Thermal Hydraulic Design and Analysis of a Large Lead-Cooled Reactor with Flexible Conversion Ratio

By

Anna S. Nikiforova

B.S. Nuclear Engineering (2006)
Oregon State University

SUBMITTED TO THE DEPARTMENT OF NUCLEAR SCIENCE
AND ENGINEERING
IN PARTIAL FULFILLMENT OF THE REQUIREMENTS FOR THE DEGREE OF

MASTER OF SCIENCE IN NUCLEAR SCIENCE AND ENGINEERING
AT THE
MASSACHUSETTS INSTITUTE OF TECHNOLOGY

[September]
AUGUST 2008

Signature of Author:_____
Anna S. Nikiforova
Department of Nuclear Science and Engineering
August 21, 2008

Certified By:_____
Neil E. Todreas
KEPCO Professor of Nuclear Science and Engineering, Professor of Mechanical Engineering (Emeritus)
Thesis Co-Supervisor

Certified By:_____
Pavel Hejzlar
Principal Research Scientist
Thesis Co-Supervisor

Certified By:_____
Jacquelyn C. Yanch
Professor of Nuclear Science and Engineering
Chair, Department Committee on Graduate Students

Thermal Hydraulic Design and Analysis of a Large Lead-Cooled Reactor with Flexible Conversion Ratio

by
Anna Nikiforova

Submitted to the Department of Nuclear Science and Engineering on August 21, 2008
in partial fulfillment of the requirements for the degree of Master of Science
in Nuclear Science and Engineering

Abstract

This thesis contributes to the Flexible Conversion Ratio Fast Reactor Systems Evaluation Project, a part of the Nuclear Cycle Technology and Policy Program funded by the Department of Energy through the Nuclear Energy Research Initiative. The goal of this project is to develop conceptual designs of fast flexible conversion ratio reactors using lead and liquid salt coolants and compare the results with the gas cooled fast reactor developed in an MIT NERI project and the sodium cooled reactor under development at ANL.

This thesis is the summary of the design and analysis of the lead-cooled reactor portion of the project. Core designs that fit in the same reactor plant were executed for two limiting conversion ratios: (1) near zero to transmute legacy waste and (2) near unity to operate in a sustainable closed cycle. To reap the benefits of economy of scale, a large power rating of 2400MWt was set as the target thermal power for both reactor designs. In addition, the achievement of inherent reactor shutdown in unprotected accidents (without scram) was set as a desirable goal. The core employs transuranic metallic fuel. The large pool vessel contains four intermediate heat exchangers (IHX) that couple the primary system to an efficient and compact supercritical CO_2 power conversion system. To prevent CO_2 from entering the core in case of intermediate heat exchanger tube rupture, a dual-free level design for the primary vessel is adopted.

Ultimate decay heat removal is accomplished by passive means through an enhanced reactor vessel auxiliary cooling system (RVACS) complemented by a passive secondary cooling system (PSACS). The transient simulation of station blackout (SBO) using the RELAP5-3D/ATHENA code shows that inherent shutdown without scram can be accommodated within the cladding temperature limit by the enhanced RVACS and PSACS by removing a fraction of decay power with the PSACS. The PSACS was designed such that the balance between two limiting cases was achieved: (1) peak cladding temperature limit is satisfied during unprotected station blackout with a minimum (two) number of PSACS trains operated, and (2) the minimum coolant temperature is kept above the freezing point with a maximum (four) number of PSACS trains operated. The PSACS design satisfies the conditions of both unity and zero conversion ratio cores. The other SBO accident conditions are bounded by the above cases. In addition, two other transients are considered: loss-of-flow accident (LOFA) and inadvertent reactivity insertion transient (UTOP). Both reactors show good performance during these additional transients.

Thesis Co-Supervisor: Neil E. Todreas
Title: KEPCO Professor of Nuclear Science and Engineering, Professor of Mechanical Engineering (Emeritus)

Thesis Co-Supervisor: Pavel Hejzlar
Title: Principal Research Scientist, Department of Nuclear Science and Engineering

Acknowledgements

Foremost, I would like to express my infinite thankfulness to my supervisors, Dr. Pavel Hejzlar and Prof. Neil Todreas, who shared with me a lot of their great expertise in reactor design and knowledge of details. I could not overemphasize my appreciation to Dr. Hejzlar's contribution to my professional growth. I am also very grateful for the honor of working with Prof. Todreas whose guidance and thoughtful advice led me through both years of this research.

I would also like to thank the person who first brought me into the world of research – Dr. James Sienicki whom I met at Argonne National Laboratory. Dr. Sienicki was my very first supervisor who sparked my interest in the reactor design.

My gratitude extends to Prof. Driscoll as I often benefited from his expertise in the reactor physics field. I thank Eugene Shwageraus for his helpfulness and knowledge.

My mother, Natasha, and sister, Masha, are two the most important people in my life. I thank them for their understanding and support when I made the decision to part with them and go across the country in order to be at MIT.

My studies and research at MIT would not be possible without the support and encouragement of my dearly loved friend Robert Erickson. To him I dedicate this thesis.

TABLE OF CONTENTS

TABLE OF FIGURES

LIST OF TABLES

1. INTRODUCTION

1.1. Motivation

With the growing demands for energy in the modern world and concerns about resource availability and global climate change, nuclear power's role in the energy supplies is projected to grow significantly. However, with the increase in the number of nuclear reactors, the nuclear waste issue grows as well. Another concern is the limited supply of fissile isotope of U-235 which is used in current generation of nuclear reactors in the US. Although, light water reactors have a capability of fulfilling the energy demands for many years, there is a need for integrating the advanced technology into the energy generation structure. Advanced fast reactors are an essential part of the Global Nuclear Energy Partnership (GNEP). Fast reactors will serve one of the goals of GNEP by consuming the usable isotopes recovered from spent LWR fuel as an alternative to their disposal in the long-term geological repository.

One of the current priorities of the Department of Energy is a time-dependent strategy of closing the fuel cycle by introducing fast reactors. However, it is difficult to predict the main purpose of the advanced reactors in the long term in addition to electricity production: actinide transmutation or production of fissile isotopes for light water reactors. Most of the designs of fast reactors are capable of doing a single task of those mentioned above. On the other hand, flexible conversion ratio reactors can respond dynamically to the emerging needs. A single reactor module is capable of operating in a zero conversion ratio mode when incineration of transuranic waste from thermal or fast reactors is necessary and unity conversion ratio mode, or self-sustainable fuel cycle mode, when better uranium utilization and resource extension is necessary.

1.2. Background

Fast reactors are an important part of the closed-cycle objective proposed by DOE. Fast reactors are capable of operating in three different modes: conversion ratio less than unity (burner), equal to unity (self-sustaining core), or larger than unity (breeder). Breeder reactors are not a part of DOE near term strategy since a significant accumulation of higher actinides from light-water reactors is present and use blankets, which raise proliferation concerns, would be required. Thus, conversion ratios of zero and unity are the limiting modes of reactor operations in this study.

Lead-cooled reactors were chosen as one of the six GEN IV reactor concept candidates. Even though lead coolant has inferior heat transfer capabilities when compared to sodium and imposes significant limits on the cladding temperatures and coolant velocity due to corrosion issues, it does not have a chemical reaction with air should the primary piping leak nor with water in the traditional Rankine cycle nor with the supercritical carbon dioxide secondary working fluid in the direct Brayton cycle. Furthermore, lead has a very high boiling point and low neutron absorption. From reactor physics stand point, lead generally has harder spectrum than sodium which is advantageous in TRU burning. On the other hand, lead reactor cores have significantly lower power density as compared to sodium cores.

Current research and design involving reactors with lead or lead-alloy primary coolants consider either a small battery-type reactors with closed fuel cycle with long (15-30 years) refueling intervals, for example SSTAR [Sienicki and Moisseytsev, 2005; Sienicki et al., 2007; Wade et al., 1999], or medium (400-700 MWth) size reactors, for example STAR-LM and STAR-H_2 [Wade et al., 2004]. Even though such reactors have many attractive attributes, their small power rating and low power density result in high fuel cycle cost. Therefore, from an economic stand point, reactors with large power ratings will be important part of the energy fleet and closed cycle.

Significant research and analysis of fast reactors with lead coolant has been done at MIT in collaboration with Idaho National Laboratory. The majority of the work was done for medium power lead-cooled actinide burners. The details can be found in Hejzlar et al [Hejzlar, 2004].

One of the major investigators of the lead-cooled reactor technology is Russia. The technology was originally applied to the development of nuclear submarines with lead-bismuth coolant with eight submarines and two ground-based facilities constructed [Gromov et al., 1997; Kagramanyan, 2008]. Current research is directed towards design of low-power systems with high efficiency balance-of-plant and passive safety characteristics. More details on current research can be found in Zrodnikov et al. [2004].

1.3. Objectives of the Present Analysis

The objective of the design and analysis is to develop a large 2400 MWth reactor system that is able to accept both zero conversion ratio and unity conversion ratio cores. Only two modes of operation rather than a full spectrum are considered due to thesis time and resource limitations. The two cores have the same size, but feature different fuels. Thus, the design of the primary coolant system must account for different peaking factors, number of control rods, and decay heat generated after the reactor shutdown. The design and analysis of the flexible conversion ratio (FCR) reactors is conducted in such way that all of the objectives of next-generation reactors including efficient utilization of resources, waste management, and inherent safety are satisfied.

A significant part of the design work is devoted to the passive safety systems including the reactor vessel air cooling system (RVACS) and passive decay heat removal loop and evaluation of their performance under unprotected transients. Neutronic design and analysis of both cores was done in parallel with this thesis work by Shwageraus et al. [2007].

1.4. Organization of the Work

The work is divided into three main parts:

- Preliminary modeling of the system using in-house codes including SUBCHAN and LOCA-COLA both written by P. Hejzlar [Todreas et al., 2008]. During this phase, the calculation of the coolant core inlet and outlet temperatures, peak cladding temperatures, and orificing arrangements needed to flatten the temperatures in the core are performed. Materials of reactor components and material behavior in lead environment are evaluated. Two main design constraints based on material study, peak cladding temperature and maximum coolant velocity in a subchannel are applied. Operational parameters are iteratively calculated to achieve the goal core power of 2400 MWth. Another part of this step is to size the intermediate heat exchangers and to ensure that enough space is provided given the constraint on the guard vessel size. The details are presented in Chapter 3 and Appendix A.
- Steady state design analysis of the reactor systems using the RELAP5-3D/ATHENA [RELAP5-3D, 2005] thermal hydraulic code. Both the conversion ratio of unity and zero reactor cores are modeled and analyzed. The model includes detailed primary system coolant flow path, secondary system configuration, and the Reactor Vessel Auxiliary Cooling System (RVACS). The details of the RVACS design are covered in Section 5.2, and the description of RELAP5-3d/ATHENA model is given in Section 6.4.
- Analysis of the reactor systems performance under protected and unprotected transients. The "unprotected" term is used to describe accidents with the failure to scram. The following transients are analyzed: loss of primary flow, station blackout, and inadvertent reactivity insertion. Reactor safety assessment based on neutronic calculation is also conducted for three transients. The results of the transient analyses are provided in Chapter 7.

1.5. Computational Tools

Preliminary modeling of the system is done using in-house code SUBCHAN written by P. Hejzlar [Todreas et al., 2008]. SUBCHAN is a computer program written in FORTRAN77 which is used to determine key thermal hydraulic parameters of interest to identify if sufficient margins to the limits are maintained. The parameters of interest include core pressure drop, flow rate distribution among assemblies and subchannels, cladding and fuel temperature distribution, and lead velocities. A separate design of the intermediate heat exchanger is performed using MS Spreadsheet. A detailed reactor system model including primary system, IHXs, RVACS, and the power conversion system is built and analyzed in RELAP5-3D/ATHENA [RELAP5-3D, 2005]. RELAP5-3D/ATHENA code has been developed for steady-state and transient simulation of the reactor system behavior. The code allows for modeling control systems, pumps, turbines and other equipment that is crucial for the analysis during protected and unprotected transients.

1.6. References for Chapter 1

Gromov B. F., Belomitcev Yu.S., Yefimov E. I., Leonchuk M. P., Martinov P. N., Orlov Yu. I., Pankratov D. V., Pashkin Yu. G., Toshinsky G. I., Chekunov V. V., Shmatko B. A. and Stepanov V. S., "Use of Lead-Bismuth Coolant in Nuclear Reactors and Accelerator- Driven Systems", *Nuclear Engineering and Design*, **173**, pp. 207-217, 1997.

Hejzlar P., Buongiorno J., MacDonald P., Todreas N. E., "Design Strategy and Constraints for Medium-Power Lead-Alloy-Cooled Actinide Burners", *Nuclear Technology*, **147**, 3, pp. 321-343, September 2004.

Hejzlar P., Davis C. B., "Performance of the Lead-Alloy-Cooled Reactor Concept Balanced for Actinide Burning and Electricity Production", *Nuclear Technology*, **147**, 3, pp. 344-367, September 2004.

Kagramanyan V. S., "Role of Fast Reactors in Addressing Energy and Environmental Issues in Russia", Sixth Tsuruga International Energy Forum, Tsuruka, Fukui, Japan, 6-8 June 2008.

RELAP5-3D Code Development Team, "RELAP5-3D© Code Manual Volume 1: Code Structure, System Models and Solution Methods," INEEL-EXT-98-00834-V1 Revision 2.3, Idaho National Engineering and Environmental Laboratory, 2005.

Sienicki J.J., Moisseytsev A.V., "SSTAR Lead-Cooled, Small Modular Fast Reactor for Deployment at Remote Sites - System Thermal Hydraulic Development", in *Proceedings of the International Congress on Advances in Nuclear Power Plants* (ICAPP'05), no. 5426, Seoul, Korea, May 15-19, 2005.

Sienicki J.J., Moisseytsev A.V., Wade D.C., Nikiforova A.S., "Status of Development of the Small Secure Transportable Autonomous Reactor (SSTAR) for Worldwide Sustainable Nuclear Energy Supply", in *Proceedings of the International Congress on Advances in Nuclear Power Plants* (ICAPP'07), no. 7218, p. 1, Nice, France, May 2007.

Shwageraus E., Hejzlar P. and Driscoll M.J., "Nuclear Design Feasibility of a Lead-cooled Fast Reactor with Flexible Conversion Ratio", 2007 ANS/ENS international Meeting, Washington D.C., November 11-15, 2007.

Todreas N.E., Hejzlar P., Shwageraus E., Petroski R., Nikiforova A., Whitman J., and Fong, C.J., "Flexible Conversion Ratio Fast Reactor Systems Evaluations", Final report, Center for Advanced Nuclear Energy Systems, MIT, MIT-NFC-PR-101, August 2008.

Wade D.C. et al., "Thermal-hydraulic Development a Small, Simplified, Proliferation-Resistant Reactor", ANL/RE/CP-98725, July 1999.

Wade D.C, J. J. Sienicki J.J, Matonis D.T., Faibish R.S., Moisseytsev A.V., Doctor R.D., "STAR-H2: a long-refueling interval battery reactor for hydrogen and water supply to cities of developing countries," in Proceedings of the 5th International Conference on Nuclear Option in Countries with Small and Medium Electricity Grids, Dubrovnik, Croatia, May 2004.

Zrodnikov A. V., Toshinskii G. I., Grigorev O. G., Dragunov Yu. G., Stepanov V. S., Klimov N. N., Kopytov I. I., Krushel'nitskii V. N. and Grudakov A. A., "SVBR-75/100 Multipurpose Modular Low-Power Fast Reactor with Lead–Bismuth Coolant", *Atomic Energy*, **97**, 2, pp. 528-533, August 2004.

Zrodnikov A. V., Efanov A. D., Orlov Yu. I., Martynov P. N., Troyanov V. M. and Rusanov A. E., "Heavy Liquid Metal Coolant – Lead–Bismuth and Lead – Technology", *Atomic Energy*, **97**, 2, pp. 534-537, August 2004.

2. DESIGN CHOICES AND CONSTRAINTS

The goal of this thesis work is to design a plant which can accommodate flexible conversion ratio cores. Thermal hydraulic design choices of the lead-cooled reactor are affected by multiple parameters. The major contributors to the design choices and constraints are:

- reactor power and vessel type,
- conversion ratio which defines the type of fuel used,
- operating temperatures which dictate the efficiency of the plant,
- choice of materials controlled by the operating temperatures as well as the susceptibility for corrosion,
- choice of balance-of-plant.

Reactivity coefficients and the decay heat curves play a key role in determining the reactor behavior during the transients. While the decay heat curves are determined by fuel type used and time of irradiation, the reactivity coefficients are part of the design choices. They were calculated to be within the self-controllability parameters a priory to the thermal hydraulic analysis.

2.1. Project Challenges

The unique challenge of the Flexible Conversion Ratio (FCR) reactor thermal hydraulic design is the requirement of the reactor systems to be able to accept cores with different fuel loadings. Two limiting cases of core configurations with zero and unity conversion ratios are considered. Due to significant variation of the fuel composition, the unity and zero conversion ratio cores have different number of control rods, power peaking maps, coolant velocities, decay heat curves, and reactivity coefficients. All of the difference must be accounted for in the thermal hydraulic design to assure that the inlet and outlet temperatures are the same for both cores. The same inlet and outlet temperature condition is necessary because of the coupling to the Power Conversion System (PCS). Transuranic (TRU) fuel and lead coolant impose temperature limits on the fuel cladding.

Therefore, both cores must be designed within both steady state and transient cladding temperature limits while maximizing the core outlet temperature for better plant efficiency. The limits and rationale behind the design constraints are discussed in Section 2.3.

Another major challenge of the FCR project is the scale of the plant. A pool-type reactor plant with 2400 MWth power output has certain advantages from the economy of scale perspective. Also, certain type of accidents is eliminated, e.g. Loss of Coolant Accident due to primary coolant pipe break. However, such a large power rating raises challenges related to the tight space within the vessel. The core, primary coolant pumps, and four Intermediate Heat Exchangers (IHX) must be placed inside the vessel. While placement of the IHX inside the vessel eliminates additional loops, there is a possibility of ingress of the secondary coolant, supercritical carbon dioxide at high pressure, into the core. Ingress of the gas would result in coolant voiding which can lead to reactivity increase and challenge proper core cooling. Therefore, the core must be protected against such an incident.

IHX design is important for the overall plant performance. Performance of the IHXs directly impacts the efficiency of the secondary side as well as the primary coolant pumping requirements. In order to achieve good efficiency of the S-CO2 cycle, the IHX pressure drop and logarithmic temperature difference should be minimized. These desirable goals favor a large IHX. However, the large IHX would result in a significant increase of the vessel size which in turn would hurt the overall plant economics. Therefore, a balance between the above parameters must be achieved.

Reactor safety is a major aspect of the plant design. A self-controllable reactor needs to demonstrate a combination of reactivity feedbacks that lead to an inherent reactor shutdown without reliance on reactor scram. The core can be designed in such way that the reactivity coefficients satisfy the self-controllability criteria [Wade et al., 1997.] However, large positive coolant void worth is one of the key design challenges. Another characteristic of a self-controllable reactor design is a capability of dissipating the decay

heat during the transients without reliance on active systems and exceeding the material temperature limits. The above requirement combined with large power of the core creates a need for design of passive decay heat removal.

2.2. Choice of Coolant

The coolant choice contributes to safety characteristics of the reactor and affects its economics. Lead coolant exhibits inherent safety features such as absence of chemical interaction with secondary fluid CO_2 and low operating pressures. Furthermore, lead is favorable neutronically for fast reactors because of its low parasitic neutron absorption, high scattering cross section (low leakage out of the core), and hard spectrum. Its high boiling temperature is also favorable for safety due to a lack of coolant voiding from boiling and consequent reactivity effects. From the thermal hydraulic perspective, lead requires considerable pumping power because of relatively high viscosity especially when compared to sodium. However, its neutronic characteristics allow for a more open lattice than sodium cores which makes it possible to reduce the pumping power requirements.

2.2.1. Thermophysical and Chemical Properties

In this section, lead-alloy coolants are compared with sodium, the other coolant commonly used in fast reactor designs. Table 2-1 compares thermophysical properties of three coolants. Sodium coolant shows the best thermal hydraulic characteristics. Sodium has a low melting point, but its boiling point is also low. Due to the high boiling temperature of lead, certain problems such as coolant voiding caused by boiling in the core during an accident are eliminated.

Because of the high density of lead and lead-bismuth, radial reflectors for gamma-rays and energetic neutrons are not required which is not the case for sodium or salt reactors. Lack of reflectors means smaller effective core diameter. On the other hand, sodium

coolant has tight core packing. Small coolant fraction is acceptable because of high thermal conductivity of sodium resulting in small film temperature drop and relatively low viscosity. As can be seen in Table 2-1, the thermal conductivity of lead-alloy coolants is nearly four times smaller than sodium, resulting in higher values for film temperatures. This affects the cladding temperatures and reactor operating temperatures. In addition to thermal conductivity, lead cores are required to have an open core lattice to maintain acceptably low pumping power and because of significant coolant velocity limits. The coolant velocity cannot exceed 3 m/s because of the protective oxide layer present on the structural components of lead systems. At high velocities, the layer can be damaged or stripped off. More details are provided in Section 2.3. Therefore, because of lower thermal conductivity and coolant velocity constraint, the lead-cooled cores must have higher coolant volume fraction in order to achieve the same power rating as in sodium reactor. Because of superior thermal properties of sodium, the power density of sodium cores is nearly three times higher than in lead-cooled reactors.

The attractiveness of sodium coolant is however counterbalanced by the drawbacks associated with its energetic reactions with air and water. Sodium is one of the most electropositive metals [IAEA TECDOC-1289, 2002] (lithium is more reactive, but has less metallic properties). The possibility of fires when sodium reacts with air or water requires employing an intermediate heat transport loop or double-wall heat exchanger tubes. Liquid lead is not chemically reactive with secondary coolants. However, lead and Pb-Bi interact with structural materials. Such interaction results in dissolution or liquid metal embrittlement (LME) [Ballinger, et al., 2004]. The issues of corrosion and LME are very important in lead-cooled reactors.

2.2.2. Neutronic Characteristics

One of the goals of a Flexible Conversion Ratio reactor is being able to either operate in a self-sustained cycle or as a TRU incinerator. Both functions require usage of a coolant with low moderating power. As was discussed above, sodium's relatively low boiling

point creates a possibility of reactivity effects from coolant voiding due to boiling. Sodium also has a softer spectrum than lead coolant.

Table 2-1. Thermophysical Characteristics of Coolants

	Lead*	Lead-Bismuth* (0.445Pb-0.555Bi)	Sodium*
Atomic Number	82	-	11
Atomic Weight	207.21	-	22.997
Boiling Point, °C	1737	1670	892
Melting Point, °C	327.4	123.5	97.8
Density, ρ, kg/m^3			
At 450°C	10536	10180	842
At 700°C	10242	9876	780
Thermal Expansion Coefficient, α, % Vol/K			
At 450°C	0.011	0.0130	0.029
At 700°C	0.012	0.0135	0.031
Dynamic Viscosity, μ, kg/m-s			
At 450°C	2.01 E-3	1.49 E-3	2.59 E-4
At 700°C	1.40 E-3	1.13 E-3	1.81 E-4
Thermal Conductivity, k, W/m-K			
At 450°C	15.4	14.9	66.1
At 700°C	17.7	16.7	59.1
Specific Heat, c_p, J/kgK			
At 450°C	147	146	1272
At 700°C	147	146	1276
Density Specific Heat Product, ρ c_p, J/cm^3K			
At 450°C	1.55	1.49	1.07
At 700°C	1.51	1.45	1.00

* Kutateladze, et. al., "Liquid Metal Coolants", Atomisdat, Moscow, 1976

One of the key challenges of lead-cooled reactors is positive coolant void worth. Coolant void worth is one of the criteria used to evaluate the core inherent safety. Because of the high boiling temperature of lead and dual-free-level design, the unlikely event of gas entering the core is not considered. The coolant void can originate from the spectral factor of reactivity response to coolant density reduction [Todreas et al., 2008]. The other components are neutron leakage and absorption in the coolant. To reduce positive void worth of coolant, the following techniques can be used in the design: use of streaming fuel assemblies [Hejzlar et al., 2004] or making the core pancake–like or very

tall to increase neutron leakage. The goal of this core design was to strive not necessarily for negative coolant temperature coefficient (since it may not be achievable in large cores without significant economic penalties), but for a combination of all reactivity feedbacks such that one can achieve passive reactor shutdown in unprotected (without scram) accidents – an approach similar to that of the ANL Integral Fast Reactor (IFR) [Wade et al., 1997].

2.2.3. Overview of Corrosion Issues Associated with Lead Coolant

With lead-cooled systems, the corrosion problem is one of the main challenges. Design limits are greatly affected by corrosion. Since most materials have finite solubility in lead, the components surfaces must be protected. The driving force for corrosion is the chemical activity of structural metals and lead. [LBE Handbook, 2007] Corrosion rate is also a function of temperature. Therefore, unless there is a protective layer between a material and lead-coolant, there is a removal of materials from hot regions and deposition of materials in cooler regions [Ballinger et al., 2004]. Such phenomenon can create a build up of corrosion products potentially plugging the heat exchanger tubes. If the coolant passages of the core are blocked by the corrosion products, it can lead to fuel pin overheating. Besides temperature, other contributing (or in some cases limiting) factors of material degradation are exposure time, flow rate, and coolant and material composition including oxygen content in coolant. The measures that can be taken in order to reduce lead effects on the system are the following:

- Reduction of operating temperatures and coolant velocity
- Use of coating (corrosion resistant but structurally unsatisfactory material to face lead environment)
- Environment with self-protective film formation
- Use of materials with low solubility in lead

Table 2-2 shows compositions of T-91 and SS316 steel. The former is used as cladding and IHX structural material in this study while the latter is for the vessels. Corrosion rates

and resistance of steels depend on the solubility of compositional elements in liquid lead which are summarized in Table 2-3. Constants A and B are parts of the Arrhenius equation. The Equation 2-1 defines the saturation concentration of an element in solution and can be used to estimate material corrosion resistance based on solubility of chemical elements. [IAEA TECDOC 1289, 2002]

Table 2-2. Composition of T-91 steel

[LBE Handbook, 2007]

	T-91	SS316
C	0.1-0.11	0.012-0.02
Cr	8.26-8.63	16-18
Ni	0.13-0.23	10-17.392
Mo	0.91-0.95	2-2.75
W	<0.01	
Mn	0.43-0.78	0.2-2
Si	0.31-0.43	0.1-1
P	0.01-0.02	0.024-0.19
S	0.003-0.06	0.0005-0.03
Cu	0.19-0.05	
Al	<0.01	
Nb	0.07-0.09	
Co	0.02	0.06-0.14
V	0.20-0.23	
Ti	0.003	
N	0.04	0.02-0.1

$$\log C_S = A - B/T \qquad \text{Equation 2-1}$$

Figure 2-1 and Figure 2-2 show corrosion behavior of T-91 steel and SS316L, respectively. The saturation line which indicates formation of PbO and the line of formation of magnetite (Fe_3O_4) are useful in determining the oxygen concentration and temperature ranges of operation in LBE environment with oxide layer formation. The upper limit of the desired operating range of temperatures of the FCR reactors is ~ 575°C (corresponds to peak cladding temperature of 625°C during steady state operation).

Dissolved oxygen can form a protective Fe-Cr oxide layer that prevents cladding dissolution into the coolant. However, careful oxygen control is required. Below the magnetite formation curve, the dissolution occurs. At temperatures above 550°C, oxygen control in lead environment becomes significantly less effective. Furthermore, it is important to keep the cladding material temperature below the transformation from ferrite to austenite that results in significant property changes as well as a volume change. This transformation depends on material composition and for 12Cr-MoVNb steels ranges between 760°C to 850°C [Klueh and Harris, 2001].

Table 2-3. Solubility of different elements in liquid lead
[IAEA TECDOC 1289, 2002]

Elements	Constants of Eq. 2-1		Temperature range, K
	A	B	
C	1.026	3850	350–1000
Co	2.60	4400	350–1650
Cr	3.74	6750	908–1210
Cu	2.72	2360	327–1000
Fe	0.34	3450	330–910
H_2	–1.946	2360	500–900
Mn	2.02	1825	327–1200
Mo	solubility <10-3 wt.% at 1000°C		
N_2	no solubility		
Nb	solubility <10-5 wt.% at 1000°C		
Ni	2.78	1000	330–1300
O2	–	2176	350–850
	0.106		
Si	3.886	7180	1050–1250
Ti	solubility ~5.6·10-4 wt.% at 500°C		
U	3.921	5121	400–800
Zr	solubility ~1.2·10-9 wt.% at 500°C		

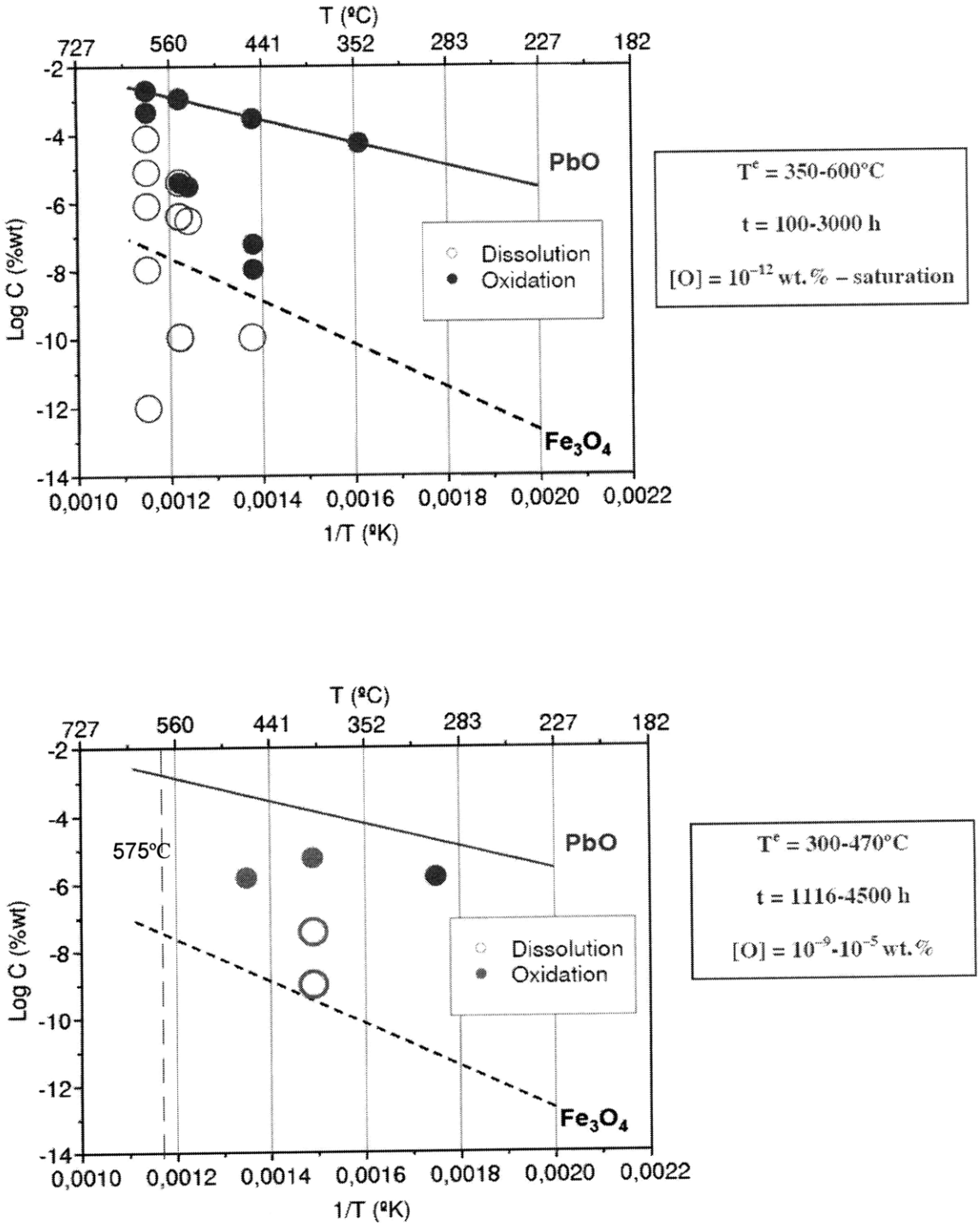

Figure 2-1. T-91 steel in stagnant (top) and flowing (bottom) LBE

[LBE Handbook, 2007]

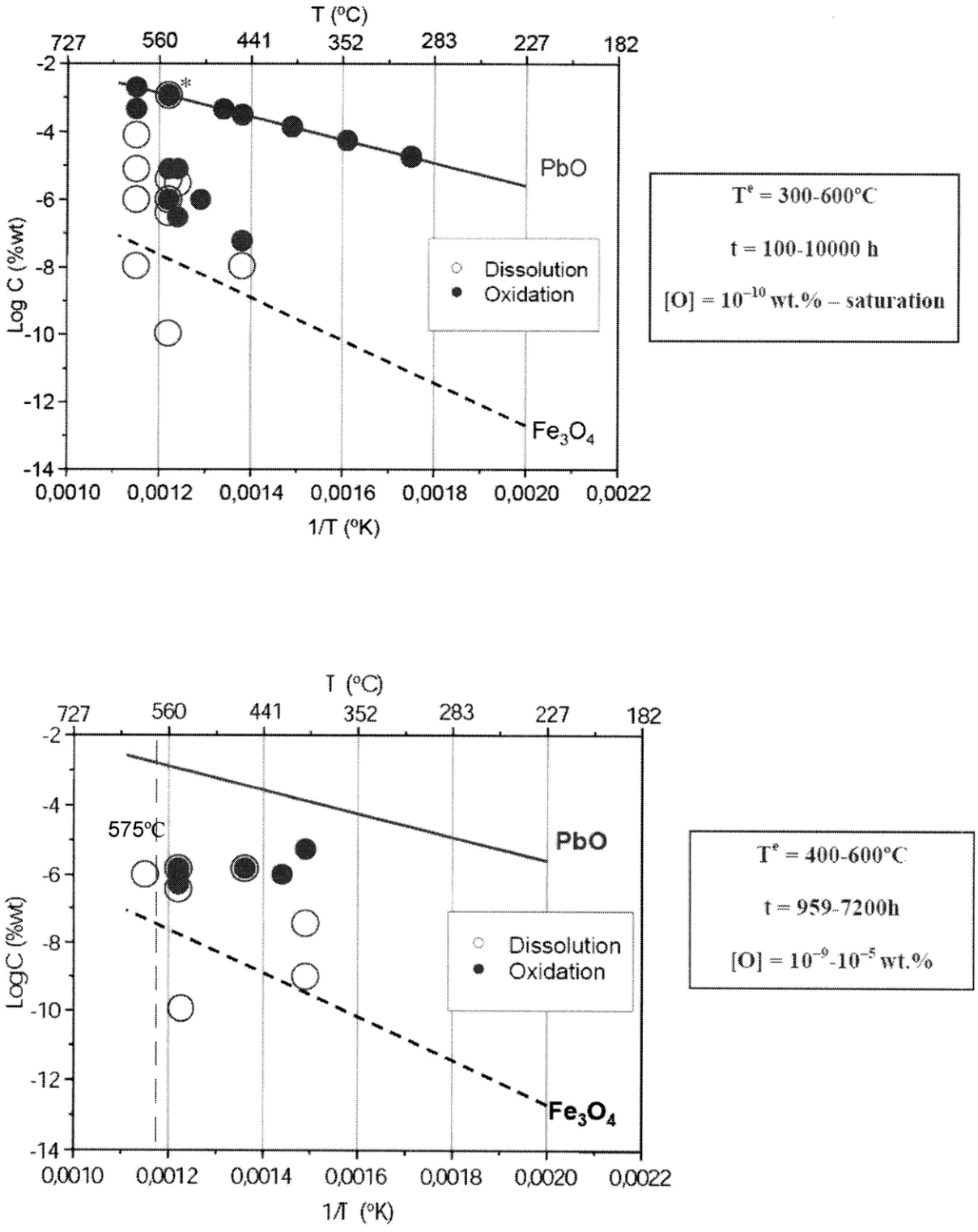

Figure 2-2. SS316L steel in stagnant (top) and flowing (bottom) LBE

[LBE Handbook, 2007]

Self-protective films, of the same kind as oxide layers, have been considered as another defense mechanism against corrosion. A protective oxide layer can be viewed as a diffusion barrier, slowing overall corrosion rate and preventing more severe materials degradation. However, material dissolution in case of low oxygen concentration and surface oxidation in case of high oxygen concentration can occur. Therefore, an oxide layer can form given sufficient oxygen dissolved in the coolant, and active oxygen control is needed. Thus, a lead-cooled system can operate in a narrow range of oxygen concentration and temperatures.

With current demand for higher operating temperatures, a collaborative effort between Los Alamos National Laboratory, Idaho National Laboratory, and MIT is directed towards development of a system that will both form a protective oxide layer over a wide range of oxygen potentials as well as demonstrate minimal solubility in liquid metal at oxygen potentials below the formation potential of SiO_2 [Ballinger et al., 2006]. Acceptable temperature goal of this project is up to 700°C. A series of Fe-Cr-Si alloys have been developed. The Fe-12Cr-2.55Si alloy has demonstrated corrosion resistance in lead-bismuth eutectic environment for temperatures up to 700°C. However, such alloy is susceptible to radiation induced embrittlement. Thus, the development of an alloy that has all required characteristics, such as low solubility in lead environment, stable oxide film formation, and invulnerability to radiation induced embrittlement, is still in progress.

2.3. Steady State and Transient Design Constraints

The design constraints are determined by the balance between materials performance and plant efficiency. To maximize the cycle efficiency, it is desired to have the reactor operating with the temperatures as high as possible; however, the issues of corrosion, stresses and mechanical integrity, and radiation embrittlement limit the operating temperatures to finite values. In the case of the FCR reactors, three main material temperature and coolant velocity constraints were identified: fuel, cladding, and vessel and structural materials.

The reactor materials can be split into three categories according to their immediate availability: available now, achievable in the near future and the materials which still require significant research and development. The materials evolution is depicted in Figure 2-3. The materials designated "available now" and "achievable" have been selected for the current design. Table 2-4 summarizes the design constraints for the reactor materials. Note that T-91 is placed into the "achievable" category. This is because lead coolant requires special protective layers for the cladding in order to operate in highly corrosive environment.

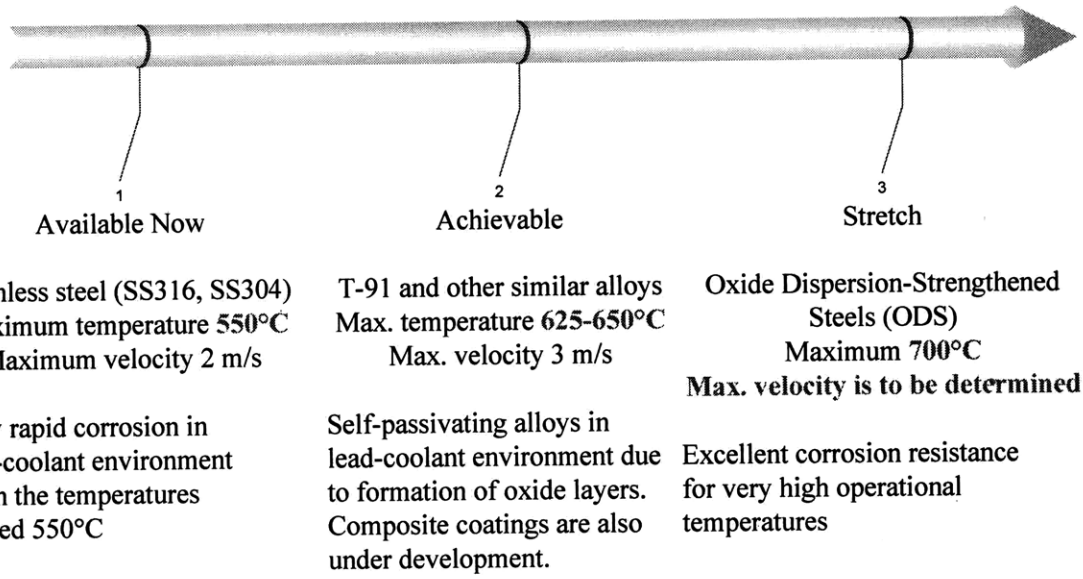

Figure 2-3. Materials evolution and operational limits

Table 2-4. Summary of Design Constraints for the Reactor Materials

(Available Now Case)

Cladding limits	Material used:	T-91 with protective layers
	Steady state membrane temperature:	650°C
	Transient inner temperature:	725°C
	Fluence (E > 0.1 MeV):	3.3-4.0 x 10^{23} n/cm^2
	Irradiation damage:	150-200 dpa
Fuel limits	Maximum temperature (CR=0/CR=1[†])	1200/1000°C
	Peak burnup[††] (CR=0/CR=1[†])	Heavy metal loading

		dependent/150 MWd/kg
Vessel limits	Material used:	SS316
	Steady state maximum membrane temperature:	430°C
	Transient maximum membrane temperature:	700°C
	Fluence (above 1 MeV)	5E+19n/cm^2
Maximum coolant velocity		3 m/s

†CR=1 fuel composition: U-TRU-Zr (10%Zr), and
CR=0 fuel composition: TRU-Zr
††Alloy-type fuel, taking into account cladding stress for given cladding dimensions and temperature limits, based on earlier analyses

2.3.1. Cladding

The high chrome boiler tube material T-91, similar in composition to HT-9, has initially been developed for nuclear application [T-91 Handbook, 1990]. T-91 alloy showed superior behavior over stainless steel TP304H in modulus of elasticity, thermal conductivity and thermal expansion in numerous experiments. T-91 (9Cr-1MoVNb) steel alloy has been approved for the ASME code Section III, Subsection NH for Class 1 [ASME, 2007] applications for temperatures up to 649°C in 2007. Thus, the 650°C steady state limit was adopted for the steady state cladding temperature limit. The transient temperature limit for cladding is 725°C. Beyond this temperature significant diffusion of actinides into the cladding from the fuel can create low-melting-point regions, resulting in thinning of the cladding and subsequent failure [Pahl et al., 1990]. The T-91 alloy appears in the "achievable" category on Figure 2-3 in spite of being currently commercially available. The alloy experiences corrosion problems in the lead environment at the temperatures above 550°C as is discussed in Section 2.2. Protective films can limit the corrosion effects, but still require significant R&D.

A cladding fluence limit of 4.0 x 10^{23} n/cm^2 (E>0.1MeV) or 150-200dpa was adopted based on proven HT-9 (Fe-12Cr-1Mo) performance [Dubberley et al., 2000]. In addition to the temperature and fluence limits, coolant velocity limits are imposed to the surfaces exposed to flowing lead alloys. The cladding materials of lead-bismuth cooled reactors used in Russian submarines required that the lead velocity not exceed a 2 m/s limit. The

main reason for such limit is the Fe-oxide layer stability. Higher velocities of the coolant can lead to oxide layer erosion especially in locations where the geometry of the structure suddenly changes [LBE Handbook, 2007]. The newer materials with Si or Al oxide based films for protection under development at MIT should allow higher velocity limits. Thus, the limit of 3m/s was adopted for ferritic-martensitic steels with the new alloy cladding surface with the expectation that with further development this limit can be raised.

2.3.2. Vessel

For the vessel, stainless steel 316 (SS316) was adopted because of the need to accommodate high temperature in transients. The ASME Code, Subsection NH, which regulates the design of pressure retaining components, shows that SS316 has higher allowable stress than other materials for the design of Class 1 components for elevated temperature service (SS304, Alloy 800H and 2.5Cr-1Mo). This steel was also used for the S-PRISM design. Buongiorno has shown that for a guard vessel of thickness greater than 15 cm and diameter of 6m, the temperature limit is for transients of lower frequency (Level C Service Loadings), and is about 750°C [Buongiorno, 2001]. The FCR design requires larger vessel. Hence, the limit of 700°C was adopted. The steady state operation limit is 430°C if the lifetime of the vessel is to be more than 34 years. The SS316 vessel needs to be equipped with a thin liner material that is corrosion resistant and prevents liquid-metal embrittlement of the vessel.

2.3.3. Fuel

The primary choice for the fuel is metallic U-TRU-Zr (10%Zr) alloy for the CR=1 core and metallic TRU-Zr alloy for the zero CR core. The limiting fuel temperature for U-Pu-Zr alloy with 10wt% Zr is 1000°C. The same temperature limit was adopted for U-TRU-Zr fuel for the CR=1 core, although more research is needed to confirm the effect of small amounts of minor actinides on the fuel alloy melting point. The fuel for the CR=0 core contains significantly larger zirconium content, and has thus a higher melting point. The 1200°C fuel temperature limit from Hejzlar et al., [2004] for fertile free zirconium-based fuel was also adopted in this analysis. The burnup limit is set at 150MWd/kgHM (average) and 200MWd/kgHM (peak) for U-TRU-Zr (10%Zr) fuel. This is based on

irradiation experience with ternary (U-Pu-Zr) metal alloy pins in HT-9 ferritic cladding, which were qualified and demonstrated for 150 MWd/kg peak discharge burnup and 100 MWd/kg average burnup and achieved 200 MWd/kg peak discharge burnup [Hill et al., 1999].

2.4. References for Chapter 2

ASME, "Boiler & Pressure Vessel Code. An International Code. Section III, Division 1, Subsection NH (Class 1 Components in Elevated Temperature Service)." ASME, 2007.

Ballinger, R.G., Lim, J., "An Overview of Corrosion Issues for the Design and Operation of High-Temperature Lead- and Lead-Bismuth-Cooled Reactor Systems," *Nuclear Technology*, **147**, 3, pp. 418-435, 2004.

Ballinger, R.G., "The Development and Production of a Functionally Graded Composite for Pb-Bi Service", quarterly report, August 15, 2006.

J. Buongiorno, "Temperature Limits for Heavy-Liquid-Metal Reactor Vessels", Proc. of the 2001 ANS Winter Meeting, Reno, NV, Nov. 11-15, 2001.

Dubberley A. E., Boardman C. E., Yoshida K., and Wu T., "SuperPRISM Oxide and Metal Fuel Core Designs", ICONE-8002, Proc. of ICONE-8, 8th Int. Conf. on Nucl. Eng., Baltimore, MD, Apr. 2-6, 2000.

INTERNATIONAL ATOMIC ENERGY AGENCY, "Comparative assessment of thermophysical characteritics of lead, lead–bismuth and sodium coolants for fast reactors," IAEA-TECDOC-1289, 2002.

Hejzlar P., Davis C.B., "Performance of the Lead-Alloy-Cooled Reactor Concept Balanced for Actinide Burning and Electricity Production," *Nuclear Technology*, **147**, 3, pp. 344-367, 2004.

Hejzlar P., Buongiorno J., MacDonald P. E., Todreas N. E., "Design Strategy and Constraints for Medium-Power Lead-Alloy-Cooled Actinide Burners," *Nuclear Technology,* **147**, 3, pp. 321-343, 2004.

Hill R. N., J. E. Cahalan, H. S. Khalil, and D. C. Wade, "Development of Small, Fast Reactor Core Design Using Lead-Based Coolant," Proc. of the Global 1999 Int. Conf., Jackson Hole, WY, August 1999.

Klueh R.L. and Harries D.R., "High-Chromium Ferritic and Martensitic Steels for Nuclear Applications", American Society for Testing and Materials, West Conshocken, 2001.

Kutateladze, "Liquid Metal Coolants," Atomizdat, Moscow, 1976.

LBE Handbook, "Handbook on Lead-bismuth Eutectic Alloy and Lead Properties, Materials Compatibility, Thermal-hydraulics and Technologies", ANE NEA, 2007.

Pahl R. G., Porter D. L., Lahm C. E., and Hofman G. L., "Experimental Studies of U-Pu-Zr Fast Reactor Fuel Pins in the Experimental Breeder Reactor-II", *Metallurgical Trans. A*, **21A**, pp. 1863-1870, 1990.

T-91 Handbook, "The T91 Book: Ferritic Tues and Pipe for High Temperature Use in Boilers", ed. G. Guntz, M. Julien, G. Kottmann, F. Pellicani, A. Pouilly, and J.C. Vaillant, Vallourec Industries, France, 1990.

Todreas N.E., Hejzlar P., Shwageraus E., Petroski R., Nikiforova A., Whitman J., and Fong, C.J., "Flexible Conversion Ratio Fast Reactor Systems Evaluations", Final report, Center for Advanced Nuclear Energy Systems, MIT, MIT-NFC-PR-101, August 2008.

Wade D.C., Hill D.J., Wigeland R.A., "The Safety of the IFR", *Progress in Nuclear Energy,* 31, 1/2, pp. 63-82, 1997.

3. OVERVIEW OF PLANT DESIGN

3.1. Overview of the Design

The main goal for the plant design for lead-cooled reactor is the ability of the plant to accommodate both unity and zero conversion ratio cores without any changes to the design or layout except for the control rod penetrations through the vessel head. The steady state thermal hydraulic design of the reactor core and the intermediate heat exchangers (IHXs) follows from the design goals and constraints. The coolant temperature rise through the core is determined by the peak cladding temperature limit, margin to freezing point, and the balance-of-plant working temperatures. Similarly, the design and configuration of the IHXs is related to the secondary cycle temperatures and pressure drop constraint and the space availability within the reactor vessel. Thus, for a successful design, it is necessary to achieve good balance between the design goals, limits discussed in Chapter 2, and economic practicability.

The key features of the plant design include:

- Forced circulation of the primary coolant under steady state conditions. The forced circulation allows for higher power density than natural circulation. Higher power density means more compact core and economic plant design. Compact core gives more freedom for the Intermediate Heat Exchanger design in case of a fixed maximum reactor vessel diameter.
- Pool-type reactor design, which is possible because of inertness of lead with respect to CO_2. While the placement of the IHXs inside the vessel creates constrains on the IHX design because of the limited space, the benefits of pool-type design include elimination of loss-of-coolant accident and additional piping.
- Supercritical carbon dioxide Brayton cycle chosen as the balance-of-plant. The compact and efficient (~44% for operating temperatures and pressures of this design) S-CO_2 cycle is expected to reduce the overall capital cost of the plant.

- Enhanced Reactor Vessel Auxiliary Cooling System (RVACS) and Passive Safety Auxiliary Cooling System (PSACS) both using coolants with natural circulation for decay heat removal during transients.
- Dual-free-level design of the reactor vessel which is used to ensure that the supercritical CO2 does not enter the core in case of an IHX tube rupture.

3.2. Reactor Core Layout

Both of the reactor cores consist of three core zones with different fuel loadings. Instead of conventional TRU/U ratio variation from zone to zone, zirconium tailoring was used while the TRU/U ratio was held fixed. Such tailoring had key beneficial impacts on thermal hydraulic design: relatively flat core power profile and constant spatial positions of assembly peaking factors in the core throughout the cycle. Flat power profile minimized the number of orificing zones to three, and the "stationary" assembly peaking allowed for fixed orificing configuration. Orificing can be used to maximize either core-average outlet temperature, and thus plant efficiency, or the margins to cladding temperature limits. In this design orificing was used to maximize the margin between the peak cladding temperature and the limit of 625°C. Note that the actual limit identified in Chapter 2 was 650°C. However, the transient limit of peak cladding temperature is 725°C. To allow more flexibility during the transient, the more conservative value of 625°C was adopted as a soft limit for the steady state model.

The preliminary reactor core analysis was performed using the in-house code SUBCHAN, in which every core subchannel was modeled to determine the core temperature map. The core models were different for the unity conversion ratio (CR=1) core and zero conversion ratio (CR=0) core due to their differences in enrichment, number of control rod assemblies, and power peaking. The layout of both cores is shown on Figure 3-1. The 2400 MWth core contains 349 canned fuel assemblies in a square lattice configuration. Each assembly is composed of 21x21 pin positions also arranged in a square lattice. The unity conversion ratio core has fewer control rods because of its

smaller reactivity swing. The control rods in both cores are double-entry rods [Todreas et al., 2008]. Such configuration helps flattening the power profile of the core. The core parameters for both cores are summarized in Table 3-1.

Table 3-1. Core model description

Parameters	**Value**
Bottom coolant mixing plenum height, cm	150.000
Core support plate thickness, cm	4.500
Core support height (shield + bottom reflector), cm	130.000
Active core height, cm	130.000
Gas plenum height, cm	130.000
Upper plate thickness, cm	1.000
Lead chimney height, cm	500.000
Core barrel inner radius, cm	244.131
Core barrel outer radius, cm	246.131
Reactor vessel inner radius, cm	316.131
Reactor vessel outer radius, cm	324.131
Number of assemblies	349
Core average power density, W/cm3	111.8
Initial core fuel inventory, kgHM	53,631
Core specific power, W/gHM	44.75

Figure 3-2 shows the radial power peaking for both zero and unity conversion ratio cores. The power peaking maps are further used in subchannel analysis described in Chapter 4. Note that the power peaking profile for the CR=1 core is shown for the middle-of-core-life which corresponds to 40 MWd/kg burnup while the map for the CR=0 core is for beginning-of-life. This is because of the time when the maximum power peaking occurs for both cores. Details on neutronic analyses and generation of power peaking maps are given in [Todreas et al., 2008].

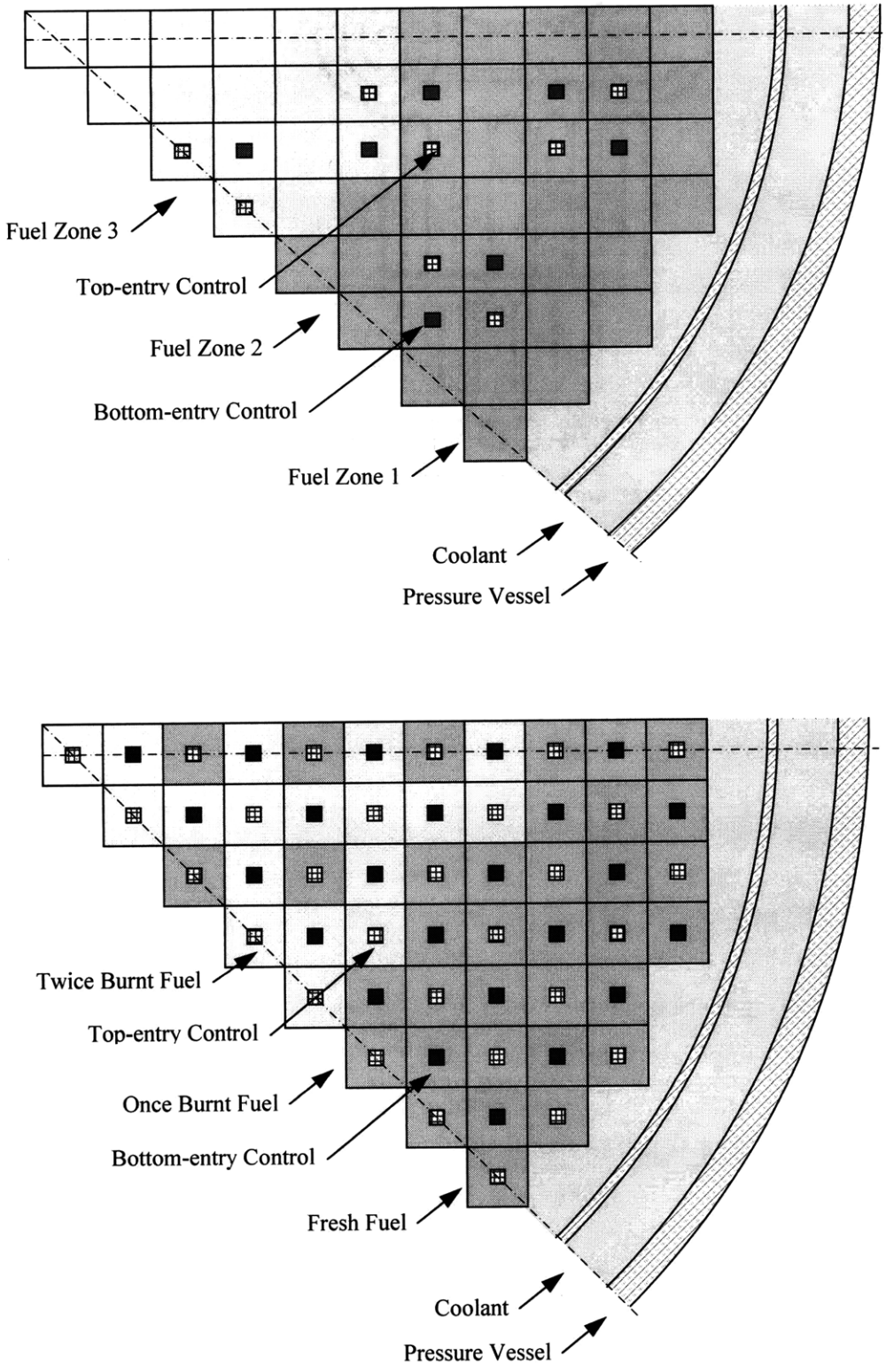

Figure 3-1. Radial core zoning. Top = unity conversion ratio; bottom = zero conversion ratio. [Todreas et al., 2008]

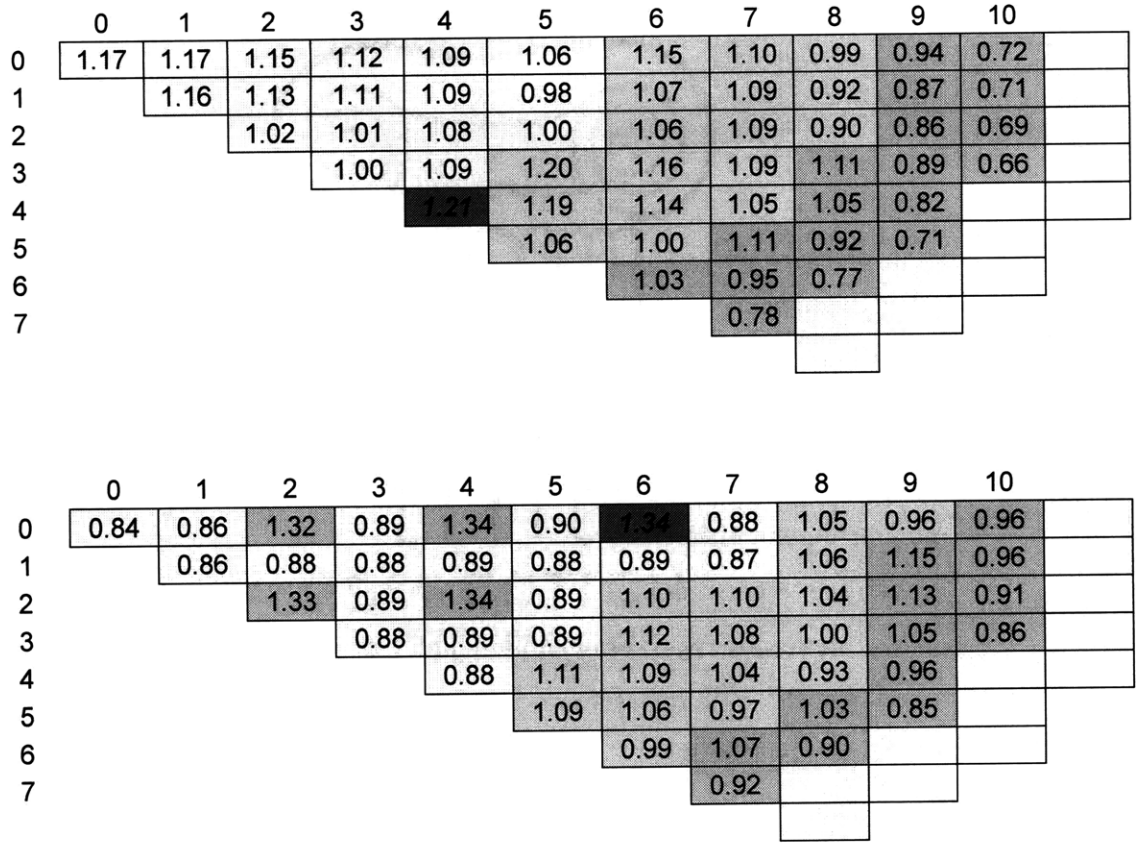

Figure 3-2. Radial Power Distribution Map. Top = CR=1 Core at MOC (40 MWd/kg); bottom = "CR=0" Core at BOL (0 days). [Todreas et al., 2008]

3.3. Intermediate Heat Exchanger

The Intermediate Heat Exchanger (IHX) is one of the key components of the plant system. IHX performance is defined by its heat removal capabilities and has an effect on the overall plant efficiency. The main IHX challenge is that the heat exchangers must be placed within the reactor vessel in a constrained space. The constraints are defined by the size of the core and by the maximum allowable diameter of the guard vessel. The diameter of the vessel is limited by manufacturer capabilities and by seismic analysis. In the present analysis, the maximum vessel diameter of 10.2 m is assumed – about 1m larger than the vessel of the S-PRISM reactor. Pool design eliminates coolant loops on the primary side leading to plant compactness and simplicity in design. Certain types of

accidents involving a primary coolant pipe break are also eliminated. Placement of IHXs inside the vessel also eliminates intermediate loops. However, the constraint on the vessel size imposes a limit on the size of the heat exchanger. Additional challenges exacerbating the problems are:

- High pressure on CO_2 side (19.7 MPa), which requires thicker tubes and gas plena walls,
- High temperature (573°C), which reduces allowable stress of IHX material
- Desirable small temperature difference between lead coolant and CO_2 to maximize plant efficiency
- Pressure drop constraints
  - on the S-CO_2 side to maintain high (45%) efficiency of the PCS,
  - on the primary side to retain reasonable pumping power and velocity limits
- Large difference in the heat transfer coefficient between lead and CO_2

The design and analysis of the intermediate heat exchangers (IHXs) have been a challenge due to high operating pressures and temperatures. The high pressure on the CO_2 side required stress analysis to determine appropriate tube thickness. Furthermore, the large difference in heat transfer coefficients between the lead coolant and supercritical carbon dioxide stimulated investigation into enhanced heat transfer on the CO_2 side. Finally, the pressure drop constraint on the S-CO_2 side is directly related to the power conversion system efficiency; thus, the minimum achievable pressure drop was pursued. The above challenges are closely linked to material choice.

3.3.1. Materials for IHX

T-91 alloy (with functionally gradient surface treatment on the lead side) was investigated for use in heat exchangers since 316SS alloy is not compatible with the corrosive environment of lead at temperatures above 550°C. A comprehensive overview of T-91

composition and associated corrosion issues in a lead-coolant environment are discussed in Chapter 5. Prior to the ASME Code 2007 Edition [ASME, 2007], T-91 alloy was ASME Code approved for temperatures up to 649°C only for Section III, Classes 2 and 3 components. Therefore, its use was limited to the applications outside the pressure boundary of the reactor systems, and its properties (e.g. allowable stress intensity which is crucial for the IHX design) as a function of service time were not available. The 2007 ASME Boiler and Pressure Vessel code included T-91 alloy as an acceptable material for Sec. III, Division 1, Subsection NB/NH for Class 1 components. Figure 3-3 Figure 3-3 depicts allowable stress intensity for T-91 alloy for a service lifetime of 20 years for the heat exchanger components.

Another important parameter that affects heat exchanger performance is thermal conductivity of the structural material. The ASME code provides thermal conductivities for a great variety of materials. Figure 3-4 compares thermal conductivity of T-91 alloy versus 316SS. At the temperature of interest, 577 °C and lower, the thermal conductivity of T-91 significantly exceeds the conductivity of 316SS. The temperature of 470 °C shown on Figure 3-4 corresponds to the heat exchanger temperature averaged for both lead and CO_2 coolants. At this temperature, the thermal conductivity of T-91 is 33% higher than 316SS, which results in better heat transfer and thus smaller IHXs.

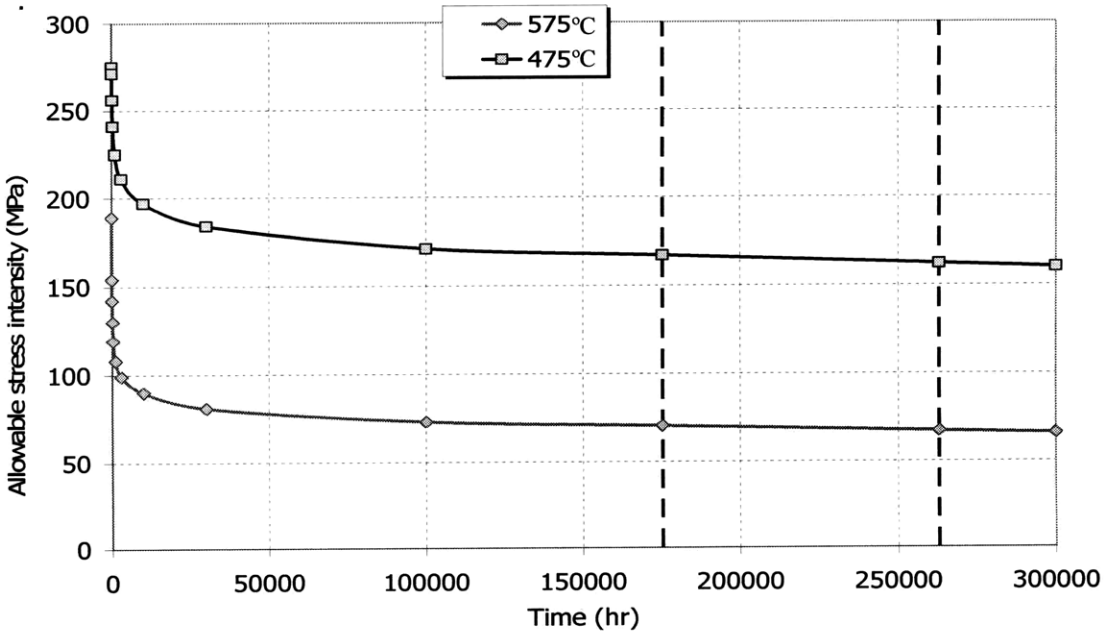

Figure 3-3. Allowable stress intensity as a function of time and temperature (in °C) for T-91 alloy (ASME code, Division 1, Section III, Class 1 components)

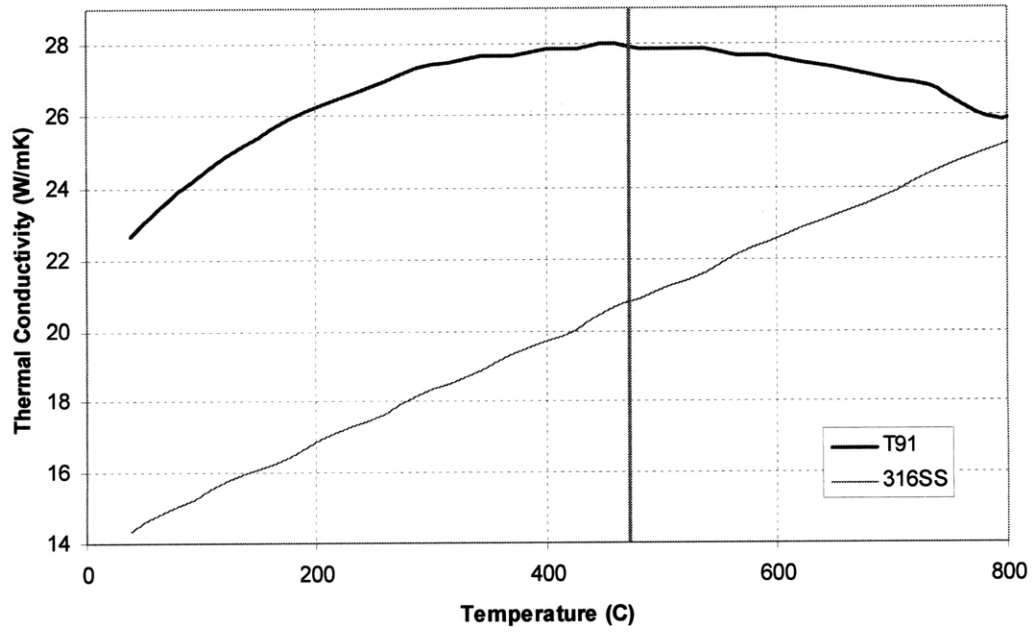

Figure 3-4. Thermal conductivity (in W/mK) vs. temperature (in °C) (ASME code, Section III, Class 2 and 3 components)

3.3.2. Overview of the IHX Design

The design of the kidney-shaped heat exchanger is shown on Figure 3-5**Error! Reference source not found.** and Figure 3-6. The gas enters the heat exchanger through the large inlet tube, and proceeds downward to the lower plenum where it is distributed into small-diameter tubes. After the heat exchange with lead coolant which is on the outside of the tubes (shell side of the IHX), the gas is collected in the upper plenum. The CO_2 outlet tube is split into two outlet tubes of smaller size. Concentric tube design could not be applied to the heat exchanger due to the large size of the main inlet tube.

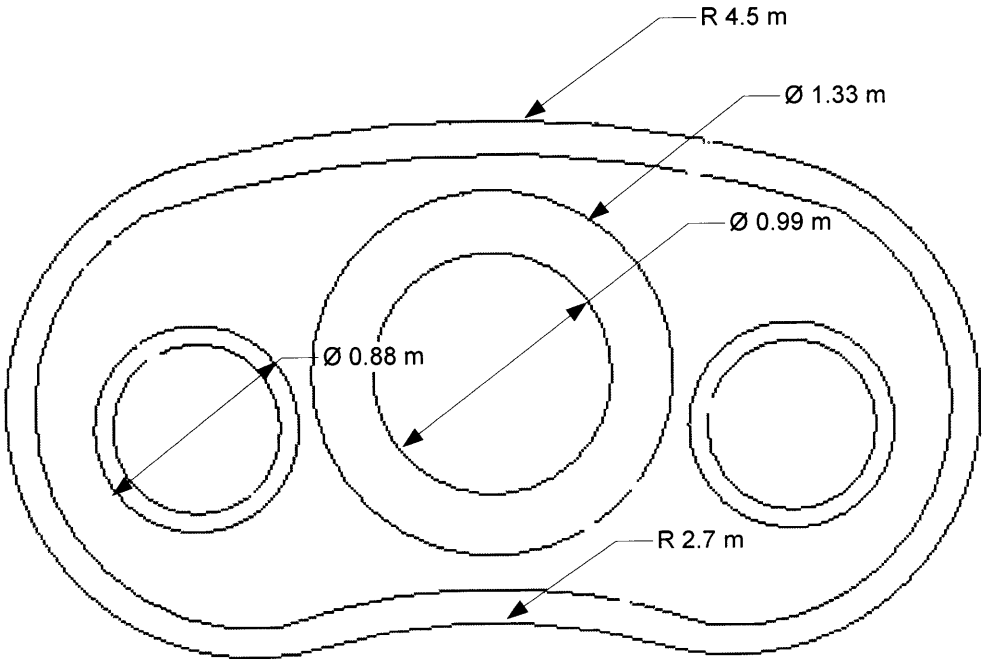

Figure 3-5. Kidney-shaped heat exchanger – top view

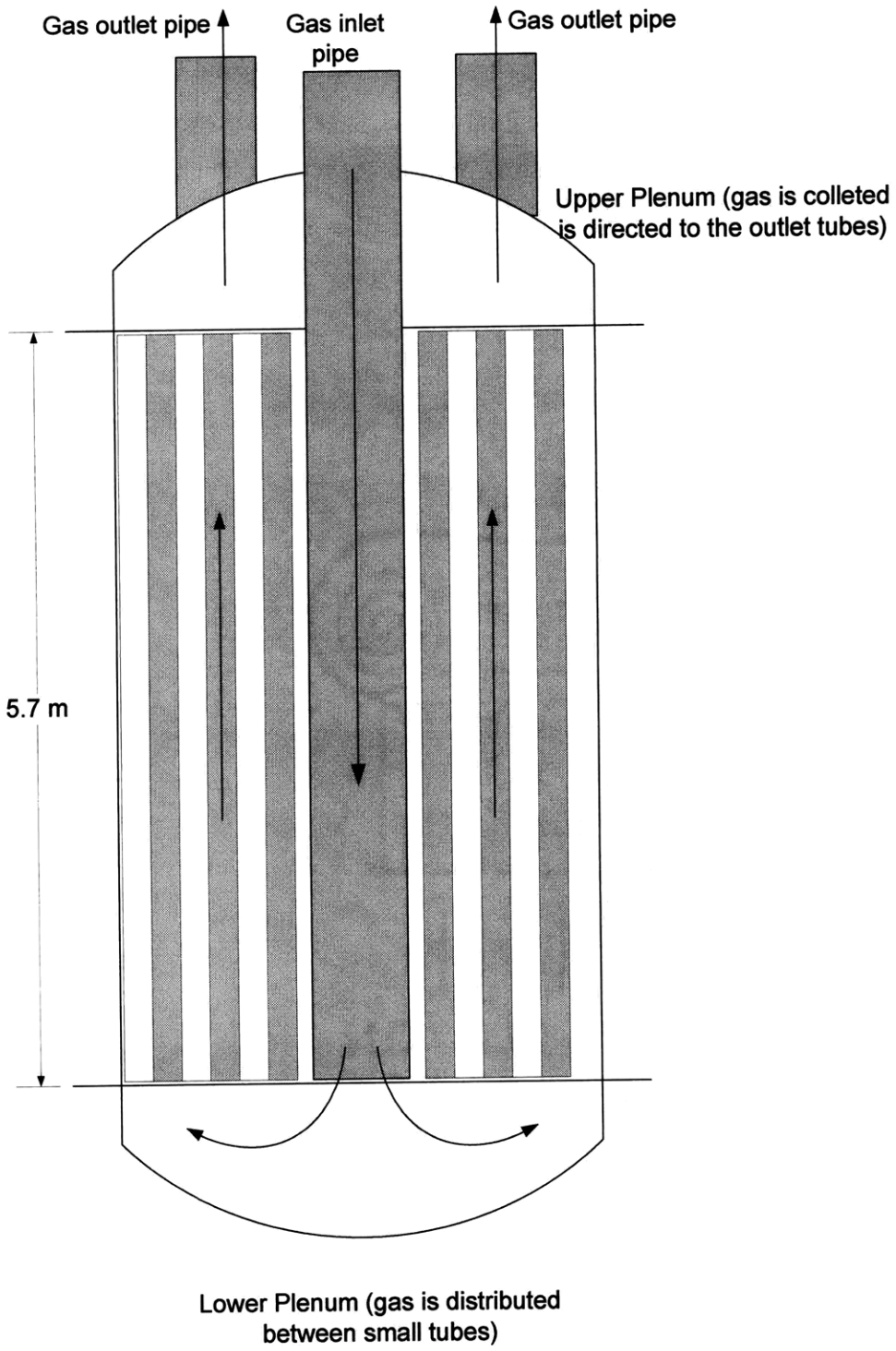

Figure 3-6. Kidney-shaped heat exchanger - vertical cross section

FCR reactor intermediate heat exchanger design is constrained by the size as well as performance and efficiency related to IHX lead inlet and outlet temperatures and CO_2 pressure drop. The radial dimensions are limited by the core and vessel size while its height is dictated by the vessel height. Azimuthal dimensions are influenced by the need for pump and other equipment space. The above challenges and space constraints within the reactor vessel motivated the exploration of the enhancement of heat transfer capabilities to reduce IHX dimensions. Heat transfer augmentation was considered for the CO_2 side because it exhibited a heat transfer coefficient 3-5 times lower than that of the lead side. One of the possible methods to increase heat transfer coefficient is through tube roughening on the inside tube surface. Repeated helical ribs were introduced on the inner tube side, which increase the CO_2 heat transfer through disturbance of the surface sublayer. [Ravigururajan, 1999] The applicable correlations for predicting friction factor and Nusselt number developed by Bergles and Ravigururajan [Bergles and Ravigururajan, 1996] were selected for the heat exchanger design due to their generality and relevance to a wide range of applicable conditions. Such tube augmentation allowed an increase of heat transfer coefficient on the CO_2 side by 20% and reduction of tube length by over 1 m.

The following requirements and assumptions were followed in the design:

Requirements:

- Pressure drop on CO_2 side is around 500 kPa (does not exceed 700kPa)
- Pitch is large enough to allow sufficiently low pressure drop on the lead side so that free level separation is not excessive

Assumptions:

- Steady state operation
- Homogeneous material
- No contact resistance between the fin and tube (extruded fins)
- Constant heat transfer coefficient of the fin to the gas flow over the entire surface of the tube

The design approach and correlations comparison for enhanced heat transfer through internally ribbed tubes are described in Appendix A. Augmented tubes allow for more compact heat exchanger without significant increase in the pressure drop. Comparison of enhanced and smooth tube heat exchanger performance is presented in Table 3-2. Reduction in tube length causes a decrease in pressure drop in both fluids which can be seen for the lead case, but the presence of ribs on the CO_2 side offsets that effect. Main characteristics of the final heat exchanger design are summarized in Table 3-3.

Table 3-2. Smooth vs. enhanced tube heat exchanger performance for the same power output.

	Smooth	Enhanced
Tube length (m)	6.76	5.64
S-CO_2 pressure drop (kPa)	216	226
Lead pressure drop (kPa)	379	323
Total heat transfer coefficient (W/m^2K)	3290	3950
Lead heat transfer coefficient (W/m^2K)	22500	22500
S-CO_2 heat transfer coefficient (W/m^2K)	5000	6812

Table 3-3. Main heat exchanger parameters.

INPUT	
Core power (MW_{th})	2400
Lead mass flow rate (kg/s)	173600
S-CO_2 mass flow rate (kg/s)	12757
Number of heat exchangers	4
Target power transmitted in the IHX (per IHX) (MW_{th})	600
Lead inlet temperature (°C)	573.3
Lead outlet temperature (°C)	477.0
S-CO_2 inlet temperature (°C)	396.5
S-CO_2 target outlet temperature (°C)	549.3
S-CO_2 pressure (MPa)	19.7
IHX GEOMETRY	
Lattice	Triangular
Number of tubes (per IHX)	19173
Outer tube diameter (mm)	14
Tube wall thickness (mm)	2.22*
Pitch to diameter ratio	1.23

Inner IHX radius (r_i)[1] (m)	2.687
Outer IHX radius (r_o) (m)	4.496
TUBE GEOMETRY	
Rib height (mm)	0.35
Number of starters	5
Helix angle (°)	27
OUTPUT	
Calculated power (MW_{th})	598.7
Logarithmic temperature difference (°C)	46.7
S-CO_2 pressure drop (kPa)	226
Lead pressure drop (kPa)	323
S-CO_2 velocity (m/s)	16.8
Lead velocity (m/s)	2.17
Tube length (m)	5.7
Total heat transfer coefficient (W/m^2K)	3950
Lead heat transfer coefficient (W/m^2K)	22500
S-CO_2 heat transfer coefficient (W/m^2K)	6812

* Tube wall thickness includes 0.5 mm of additional thickness for corrosion allowance.

[1] Radius here refers to the heat exchanger tube lattice radius.

3.4. Reactor Vessel and Plant Layout

The large pool type vessel, selected for the analysis, has two main advantages over the conventional LWR design: elimination of primary loops results in more compact and simpler plant, and maintenance of large inventory of lead coolant in the vessel allows for considerable heat storage capacity during transient response. However, the main challenge of this design is that the Intermediate Heat Exchangers (IHXs) must fit inside the constrained space of the vessel between the core shroud and the vessel liner. The IHXs have to transfer the large thermal power of the 2400 MWth core to the supercritical CO_2 (S-CO_2) power conversion system while minimizing the temperature difference between the core outlet temperature and CO_2 working fluid to maximize plant efficiency. Because of a large difference in heat transfer coefficients between lead and S-CO_2, heat transfer enhancement on the gas side was implemented.

Table **3-4** provides the summary of main parameters and results of the analysis which are described in the following sections.

Vessel and plant design are such that either CR=1 or CR=0 cores can be accommodated without any changes except for plugging penetrations in the vessel head that are not used after transition from the CR=0 to the CR=1 core. With the current heat exchanger design, four intermediate heat exchangers and four pumps can be placed in the reactor vessel. Four pumps are preferable because they are of smaller size and provide a better match to the SCO_2 power conversion system (PCS) units, since if one PCS fails, operation of three PCSs with three coolant pumps at reduced power is possible. Overall, it is possible to fit 4 IHXs, each supplying one 600MWth SCO_2 power conversion system within the vessel of 10.2 m outer diameter.

Figure 3-7 illustrates the top view of vessel layout with four IHX and pumps.
Figure 3-8 shows the schematic of the vessel with the dual-free-level design. Because supercritical CO_2 is at the high pressure of 20MPa, while the lead coolant is at atmospheric pressure, the design of the vessel and flow paths needs to assure that ingress of CO_2 into the core is prevented in case of IHX tube rupture. This is accomplished through a dual-free-level vessel design first proposed by Russian scientists for the BREST reactor [Adamov et al., 1994] and adopted later by the MIT/INL team for a lead-cooled actinide burner of lower power rating.

The upper core barrel contains many large holes that direct the coolant into portions of the annulus between the core barrel and the reactor vessel liner. The upper plenum, defined as the region above the first level of holes in the core barrel, below the upper head, and inside the vessel liner, contains the free level of the hot pool. An inert cover gas fills the space between the hot free level and the upper head. The lead-alloy coolant flows downward through portions of the annulus between the core barrel and reactor vessel liner where four counter-flow heat exchangers are located. The lead-alloy flows down on the shell side of the heat exchangers. After exiting the bottom of the heat exchangers, the coolant flows down through a downcomer region until reaching holes in the reactor vessel liner located near the elevation of the seal plate. These holes direct the coolant into the annular gap between the liner and the reactor vessel, which is called the vessel riser. The coolant flows upward through the riser until reaching holes located in

Table 3-4. Summary of Main Parameters of the Lead-Cooled Reactor

Core thermal power (MWth)			2400
Core electric power (MWe)			~1000
Reactor vessel geometry	Guard vessel	Outer diameter (m)	10.2
		Inner diameter (m)	10.0
		Wall thickness (m)	0.10
	Reactor vessel	Outer diameter (m)	9.94
		Inner diameter (m)	9.84
		Wall thickness (m)	0.05
	Liner	Liner-to-vessel gap (m)	0.19
		Wall thickness (m)	0.01
Fuel geometry	Fuel assembly	Assembly pitch (m)	2.175E-01
		Assembly can thickness (m)	3.940E-03
		Inter assembly gap (hot) (m)	2.229E-03
		Total number of fuel assemblies	349
		Number of FA with CRDs (CR=1)	96
		Number of FA with CRDs (CR=0)	349
		Number of fuel pins (per assembly with control rods)	416
		Number of fuel pins (per assembly without control rods)	441
		Number of CRDs (per assembly)	25
	Fuel pin	Pin outer diameter (m)	7.520E-03
		Cladding thickness (m)	6.300E-04
		Gap thickness (m)	4.200E-04
		Fuel outer diameter (m)	5.420E-03
		Fuel heated length (m)	1.3
		Fuel pin pitch (m)	9.776E-03
		Pitch-to-diameter ratio	1.3
		Plenum height (m) top/bottom	1.3/1.3
		Cladding material	T-91 (9Cr-1Mo-V-Nb)
		Gap bond	Lead
Fuel type	CR=0	Zone 1 (U/TRU/Zr), (wt. %)	0.00/34.00/66.00[1]
		Zone 2 (U/TRU/Zr), (wt. %)	Once burnt (middle zone)
		Zone 3 (U/TRU/Zr), (wt. %)	Twice burnt (inner zone)
	CR=1	Zone 1 (U/TRU/Zr), (wt. %)	75.00/15.00/10.00
		Zone 2 (U/TRU/Zr), (wt. %)	70.83/14.17/15.00
		Zone 3 (U/TRU/Zr), (wt. %)	67.50/13.50/19.00
Intermediate Heat exchanger	Type		Tube-and-shell
	Material		T-91 (9Cr-1Mo-V-Nb)
	Geometry	Number of heat exchangers	4
		Number of tubes (per IHX)	19173
		Outer tube diameter (m)	14.0E-03
		Tube wall thickness (m)	2.22E-03
		Tube pitch to diameter ratio	1.23
		Tube length (m)	5.70
	CO_2 side rib geometry	Rib height (m)	3.50E-04
		Number of starters	5
		Helix angle (degrees)	27

[1] The CR=0 core was designed as a 3-batch core with TRU-Zr fuel to accommodate the large reactivity swing. Zone 1 is the outer core zone, and numbers correspond to initial (fresh) fuel composition.

the upper liner, which directs the fluid into annular regions containing four primary coolant pumps. The coolant flows down through these annular regions, which are referred to as the pump downcomer, until flowing through the coolant pumps into the lower plenum. The upper portions of the vessel riser and the pump downcomer regions are connected to the cover gas in the upper plenum. These connections result in the formation of free levels of relatively cold fluid in the riser and pump downcomer. The levels of these cold pools are considerably lower than the level in the hot pool because of the pressure loss across the heat exchangers. This circulation scheme prevents dragging a significant amount of gas into the core in case of a heat-exchanger-tube-rupture event, which could otherwise cause undesirable reactivity perturbations.

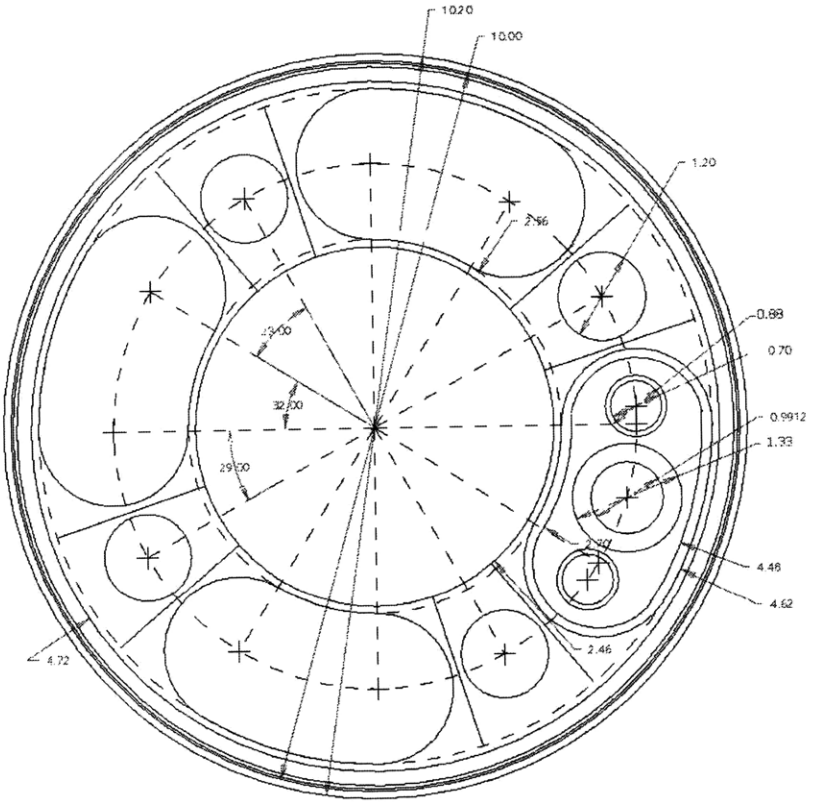

Figure 3-7. Vessel layout with IHXs and pumps.

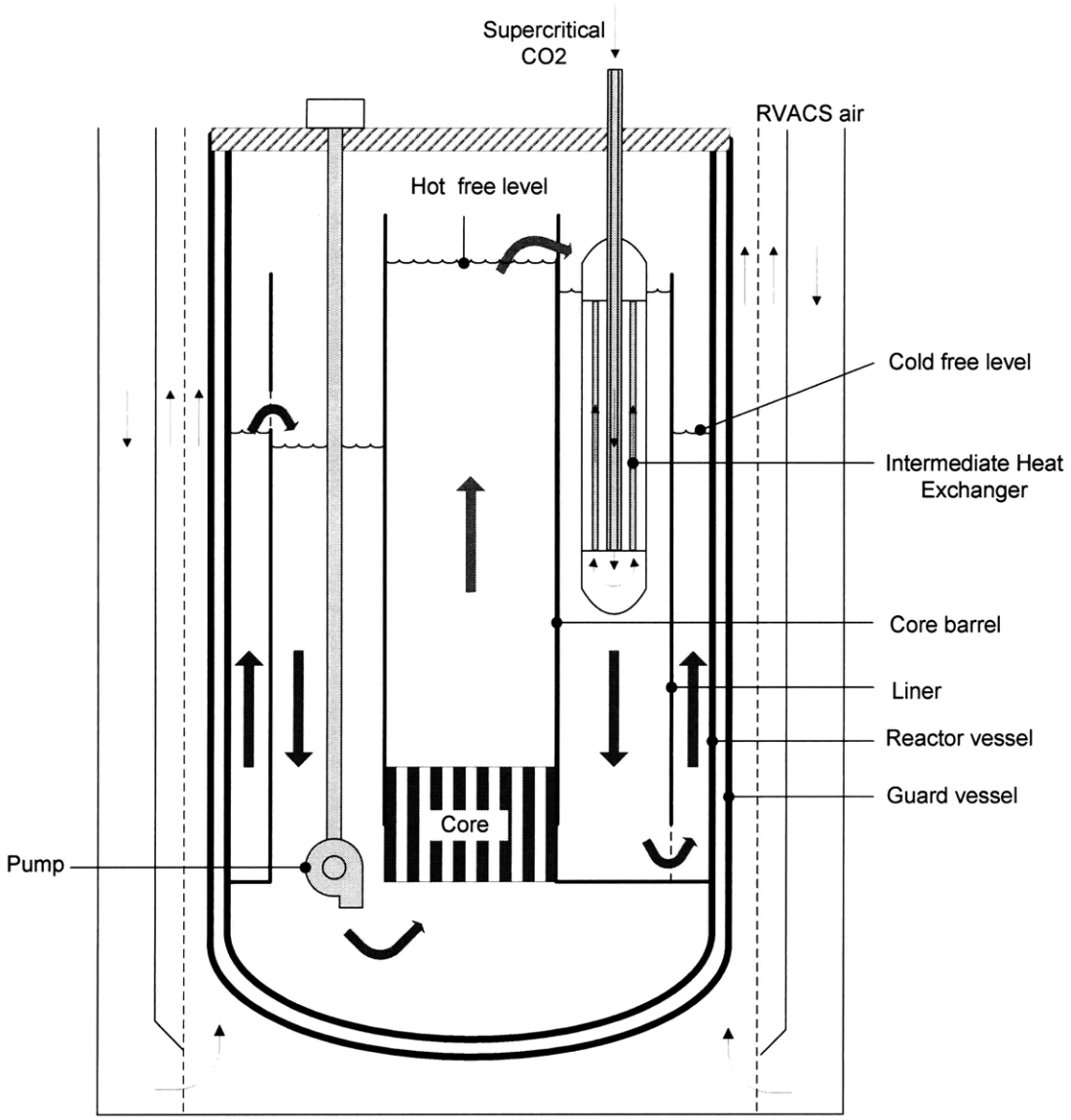

Figure 3-8. Schematic of reactor vessel with dual-free-level.
[adapted from Hejzlar et al., 2004]

The heat is transferred from lead coolant to a supercritical CO_2 through IHXs. S-CO_2 is part of the power conversion system (PCS) and drives turbomachinery and a generator. A four loop design has been adopted where each IHX rated at 600MWt supplies CO_2 to PCS loops generating about 265MWe, thereby providing a reactor electric power rating

of 1060MWe. The advantage of the SCO_2 power cycle is its high efficiency, high power density and simplicity, which is expected to reduce plant overnight cost. The SCO_2 power cycle is optimized for the IHX outlet temperature and IHX pressure losses. The balance of plant for the lead is formed by PCS in the distributed horizontal arrangement, as developed by Gibbs et al. [2006] under direct Generation IV funding via Sandia National Laboratory. This is the third generation of the S-CO_2 PCS developed at MIT [Dostal et al., 2004; Pope et al., 2006], which minimizes pressure losses in piping and maximizes modularity and ease of maintenance. Figure **3-9** shows the layout of one out of four 600MWt power conversion system units. Figure 3-10**Error! Reference source not found.** shows the horizontal arrangement of four 265MWe trains of the SCO_2 PCS connected to the IHXs.

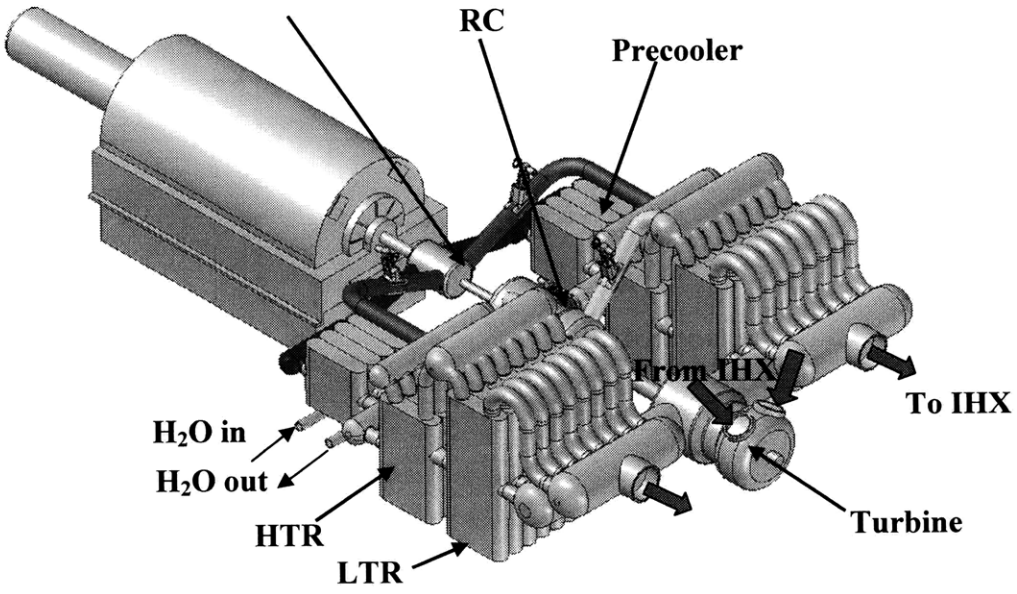

Figure 3-9. Isometric view of 600 MWt PCS layout (from Gibbs et al., 2006)

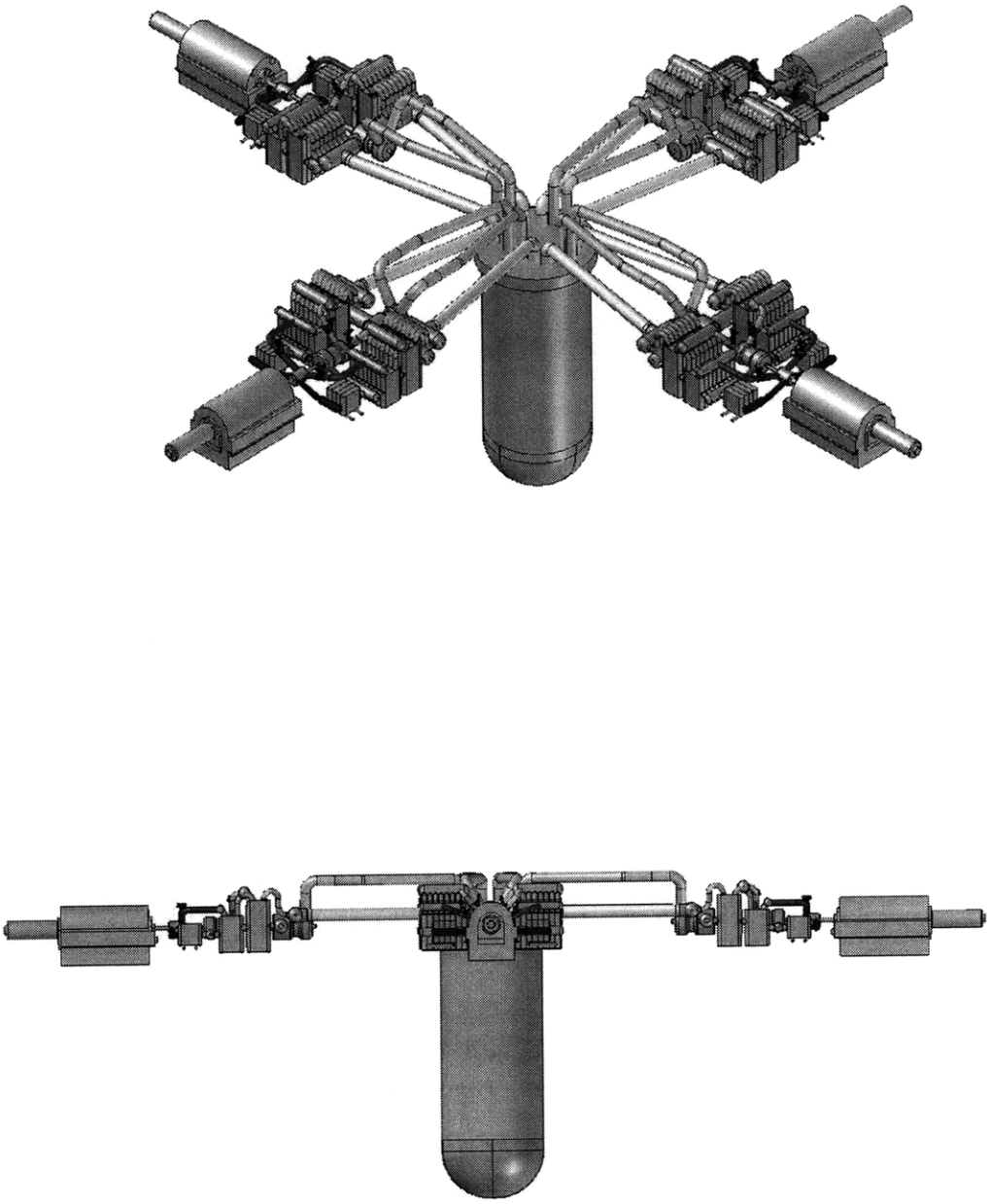

Figure 3-10. Possible arrangement of 600MWt PCS units around reactor vessel. Top = isometric view; bottom = front view (from Todreas et al. [2008])

3.5. References for Chapter 3

Adamov E., Orlov V., Filin A., Tsikunov V., Sila-Novitski A., Smirnov V., and Leonov V., "Conceptual Design of BREST-300 Lead-Cooled Fast Reactor," Proc. Int. Topl. Mtg. Advances in Reactor Safety (ARS'94), Pittsburgh, Pennsylvania, April 17–21, 1994.

Bergles, A. E., Ravigururajan, T. S., "Development and Verification of General Correlations for Pressure Drop and Heat Transfer in Single-Phase Turbulent Flow in Enhanced Tubes," *Experimental Thermal and Fluid Science*, 13, pp. 55-70, 1996

"Boiler & Pressure Vessel Code. An International Code. Section III, Division 1, Subsection NH (Class 1 Components in Elevated Temperature Service)" ASME, 2007.

Dostal V., Driscoll M. J. and Hejzlar P., "A Supercritical Carbon Dioxide Cycle for Next Generation Nuclear Reactors", MIT-ANP-TR-100, March 2004.

Gibbs J.P., Hejzlar P.. and Driscoll M.J., "Applicability of Supercritical CO_2 Power Conversion Systems to Gen IV Reactors", MIT-GFR-037, Center of Advanced Nuclear Energy Systems, September, 2006.

Hejzlar P., Davis C.B., "Performance of the Lead-Alloy-Cooled Reactor Concept Balanced for Actinide Burning and Electricity Production," *Nuclear Technology*, 147, 3, pp. 344-367, 2004.

Pope M.A., Hejzlar P., and Driscoll M.J.,"Thermal Hydraulics of a 2400 MW_{th} Supercritical CO_2-Direct Cycle GFR", MIT-ANP-TR-107, Center for Advanced Nuclear Energy Systems, Massachusetts Institute of Technology, 2006.

Ravigururajan, T. S., "A Comparative Study of Thermal Design Correlations for Turbulent Flow in Helical-Enhanced Tubes," *Heat Transfer Engineering*, 20, pp. 54-70, 1999

Todreas N.E., Hejzlar P., Shwageraus E., Petroski R., Nikiforova A., Whitman J., and Fong, C.J., "Flexible Conversion Ratio Fast Reactor Systems Evaluations", Final report, Center for Advanced Nuclear Energy Systems, MIT, MIT-NFC-PR-101, August 2008.

4. STEADY STATE ANALYSIS

4.1.Subchannel Analysis

Subchannel analysis of the core was conducted to determine the preliminary temperature and velocity distribution, and pressure drop across the core. The objective of the present subchannel analysis was twofold: to determine whether the core design constraints are satisfied and to maximize the margin to temperature and velocity limits through orificing. The in-house subchannel code SUBCHAN written by P. Hejzlar [Todreas et al, 2008] was used to calculate reactor operating parameters. The impact of three-zone core orificing on core outlet temperature distribution was also investigated. The analysis was completed using the power peaking maps from reactor physics analysis. The results of the subchannel analysis were further used as an input for RELAP5-3D/ATHENA.

4.1.1. Unity Conversion Ratio Core

The fuel assembly of the unity conversion ratio core consists of 441 fuel pins or 416 fuel pins and 25 control rods per assembly (96 assemblies in the core have control rods). In the current investigation, three types of channels are considered: fuel channel ("hot") with further division into inner, corner and edge subchannels, control rod channel ("cold"), and inter-assembly channel ("cold"). Gamma heating is assumed for both types of cold channels (5% of the average pin heat flux). The schematic of the assembly layout and different channel classification is depicted in Figure 4-1.

Reactor physics analysis determined the core power map and intra-assembly pin peaking. The power maps corresponding to each core are shown in Chapter 3. In the thermal hydraulic model, each channel represented either one assembly or several assemblies depending on peaking factor. This involved collapse of 349 assemblies into 41 groups, which were modeled in the SUBCHAN code. Each group represents assemblies with unique peaking factor. The core temperature map was plotted. Such an approach allows

applying the orificing coefficients to every individual assembly rather than using core-average values. Three-zone orificing used in this analysis was manipulated until the desired core temperature distribution was obtained. In this analysis, a fixed orificing configuration was applied.

Benefits of the aforementioned three-zone orificing technique were explored by considering every assembly individually. First, non-orificed core cladding and outlet temperature distributions were analyzed. Figure 4-2 depicts the core peak cladding and outlet temperature maps of $1/8^{th}$ of the core without any orificing applied. The peak cladding temperatures range from 556.5°C to 622.6°C. The outlet temperatures range from 594.6°C to 541.2°C. Based on the core outlet temperature distribution, hotter assemblies were left non-orificed, while two-zone orificing was applied to the rest of the assemblies. Generally, orificing is used to maximize core average outlet temperature within the peak cladding temperature constraint. However, the steady state value of the peak cladding temperature is already below the limit, and the coolant outlet temperature is set by the secondary side. The approach to maximize the margin to clad temperature limit was chosen because of the relatively low transient peak cladding temperature limit of 725°C.

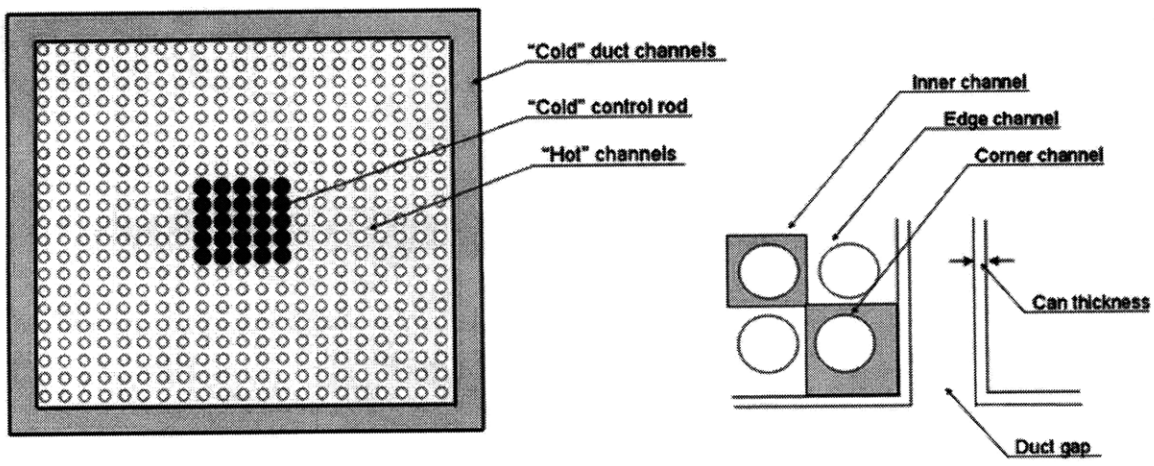

Figure 4-1. Fuel assembly layout and channel classification.

Three-zone orificing was found to be sufficient to significantly flatten the peak cladding and outlet coolant temperature distribution. The highest assembly peak cladding temperature was reduced from 622.6°C to 609.9°C. The highest assembly outlet temperature was reduced from 594.6°C to 581.8°C. The peak cladding (top) and outlet (bottom) temperature maps of the orificed core are given in Figure 4-3. Table 4-1 summarizes peak velocity and assembly-average peak cladding temperature before and after orificing. A considerable margin exists between the cladding temperature limit of 625°C (soft limit) and the calculated value of the orificed core. The maximum velocity in the core is in the hottest assembly. Core orificing resulted in increased velocity through the channels with lesser flow resistance.

Table 4-1. Summary of peak assembly-average temperatures and velocity before and after orificing.

	Unorificed core	Orificed core
Orificing coefficients (zone1/zone2/zone3)	N/A	0.4/4.96/13.24
Peak cladding temperature (°C)	622.6	609.9
Velocity (m/s)	2.05	2.30

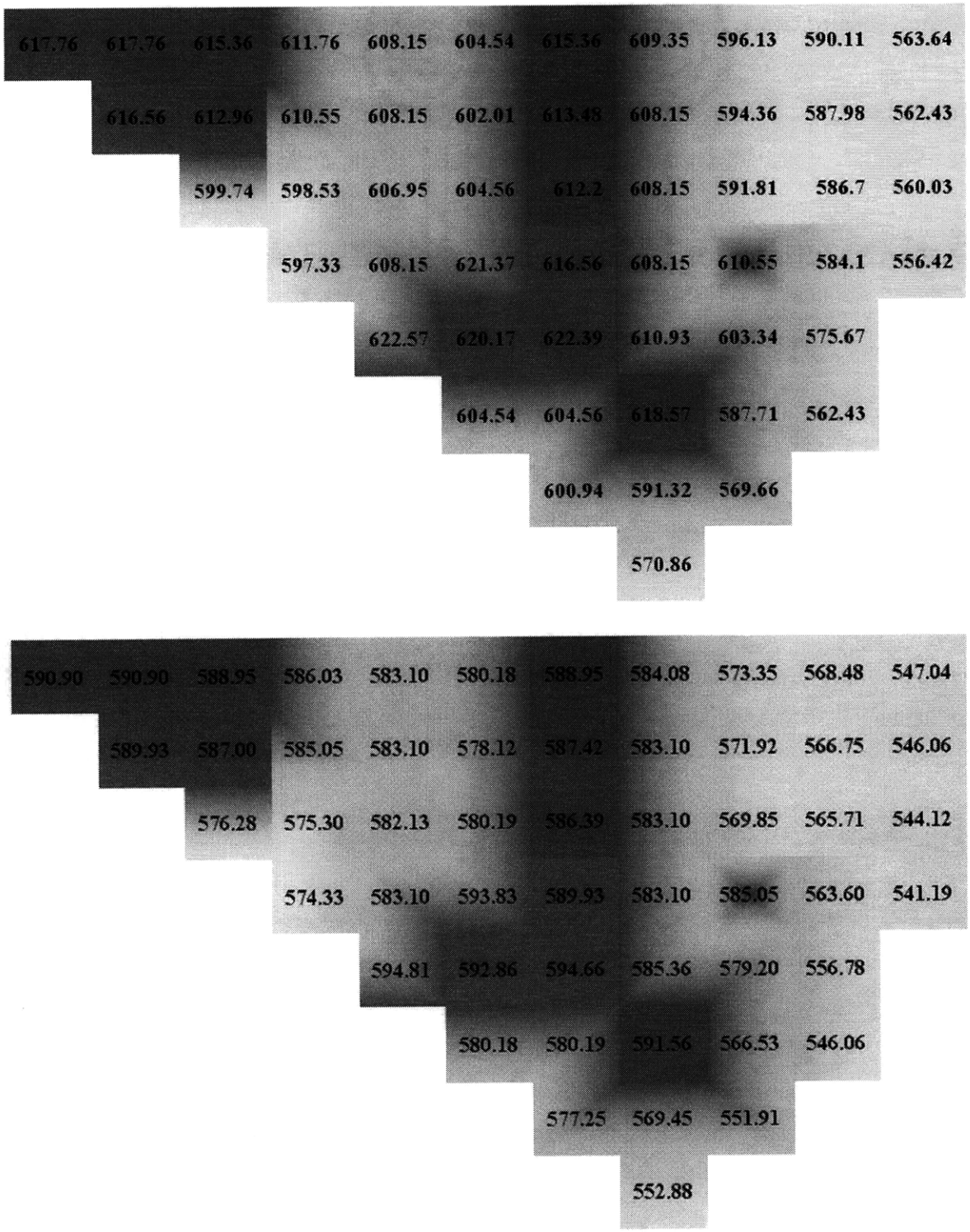

Figure 4-2. Assembly-average peak cladding (top) temperature (°C) and outlet (bottom) temperature map for unorificed core.

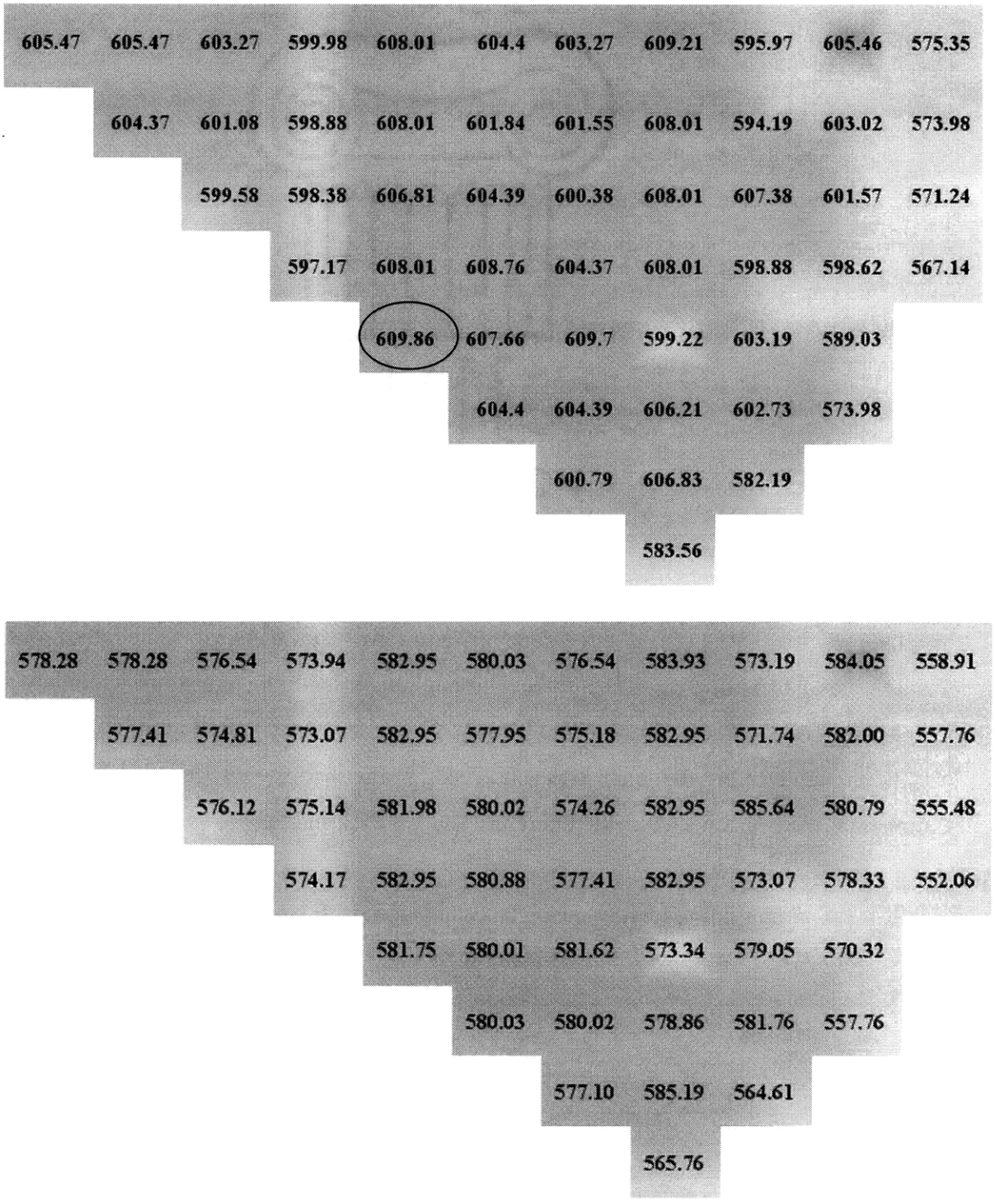

Figure 4-3. Assembly-average peak cladding (top) and outlet (bottom) temperature (°C) map for orificed core.

4.1.2. Zero Conversion Ratio Core

The methodology for zero conversion ratio core thermal hydraulic steady state parameter calculation is the same as for the unity conversion ratio core. In contrast to the CR=1 core, higher radial power peaking is associated with the CR=0 core. The maximum radial power peaking for the zero conversion ratio core occurs at the beginning of fuel cycle according to the reactor physics analysis. [Todreas et al., 2008] Thus, the BOC peaking factors were used for the thermal hydraulic analysis of the core. Similarly to unity core, the CR=0 core consists of 349 fuel assemblies. However, every assembly contains control rods, and therefore the effect of "cold" channels is greater for the CR=0 core. The peak cladding temperature and maximum velocity constraints are the same as for the unity conversion ratio core. To assure the same performance of heat exchangers for both CR=1 and CR=0 cores, the inlet and outlet core average temperatures are kept constant for both cores.

Similarly to the CR=1 case, three-zone orificing was sufficient to flatten the core temperature distribution significantly. The highest assembly-average peak cladding temperature was reduced from 645.4°C to 617.4°C as shown on Figure 4-4. The maximum velocity in the core was observed at the hottest assembly. Table 4-2 summarizes the peak subchannel temperature and velocity and the margin to the limit.

Table 4-2. Summary of assembly-average peak cladding temperature and velocity before and after orificing.

	Unorificed core	Orificed core
Orificing coefficients (zone1/zone2/zone3)	N/A	0.4/8.19/29.68
Cladding temperature (°C)	645.4	617.4
Velocity (m/s)	2.09	2.64

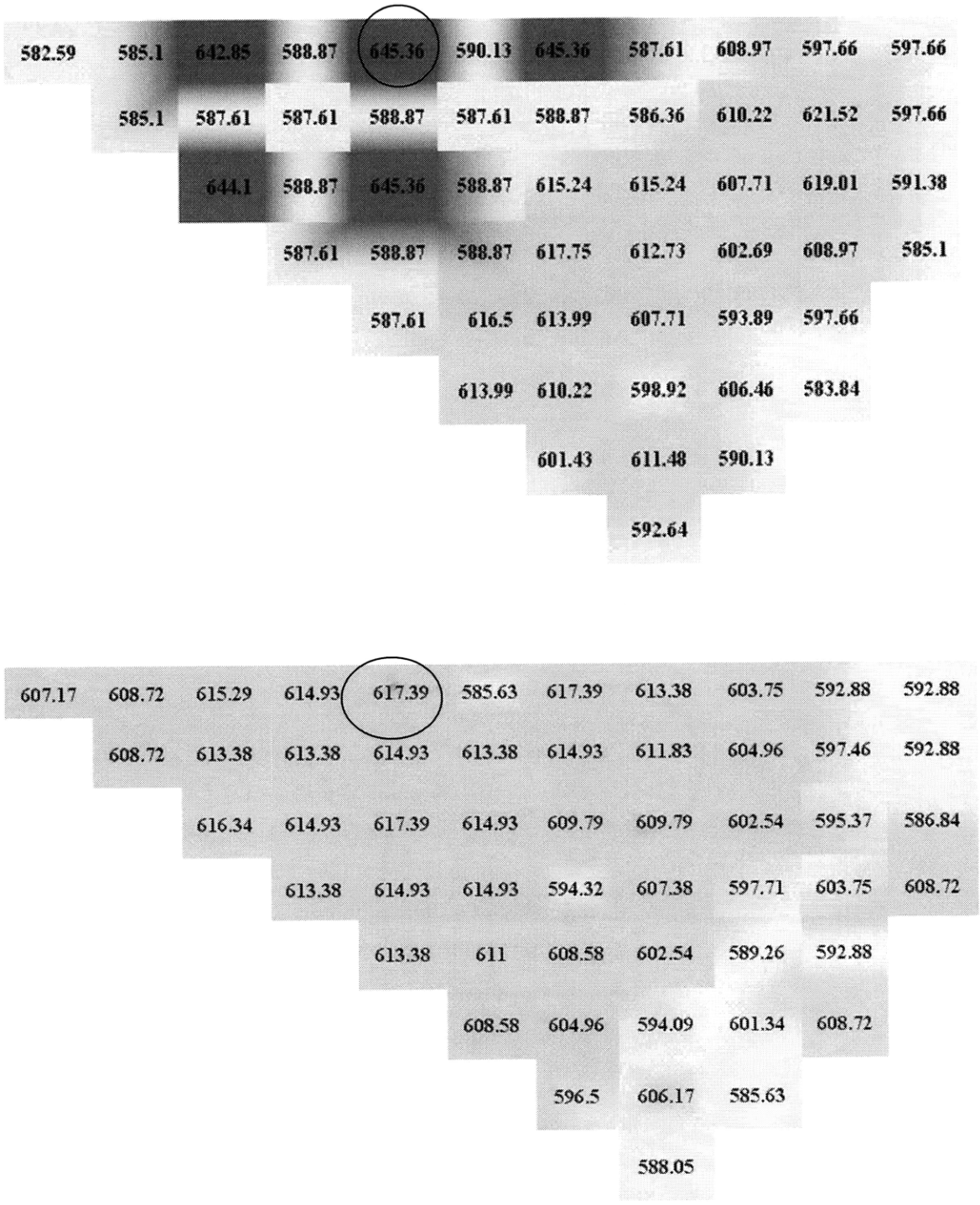

Figure 4-4. Assembly-average peak cladding temperature (°C) map for unorificed core (top) and for orificed core (bottom).

4.2. RELAP5-3/ATHENA Results for Full Power Operation

Figure 4-5 and Figure 4-6 compare hot subchannel cladding temperature as evaluated using SUBCHAN and RELAP5-3D for CR=1 and CR=0 cores, respectively. Both calculations are in good agreement. Minor discrepancies are due to numerical and calculational uncertainties. Another source of difference comes from the fact that RELAP5-3D [RELAP5-3D, 2005] uses lead-bismuth alloy as a coolant while pure lead was used for SUBCHAN calculations. Maximum peak guard vessel temperature during steady state full power operation is the same for both reactors. The maximum peak membrane temperature is 428°C which below the steady state limit of 430°C.

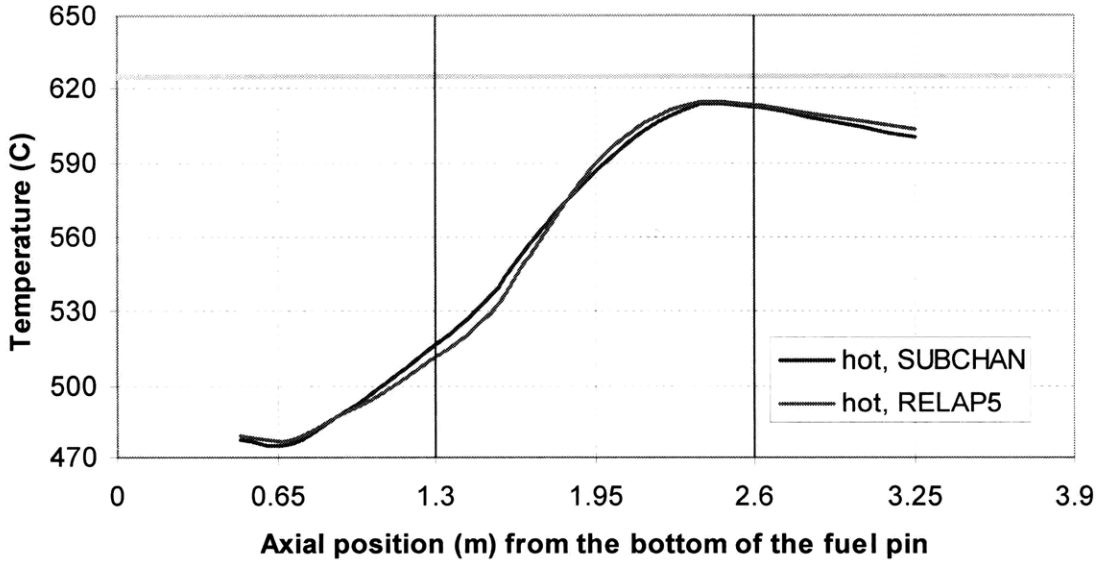

Figure 4-5. Comparison of hot subchannel temperature (in °C) produced by SUBCHAN and RELAP5-3D for CR=1 core

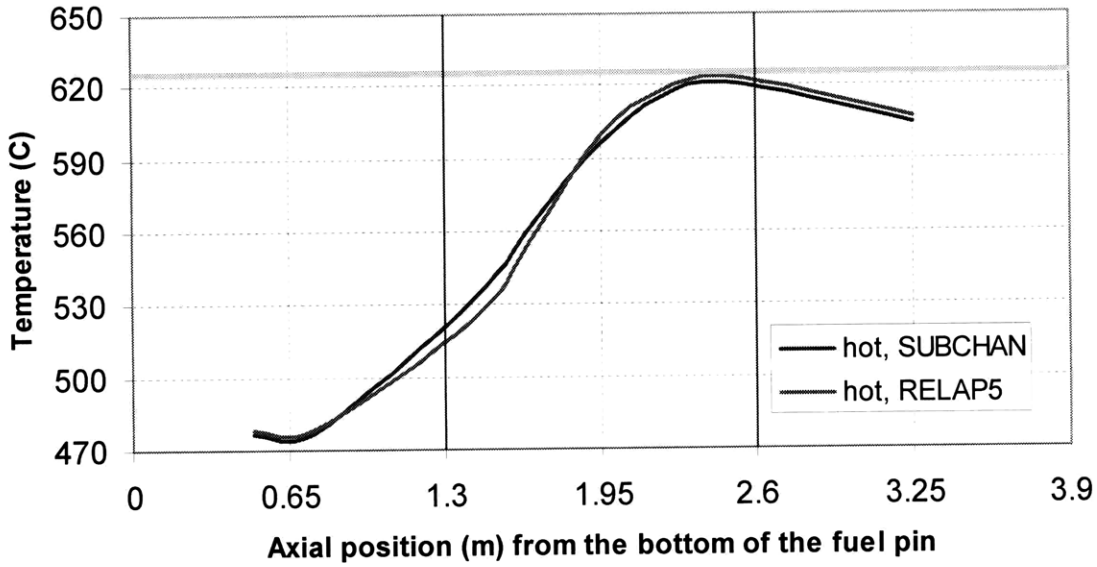

Figure 4-6. Comparison of hot subchannel temperature (in °C) produced by SUBCHAN and RELAP5-3D for CR=0 core

Figure 4-7 shows temperature evolution as air goes through RVACS. When air proceeds through the downcomer, minor temperature rise due to heat conduction through the collector is observed. The area enclosed between red lines corresponds to the part of the vessel in contact with lead coolant. The most rapid air temperature increase happens in this area. The last part of the graph is the part of the vessel in contact with cover gas. Heat transfer in this area is also almost negligible.

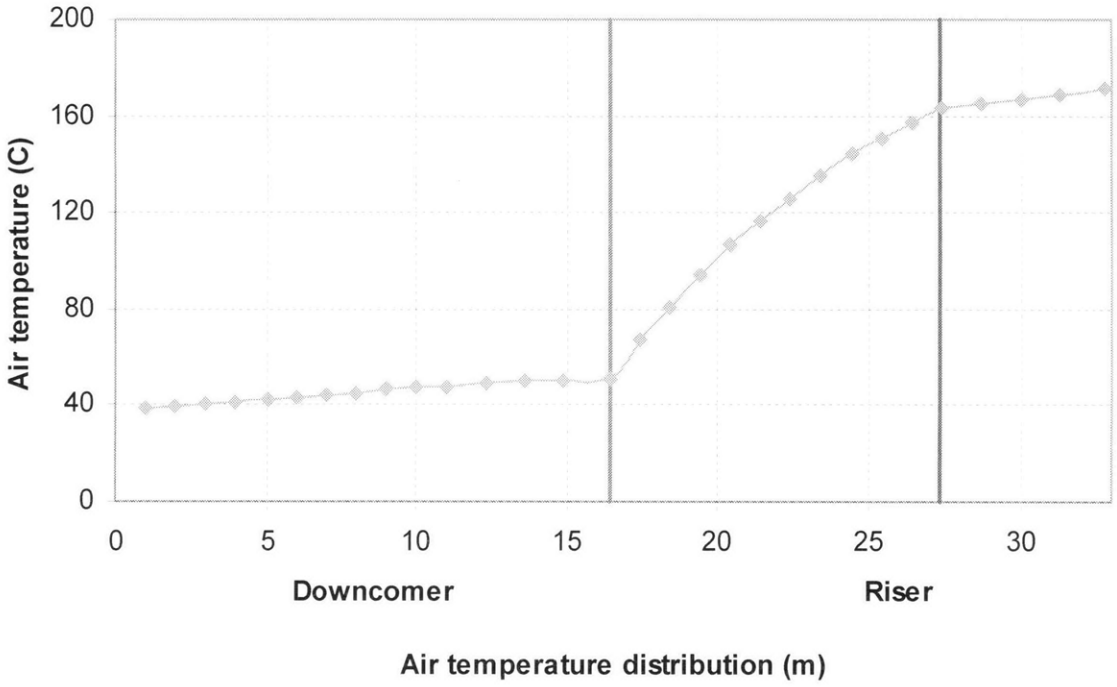

Figure 4-7. RVACS steady state performance

4.3. References for Chapter 4

RELAP5-3D Code Development Team, RELAP5-3D© Code Manual Volume 1: Code Structure, System Models and Solution Methods, INEEL-EXT-98-00834-V1 Revision 2.3, Idaho National Engineering and Environmental Laboratory, 2005.

Todreas N.E., Hejzlar P., Shwageraus E., Petroski R., Nikiforova A., Whitman J., and Fong, C.J., "Flexible Conversion Ratio Fast Reactor Systems Evaluations", Final report, Center for Advanced Nuclear Energy Systems, MIT, MIT-NFC-PR-101, August 2008.

5. SYSTEMS FOR DECAY HEAT REMOVAL AND ACCIDENT MANAGEMENT

5.1. Overview of the Systems

This chapter reviews the design and analysis of passive decay heat removal systems. A significant part of the design and analysis of FCR systems was related to the feasibility of removal of decay heat generated during transients. The design was complicated by the various challenges: large power rating, tight vessel geometry, and the goal of reliance on passive systems for decay heat removal during transients. Large power rating results in significant amount of decay heat generated whereas tight vessel geometry limits the options for decay removal concepts. The issue with tight pool-type vessel design ultimately excluded the option of in-vessel heat exchangers such as Direct Reactor Auxiliary Cooling System (DRACS).

Two systems were designed to remove the decay heat from the primary coolant in case of a transient. The Reactor Vessel Auxiliary Cooling System (RVACS) design is based on the design proposed for S-PRISM [Boardman et al., 2000]. The RVACS design in this thesis includes various enhancements to increase the heat removal rate. However, after the transient analysis of the reactor under station blackout accident conditions was performed, it was determined that even though the reactor can be shutdown without scram, the Reactor Vessel Auxiliary System (RVACS) was not sufficient to remove the decay heat generated after reactor shutdown. Therefore, due to large amount of decay heat generated, the Passive Safety Auxiliary Cooling System (PSACS) was designed to supplement the RVACS heat removal during the earlier stages of the accident sequence.

5.2. Enhanced Reactor Vessel Auxiliary Cooling System

The design of RVACS is based on the 1000 MWth S-PRISM design. Because of higher power rating of the FCR reactor, several modifications and enhancements were adopted

in order to increase the heat transfer rate from the reactor vessel into the air. The schematic of enhanced RVACS air flow path is shown on Figure 5-1. RVACS enhancements include a liquid metal bond in the gap between the reactor vessel and guard vessel and a number of enhancements in the guard-vessel-to-air heat transfer path. The former consist of dimples on the guard vessel wall and a perforated plate in the air riser gap. Addition of dimples to the exterior of the guard vessel significantly increases heat transfer enhancement without significant increase in pressure drop. The heat transfer enhancement is possible because of the combination of increased surface area and boundary layer separation. Because of limited information available, more research on dimple performance applied to large systems such as FCR is necessary [Todreas et al., 2008]. The perforated plate is modeled as an additional heat structure in the air riser. The holes on the plate occupy 40% of the surface area. The main reason for the holes is to provide the ability of the guard vessel to radiate not only to the plate, but also to the collector. The heat removal rate is also directly proportional to the diameter of the vessel. However, the vessel size is constrained by the manufacturing and transportability limitations. The heat removal rate also increases as the primary coolant temperature rises during the transients.

RVACS was further modeled in RELAP5/ATHENA. The unprotected station blackout accident simulation revealed that an enhanced RVACS with dimples alone would not be sufficient to remove the required decay heat. Moreover, the decay heat rate calculated for the transuranic cores is appreciably higher than the decay power curve used for preliminary scoping studies of RVACS performance, making it even more difficult for RVACS with dimpled surface and perforated plate to assure adequate performance. Therefore, it was decided to no longer pursue a reduction of heat transfer uncertainties from dimpled surfaces, in favor of researching additional DHR options, which would aid RVACS. These options are described in the next section.

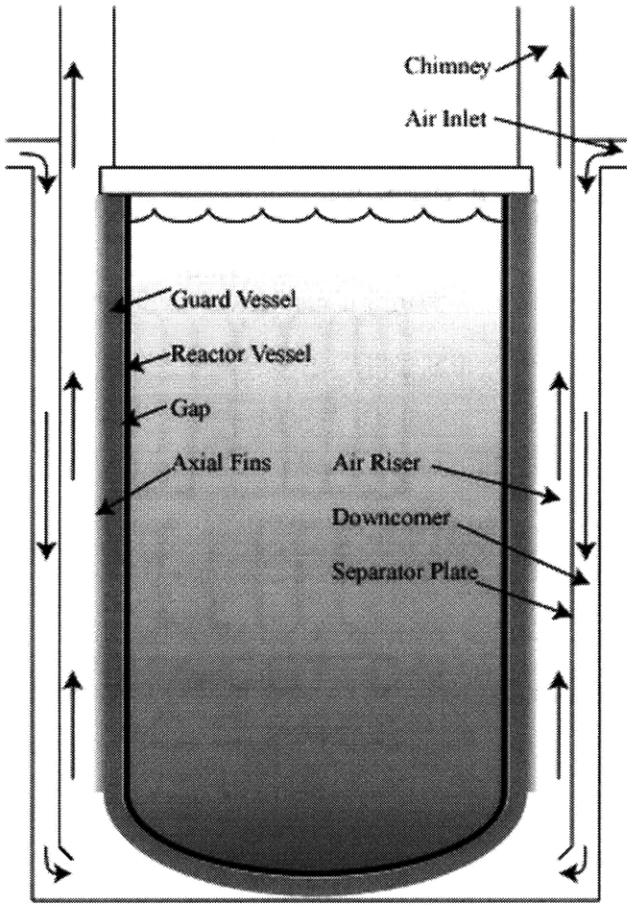

Figure 5-1. Side view of RVACS system, showing air-side flow path
[Todreas et al., 2008]

5.3. Passive Safety Auxiliary Cooling System

Passive DHR auxiliary systems that were considered and evaluated include:

- A Direct Reactor Auxiliary Cooling System (DRACS) consisting of the In-Vessel Heat Exchanger connected by lead-bismuth eutectic loop to the air cooled Passive Auxiliary Heat Exchanger (PAHX) located in the chimney of RVACS riser

- A Passive Secondary Auxiliary Cooling System (PSACS), which removes decay heat via the IHX and standby loop filled with secondary SCO_2 that transports heat by natural circulation from the IHX to (1) CO_2/air (PSACS-Air) or (2) CO_2/water heat exchangers (PSACS-Water).

The DRACS system uses a Lead-Bismuth Eutectic cooling loop to remove decay heat from the reactor vessel. The loop consists of two heat exchangers. The In-Vessel Heat eXchanger, or IVHX, is located within the reactor vessel. Because of the issue with tight in-vessel geometry and an additional loop of lead-coolant which must be preheated in order to circulate constantly, the option of a DRACS was discarded from the analysis. The other two PSACS options are simpler in design. Rather than use a separate fluid and IVHX for the decay heat removal, both PSACS options use the PCS working fluid along with the IHXs to remove decay heat. Since both the PSACS air and water designs were deemed to have merit, a formal decision-making process developed at MIT was utilized to select the most favorable design option. The Analytic Deliberative Process (ADP) [Apostolakis et al, 2007] was used to assess the two design options against a variety of performance measures such as economics, reliability, and thermal hydraulic performance. Based on insights from the ADP, the PSACS-Water option was selected as the final design option, and RELAP5 simulations were used to test and optimize the design.

The final PSACS design consists of four independent, 50% capacity, safety-grade cooling loops. Each loop is composed of an inlet connection from the IHX outlet leg (inlet to turbine), a passive auxiliary heat exchanger (PAHX) submerged in a water storage tank, and a return line to the IHX. A schematic is shown on Figure 5-2. The PSACS is isolated under normal operating conditions. During an SBO event, the main turbine will be tripped and isolated and the PSACS isolation valves will open, allowing CO_2 natural circulation flow into the Passive Auxiliary Heat Exchanger (PAHX). This can be accomplished with a high degree of reliability and without operator action by using a series configuration of fail-closed and parallel configuration of fail-open valves common in industry today. Upon loss of normal power, the turbine isolation and PSACS valves will swap positions thereby placing the PSACS in service. S-CO_2 flow will leave the

IHX and flow into tubes passing through the PAHX, which is located higher than the IHXs. The PAHX is a vertically oriented bank of tubes submerged in an in-containment water storage tank. The S-CO_2 will flow through parallel banks of tubes and transfer heat into the water via convection. No external driving force will be required as the PAHX will be located at a suitable elevation so as to establish natural circulation via thermal head. The amount of water in the tank is established to provide a heat sink sufficient for the period of the transients or until all decay power can be removed solely by the RVACS. The system has been optimized to ensure that flow rates appropriate for worst-case decay heat loads are established and maintained under all credible scenarios.

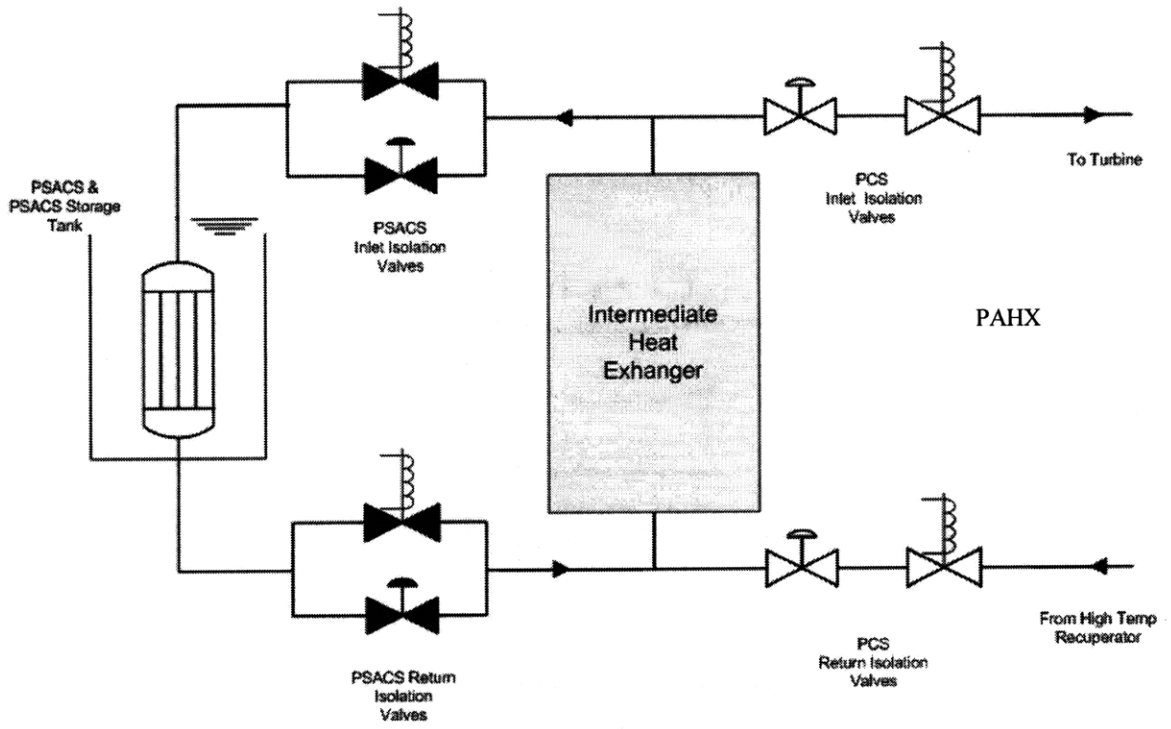

Figure 5-2. Schematic of PSACS-Water system

The PSACS relies on a density differential between its hot and cold legs (i.e. thermal head) and elevation difference (PSACS is located 2.0 meters above the in-vessel IHXs) to provide cooling based on natural circulation. Because no external energy sources (e.g. pumps, blowers) are used, the PSACS is classified as a passive safety system. Unlike the

RVACS, the PSACS must be isolated during normal operation. This prevents boiling of the PSACS Storage Tank water and improves economics by limiting heat loss from the power conversion system (PCS). PSACS main design parameters are summarized in Table 5-1.

The PCS must be isolated during a transient such as an SBO. Failure to isolate a PCS train creates a flow bypass around the corresponding PSACS train. Hot CO_2 exiting the IHX could instead flow through the PCS rather than the PSACS. Furthermore, PCS piping is non-safety related and therefore less robust than the PSACS piping. Without isolation, a rupture or leak in the PCS could depressurize the PSACS thereby challenging its effectiveness.

Table 5-1. Passive Secondary Auxiliary Cooling System Data

Reactor			Lead
Passive Secondary Auxiliary Cooling System	Water Tank	Height (m)	14.0
		Diameter (m)	8.0
	Passive Auxiliary Heat Exchanger (PAHX)	Number of tubes	350
		Tube length (m)	4.0
		Inner diameter – CO_2 side (m)	8.00E-03
		Tube thickness (m)	2.80E-03
		Outer diameter – water side (m)	1.36E-02
		P/D ratio	3

5.4. DHR through the Power Conversion System

The supercritical CO_2 power conversion system offers the unique opportunity to use the decay heat to drive the turbomachinery and to remove the decay heat [Pope et al., 2006]. In this case, the gas is circulated through the turbine which is mounted on the same shaft as compressors. The decay heat is removed from the core through the IHXs and then further rejected through the precoolers. Similarly to the PSACS, the PCS can also serve as a heat sink in case of an accident. However, this would require that the entire PCS to be classified as Safety Related. Within the current regulatory framework, Safety Related components must be seismically qualified to withstand the Safe Shutdown Earthquake, also known as the Design Basis Earthquake 10 (CFR 100, Appendix A (Seismic

Requirements)). In addition, the Quality Assurance rules of 10 CFR 50, Appendix B (Quality Assurance Requirements for Nuclear Power Plants) would have to apply to the whole balance of plant. The reclassification of nearly the entire PCS as Safety Related would lead to a substantial increase in construction, maintenance, and procurement costs. Moreover, it would likely pose operational challenges. Because of the considerable increase in cost associated with upgrading the PCS to the Safety Grade system for decay heat removal, the PSACS was designed as a Safety Related system. However, the PCS can still be used to remove the decay heat in case of an accident provided that the safety-grade PSACS is always available to perform as an ultimate backup. This section describes the approach of decay heat removal using PCS.

When the station blackout accident is initiated, the generators are disconnected from the power grid. However, the turbomachinery does not immediately stop. Moreover, since turbine energy can no longer be transferred into the grid, any additional energy input into the turbine is converted into kinetic energy, driving the shaft and the compressors, which deliver significant CO_2 flow through the IHXs. It is assumed that all four PCS loops are in operation and that some cooling water flow can be maintained through the precoolers either by natural circulation or by pumps in case of loss of primary flow scenario when electricity to precooler pumps is available.

When the generator is disconnected from the grid during the SBO accident, imbalance in angular momentum leads to a rapid increase in shaft speed. To protect against shaft overspeed, the overspeed protection system, described in Section 5.5, is invoked first using turbine bypass valve. After the speed of turbine is reduced to safe values, the turbine bypass valve can be also used using to control turbine speed in such a manner that the turbine provides enough power to drive compressors on the same shaft to provide sufficient flow rate through IHXs to remove decay heat. This can be accomplished using a shaft speed signal controller that acts on the bypass valve. A proportional-integral controller (PI controller) was selected for this purpose. The PI controller uses the error between the actual (measured) shaft speed and the desired speed value to adjust the

bypass valve position. The following algorithm of the PI controller was used in the model:

1. Desired shaft speed value (setpoint) is determined;
2. The actual shaft speed (process variable) is measured;
3. The error between set and actual shaft speeds, V_1, is calculated;
4. The proportional value, P, determines the reaction to the current error;
5. The integral value, I, measures the reaction based on the sum of past errors;
6. The weighted sum of P and I parameters is further used to adjust the control variable, i.e. speed.

The diagram of a PI controller is depicted on Figure 5-3. The very first estimate of the variable (output from the controller) is the proportional reaction of the controller used to obtain the rough estimate. The integral controller is further used for fine tuning until the setpoint is reached. Once tuned, the controller relies mostly on the integral response.

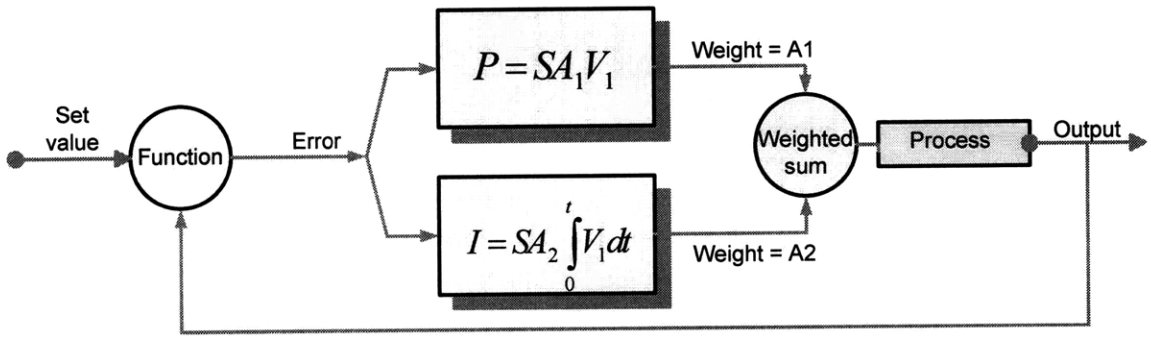

Figure 5-3. PI controller diagram

Ideally, the turbine speed is held nearly constant, so the decay heat can be removed for as long as possible through the PCS. In this case, the mass flow rate through the turbine must be adjusted in such way that the speed of the shaft remains constant. This can be done through control of the turbine bypass valve open area or can also be extended to other valve configurations. The list below represents the values that are either assumed or calculated following the algorithm specific for tuning the turbine shaft speed:

- Desired turbine speed
- Measured turbine speed
- The error between them is an input to the function
- Estimated factor S
- Estimated weights A1 and A2
- The obtained correction is fed into the valve stem displacement function
- The valve area is itself a function of valve stem displacement (non-linear)
- The flow rate responds to the change in the valve area
- The shaft reacts to the flow rate -> new value is measured

Careful tune up of the PI controller parameters is needed to ensure desired performance. As the turbine bypass valves begins to open, the mass flow rate through the turbine decreases. Turbine velocity increases due to the turbine energy which can no longer be transferred into the grid and is being converted into kinetic energy. Heat removed from the primary system through the intermediate heat exchangers temporarily increases since the primary coolant and fuel temperatures rise, and the primary and secondary coolant mass flow rates rapidly decrease. When the difference between the setpoint of the turbine velocity and the initial turbine speed, 368 rad/sec, is small, the PI controller iteration converges to the setpoint very quickly. However, sustaining high value of turbine velocity is not necessary since the amount of heat removed through the IHXs is higher than the decay heat produced. When the setpoint is fixed at a smaller value, the convergence is slower because the difference is large.

The value of the proportional weight was also iterated: (1) if the value was taken too large, system instabilities were observed; (2) for small values (given a large error), the controller was not sensitive enough. The integral term accounts for both: magnitude of the error as well as the duration. Integral weight accelerates the conversion of the variable to the setpoint. However, in the case of a station blackout accident, the decay heat curve decreases in a relatively slow fashion. Therefore, a small integral weight should be applied to ensure that the turbine velocity (and the amount of decay heat removed

through the IHX) has a smoothly decreasing behavior comparable to the decay heat curve.

Error! Reference source not found. Table 5-2 summarizes the PI controller factors and values used for the model based on tune up calculations using RELAP5-3D. The PI controller is used in the loss of flow accident analysis which is discussed in Chapter 7.2.

Table 5-2. PI controller factors used in loss of flow accident simulation

Factor	Value
Setpoint	50 rad/sec
Estimated factor S	0.04
Proportional weight A_1	2.50
Integral weight A_2	0.01

Analyses in Chapter 6 show that the shaft speed control using a well tuned PI controller is very effective in removing decay heat from the primary system through the PCS after the generator is disconnected from the grid. The PI controller parameters can be tuned to take into account the dependence on the difference between the decay heat and the amount of heat removed by RVACS.

5.5. Approaches for Managing Turbine Overspeed

When the generator is disconnected from the grid during the SBO accident, imbalance in angular momentum leads to a rapid increase in shaft speed. The speed and acceleration of the turbine shaft are primarily determined by the torques of the turbine and compressors and the shaft moment of inertia [Pope et al., 2006]. It is imperative that the rotational speed of the turbine remains below the overspeed limit to prevent potential damage of the equipment. The exact overspeed limit is uncertain at this stage of gas turbine development, but it is expected that the turbine should be able to withstand 130% overspeed due to its small size. In this analysis, a conservative value of 120% for the turbine overspeed limit was adopted.

To protect against excessive turbine overspeed and evaluate the effectiveness of various options to limit the overspeed to allowable levels, a number of possible bypass paths were investigated. The bypasses include fast acting valves that are closed during normal operation and are actuated when the turbine rotational speed increases. To prevent turbine overspeed requires very fast-acting valves. This is because in case of generator trip, the rate of the shaft speed increase is high. The initial rotational speed of the turbine is 376.99 rad/sec, and the 120% (452.4 rad/sec) overspeed limit is exceeded in less than 0.5 seconds if no action is taken. The valve opening time must be on the order of 0.5 seconds or faster as can be seen on Figure 5-4. However, such rate of valve opening is consistent with fast acting valves for steam turbines and should not pose significant challenge for valve design. The performance of three types of bypass options was evaluated:

- Turbine bypass;
- Intermediate heat exchanger bypass (IHX bypass);
- Power cycle bypass (PC bypass);

All bypass options were modeled in RELAP5-3D, and the models discussed in more detail in the current chapter are shown on Figures 5-7, 5-9, and 5-13. The valve components were modeled in RELAP5-3D as motor valves. That allowed simulation of the valve that is driven open or closed at a given rate following a trip command. There are two ways to model valve's response: linear where the rate of area change is specified by a constant; non-linear where the normalized valve flow area is correlated with the stem position. Table 5-3 shows the non-linear case.

Table 5-3. Turbine bypass valve position

Normalized stem position	Normalized valve area
0.00	0.00
0.33	0.00
0.75	0.95
1.00	1.00

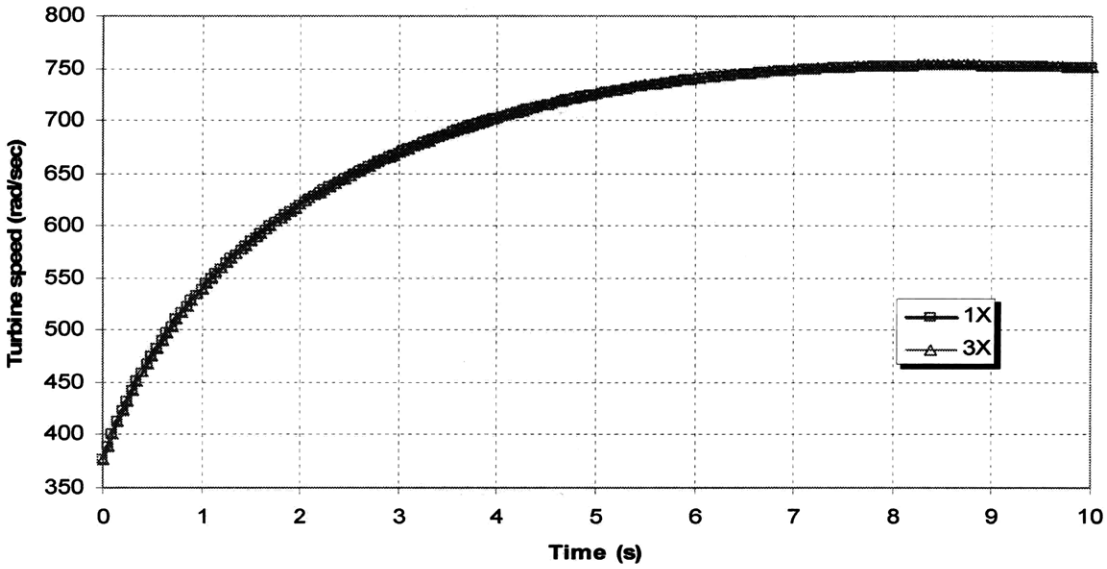

Figure 5-4. Turbine rotational speed after the generators are decoupled from the grid. Case of no bypass (1x and 3x show response of 1 and 3 lumped PCS trains)

In this model, it is assumed that the valves are actuated at the instant the accident starts. Because real valves cannot respond to an event immediately, the second option with delay in valve opening is more realistic. Normalized stem position is then correlated to the rate of opening the valve. By manipulating the rate of opening, the turbine overspeed can be managed to obtain the desired value. The dependence of the turbine speed on the rate of valve opening is presented in Figure 5-5 and Figure 5-6. The first case (labeled as "rate=1") assumed a constant change in stem position with rate of 1.0 Hz. Thus, the valve is fully open in 1 second. The second case (labeled as "rate=2") is twice as fast as the first one with rate of 2.0 Hz.

Figure 5-5 shows normalized valve area during first 3 seconds into the accident. Because in Case 2 the valve is twice as fast as in Case 1, it takes half of the time to turn fully open. As can be seen on Figure 5-5, at a rate of 2 Hz, the turbine overspeed is below 120%. This shows that such fast acting valve can hold the turbine overspeed to the peak value of only 18% which occurs at 0.7 seconds into the accident. Therefore, the rate of change of stem position of 2Hz, which is equivalent to change of normalized valve area from 0 to 1 in 0.5 seconds, was selected and used in all transients throughout this report.

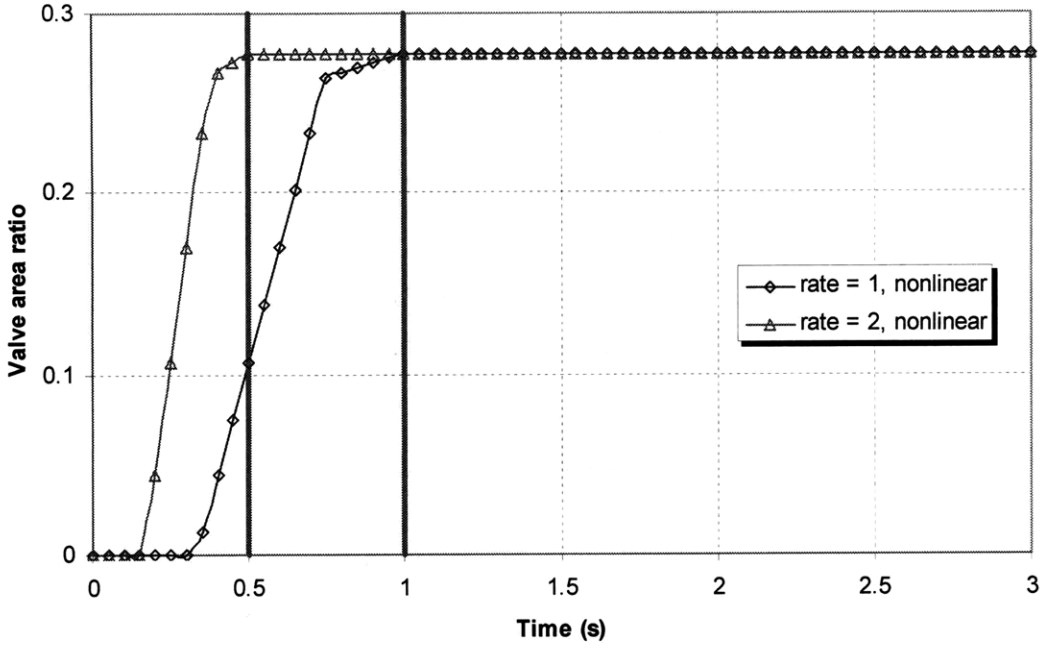

Figure 5-5. Normalized valve area during first 3 seconds of the accident

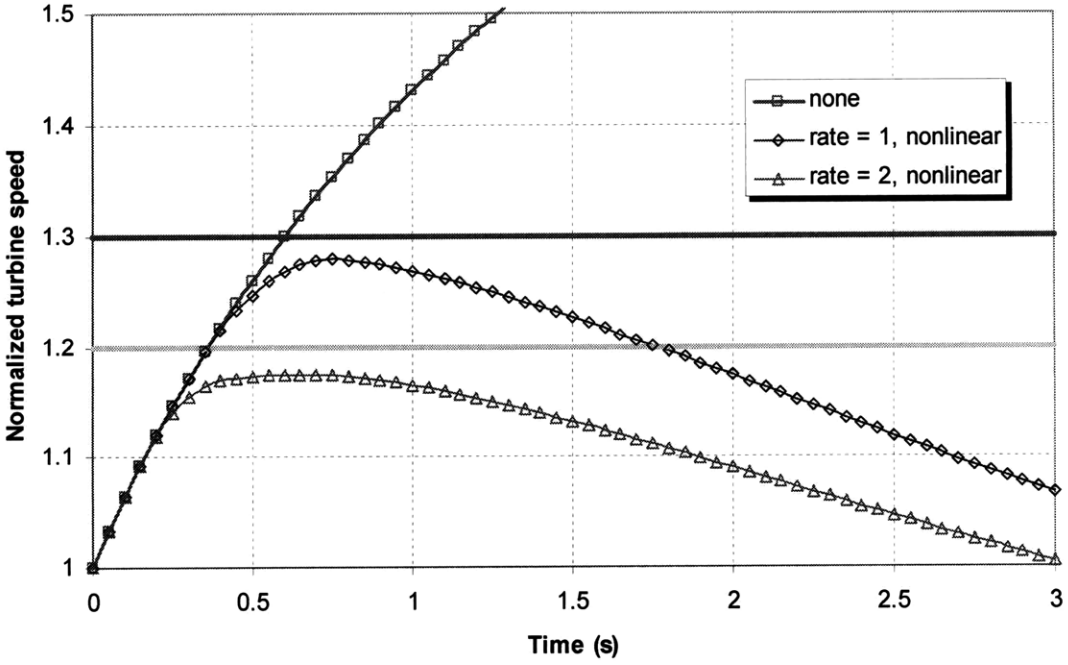

Figure 5-6. Normalized turbine speed during first 3 seconds of the accident

5.5.1. *Turbine Bypass Placement Considerations*

In the turbine bypass arrangement used in the above study, the fluid from the IHX outlet (turbine inlet) is diverted around the turbine and rejoins the stream before entering the high temperature recuperator (HTR). The schematic of the bypass is shown on Figure 5-7. Resulting reduction in flow rate through the turbine and increase in pressure at turbine exit helps to prevent the shaft rotational overspeed. However, since part of the flow does not pass through the turbine, the temperature of the fluid entering the high temperature recuperator is higher than during normal operation which increases thermal stresses in the HTR. In addition, the turbine bypass is generally undesirable because the valves are exposed to high-temperature gas from the outlet of the IHX. Figure 5-8 shows HTR gas inlet temperature (in °C). Nominally, the temperature is around 436°C, but during the transient with the turbine bypass, the temperature increases to almost 480°C. The increase in temperature is nearly 40°C which is significantly smaller than in helium Brayton cycles, but not negligible in terms of thermal stress increase. Because it is of high interest to minimize thermal stress in the HTR, other bypass locations were explored.

5.5.2. *Intermediate Heat Exchanger Bypass*

The IHX bypass location is shown on Figure 5-9. The IHX valve which is closed during normal operation opens due to de-energized actuators. The bypass pipe connects the high pressure HTR cold side outlet (at 19.8 MPa) with the turbine outlet which is at significantly lower pressure of 7.97 MPa. The difference in pressures drives the flow to the low pressure line through the bypass and reduces the flow through the turbine. As in case with the turbine bypass, the IHX bypass keeps the shaft overspeed under the limit of 120%. This bypass location is generally preferred over the turbine bypass since it is expected not to lead to an increase of HTR inlet temperature. However, as can be seen from Figure 5-10, there is still significant temperature transient on HTR inlet, albeit in the direction of reduced temperatures. Hence the potential for thermal shock is not avoided using the IHX bypass.

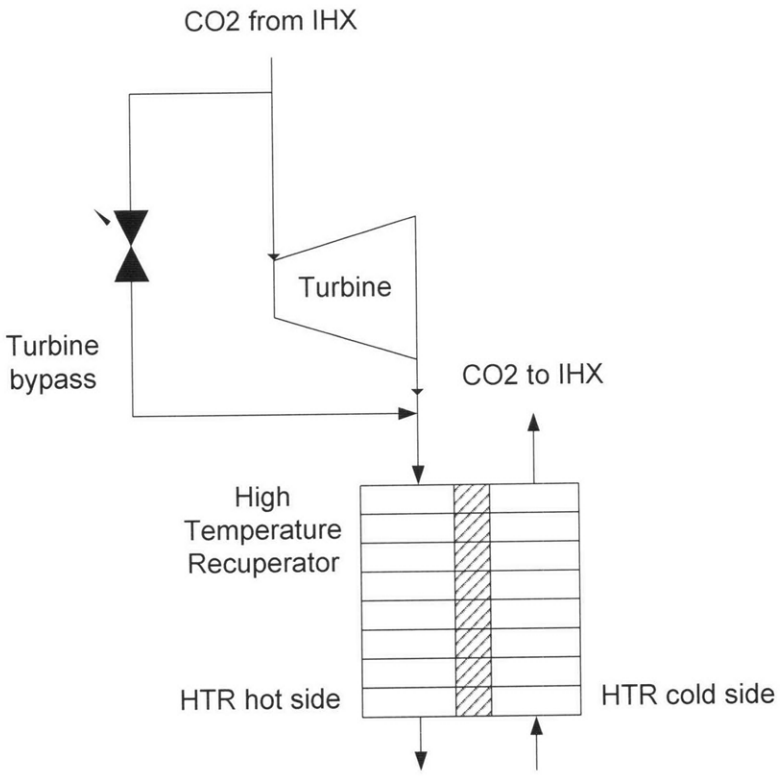

Figure 5-7. Schematic of the turbine bypass location

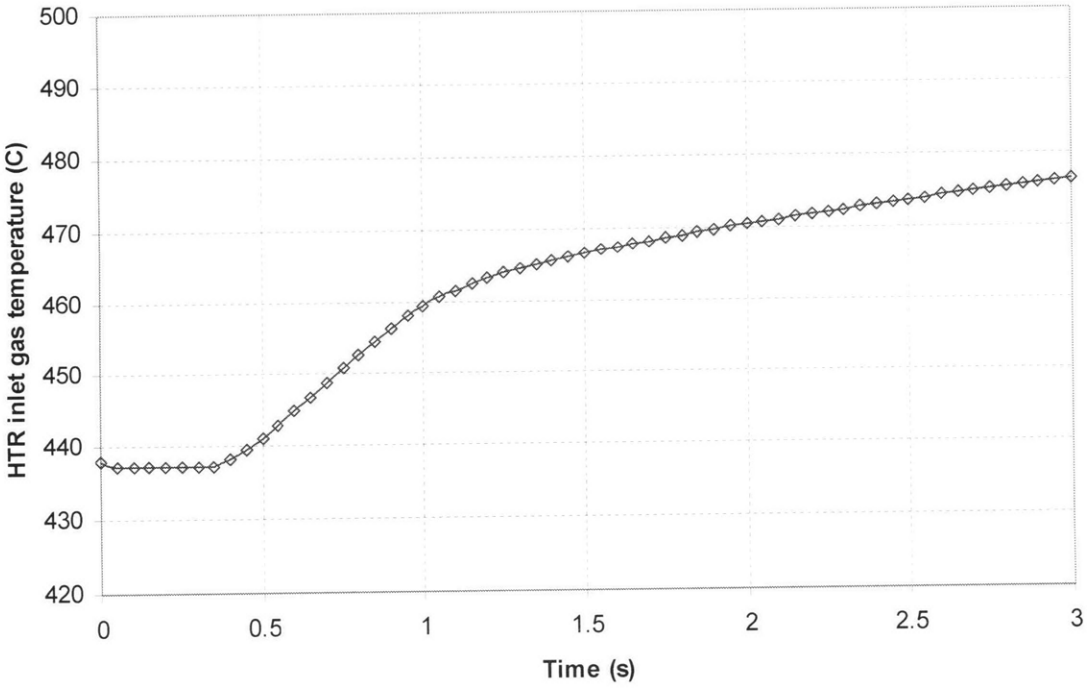

Figure 5-8. HTR gas inlet temperature (°C) for turbine bypass valve case

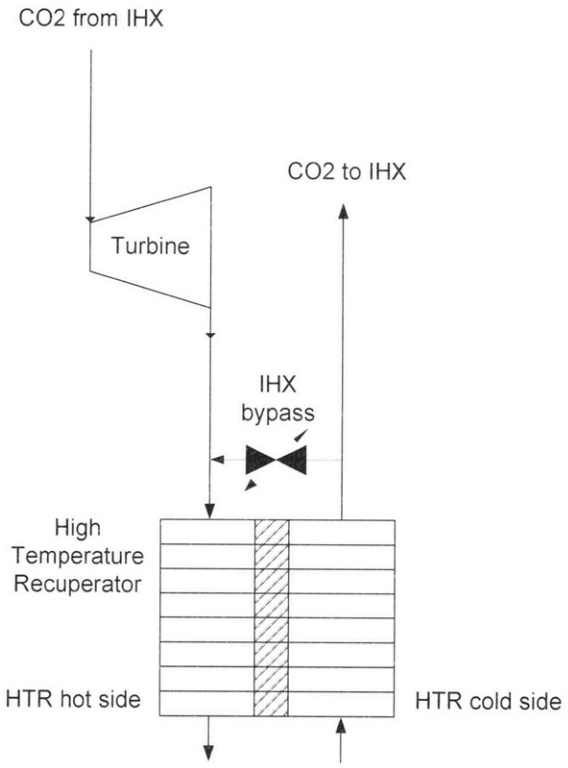

Figure 5-9. Schematic of the IHX bypass location

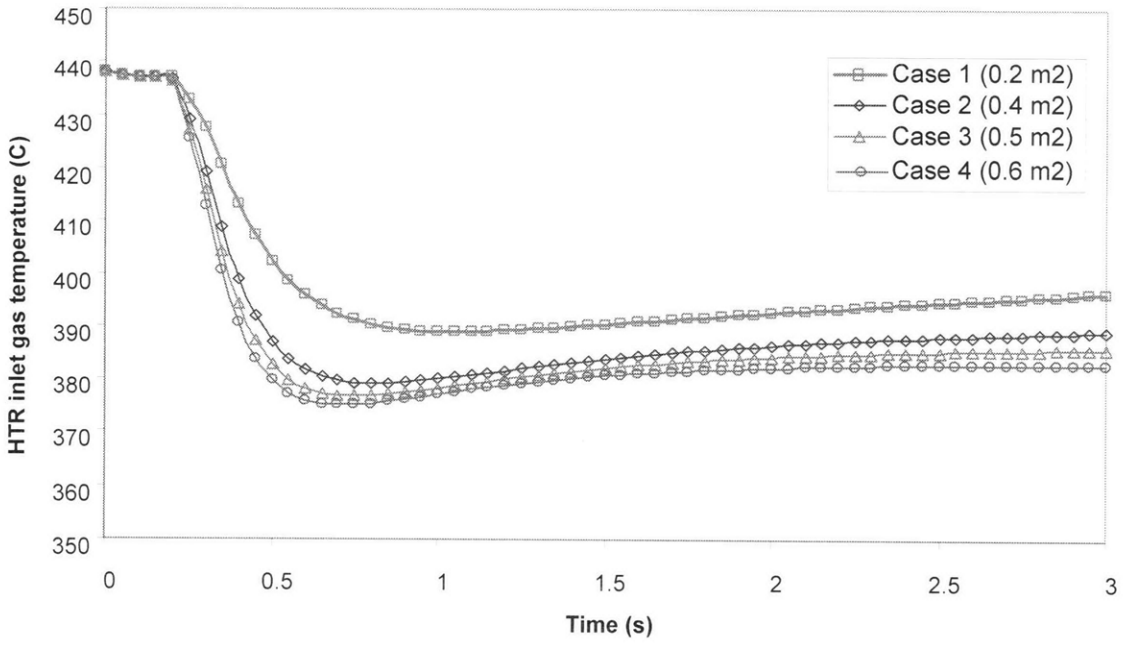

Figure 5-10. HTR gas inlet temperature (°C) for IHX bypass valve case

All cases considered for IHX bypass are for non-linear valves identical to the ones considered for turbine bypass. The rate of change in stem position was 2 Hz, but different valve areas, indicated by numbers 1-4 on the legend of Figure 5-10 were explored. Figure 5-11 shows the valve area ratios for these cases, where the valve area ratio is defined as the ratio of the valve area to the area of the adjacent piping. The **actual** area (in m^2) of the valve is given for every case in parentheses. Figure 5-12 shows normalized turbine speed for different cases. The limit for the turbine rotational speed of 120% adopted earlier requires the area of the valve to be 0.6 m^2 or more. Thus, case 4 was used for further comparison with the other bypass options.

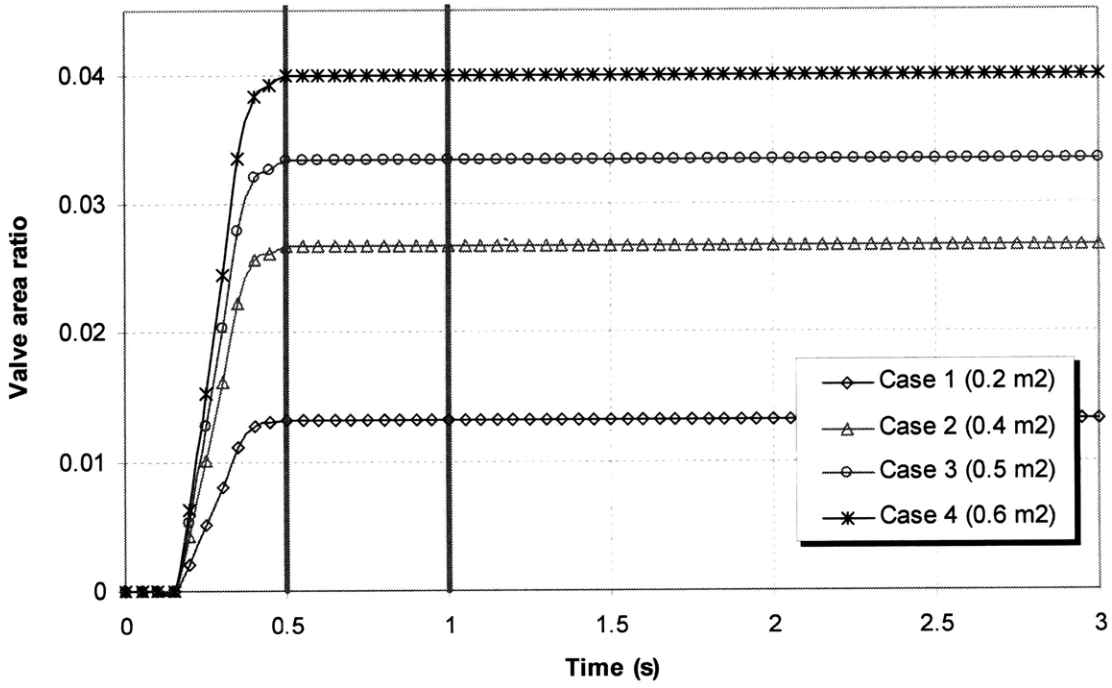

Figure 5-11. Normalized valve area during first 3 seconds of the accident

5.5.3. Power Cycle Bypass (PCB)

The PCB bypass location is shown on Figure 5-13. Similarly to previous cases, the bypass valve which is closed during normal operation opens due to de-energized actuators. The bypass pipe connects the outlet of the main compressor which is at high

pressure of 19.98 MPa with the precooler inlet which is at a significantly lower pressure of 7.69 MPa. Thus, this case is similar to the IHX bypass, but the temperature difference between main compressor outlet and precooler inlet is small, which was expected to yield a small thermal shock at precooler inlet.

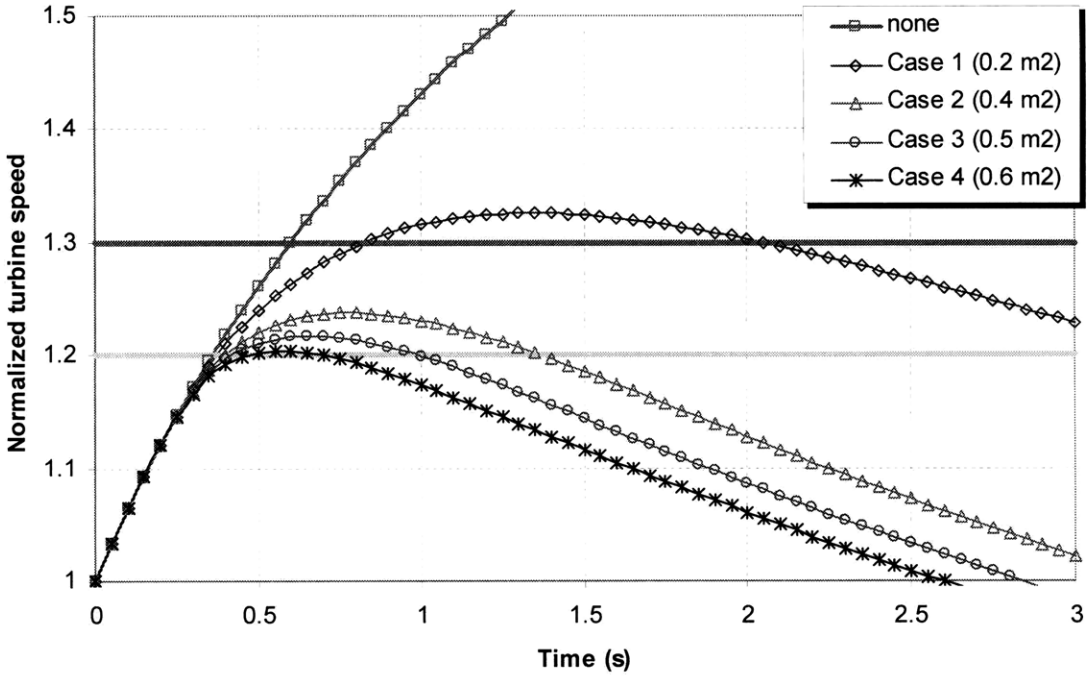

Figure 5-12. Normalized turbine speed during first 3 seconds of the accident

As can be seen from Figure 5-14, the PCB bypass can maintain the shaft overspeed under the limit of 120%. However, an appreciable temperature transient on the inlet of the precooler is still observed and potential for thermal shock is not eliminated. This is because the high pressure CO2 from main compressor outlet undergoes substantial cooling during expansion through the bypass valve resulting in cooling of precooler inlet stream. The magnitude of the temperature difference between nominal value and the minimum shown on Figure 5-15 is even higher than for the other bypass cases.

Normalized gas inlet temperatures for all three cases are compared in
Figure **5-16**. As can be observed, the PCB bypass creates the largest relative temperature difference. The most favorable case in terms of relative temperature stress on

components appears to be turbine bypass. Therefore, this bypass location was selected as preferable and was used for all studies in this report. It is also noted that turbine bypass provides the most rapid response of turbine speed reduction since it bypasses only turbine and has the smallest stored mass between the inlet and outlet of the bypass line.

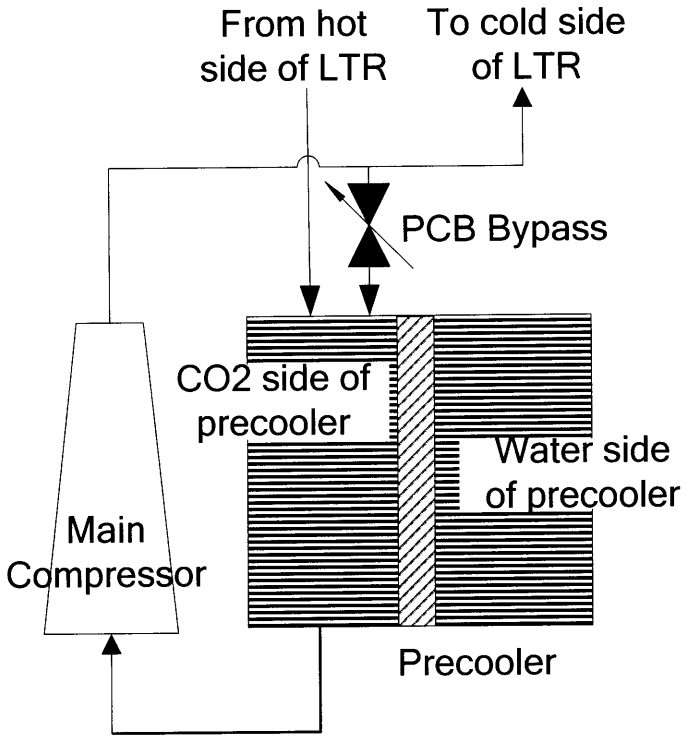

Figure 5-13. Schematic of the power cycle bypass location

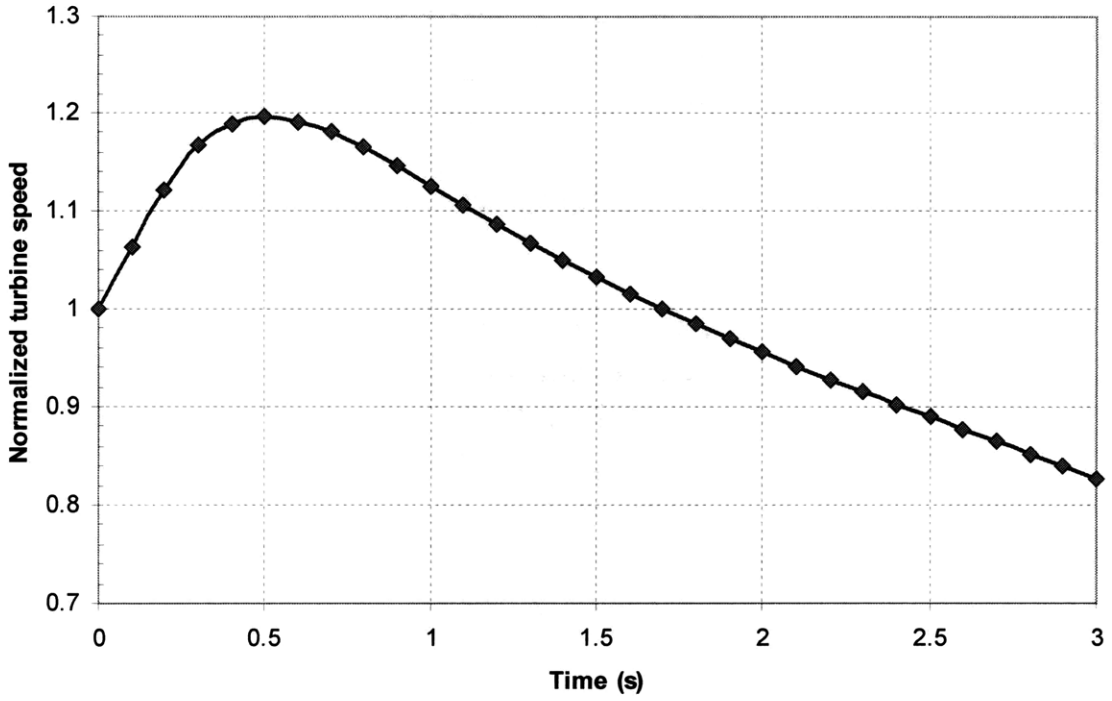

Figure 5-14. Normalized turbine speed during first 3 seconds of the accident

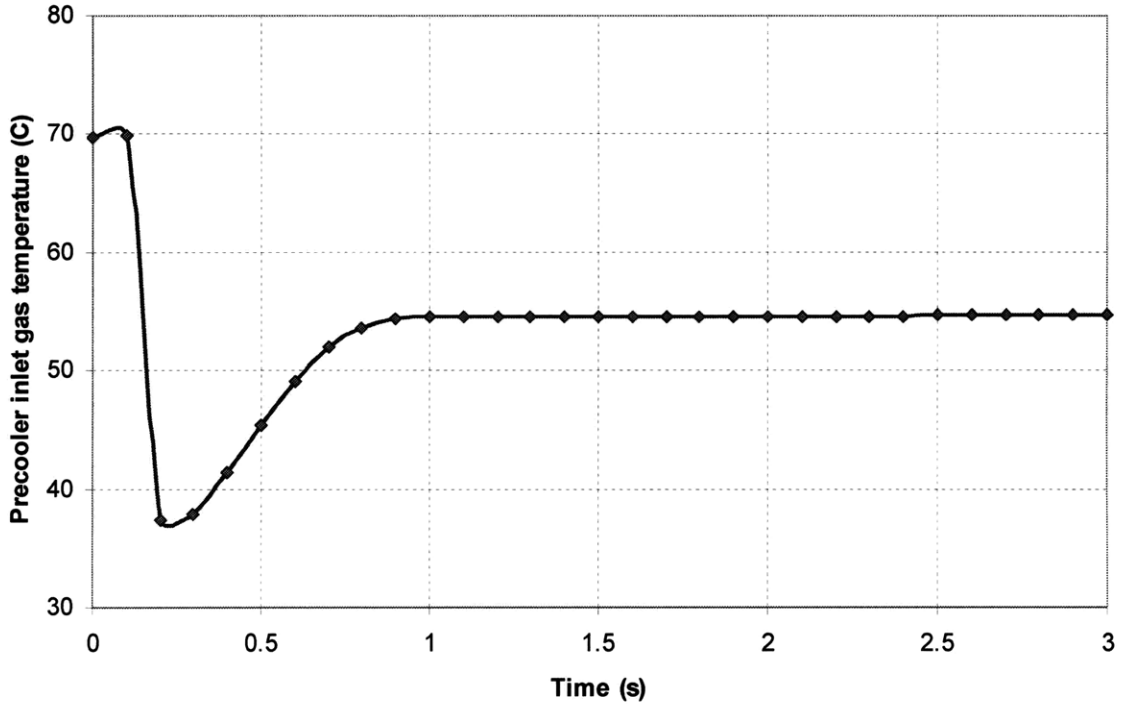

Figure 5-15. Precooler gas inlet temperature (°C) for PCB valve case

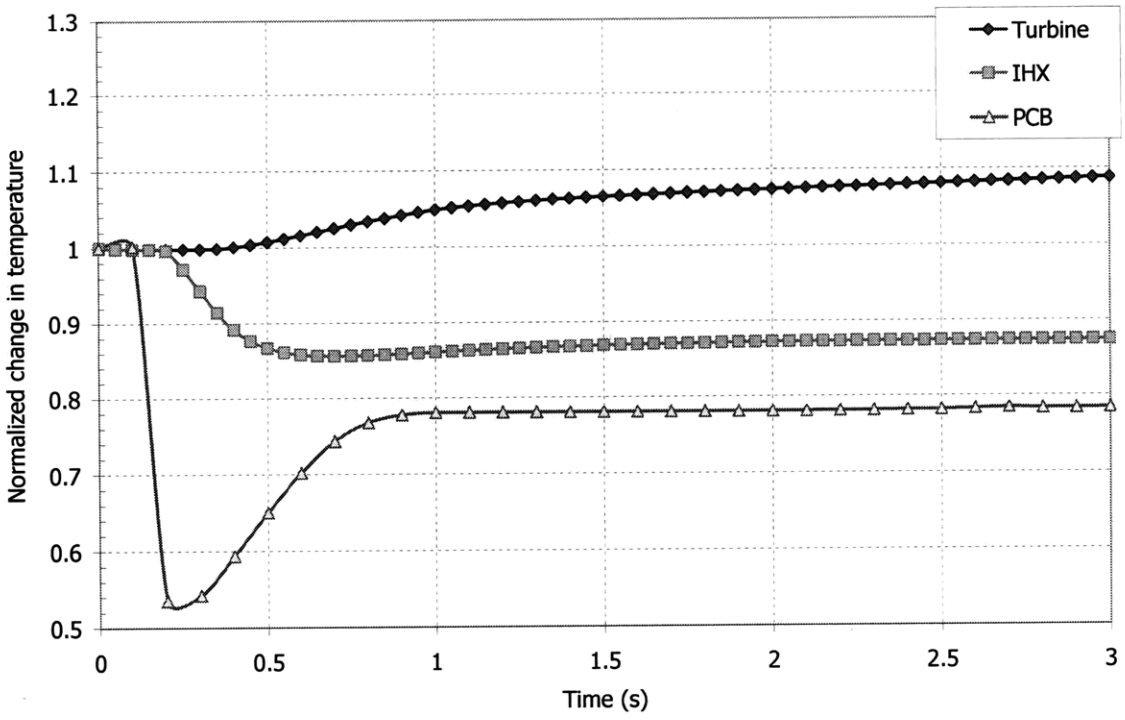

Figure 5-16. Comparison of normalized gas inlet temperature for three cases

5.6. Comprehensive Strategy for Managing Transients

One of the objectives for the FCR concept is to achieve self-controllability and reactor shutdown without exceeding structural temperature limits even in case of failure to scram. The most challenging accident without scram is the unprotected station blackout, since unprotected loss of flow and unprotected control rod withdrawal can be accommodated through the self-sustained operation of the S-CO_2 PCS (assuming pumps for precooler cooling water are available). Therefore, the discussion will focus on SBO, but also applies to other accidents in case the PCS is not available.

Transient simulations indicated that an SBO coincident with a failure to scram and operation of PSACS trains can be accommodated within the peak cladding temperature limit of 725°C. This can be done independently on the number of operating PSACS

trains since the reactor power self-adjusts to RVACS plus PSACS heat removal capacity. However, because unprotected accidents have extremely low probability, it is more important to assure safe reactor performance under protected accidents. This is typically easier to do than for unprotected accidents because of the smaller amount of heat generated and lower temperatures. However, lead coolant has a high melting point of 327°C. Thus, lead cooled reactor poses a challenge in this aspect because of potential of coolant freezing. One needs to guarantee not only sufficient decay heat removal in order not to exceed maximum cladding temperature, but also to avoid excessive cooling to avoid coolant freezing. Since it is not known a priori how many of the 4x50% trains will be operating, the PSACS system must be designed in such way to accommodate both protected and unprotected accident conditions.

The six plausible PSACS configurations during an SBO are listed in Table 5-4. The first letter of the Configuration ID indicates the state of the reactor protection system: P = protected/SCRAMED, U = unprotected/UNSCRAMED. The number following this letter indicates the number of PSACS trains initially available during the event. P1 and U1 are not considered in this analysis since they are extremely unlikely.

The challenge with mitigating an SBO is that design changes that improve the PSACS with respect to one configuration may degrade PSACS performance in another configuration. For example, a larger heat exchanger would help U2 but hurt P4. Therefore, a comprehensive design strategy is needed. Unprotected SBOs are beyond design basis and extremely unlikely. They assume a loss of two independent offsite power sources, two independent onsite power sources, and two independent scram trains. Therefore, it was chosen to focus on design basis events, P4, P3, and P2. The design philosophy was that design changes should not be made that adversely affect PSACS performance in these configurations even if they improve performance for U4, U3, and U2.

Table 5-4. PSACS Configuration Table

Configuration ID	Comments	Concern	Status
P4	Most likely	Freezing	Analyzed, OK
P3	Expected to occur during plant life (e.g. one train out for maintenance)	Freezing	Not analyzed – bounded by P4 or P2,
P2	Unlikely, but within design basis	Clad Damage	Analyzed, OK
U4	Beyond design basis	Clad Damage	Not analyzed – bounded by P4.
U3	Beyond design basis	Clad Damage	Not analyzed – bounded by U2.
U2	Beyond design basis	Clad Damage	Analyzed, OK

5.6.1. Design Strategy

The initial concern was that the most likely PSACS configuration, P4, would result in coolant freezing. The solution to this approach was to reduce the decay heat removal during P4 to an acceptable level without introducing additional failure modes or increasing system complexity.

Initially, changing the PSACS isolation valves to a battery operated design was considered. This approach would allow manual or automatic isolation of one or more PSACS trains to prevent over-cooling. The downside to this change is that several new failure modes are introduced. First, each PSACS train has two isolation valves in a parallel configuration. Therefore, to isolate a train, both valves must fully close and there is a possibility that this will not be successful. Furthermore, the current PSACS isolation valves are of a highly reliable fail-safe design that fails open upon loss of AC. Changing this valve design to one that can open and close reduces their reliability and increases the probability that a PSACS train will fail to actuate when needed or fail spuriously during a transient.

With these considerations in mind, a more passively safe design was selected. Rather than altering the PSACS valves, the size of the PSACS heat exchanger and water tank can be adjusted to accommodate both P4 and U2. The goal of SBO mitigation is to survive the accident while preventing the peak cladding, the maximum guard vessel membrane, and the peak fuel centerline temperatures from exceeding the limits defined in Chapter 2 and maintaining coolant temperature above the freezing for 72 hours. The final design removes enough heat during U2 to prevent clad damage, but does not overcool and freeze the primary system during P4. The design provides margin with respect to both failure criteria as shown in Figure 5-17 and Figure 5-18 for CR=1 and CR=0 cores, respectively.

This design modification maintains the passive philosophy of the PSACS and ensures that the appropriate level of decay heat removal is provided under all credible SBO scenarios. The PSACS provides a robust SBO mitigation capability with two, three, or four operational trains and does not under or over cool the primary system. In the extremely unlikely event of a SBO coincident with a failure to scram, the PSACS provides a long term mitigation capability.

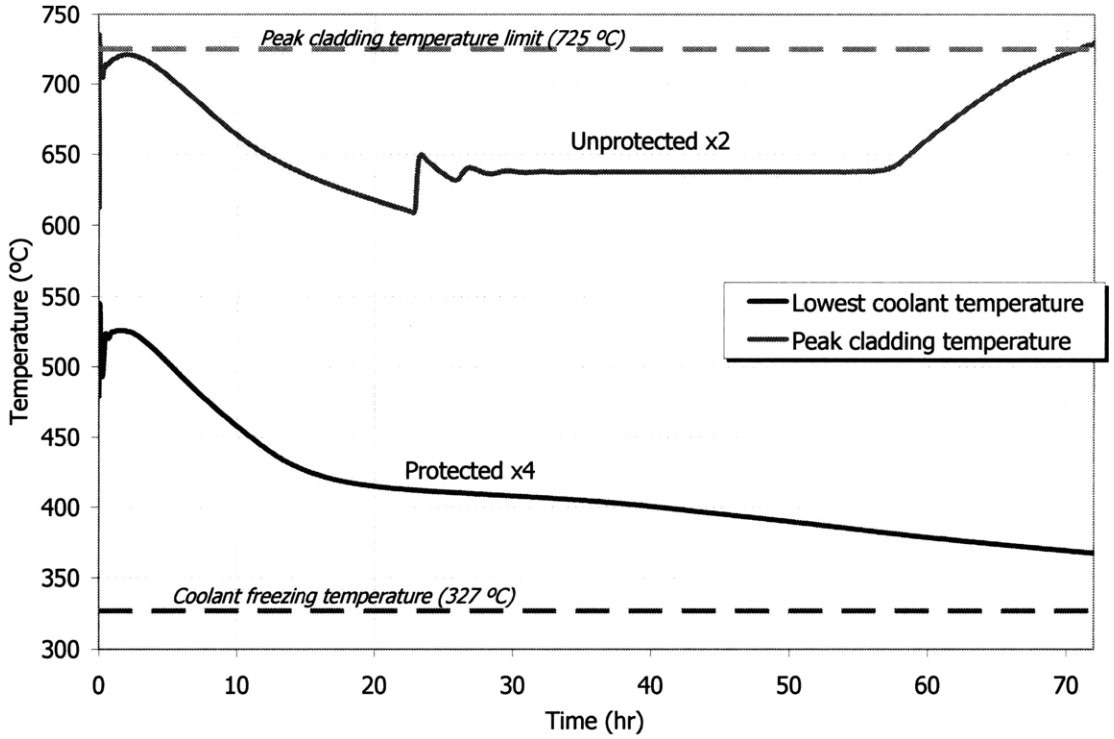

Figure 5-17. SBO bounding cases for CR=1

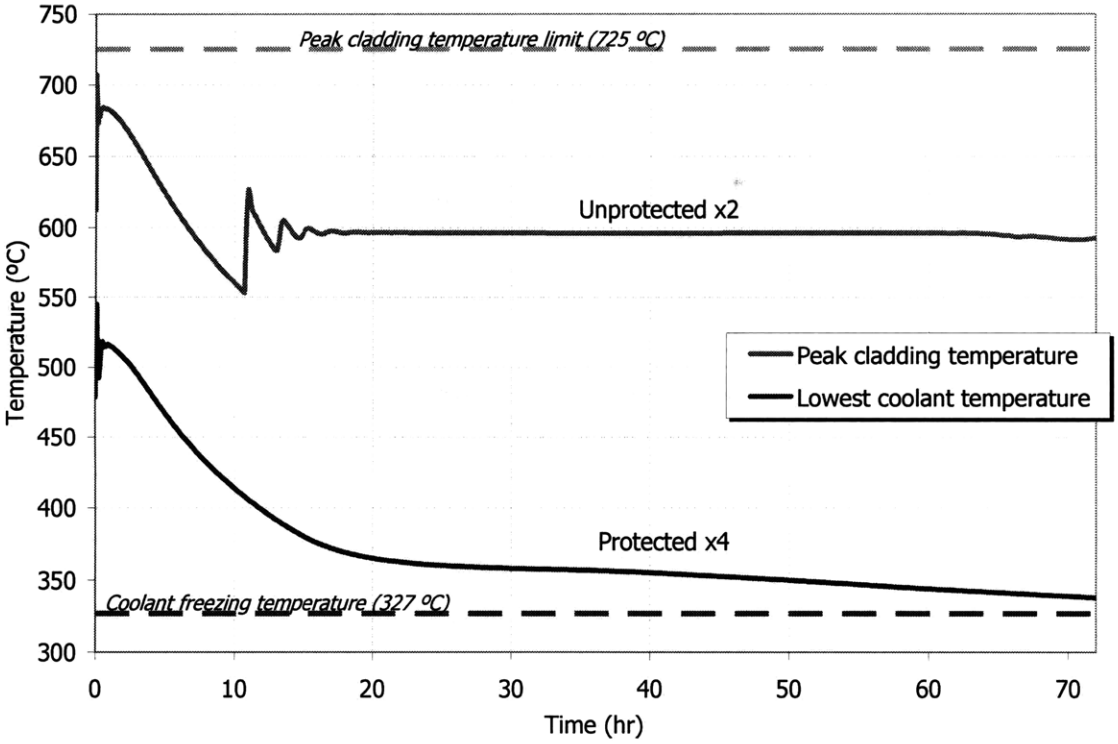

Figure 5-18. SBO bounding cases for CR=0

5.7. References for Chapter 5

Apostolakis, G., Hoffman, J., Kadak, A., Stawicki, M., "Methods for Risk Informed Decision Making for Multiple-attribute Design Decisions", unpublished, 2007.

Boardman C., Dubberley A., Carrol D., Hui M., Fanning A., and Kwant W., "A Description of the S-PRISM Plant," Proceedings of ICONE 8, Baltimore, MD, USA, 2000.

Pope M.A., Hejzlar P., and Driscoll M.J.,"Thermal Hydraulics of a 2400 MW_{th} Supercritical CO_2-Direct Cycle GFR", MIT-ANP-TR-107, Center for Advanced Nuclear Energy Systems, Massachusetts Institute of Technology, 2006.

Todreas N.E., Hejzlar P., Shwageraus E., Petroski R., Nikiforova A., Whitman J., and Fong, C.J., "Flexible Conversion Ratio Fast Reactor Systems Evaluations", Final report, Center for Advanced Nuclear Energy Systems, MIT, MIT-NFC-PR-101, August 2008.

6. RELAP5/ATHENA MODEL OF THE REACTOR SYSTEMS

Significant part of the thermal hydraulic design and analysis of the FCR systems involved working with RELAP5/ATHENA (Advanced Thermal Energy Network Analysis) code [RELAP-3D, 2005]. The RELAP5-3D code has been developed at Idaho National Laboratory for simulation of steady state and transient behavior of reactor system [RELAP-3D, 2005]. ATHENA supports the working fluids commonly used in the GEN. IV systems design, in particular Pb-Bi and S-CO_2. In the current version of the code, liquid lead coolant properties are not available; thus, lead-bismuth, which has almost the same properties as lead, was used in the analysis. The work on FCR RELAP5-3D/ATHENA model was conducted in six main stages:

1. An overall model of the primary system was built with the core represented as two channels: hot channel representing group of hot fuel assemblies and average channel modeling the rest of the core.
2. A detailed intermediate heat exchanger model was created separately, optimized, and then connected to the primary loop within the reactor vessel.
3. The RVACS with guard vessel, the lead-bismuth gap between the reactor and guard vessels, dimples on the outer guard vessel wall and perforated plate for heat transfer enhancement were added, and analysis of the RVACS decay heat removal capability was conducted.
4. A complete power conversion system (PCS) with the turbine, compressors, recuperators and the precooler was connected to the primary system through the IHX to simulate overall system response to accident conditions.
5. A preliminary design of a Passive Secondary Auxiliary Safety System (PSACS) to aid RVACS decay heat removal was conducted. The passive system was built in RELAP5-3D and connected to the PCS.
6. Transient analysis of the accidents of interest was completed using RELAP5-3D/ATHENA.

6.1. Overall RELAP5-3D Model Nodalization

The overall reactor RELAP5-3D model nodalization is illustrated in Figure 6-1. RELAP5-3D model is applicable to both unity conversion ratio and zero conversion ratio cores with a modification in the core modeling due to different radial peaking factors and orificing arrangements.

Both the primary coolant system (components 500 through 595) and RVACS (components 800 through 830) are depicted. The nodalization starts with the lower plenum, 500. The flow is subsequently split into two parallel channels: hot channel (component 516) and average channel (component 510). The active core components were further nodalized into 5 axial volumes. The flow is recombined in the chimney, 520. Component 540 corresponds to the upper plenum.

Four heat exchangers are represented by components 560 and 561. Component 560 depicted in Figure 6-1 corresponds to one heat exchanger's lead coolant channels. The other three are lumped together in component 561 (not shown). Detailed illustration of a heat exchanger with both lead and CO_2 sides is shown in Figure 6-2. Heat exchanger downcomer, vessel riser (liner), and the pump downcomer are represented by components 570, 580 and 590, respectively. The above volumes are connected by perforation holes to allow the coolant to follow its path. The perforation holes are modeled as a single junction with flow area corresponding to the total connection area, but the hydraulic diameter corresponding to a single perforation hole. Such simplification is necessary because of 1-D nature of the model. The geometry of perforations is calculated based on the velocity limit of the coolant. Four centrifugal pumps are lumped together as component 595.

Hatched components correspond to the heat structures. Heat structures are connected thermally to the attached hydrodynamic volumes. The primary system includes five main structures: average fuel pins, hot fuel pins, core barrel, heat exchanger tubes, and the reactor vessel liner. The RVACS heat structures contain the reactor and guard vessels

with lead-bismuth as the conducting fluid modeled as one component, perforated plates and the collector cylinder.

The reactor power is calculated using a point reactor kinetics model.

Two time-dependent volumes, 800 and 830, set the air supply and exhaust conditions and are at atmospheric pressure. The downcomer is represented by component 810. Volume 820 is the riser with the perforated plate installed in the middle. Radiation heat transfer from the guard vessel through the perforated plate to the collector was represented as a radiation enclosure model; thus, there are four radiation enclosure heat slabs.

6.2. RELAP5-3D Core Model

In the core model, the flow through the core is represented as two parallel channels: hot channel and average channel. The hot channel contains four assemblies with the highest peaking factor of 1.21 for CR=1 or 16 assemblies with the highest peaking factor of 1.34 for CR=0 lumped together. Average channel represents remaining assemblies.

Detailed subchannel calculations were performed using SUBCHAN to flatten the core coolant temperature distribution and to minimize the peak cladding temperature through three-zone orificing. The calculations resulted in the desired flow split between the average and hot channels. In RELAP5-3D model such flow split was represented through form losses (forward and reverse loss coefficients) associated with the orifices. Table 6-1 shows the orificing and the calculated flow split for both cores.

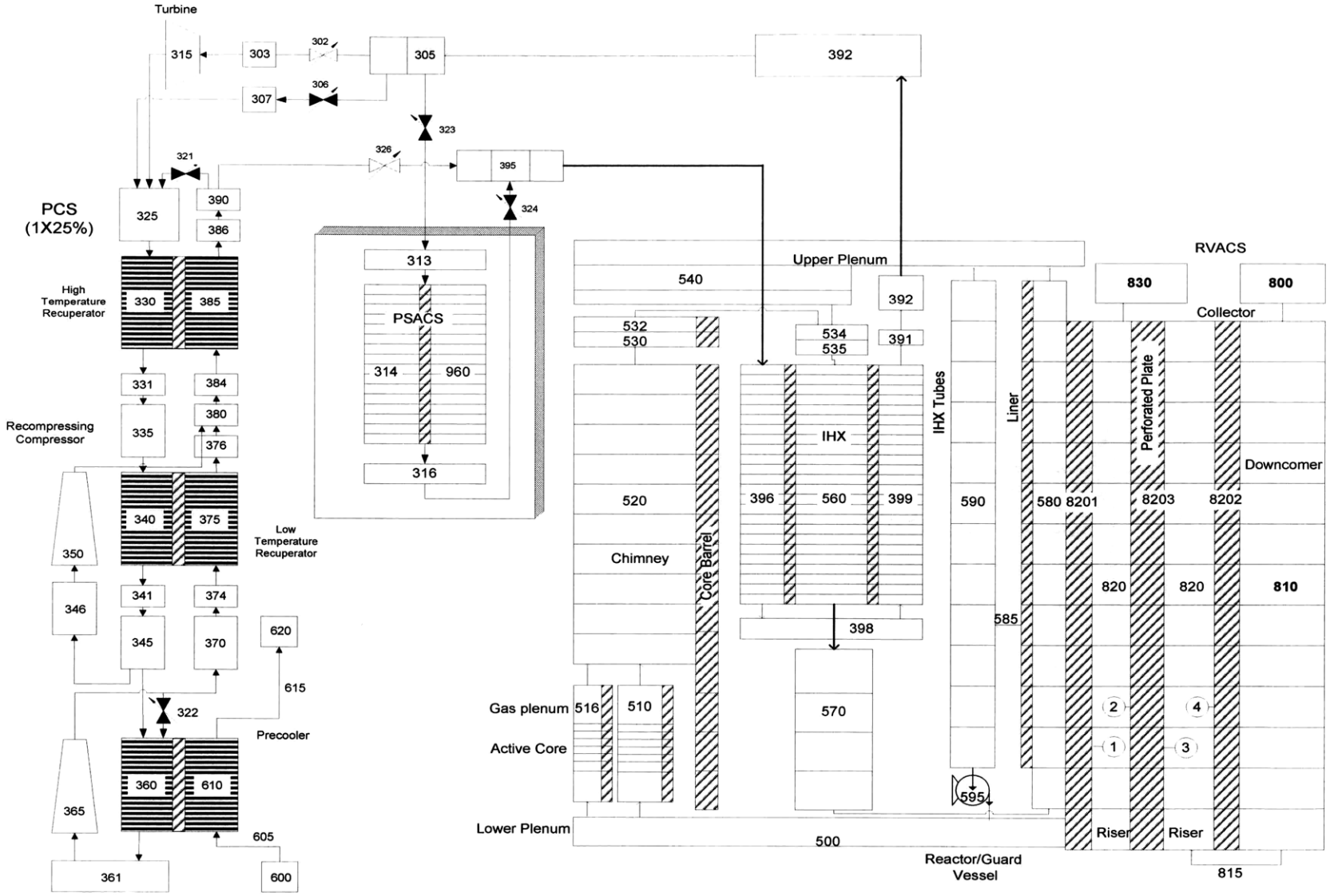

Figure 6-1. Integrated layout of the primary and secondary (PCS and PSACS) reactor coolant systems and RVACS

Table 6-1. Orificing and the flow split in the core

		CR=1	CR=0
Highest peaking factor		1.21	1.35
Number of assemblies		4	16
Orificing coefficients (zone1/zone2/zone3)		0.4/4.96/13.24	0.4/8.19/29.68
Flow split (kg/s)	Hot	2196.5	9511.8
	Average	171403.5	164088.2

Fuel pins are modeled in detail including fuel pellets, lead-alloy bond, cladding and the oxide layer on the outside of cladding. The active core components were further nodalized into 5 axial volumes 0.26 m in length and 8 radial meshes. The axial power distribution was then applied to heat structures connected to both hot and average channels. The power distribution simulates the heat generated in the fuel pins. An internal source multiplier used in RELAP5-3D core model allows for distinguishing between average and hot channels by applying higher peaking factor to the hot channel. Another purpose of the internal source multiplier is to account for the number of channels included either in the average or hot channel. Table 6-2 summarizes the multipliers. The unity conversion ratio core has significantly lower hot channel multipliers due to fewer hot channels and lower peaking factor.

Table 6-2. Internal power multipliers

Relative axial flux multiplier	CR = 0		CR = 1	
	Average	Hot	Average	Hot
0.813	0.16443	0.01086	0.17286	0.00243
1.06	0.21439	0.01416	0.22537	0.00317
1.23	0.24877	0.01643	0.26152	0.00368
0.95	0.19214	0.01269	0.20199	0.00284
0.585	0.11832	0.00781	0.12438	0.00175

Another significant difference between the unity and zero conversion ratio cores is the fuel composition. The zero conversion ration core has larger transuranic content that lowers the fuel conductivity. The comparison of estimated fuel conductivities used in the

model is provided in Table 6-3. Thus, the maximum fuel temperature of the CR=0 is expected to be higher than for the CR=1 core.

Table 6-3. Fuel conductivities (W/mK)

Temperature (K)	CR = 0	CR = 1
293	3.75	8.22
373	4.60	9.00
873	10.95	15.26
1173	13.70	20.14
1873	22.80	34.81

6.3. RELAP5-3D Model of Intermediate Heat Exchanger

The IHX design is an important part of the RELAP5-3D/ATHENA model. To avoid multiple design iterations of the heat exchanger design and to save computational time, the IHX was first modeled separately from the rest of the reactor system. The following constraints were taken into account:

1. Inlet and outlet temperatures on both sides are fixed by the core thermal hydraulic design and the S-CO_2 power cycle.
2. Mass flow rates on both sides are fixed by the core thermal hydraulic design and the CO_2 cycle.
3. Heat exchanger size is constrained by the annulus size between the core barrel and the liner including space needed for the pumps.
4. Pressure drop on CO_2 side must be minimized to ensure good efficiency of the CO_2 cycle. It is directly related to the size of the heat exchanger.
5. Pressure drop on lead side must be minimized to ensure reasonable pumping power.
6. Component wall thicknesses are calculated based on material properties as function of design pressure and temperatures.

6.3.1. Design Methodology

The initial design of the intermediate heat exchanger was performed using MS Excel worksheet. The details of the design and optimization of the intermediate heat exchanger in Excel are provided in Appendix A. Enhanced heat transfer applied to the inner surface of the heat exchanger tubes allows for the reduction in heat exchanger size without a significant increase in the pressure drop on the CO_2 side. The increase in heat transfer coefficient between the ribbed and smooth tubes was calculated using Excel worksheet. The ratio of enhanced heat transfer coefficient and smooth heat transfer coefficient was calculated and then further applied to the RELAP5-3D/ATHENA model. To simulate the enhanced heat transfer in RELAP5-3D/ATHENA, the obtained ratio was factored into the gas heat transfer coefficient. In addition the small increase in the pressure drop through the gas-side of the IHX tubes due to the helical ribs was included in the model. The heat exchanger length was reduced from 6.8 m to 5.7 m which resulted in a lead-side pressure drop cutback from 380 kPa to 325 kPa.

In the RELAP5-3D/ATHENA model, coolant mass flow rates, inlet and outlet temperatures, and inlet pressures were used as boundary conditions. The values are shown in Table 6-4. Optimized geometric parameters were taken from the Excel model. For quick optimization purpose, the secondary side was modeled through time-dependent volumes and junctions to avoid remodeling the entire power conversion system in RELAP5-3D/ATHENA. The output values of pressures and temperatures were then compared to the Excel model.

Table 6-4. Design boundary conditions for the heat exchangers

	CO_2 side	Lead side
Mass flow rate (kg/s)	3189.2	43400.0
Inlet temperature (°C)	393.1°C	573.3°C
Outlet temperature (°C)	546.0°C	477.0°C
Inlet pressure (MPa)	19.5 MPa	465 kPa

Figure 6-2 depicts schematic representation of the RELAP5-3D/ATHENA heat exchanger model. "Gas-side source" is a time-dependent volume that sets the boundary conditions for CO_2 temperature and pressure simulating the turbine outlet. Junction 370 is a time-dependent junction that sets the gas mass flow rate. Similarly, on the lead side, time-dependent volume 535 and junction 536 specify the boundary conditions for the primary side. Thus, CO_2 gas enters through volume 360, goes through the main inlet tube (modeled as pipe-volume 380), mixes in the bottom plenum 384, heats up while going through the small tubes represented by volume 385, enters top mixing plenum (volume 386), and exits through two outlet tubes (390) into the sink (398). For the lead side, the path is much simpler: lead-coolant enters through the "source" volume, transfers heat to the gas-coolant through channels modeled as volume 560, and exits through sink 565.

Similarly to core model, hatched areas correspond to the heat structures: 3401 is the CO_2 inlet tube wall, and 5601 represents all of the small tubes. Small tubes were nodalized radially into five meshes including the oxide layer on lead side.

After the model was built, the output was compared to the Excel model. Originally, a large difference between the two models was observed. In the initial setup of the model, coarse axial meshing for the tubes in RELAP5-3D/ATHENA was used because of single-phase fluids in the system. Coarse vs. fine meshing allows a significant savings in computational time. However, large discrepancies in the power removed from the lead coolant between that calculated using RELAP5-3D/ATHENA and that estimated by Excel using Log Mean Temperature Difference approximation were observed. This led to investigation of the effects of mesh size on the model performance. RELAP5-3D/ATHENA model of IHX shows a strong dependence of the results on meshing as can be seen from Figure 6-3. Even though the fluids are both single-phase, large difference in heat transfer coefficients and other thermal properties can lead to poor numerical results. As the mesh becomes finer, the transmitted power calculated using RELAP5-3D/ATHENA saturates around the target value of 600 MW. Thus, it was concluded that 50 meshes per heat exchanger length is sufficient to acquire adequate results.

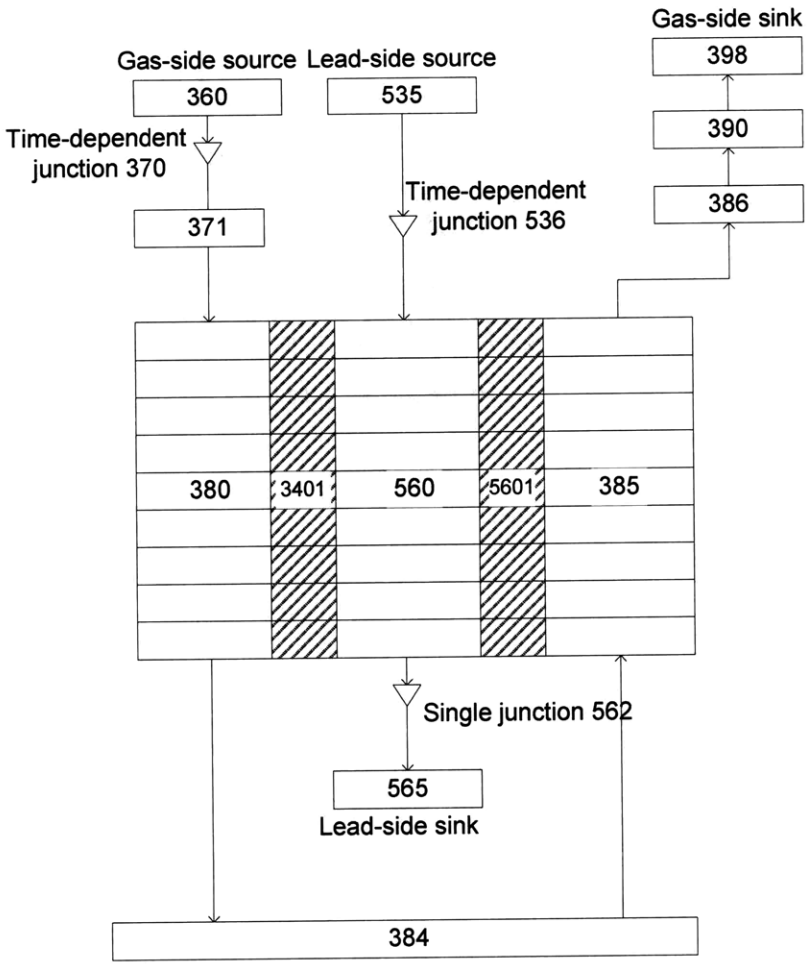

Figure 6-2. RELAP5-3D/ATHENA schematic of the heat exchanger

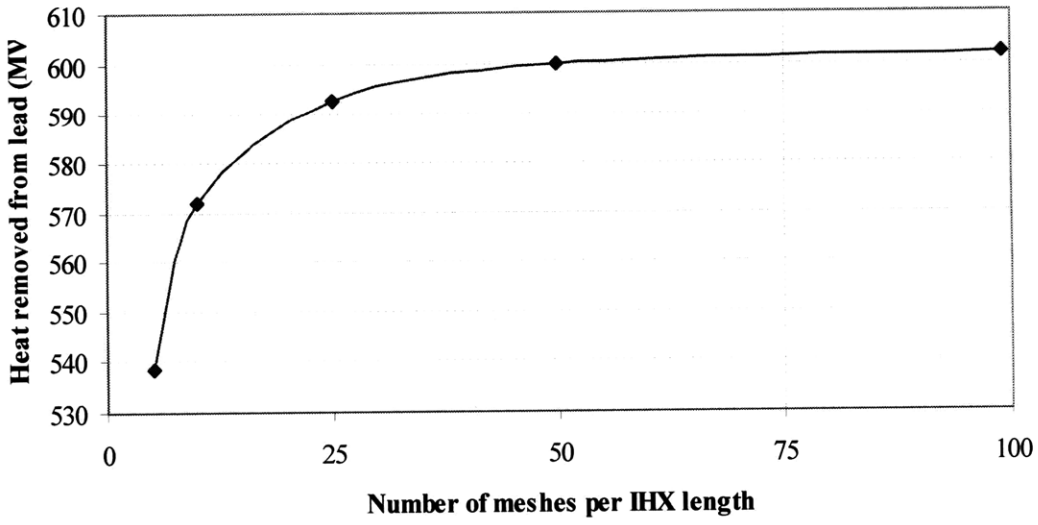

Figure 6-3. Effect of axial mesh size (RELAP5-3D/ATHENA) on the model performance

6.3.2. Verification of the RELAP5/ATHENA model

The major heat exchanger design parameters obtained from Excel worksheet and RELAP5-3D/ATHENA simulation are summarized in Table 6-5. Note that RELAP5-3D/ATHENA simulation was run with lead-bismuth alloy coolant since pure lead is not yet available as a fluid in RELAP5-3D/ATHENA. Nonetheless, lead and lead-bismuth have very close thermal properties. Table 6-6 provides a comparison of a few thermal hydraulic parameters of lead and lead-bismuth eutectic (Martynov, 1998). Average values for heat transfer coefficients of lead and CO_2 are in good agreement when estimated using Excel worksheet and RELAP5-3D/ATHENA model.

6.4. RELAP5-3D Model of RVACS

A brief description of the nodalization was given in the overview. In this model, the RVACS chimneys were lumped together. The model consists of three hydrodynamic volumes, downcomer and two risers separated by the perforated plate, and three structures, collector wall, perforated plate and the vessel. Reactor vessel, guard vessel, and the liquid metal gap between them are lumped into one structure with material properties preserved.

The view factors for each surface are given in Table 6-7. The numbers for each view surface are identified on Figure 6-1. The emissivity of the surfaces was taken to be 0.75 [Hejzlar et al., 2004]. In the perforated plate, 40% of the total area was voided to account for the presence of holes. The description of the effects of heat transfer enhancement through placement of dimples on the outer surface of the guard vessel is provided in Todreas et al. [2008]. Description of the RVACS design is given in Section 4.2.

Table 6-5. Comparison of heat exchanger performance between Excel calculations and RELAP5-3D/ATHENA simulation

INPUT	Excel calculations	RELAP5-3D simulation
Core power (MW_{th})	2400	
Lead mass flow rate (kg/s)	173600	
S-CO_2 mass flow rate (kg/s)	12848	
Number of heat exchangers	4	
Target power transmitted in the IHX (per IHX) (MW_{th})	600	
Lead inlet temperature (°C)	573.3	
Lead outlet temperature (°C)	477.0	
S-CO_2 inlet temperature (°C)	398.0	
S-CO_2 target outlet temperature (°C)	549.6	
S-CO_2 pressure (MPa)	19.7	
GEOMETRY		
Lattice	Triangular	
Number of tubes (per IHX)	16356	
Outer tube diameter (mm)	14	
Tube wall thickness (mm)	2.8	
Pitch to diameter ratio	1.23	
Inner IHX radius (r_i) (m)	2.711	
Outer IHX radius (r_o) (m)	4.471	
OUTPUT		
Calculated power (MW_{th})	598.7	598.2
Tube length (m)	5.7	5.7
Logarithmic temperature difference (°C)	46.7	N/A
S-CO_2 velocity (average) (m/s)	16.8	17.0
Lead velocity (average) (m/s)	2.17	2.18
S-CO_2-side pressure drop (through small tubes) (kPa)	226	230

Table 6-6. Comparison of lead and lead-bismuth eutectic selected physical parameters

Temperature (°C)	Density (kg/m^3)		Thermal conductivity (W/mK)		Specific heat (kJ/kgK)		Pr number	
	Lead	Pb-Bi	Lead	Pb-Bi	Lead	Pb-Bi	Lead	Pb-Bi
300	10709	10364	14.88	12.67	147	146	0.0268	0.0224
400	10593	10242	15.11	13.72	146	146	0.0213	0.0172
500	10477	10120	15.45	14.65	144	146	0.0171	0.0137
600	10360	10000	15.96	15.81	142	146	0.0141	0.0115

Table 6-7. View Factors

Surface Emitting	View Factor	Surface Receiving
1	0	1
1	0.6	2
1	0	3
1	0.4	4
2	0.980592	1
2	0.019408	2
2	0	3
2	0	4
3	0	1
3	0	2
3	0	3
3	1	4
4	0.384384	1
4	0	2
4	0.588589	3
4	0.027027	4

6.5. Details of RELAP5-3D Model of PSACS

The PSACS model consists of a large tank of water with the tube-and-shell auxiliary heat exchanger placed inside. To enhance natural circulation, the PSACS is located 2.0 meters above the in-vessel IHXs. In case of an accident, the CO_2 gas from the power cycle is directed into the PSACS by opening the PSACS isolation valve (shown as 323 on Figure 6-4). CO_2 is then distributed into the auxiliary heat exchanger tubes in the upper plenum 313. The coolant then travels downward through the gas-to-water heat exchanger tubes 314, while cooling, providing additional driving head for the natural circulation. The gas is collected in the bottom plenum and directed back to the IHX. The size of the water tank and the size of the PAHX can be adjusted depending on the requirements of the incremental strategy for beyond DBA accidents. The inner diameter of the pipes connecting the PSACS and PCS are the same as used throughout the PCS (0.7 m);

however, such large diameter might be unnecessary because of low gas mass flow rate through the PSACS. Table 6-8 provides the summary of the PSACS parameters. The final PSACS design consists of four trains (4x50%), i.e., for each IHX, but the operation of only two trains out of four is sufficient for satisfactory performance during an SBO.

Table 6-8. Design parameters of the PSACS

Parameter	Initial Value	Comments/Remarks
Water Tank - H_2O initial conditions		
H_2O temperature (°C)	25	Room pressure and temperature
Tank diameter (m)	8.0	The volume of the water was estimated based on water properties and possible duration of the accident.
Tank height (m)	16.0	
Passive Auxiliary Heat Exchanger (PAHX)		
Number of tubes	350	
Tube length (m)	4.0	
Inner diameter – CO_2 side (m)	10.5E-03	
Outer diameter – water side (m)	1.40E-02	
P/D ratio	3.0	

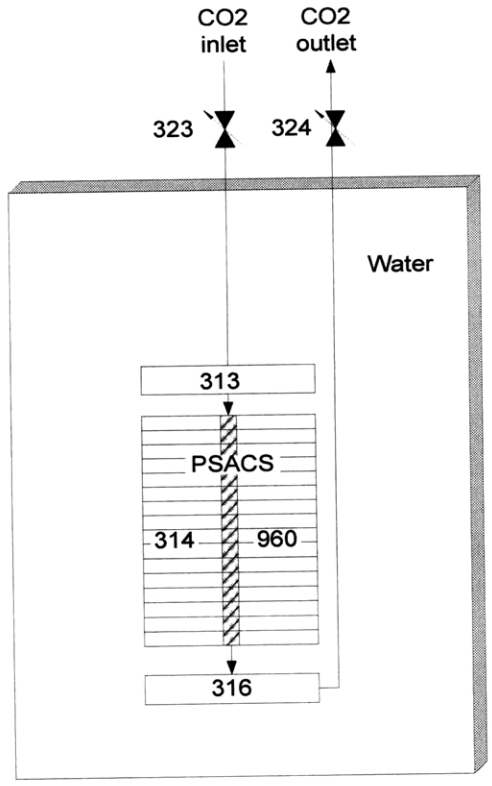

Figure 6-4. RELAP5-3D schematic of PSACS

In case of the station blackout accident, the valves that would normally isolate the PSACS from the rest of the gas cycle start opening. Simultaneously, power conversion cycle valves close in order to isolate the turbomachinery from the rest of the loop. The purpose of the turbomachinery isolation is twofold: the gas must be directed through the PSACS equipment to remove as much heat as possible and to prevent the turbine rotational overspeed that would result in turbomachinery damage. The turbine overspeed and the potential ways to overcome the problem are discussed in Section 5-5. During SBO accident, the valves 302, 306 and 326 shown on Figure 6-1 will shut closed isolating the PCS while the valves 323 and 324 will be open letting CO_2 enter PSACS. The timeline of the station blackout accident with PSACS used to aid RVACS with the decay heat removal is presented in Table 6-9. Time nodes t_1 and t_2 are to be determined by transient analysis and depend on the strategy chosen to mitigate the accident.

Table 6-9. Timeline of the station blackout accident with PSACS

Time	Event
0 seconds	Both independent sources of offsite power are simultaneously lost
0 - 0.5 seconds	Failure to energize onsite emergency buses Failure to SCRAM reactor PCS isolation valves close due to loss of AC PSACS-Water isolation valve actuators de-energized;
0.5 seconds – t_1	Static head differential between IHX outlet header and PSACS loop prevents S-CO2 flow in "normal" direction
$t_1 - t_2$	Natural circulation is established in PSACS loops; decay heat is removed via PSACS and RVACS
t_2	RVACS-only cooling adequate for decay heat level; PSACS no longer needed
72 hours	Offsite power is restored. Exit SBO Emergency Operating Procedures. Initiate Standard Cool down Procedure. Active systems may be available to augment RVACS cooling.

6.6. RELAP5-3D Model of PCS

The SBO is the limiting transient case, and therefore requires PSACS for the decay heat removal. Moreover, the PSACS is required to be a part of the reactor systems decay heat removal because the PCS is classified as non-safety-grade. However, in case of the less severe transients, Loss of Flow and Transient Overpower, the PCS can be used to mitigate the accident while the PSACS is still available as the ultimate safety-grade equipment in case PCS fails to perform its function. Note that the case when LOFA is accommodated with PSACS becomes identical to SBO since in order for PSACS to operate, the PCS isolation valves must fail closed.

The PCS is a recompression S-CO_2 cycle developed at MIT under other NERI and direct Generation IV funding via Sandia National Laboratory. Each loop of the SCO_2 PCS is 265MWe (600 MWth) power corresponding to one intermediate heat exchanger. Brief description and a schematic of the PCS is provided in Section 3.4. Figure 6-5 shows the nodalization diagram of the PCS in RELAP5. Volumes 300 and 398 are the pressure and temperature boundary conditions of the cycle, since the cycle model was first generated and tested separately from the rest of the reactor systems.

The main components of the cycle shown on Figure 6-5 include turbine, compressors, high and low temperature recuperators, precooler, and shaft and generator. The PCS is split into four loops. However, for computational efficiency, the loops are lumped into two loops (2x2). Thus, loop 300 is identical to loop 400. The turbine represented by volume 315 is modeled with shaft speed of 3600 rpm and efficiency of 94%. The turbine is connected to the hot side of high temperature recuperator (HTR) shown as volume 330. The flow is then directed into the hot side of low temperature recuperator (LTR) represented by volume 340. Both HTR and LTR are modeled as heat exchangers with vertical semicircular channels. The diameter of the channels is 2 mm. In volume 345, the flow is split into two streams. 40% of the original flow is directed into the recompressing compressor 350. The other 60% is cooled in the precooler 360 to 32°C, after which it is pumped through main compressor 365. Precooler is a heat exchanger in

which the gas is the primary fluid on the tube side, and water is secondary on the shell side. The water flow is simulated by time-dependent volumes 600 and 620. The mass flow rate of water through a precooler is kept constant at 4625 kg/s, and the inlet temperature is assumed to be 20°C. Both compressors are modeled as homologous pumps. RELAP5/ATHENA code has a capability of modeling compressors with detailed performance curves. However, the band of operating conditions for the axial compressors is generally rather constricted which can result in flow surge or choke during transient simulation [Pope et al., 2006]. The transient resulting in choke or surge would immediately be stopped. This is the main reason for the approximation of compressors as homologous pumps. The model can be advanced with radial compressors which allow for wider operating range, but this is left for the future work.

Once disconnected from the grid, the turbine provides energy to drive compressors mounted on the same shaft and circulate CO_2 flow through the IHXs, making possible to remove significant power from the reactor vessel without electrical power supply. A proportional-integral (PI) controller can be used to periodically adjust valve position to maintain an acceptable turbine speed.

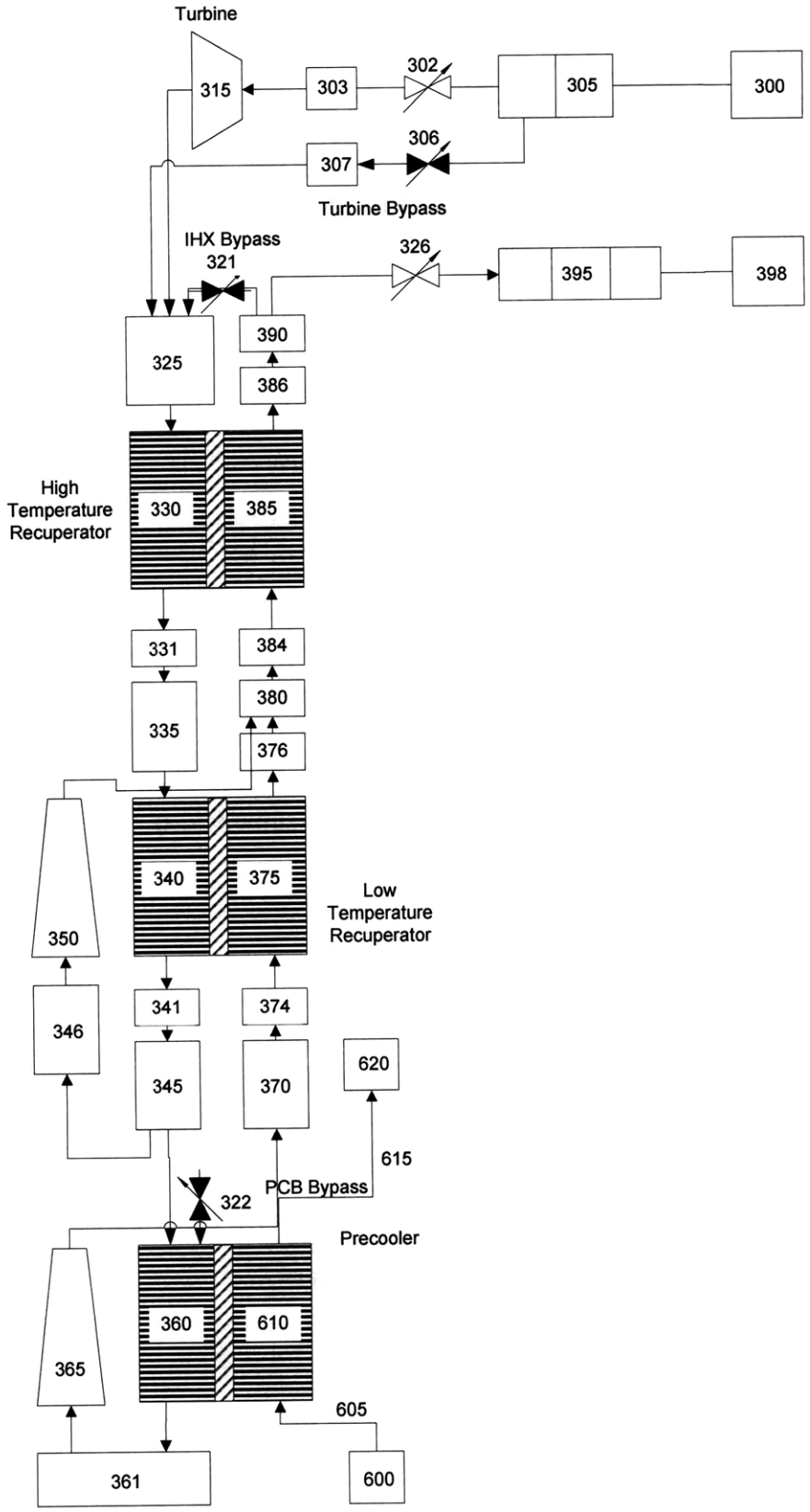

Figure 6-5. RELAP5-3D schematic of components and layout of PCS (with all bypass options shown)

6.7. RELAP5-3D Model of Reactivity Coefficients

The reactivity coefficients are an important factor in determination of the reactor power generation during transients. The reactivity can be adjusted manually using control rods. In addition, the reactivity can be influenced by change in the operating temperatures of the reactor. The change in temperature affects the density of the coolant, Doppler feedback, swelling of the fuel, core structures and control rod expansion or contraction, and neutron leakage.

Reactivity coefficients were determined using a quasi-static analysis. The quasi static approach to reactor safety was originally developed at Argonne National Laboratory in the framework of Integral Fast Reactor development [Wade and Chang, 1988]. The method suggests that the reactor can be considered passively safe if, as a result of any external reactivity insertion due to an accident, this reactivity will be compensated by a combination of the inherent reactivity feedbacks without crossing the safety limits on any of the core operating parameters. Extensive theoretical background of the method is provided in Wade et al. [1997]. In this section, the summary of the reactivity feedback model for RELAP5-3D is provided.

The reactivity coefficients were shown to be within the constraints of the self-controllability criteria. A more detailed description of core reactor physics analysis and self-controllability analysis are given in Hejzlar and Shwageraus [2008]. The values of the reactivity coefficients were incorporated into the RELAP5-3D model. Table 6-10 summarizes the reactivity feedback coefficients for lead-cooled unity and zero conversion ratio cores. The beginning-of-life values for the CR=0 and CR=1 cores are used because they constitute the worst case. Coolant density coefficients as well as fuel temperature (Doppler) coefficients are modeled as functions of density and temperature, respectively, and the example of input for the models for CR=1 core are shown in Table 6-11 and Table 6-12 and on Figure 6-6 and Figure 6-7.

Table 6-10. Summary of reactivity feedback parameters

		CR = 1		CR = 0			
	Units	BOL value	Error	BOC value	Error	EOC value	Error
β		0.0036	±0.0001	0.0029	±0.0001	0.0028	±0.0001
α_{DC}	¢/K	-0.111	±0.030	-0.016	±0.030	-0.041	±0.030
α_e	¢/K	-0.117	±0.026	-0.198	±0.034	-0.267	±0.043
α_{Co}	¢/K	+0.131	±0.052	-0.006	±0.044	-0.030	±0.038
α_{RD}	¢/K	~0	N/A	~0	N/A	~0	N/A
α_R	¢/K	-0.135	±0.013	-0.161	±0.032	-0.248	±0.043
A	¢	-22.92	±3.99	-21.57	±4.54	-30.95	±5.24
B	¢	-17.43	±2.43	-25.79	±2.75	-39.60	±5.08
C	¢/K	-0.23	±0.05	-0.38	±0.05	-0.59	±0.06
A/B		1.31	±0.29	0.84	±0.20	0.78	±0.17
CΔTc/B		1.27	±0.31	1.41	±0.24	1.41	±0.23
$\Delta\rho_{TOP}$/B		0.33	±0.05	0.98	±0.10	0.18	±0.02
A/B limits		x < 1.06 (1.59**)		x < 1.06 (1.59)		x < 1.06 (1.59)	
CΔT_c/B limits		1< x < 1.99 (2.39)		1< x < 1.99(2.39)		1< x < 1.99(2.39)	
$\Delta\rho_{TOP}$/B limits		x < 1.06 (1.59)		x < 1.06 (1.59)		x < 1.06 (1.59)	

Table 6-11. Density reactivity model for RELAP5-3D model for CR=1

T(°C)	Pb-Bi density (kg/m3) from RELAP	Fitted reactivity (pcm)[a]	Reactivity ($) with β=0.0036
300	10439.46*	1912.74	5.313
350	10345.42*	1948.10	5.411
420	10222	1992.30	5.534
450	10188	2009.35	5.582
495	10137	2032.79	5.647
519	10110	2044.25	5.678
534	**10093.24**	**2051.05**	**5.697**
547	10079	2056.71	5.713
568	10055	2065.40	5.737
581	10040	2070.50	5.751
600	10020	2077.57	5.771
650	9976.24*	2094.00	5.817
700	9932.94*	2107.29	5.854
800	9855.39*	2124.39	5.901
1000	9727.14*	2120.76	5.891
1500	9498.36*	1890.96	5.253

* Extrapolated linearly $\rho=14{,}591\cdot T^{-0.0587}$

[a] ρ=-6.3064E-04T^2+1.1170T+1.6344E+03

The reason the curves are used for coolant density and Doppler reactivity models rather than simple coefficients is the strongly non-linear dependence of the reactivity coefficients on temperature. As can be seen on Figure 6-6, the feedback is positive at nominal temperature but with decreasing slope as the temperature of the coolant increases. Hence the effect of the positive reactivity feedback of the coolant diminishes as the coolant heats up. On the other hand, the negative feedback of the fuel temperature is stronger when the temperatures are lower. Both effects result in very strong feedback when the core is cooled down. As is observed in Section 7.1.1, during unprotected station blackout accident, once the core is cooled to a temperature corresponding to peak cladding temperature of about 608°C, the restart of the reactor happens.

The core radial expansion and fuel thermal expansion effects are modeled with constant coefficients. The core radial expansion, Doppler, fuel thermal expansion, and coolant density coefficients are computed using the power squared weighting technique. The internal multipliers discussed in Section 6.2 are used to calculate the average temperature of the coolant and fuel or the averaged density which is further applied to the reactivity model.

Table 6-12. Fuel temperature reactivity model for RELAP5-3D model for CR=1

T (K) of fuel	Fitted reactivity	Reactivity ($) with β=0.0036
300	0.024361	6.767009
400	0.023472	6.519953
500	0.022671	6.297389
600	0.021958	6.099318
700	0.021333	5.925739
800	0.020796	5.776652
900	0.020347	5.652058
1000	0.019987	5.551956
1100	0.019715	5.476346
1200	0.019531	5.425229
1300	0.019435	5.398604
1400	0.019427	5.396471
1500	0.019508	5.418831
1600	0.019676	5.465683
1700	0.019933	5.537027
1800	0.020278	5.632864

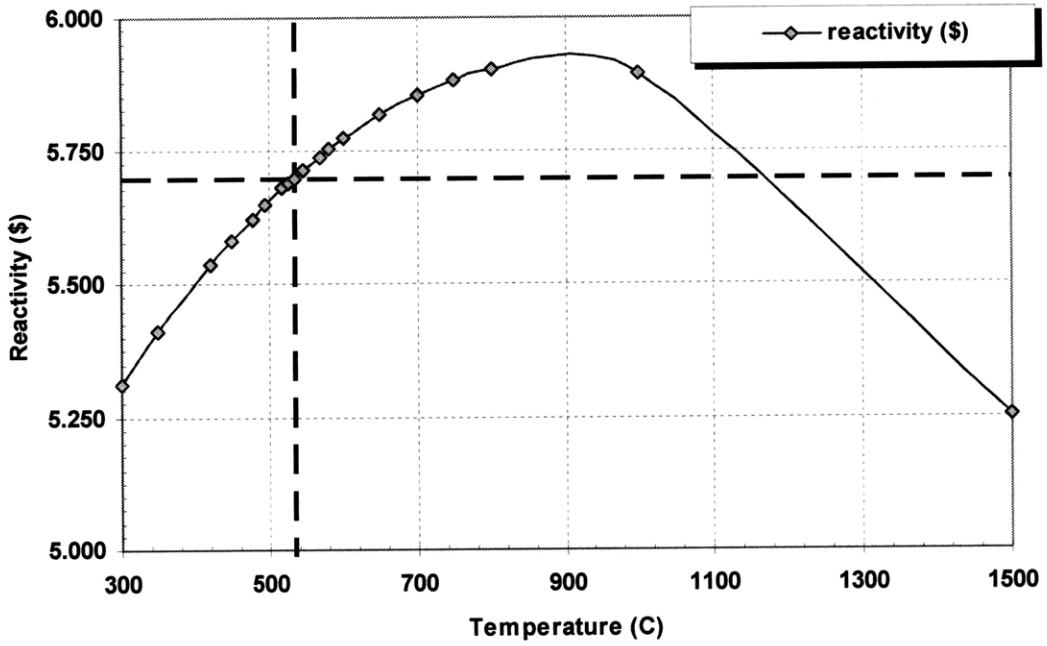

Figure 6-6. Reactivity ($) vs. coolant temperature.

Dashed lines represent steady state active core average coolant temperature (534°C) and corresponding reactivity

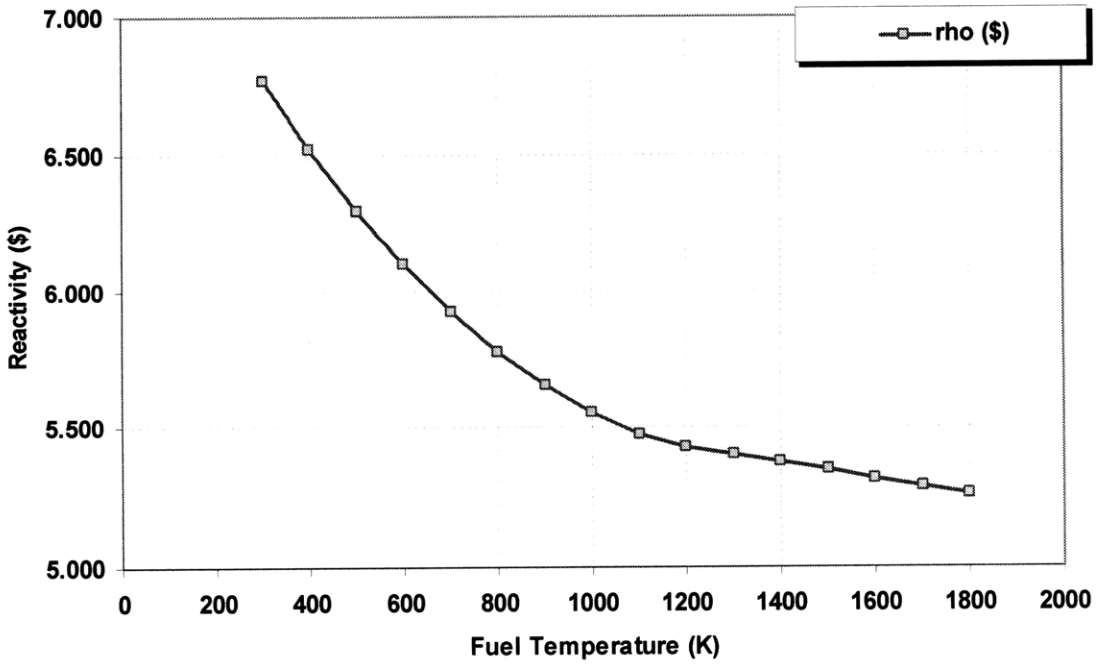

Figure 6-7. Reactivity ($) vs. fuel temperature

Neutronic analysis of both cores was done assuming All Rods Out (ARO) conditions. Therefore, the temperature dependence of Doppler and coolant density reactivity coefficients shown on Figure 6-6 and Figure 6-7 is several dollars. Although, the reactivity of the core for the steady state conditions is zero, this representation is fine for RELAP5-3D calculations since RELAP5-3D uses the deviation in reactivity from the nominal conditions as a function of either temperature or density to calculate the reactivity dynamics during transients. The ARO reactivity coefficients were used because they provide conservative results because: (1) coolant temperature coefficient is less positive for CRDs in and (2) power peaking is reduced through appropriate control rod insertion management.

6.8. References for Chapter 6

Hejzlar P., Davis C. B., "Performance of the Lead-Alloy-Cooled Reactor Concept Balanced for Actinide Burning and Electricity Production", *Nuclear Technology*, **147**, 3, pp. 344-367, September 2004.

Pope M.A., Hejzlar P., and Driscoll M.J.,"Thermal Hydraulics of a 2400 MW_{th} Supercritical CO_2-Direct Cycle GFR", MIT-ANP-TR-107, Center for Advanced Nuclear Energy Systems, Massachusetts Institute of Technology, 2006.

RELAP5-3D Code Development Team, RELAP5-3D© Code Manual Volume 1: Code Structure, System Models and Solution Methods, INEEL-EXT-98-00834-V1 Revision 2.3, Idaho National Engineering and Environmental Laboratory, 2005.

Shwageraus E., Hejzlar P., "Flexible Conversion Ratio Lead Cooled Reactor Design," International Conference on Reactor Physics, Nuclear Power: A Sustainable Resource, Interlaken, Switzerland, September 14-19, 2008.

Todreas N.E., Hejzlar P., Shwageraus E., Petroski R., Nikiforova A., Whitman J. and CJ Fong, "Flexible Conversion Ratio Fast Reactor Systems Evaluations", Final report, Center for Advanced Nuclear Energy Systems, MIT, MIT-NFC-PR-101, August 2008.

Wade, D.C., Chang, Y.I., "The Integral Fast Reactor Concept: Physics of Operation and Safety", *Nuclear Science and Engineering*, 100, 507-524, 1988.

Wade D.C., Wigeland R.A., Hill D.J., "The safety of the IFR", *Progress in Nuclear Energy*, Vol. 31, No. 1/2, pp. 63-82, 1997.

7. TRANSIENT ANALYSIS

The analysis of the reactor behavior during transients is an important part of the design. The reactor must demonstrate acceptable performance during a range of potential initiating events. Currently there are no regulatory requirements for the initiating events for fast reactors analogous to light water reactors. However, lead-cooled reactors are still vulnerable to a number of events similar to those common in LWRs. Such events include loss of offsite power, withdrawal of control rods, and failure of primary pumps. Because an aggressive safety goal of accommodating unprotected accidents in a self-controllable manner, as for the IFR design [Wade et al., 1997], was set for this project, the transients will be modeled with an assumption of failure to scram. Because of high melting point of lead coolant, protected station blackout accidents were also modeled to ensure that the reactor is capable of safe shutdown without freezing the primary coolant. Section 5.6 provides the overview of the comprehensive strategy for SBO transient management.

First, three unprotected accidents were analyzed: station blackout, unprotected primary coolant pump trip, and unprotected inadvertent reactivity insertion (unprotected overpower). The analysis of the reactor performance during transients allowed for determining whether the passive safety features of the reactor are adequate to ensure the core safety. The models used in the transient simulation are described in detail in Chapter 6. In all models, four IHX/PCS loops were lumped into 2x2 loops to reduce the computational time. The decay heat curves calculated specifically for TRU fuel were implemented in the RELAP5-3D model. The reactivity coefficients specific for each core were also incorporated into the model.

During station blackout accident, the main decay heat removal system is RVACS. As described in Chapter 4, an additional Passive Secondary Auxiliary Cooling System (PSACS), which assists RVACS, is needed to keep peak cladding temperature below the limits. In addition, heat removal capabilities of the power conversion system for unprotected loss of coolant accident were analyzed, and the turbine overspeed protection options were modeled. The overspeed protection options are discussed in Section 5.5.

Table 7-1 summarizes the initial conditions of the reactor at rated power. This chapter summarizes the main results and conclusions from the transient analysis.

Table 7-1. Initial conditions at full power

Primary coolant system	
Core power (MWth)	2400
Mass flow rate (kg/s)	173600
Core inlet temperature (°C)	479
Core outlet temperature (°C)	574
Maximum cladding temperature (°C) (CR=1/CR=0)	610/624
Maximum fuel temperature (°C)	725
Secondary system	
Pressure (MPa)	19.96
Mass flow rate (kg/s)	12848
Inlet temperature	397
Outlet temperature (°C)	548
RVACS	
Power removed (MW)	6.8
Air flow rate (kg/s)	79.1
Air inlet temperature (°C)	25.0
Air exit temperature (°C)	118.1
Maximum guard vessel temperature (°C)	430.0

7.1.Station Blackout Accident

The safety approach of the FCR reactor is based on the defense-in-depth philosophy which includes multiple barriers to a radiation release during an accident. In addition, the reactor systems are designed not to exceed structural limits using passive means for reactor shutdown and cooling even during unprotected accidents such as LOFA or UTOP. The unprotected SBO accident is considered to be the limiting event in terms of its severity because:

- Loss of forced circulation as reactor coolant pumps trip due to loss of AC;
- Loss of AC causes loss of precooler pumps;
- Generators are isolated from the grid due to loss of load;

- The reactor fails to scram and therefore must shut down due to negative reactivity feedback.

The accident was initiated at 0.0 seconds. During an SBO, the PSACS isolation valves fail open and the PCS isolation valves fail closed. The purpose of the turbomachinery isolation is twofold: the gas must be directed through the PSACS equipment to remove as much heat as possible, and to prevent the turbine rotational overspeed that would result in turbine and compressor blade damage. In this case, when the power conversion system is isolated, the IHX bypass valves open to prevent flow stagnation in the loop. In the RELAP5-3D model described in Chapter 5 the PCS was isolated at the beginning of the accident. Thus, in order to simplify the model and to reduce computational time, the PCS was modeled as time-dependent boundary conditions. Because the PCS is not part of the SBO accident sequence, such simplification does not have any effect on the results of this transient.

The PSACS and PCS valves are not operational during an SBO; their actuators are held closed (PSACS) or open (PCS) during normal operations by solenoid or instrument air. An SBO causes a complete loss of the onsite and offsite AC causing the valves to de-energize and fail to their appropriate positions via stored potential energy. The PSACS design and function was described in Section 5.3 and will not be repeated here. Current regulations (10 CFR 50.63) require a SBO mitigation strategy of up to 8 hours. Future reactor designs such as AP1000 and ESBWR have 72 hour SBO mitigation strategies allowing for the elimination of safety-related emergency diesel generators. Seventy-two hours is a time typically considered for sufficient recovery of onsite or off-site AC power and was therefore adopted for this analysis.

The PSACS-Water version consists of four trains (4x50%), each for one intermediate heat exchanger as shown on Figure 7-1. Operation of only two trains should be sufficient for satisfactory performance during the station blackout accident. This fact was taken into account when the design parameters were calculated. The integrated layout of the

primary and secondary (PCS and PSACS) reactor coolant systems and RVACS is shown on Figure 6-1.

In the initial analysis, the ANS-79 standard decay heat curve available in RELAP5-3D had been used before decay heat curves specific for FCR core designs were developed. The ANS-79 decay heat curve includes only four fissionable nuclides: U-235, U-238, Pu-239, and Pu-241. However, the FCR reactor cores contain TRU fuel with a variety of actinides (Pu, Am, Cm, Np) that uniquely determine the amount and variety of the fission products generated, resulting in significant differences in decay heat. Figure 7-2 compares the decay heat generated by the CR=1 and CR=0 TRU cores with the ANS-79 standard. As can be observed, the CR=1 core is the limiting case with respect to peak cladding temperature due to its higher decay heat generation rate. Moreover, it has inferior reactivity feedback coefficients in comparison with the CR=0 core. On the other hand, the CR=0 case is more vulnerable to coolant freezing if all PSACS trains operate during protected SBO. More details on the decay heat curve calculation can be found in Todreas et al., [2008].

The response of the FCR CR=1 reactor to the station blackout accident with the ANS-79 decay heat curve standard and with the BGCORE*-generated decay heat curve for the same PSACS design is presented in Figure 7-3. The considerable increase in the amount of the decay heat generated necessitated a redesign of the PSACS. First, the increase in the net amount of the decay heat generated required additional water in the PSACS water tank. Second, the PSACS heat exchanger size was adjusted to obtain the desired heat removal rate. Figure 7-4 depicts peak cladding temperature for both cores. Two peaks can be observed: the early peak around 2-3 hours and the delayed peak around 50 hours after the accident was initiated. The first peak is controlled by the rate at which PSACS removes heat from the primary system. The second peak is the equilibrium point between the heat generated by the core and the heat removed by the RVACS. However,

* BGCore code [Shwageraus et al., 2006; Fridman et al., 2008] was developed for the neutronic analysis of reactor systems. BGCore couples the continuous energy Monte Carlo particle transport code MCNP-4C with the decay and burnup module SARAF.

the second peak depends also on the amount of water in the PSACS tank. Note that the minimum in peak cladding temperature corresponds to the time of isolation of the PSACS or complete evaporation of water. The final design parameters calculated after the actual decay heat curve was implemented and the PSACS was redesigned are presented in Table 5-1. The RELAP5-3D model of the PSACS is described in detail in Chapter 6.

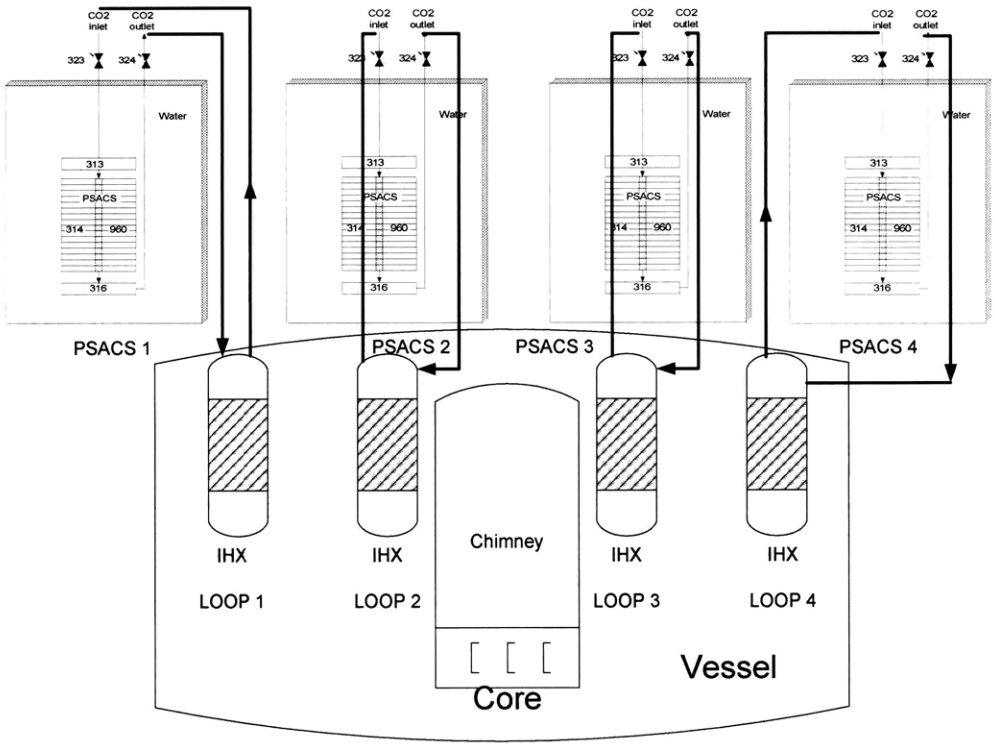

Figure 7-1. Relative layout of the reactor and PSACSs

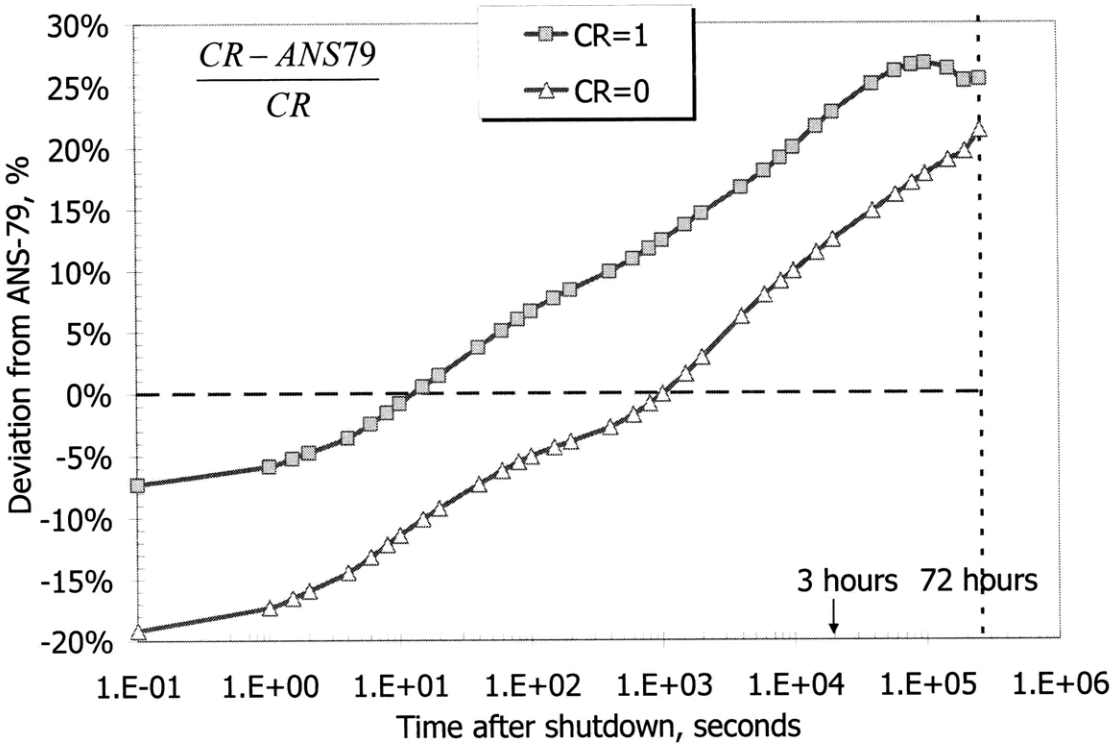

Figure 7-2. Decay heat generation rate deviation (%) from ANS-79 decay heat curve

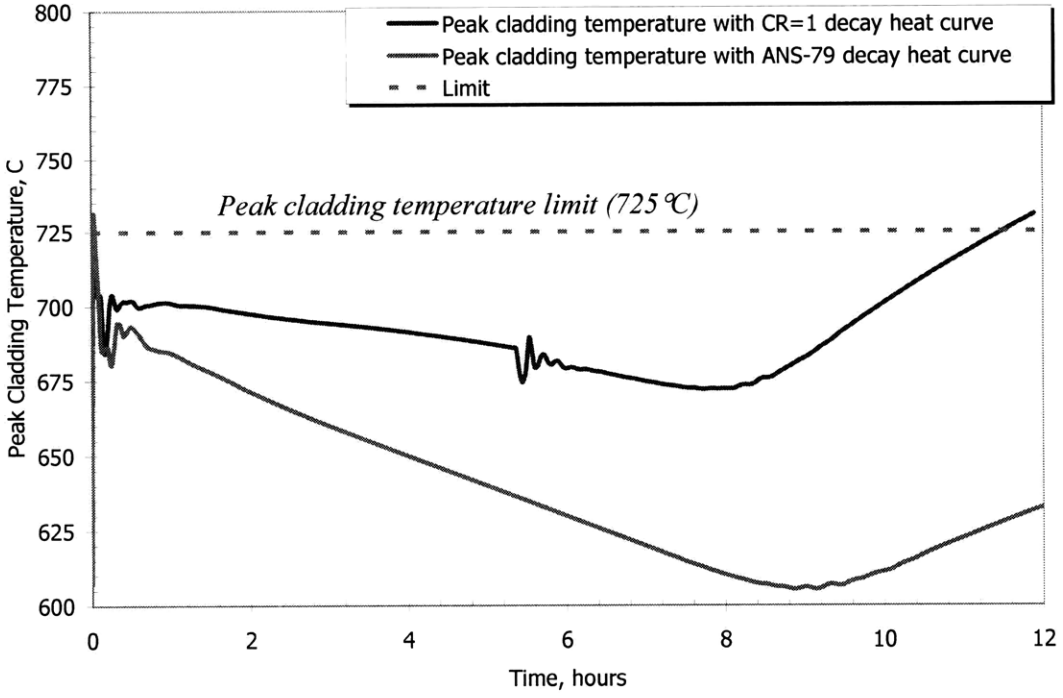

Figure 7-3. Comparison of peak cladding temperature for CR=1 core with different decay heat curves

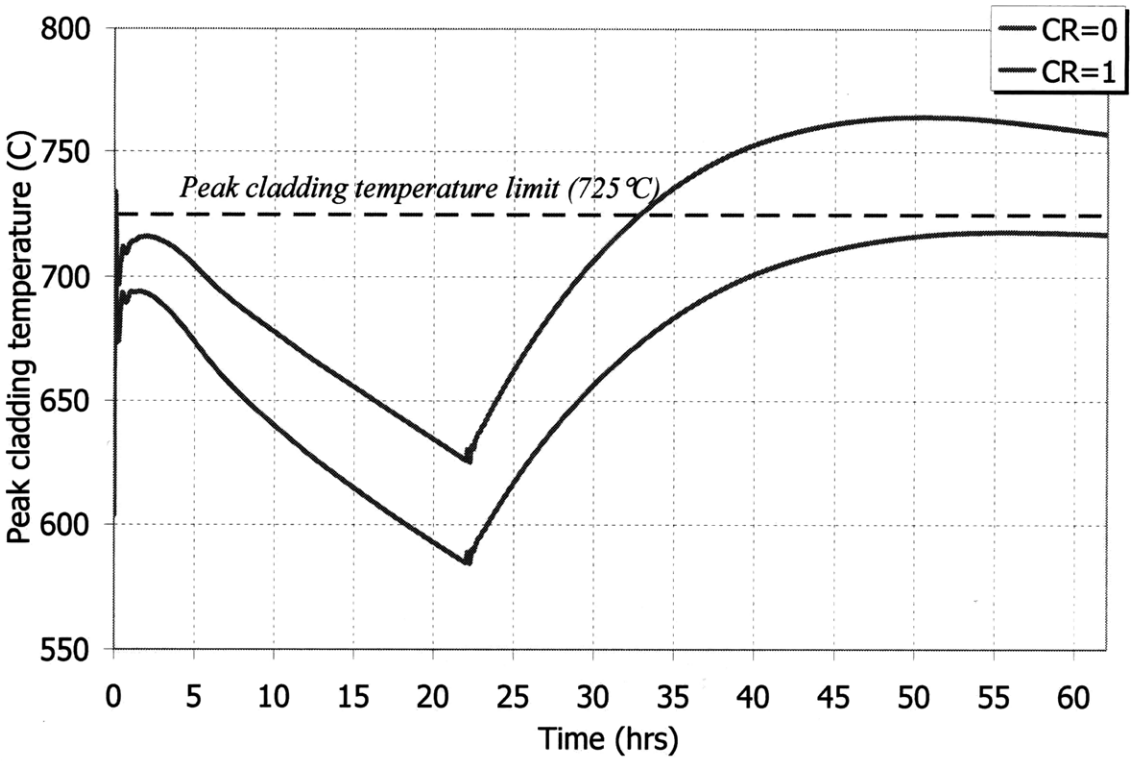

Figure 7-4. Peak cladding temperature during an unprotected SBO accident

One of the design goals of the FCR reactor is its ability to undergo inherent shutdown due to reactivity feedbacks. However, if the temperatures of the fuel, coolant and structures become low enough to result in zero or positive reactivity, the reactor restarts itself, causing temporary power increase and associated temperature rise, which leads to a new equilibrium after minor oscillations. Therefore, the PSACS heat exchanger would ideally have to be designed such that the peak cladding transient limit temperature is not exceeded and at the same time its heat removal rate is sufficiently low to avoid achievement of low temperatures at which the reactivity becomes positive. For the zero conversion ratio reactor, the PSACS size that ensured smooth reactor shutdown without restart and PCT temperature below the limit of 725°C was identified.

However, it turned out to be difficult to size the PSACS heat exchanger for the CR=1 concept. Low heat removal rate leads to early peak cladding temperatures above the limit, since the high decay heat generation rate at the beginning of the transient cannot be accommodated. On the other hand, if the heat exchanger size is too large, PCT will rapidly decrease leading to reactor

restart or coolant freezing in case of protected accident. Figure 7-5 illustrates the case when the PSACS heat exchanger is too large. The decay heat is rapidly removed from the primary system causing the coolant and fuel temperatures to drop below the point at which the reactivity becomes positive. Once the temperature of the primary system becomes too low, reactivity increases, resulting in power rise and low power oscillations. But even if one could find the right size of the PSACS to accommodate both conversion ratio cores, it would be difficult to size the PSACS HX for different numbers of operating loops (note that there are 4x50% PSACS loops) and avoid reactor restart. This is because there is no guarantee a priori how many PSACS loops will be operating (2x50%, 3x50% or 4x50%). Note from the Figure 7-5 that there is much additional power to be removed in case the reactor restarts. The additional power will result in faster evaporation of water from the PSACS tanks. On the other hand, the strategy discussed in Section 5.6 identified a major concern with coolant freezing in case of a reactor scram. In fact, since the unprotected accidents are beyond design basis, the coolant freezing in case of three or four operating PSACS trains in SBO with scram poses significant challenge to PSACS design. The PSACS can be designed such that cladding damage can be avoided in unprotected accidents by adding enough water in the PSACS water tank, but such a design can be counterproductive in much more likely accidents with scram. Thus, there are three PSACS design constraints assuming that the reactor restart due to positive reactivity is acceptable and does not pose safety concerns:

(1) PCT during the first peak, which depends on PSACS heat exchanger size, needs to remain below the PCT limit,
(2) PCT during the second peak, which depends on the RVACS performance, but also on the amount of water in the tank, needs to remain below the PCT limit,
(3) Coolant freezing, which can be a result of primary system overcooling during protected accidents when more than two PSACS trains are operating, should be prevented.

To satisfy all three constraints is not an easy task. Several configurations of the PSACS were considered. However, due to the complexity of the problem, no satisfactory results were obtained. The operating "window" for the PCT is slightly over 100°C (PCT is constrained by a 725°C upper limit and ~605°C lower limit to prevent reactor restart) which is not enough to

handle this type of accident. Protected accidents are easier to handle since they do not result in reactor restart, and the operating temperature window is between 725°C for peak cladding and 327°C for minimum coolant. However, because of the lesser amount of heat generated, the cooling with PSACS occurs at a higher rate than in unprotected accidents. Considering the additional issue of accommodating operation of different number of PSACS trains, a new strategy for the unprotected station blackout accident, described in Section 5.6, was devised.

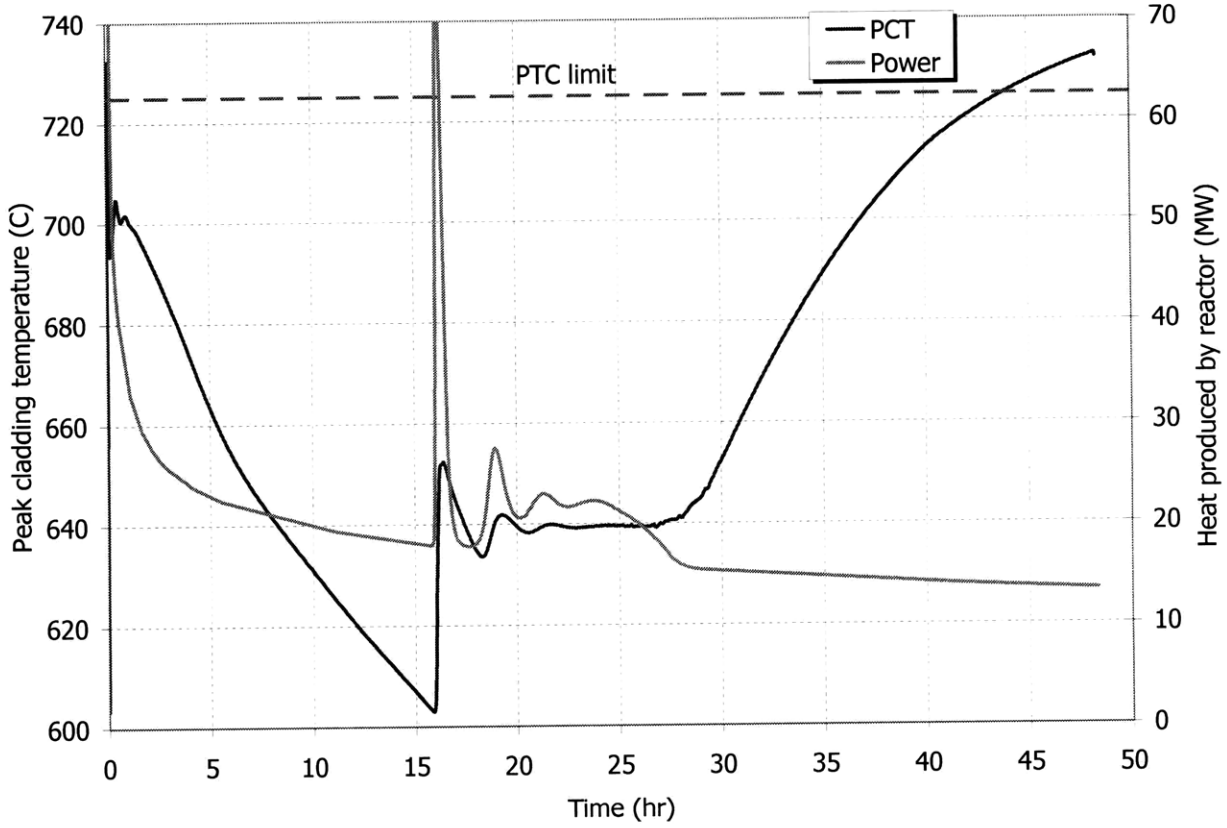

Figure 7-5. PCT response for a case of large size of PSACS heat exchanger

7.1.1. Results for Unprotected Station Blackout for CR=1 core

The unprotected station blackout exhibits first an overall primary system temperature increase since the heat generation exceeds the heat removal by RVACS and PSACS. The amount of heat that can be removed through PSACS depends on two parameters: the size of the gas-to-water heat exchanger and the amount of water in the PSACS tank. After reactivity feedbacks from increased core temperatures shutdown the reactor, RVACS plus PSACS heat removal exceeds

decay power, which results in reactor cooling until reactivity reaches zero and the reactor restarts at low power. Once the reactor restarts, core power settles at a level equal to the heat rate that the PSACS plus RVACS can remove together. This causes increased water evaporation from the PSACS tank and faster tank depletion. Figure 7-6, plots the peak cladding temperature for the case of 2x50% PSACS trains and 4x50% PSACS trains operating. For both cases, the PSACS water tank was increased to 16 m in height and 8 m in diameter in order to accommodate the additional heat generated from reactor low-power restart. The heat exchanger has 350 four-meter-long tubes.

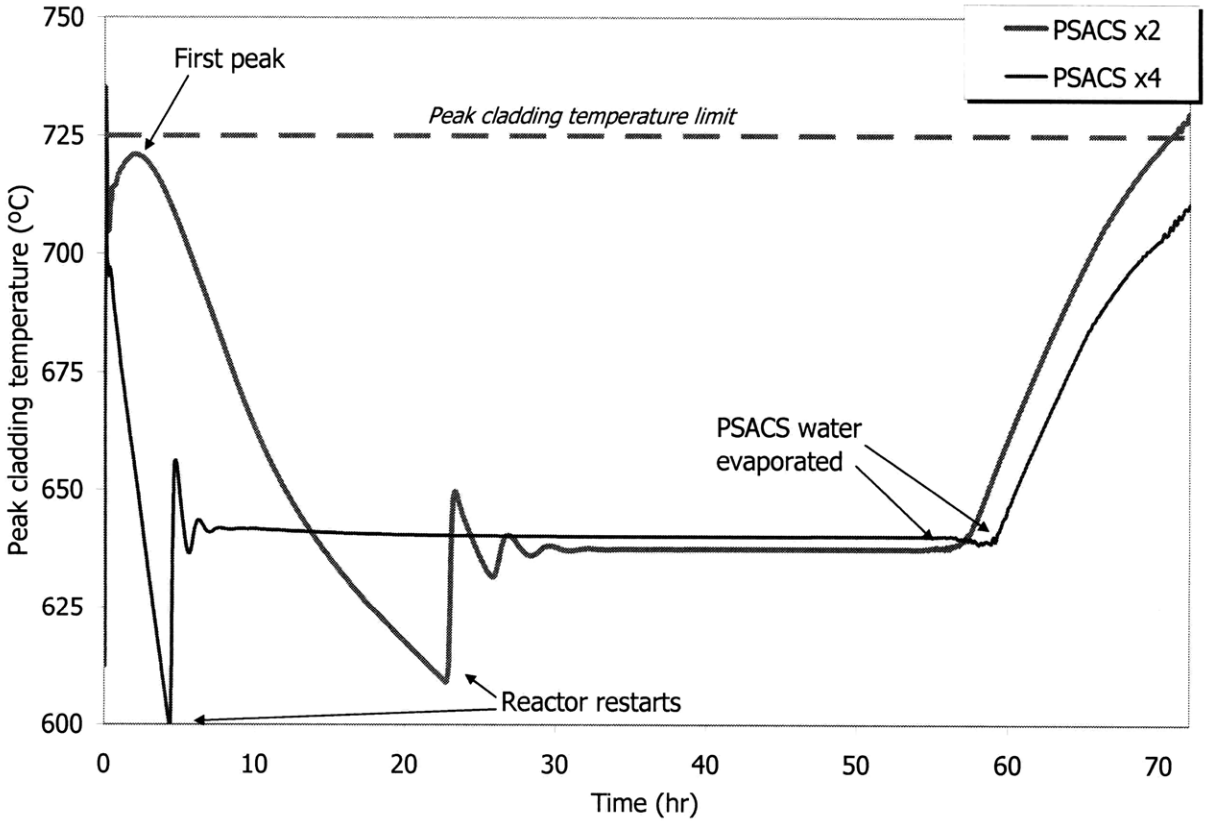

Figure 7-6. Comparison of PCT for PSACSx2 and PSACSx4 cases

This example illustrates the effect of the number of PSACS trains operating on the peak cladding temperature. The decay heat can be handled by only two trains, but PCT results for four operating trains are similar because of extra heat generated due to reactor restart. Both cases show complete PSACS water evaporation at 55-60 hours. The heat exchanger size was decreased to the smallest size for which the first PTC peak does not exceed the 725°C

temperature limit. The small size of the heat exchanger allows for a slow cool down of the system, while the large size PSACS water tank increases the time to evaporate the PSACS tank water. Slow cool down is favorable because of delayed reactor restart and is necessary for the protected accidents because of possibility of coolant freezing further discussed in Section 7.1.3.

The first peak occurs at ~3 hours into the accident. The restart for the PSACS x2 case happens at ~22 hours, while the restart for the PSACS x4 case happens much earlier at ~4.5 hours. This difference arises from a faster primary system cool down of the x4 case causing earlier reactor restart. The reactivity for both cases is illustrated on Figure 7-7. It can be observed that the reactivity becomes positive at ~2.7 hours for PSACS x4 case and at ~14.6 hours for PSACS x2 case. This is because of the decrease of core temperatures which inserts reactivity due to net negative reactivity feedback. Comparison of Figure 7-7 with Figure 7-8 shows that there is a significant delay between the time when reactivity exceeds zero and reactor restart. This is because the model did not consider neutron source from spontaneous fissions and fission reactor power exhibited an extremely small value after prolonged reactor shutdown, resulting in a negligible fission power increase in comparison to decay heat until positive reactivity increased sufficiently to cause visible fission power increase.

Figure 7-8 and Figure 7-9 illustrate the heat added to or removed from the primary system for the case with two and four operating PSACS trains, respectively. Both figures are consistent with observations from Figure 7-6. While the case with 4x50% trains has twice the water mass in the PSACS tanks than the 2-train case, the restart results in a significantly higher peak and equilibrium power to be removed from the primary system. While the power for the PSACS x2 case settled at ~19 MWt, the x4 case reached equilibrium at 30 MWt. This difference is a consequence of the different power from which initial restart occurs and of different primary system temperatures prior to restart. It can be observed that the cores of the x2 and x4 cases restarted from power of ~16 and ~24MWt, respectively. Lower temperature at the time of restart results in larger power peak because of more negative net reactivity feedback (and thus larger positive reactivity insertion on cooldown).

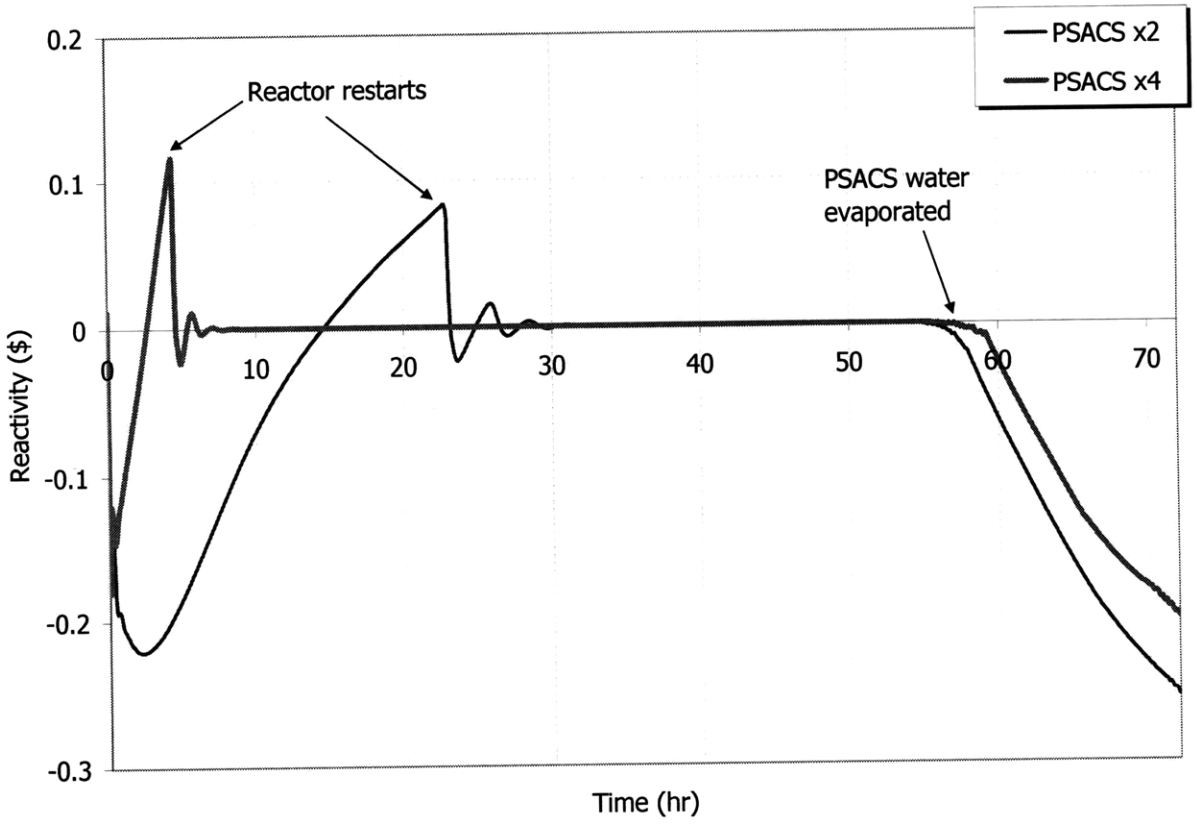

Figure 7-7. Reactivity during unprotected SBO for two and four trains of operating PSACS

Figure **7-10** shows the difference between the core power and heat removed through PSACS (x2 and x4) and RVACS during the unprotected SBO. The equilibrium discussed earlier corresponds to the balance between heat generated by the core and removed by PSACS and RVACS together. The net heat balance drives the PCT response observed on Figure 7-6. It is also noted that the heat balance and PCT trend suggest that the PCT would exceed the 725°C limit after 72 hours. Because 72 hours is the sufficient time window for restoring AC power or initiate other corrective action, this overshoot beyond 72 hours is not of concern.

Figure 7-11 shows peak vessel reactor and guard vessel temperatures. The limit for peak vessel membrane temperature is 700°C. For the case of two PSACS operating, the first peak reactor vessel temperature is 656°C occurring around 2.5 hours. The maximum peak vessel temperature of 670°C happens at 72 hours and would be increasing further if the transient was not terminated. The case with four operating PSACS trains illustrated on Figure 7-12 is not limiting with the first peak reactor vessel temperature of 615°C taking place around 0.4 hours.

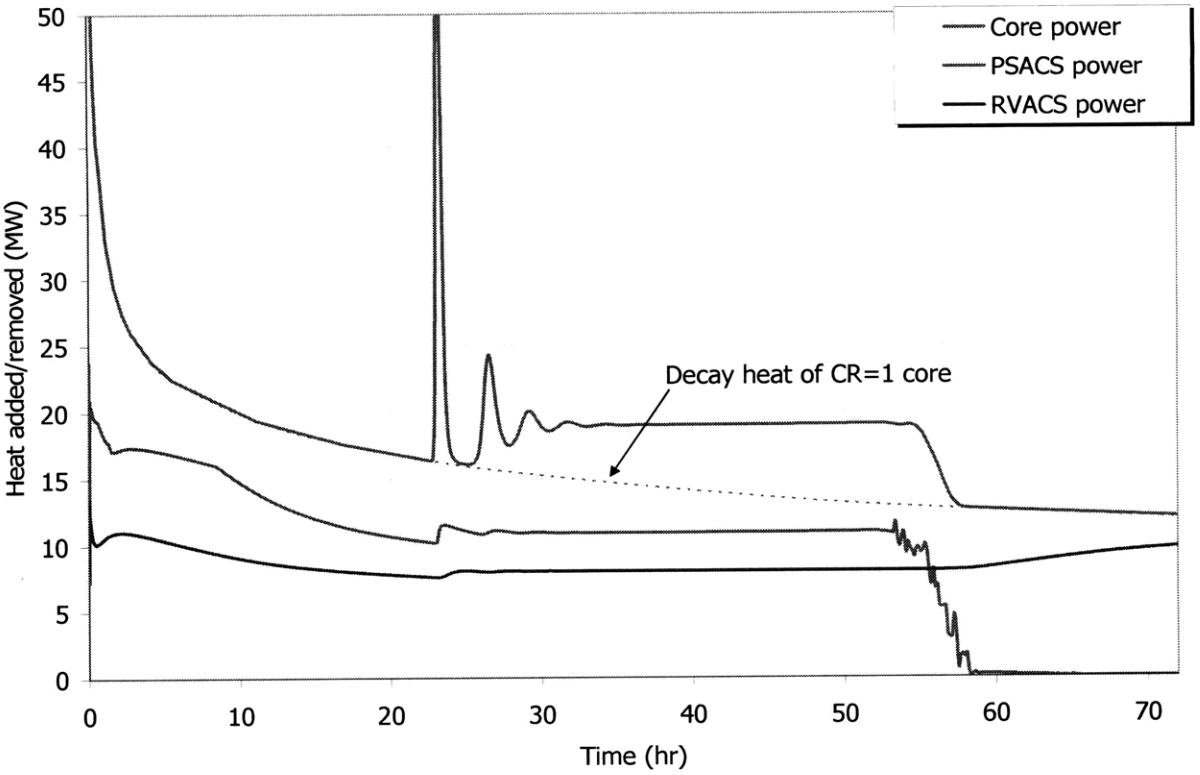

Figure 7-8. Heat added/removed during SBO with two operating PSACS trains

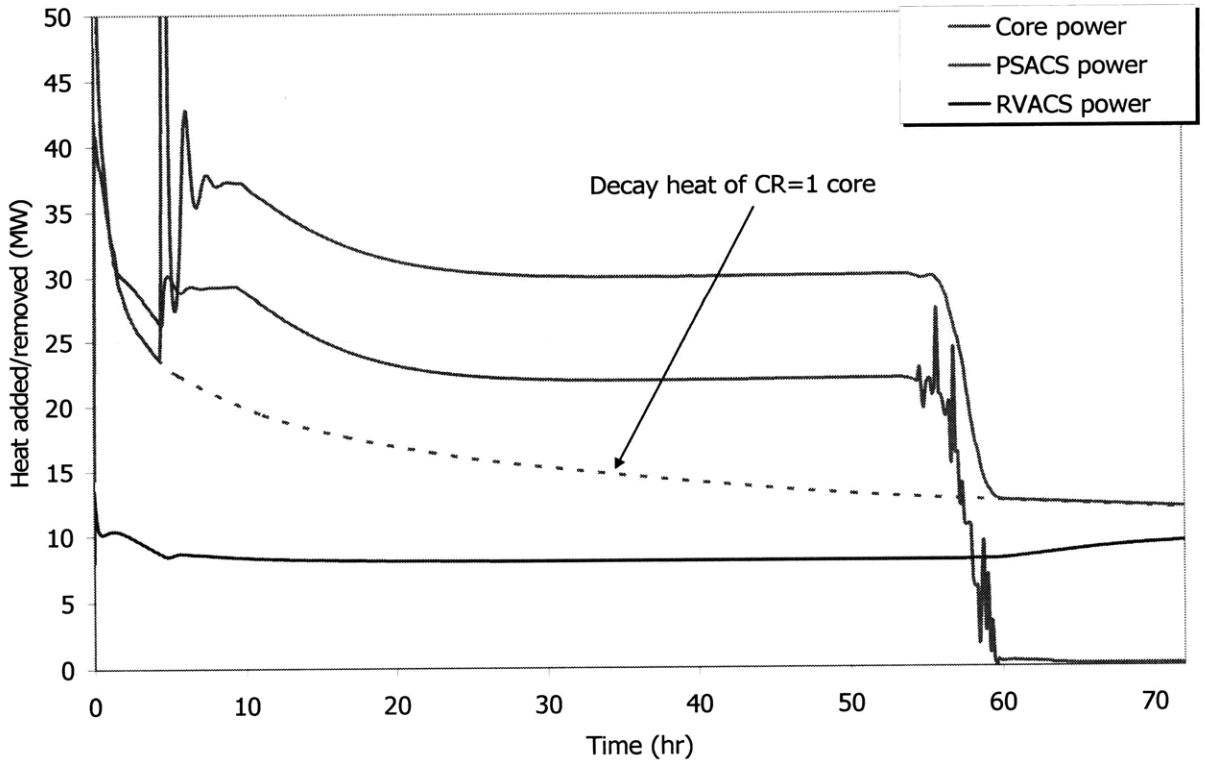

Figure 7-9. Heat added/removed during SBO with four operating PSACS trains

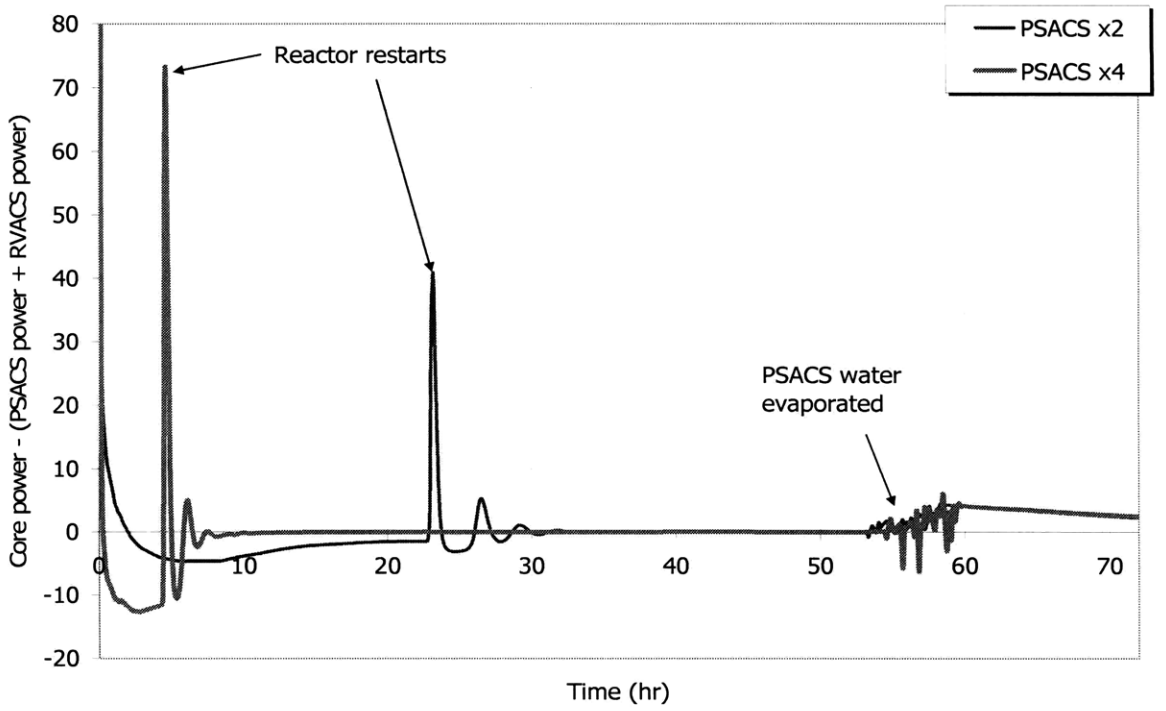

Figure 7-10. Difference between the core power and heat removed through PSACS (x2 and x4) and RVACS during unprotected SBO

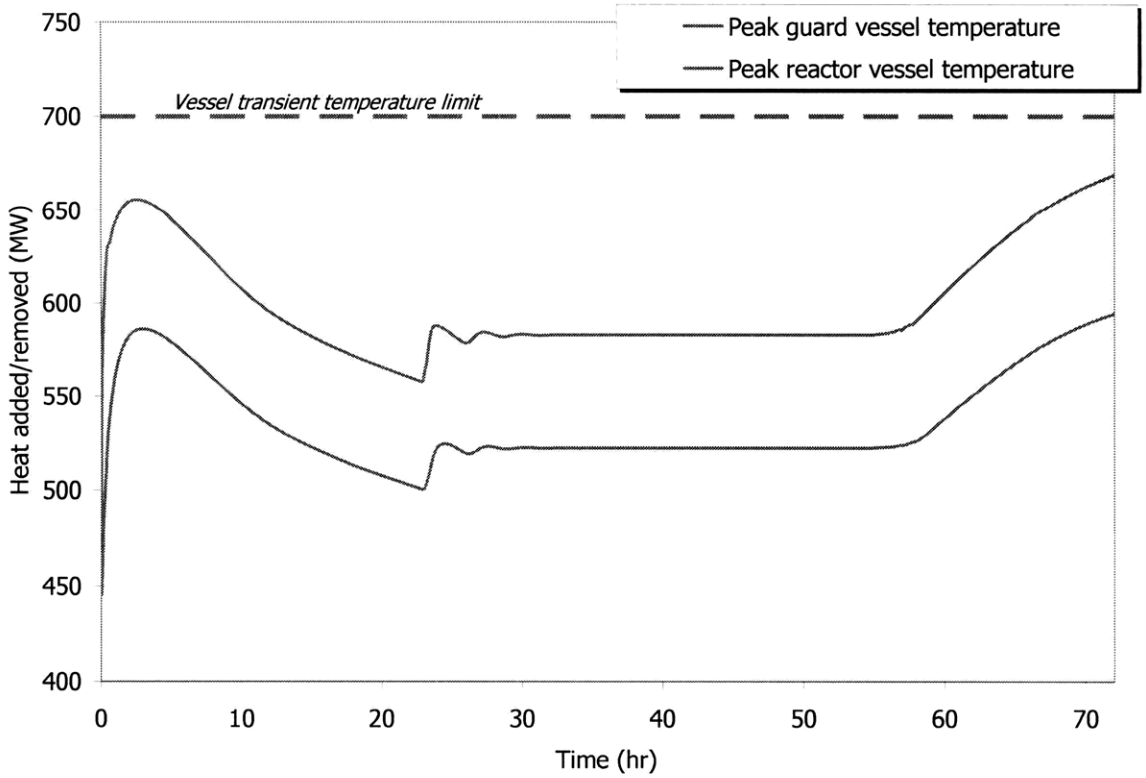

Figure 7-11. Peak vessel membrane temperature for unprotected SBO with two trains

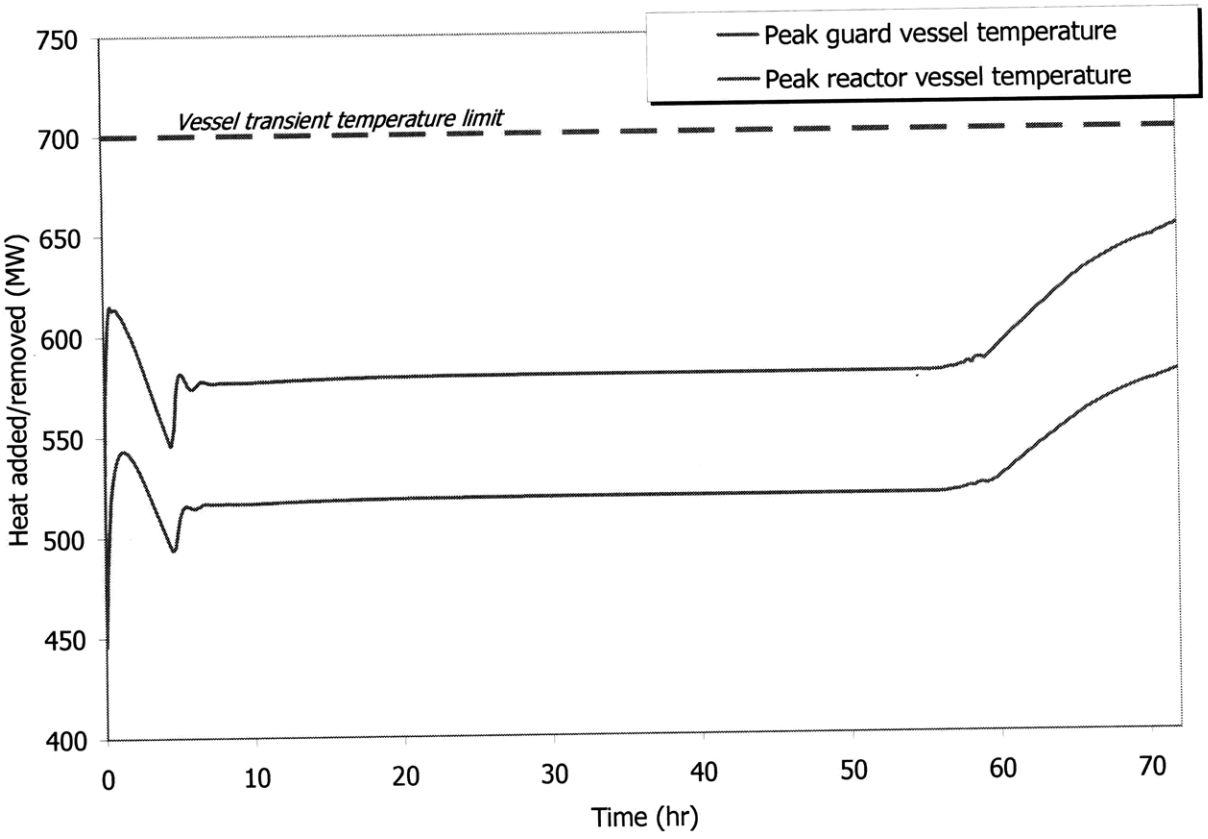

Figure 7-12. Peak vessel membrane temperature for unprotected SBO with four trains

7.1.2. Results for Unprotected Station Blackout for CR=0 core

The unprotected station blackout accident for the zero conversion ratio core is similar to unity conversion ratio core case. Two fundamental differences between the two cores are decay heat generated after shutdown and the reactivity coefficients. Since the decay heat generated by CR=0 core is less than for CR=1, the case is easier to manage during the SBO transient. The difference in reactivity coefficients is reflected in the magnitude of the power oscillations and how quickly the oscillations come to equilibrium.

Figure 7-13 shows the results for peak cladding temperature for the CR=0 core with two out of four operating trains of PSACS. The first peak in PTC occurs at 1.8 hours and is equal to 694°C. It occurs earlier than for the CR=1 core, and the magnitude is smaller in spite of higher peak cladding temperature during steady state full power operation. This phenomenon can be explained by difference in reactivity coefficients. Figure 7-14 compares reactivity for both

cores. The reactivity of the CR=0 core reaches the minimum quicker which is reflected in earlier peak. However, the duration of positive reactivity for the CR=0 core is ~7 hours while for the CR=1 core is ~8.6 hours. Therefore, the maximum peak cladding temperature for the CR=1 core is higher than for the CR=0 core.

Figure 7-15 and Figure 7-16 show the heat balance for the zero conversion ratio core. The reactor restarts around 21.4 hours with the core power peak of 64 MW. The magnitude of peak power for the CR=1 core is 60 MW. The magnitude of the restart is largely affected by the reactivity. The power equilibrated at 19 MW which is comparable to the CR=1 case.

Finally, Figure 7-17 illustrates the peak membrane temperature for the CR=0 core. The maximum peak membrane temperature for reactor vessel is 631°C occurring around 2.3 hours. The temperature is smaller when compared to the CR=1 case which expected since the overall system temperatures are lower for the CR=0 core during the unprotected SBO transient.

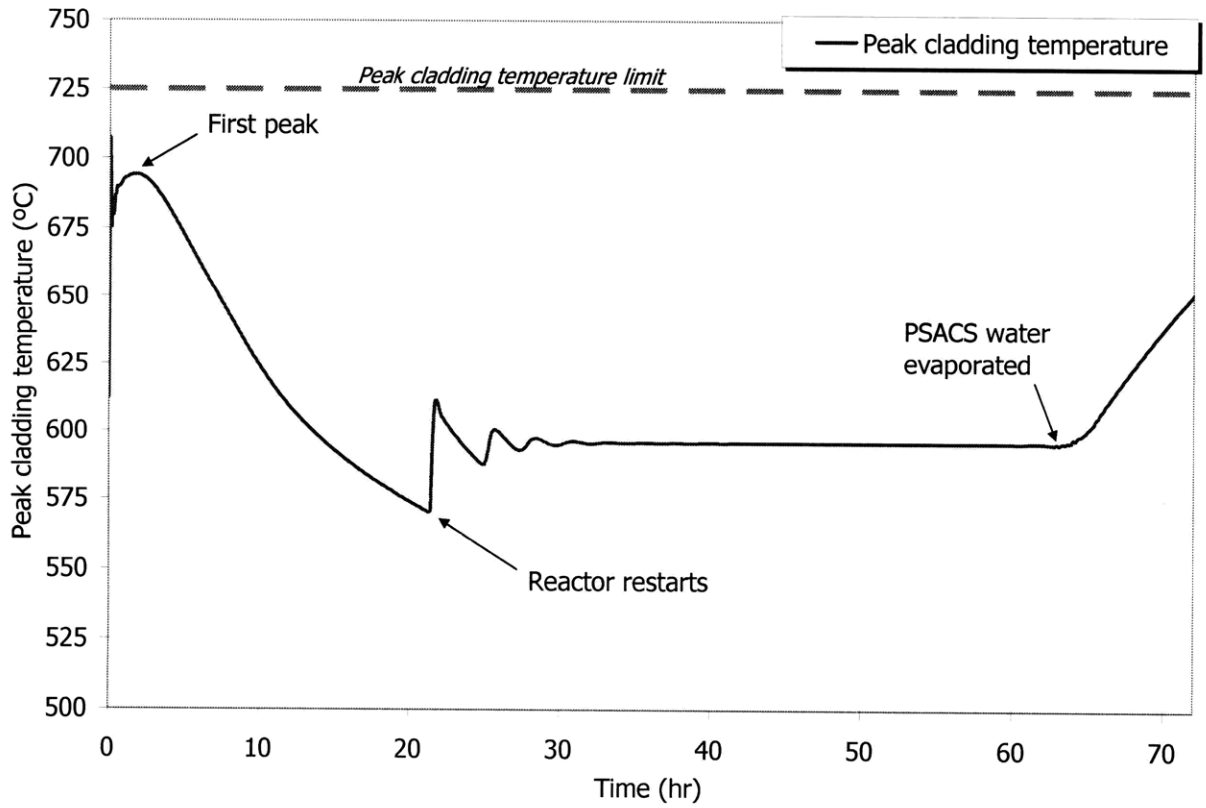

Figure 7-13. Peak cladding temperature for unprotected PSACSx2 case for the CR=0 core

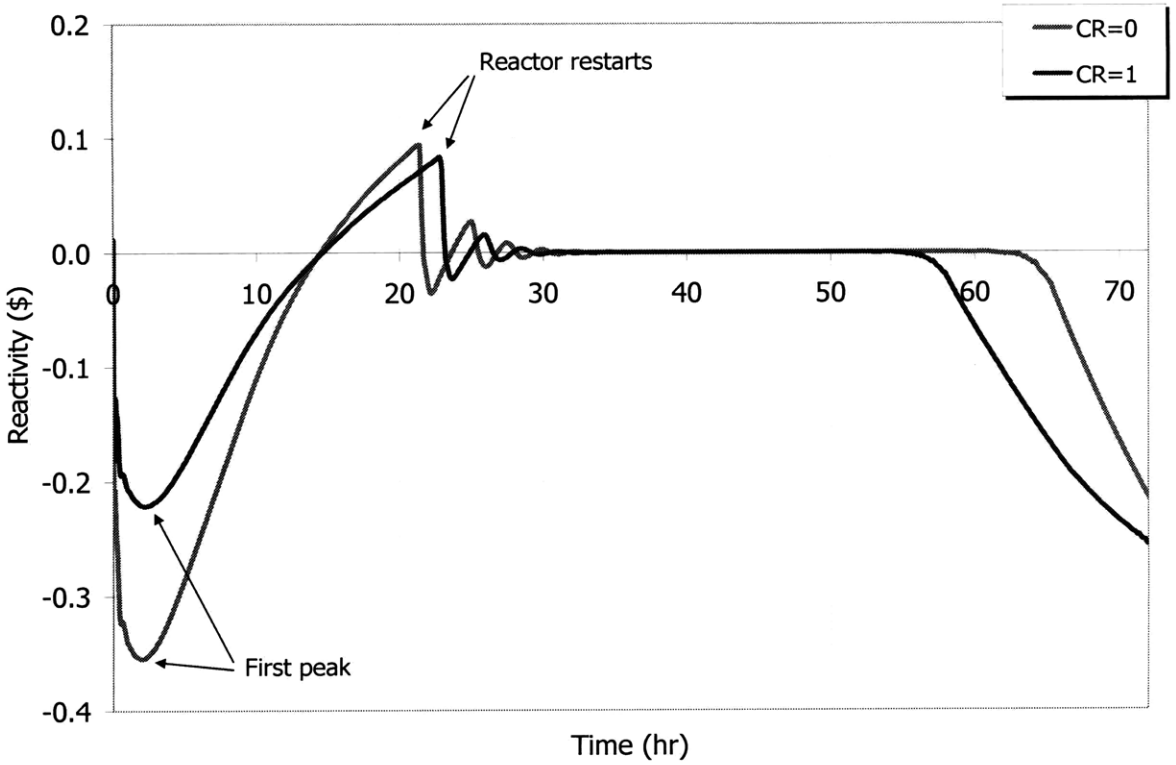

Figure 7-14. Reactivity during unprotected SBO for the CR=1 and the CR=0 cores for two trains of operating PSACS

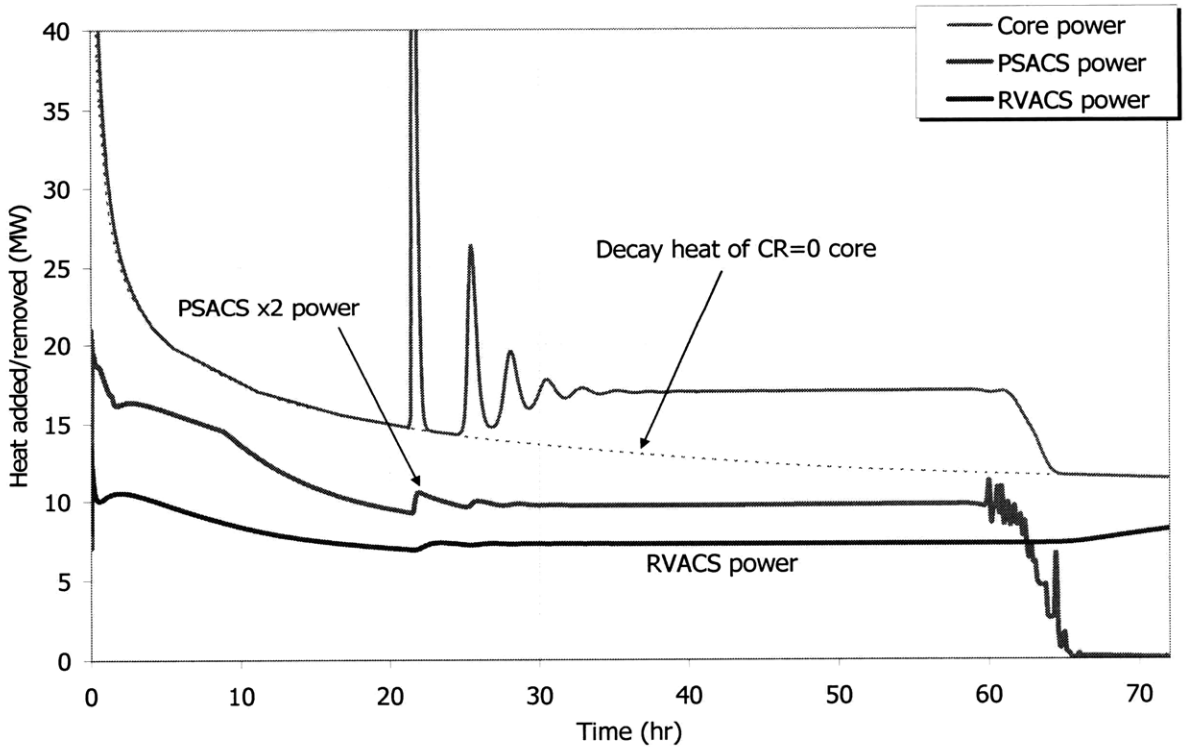

Figure 7-15. Heat added/removed during SBO with two operating PSACS trains for the CR=0 core

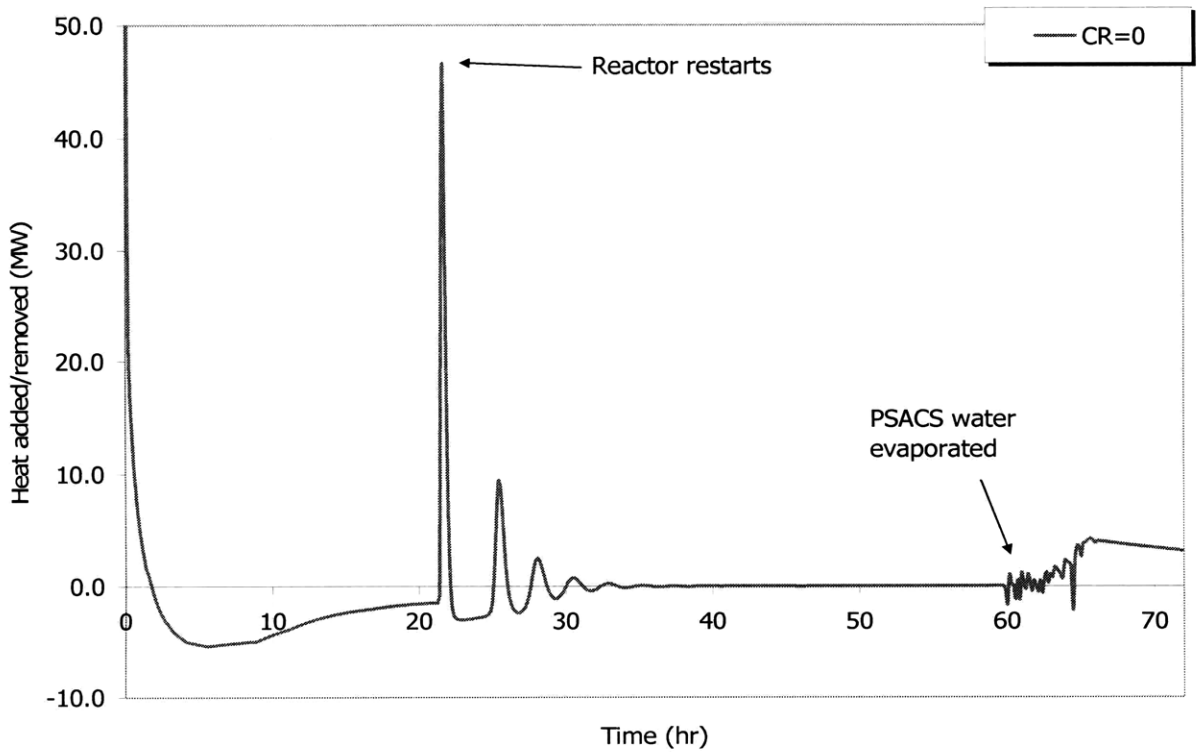

Figure 7-16. Difference between the core power and heat removed through PSACS and RVACS during unprotected SBO with two PSACS trains for the CR=0 core

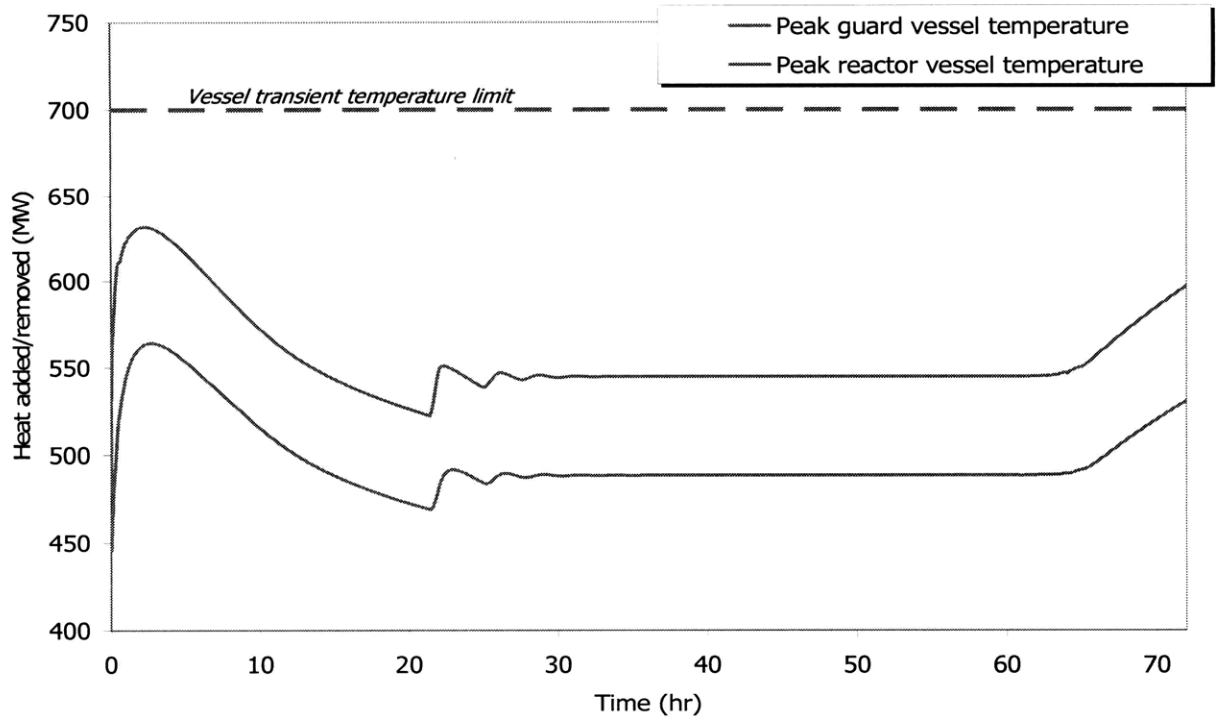

Figure 7-17. Peak vessel membrane temperature for unprotected SBO with two PSACS trains for the CR=0 core

7.1.3. Results for Protected Station Blackout for CR=1 core

As discussed in Section 5.6, the protected station blackout accident poses the concern of coolant freezing in case of system overcooling. Since any number of PSACS train between 2 and 4 can be operating, the PSACS design must ensure that freezing is avoided regardless of the number of the PSACS trains operating. Therefore, the PSACS water tank size has to be sufficiently large to assure enough water to keep PCT below its 725°C limit, but not too large to avoid coolant freezing. In addition, PSACS heat exchangers need to be selected to keep PCT below the limit during the first peak of unprotected SBO, but minimize cooling rate after reactor shutdown.

For the unprotected SBO case, the peak cladding temperature is bounded by the configuration of two operating trains. On the other hand, the limiting case for coolant freezing is a more likely event for the protected SBO (with scram) when all four PSACS trains are operating. This limiting case is described in this section.

Figure 7-18 shows the peak cladding temperature for the case of 4 operating PSACS trains. Because the reactor was scrammed, the PCT during the first peak is not a concern. Figure 7-18 also shows the minimum coolant temperature which remains above freezing for the entire duration of the accident. Because coolant freezing is prevented with all four trains operating, it can be concluded that freezing will not occur in case of two or three operating PSACS trains. This is because heat removed from the core is smaller for 2 or 3 trains operating than for the bounding case of 4 trains.

The heat generated (decay heat) and heat removed from the primary system through the PSACS and RVACS is shown on Figure 7-19. A more illustrative figure of merit showing difference between core power and total heat removed through PSACS and RVACS is depicted on Figure 7-20. The difference between heat produced by the core and heat removed by the safety systems (MW) explains the behavior of the primary system temperature. When the difference is positive, the temperature increases and vice versa. The difference becomes negative around 0.8 hours (~2900 seconds) causing the temperature to peak. The difference remains negative throughout the rest of the transient which is reflected in consistently decreasing temperature. Figure 7-21

shows the peak reactor and guard vessel temperature for the protected SBO with four trains. The reactor vessel temperature is always below the limit of 700°C.

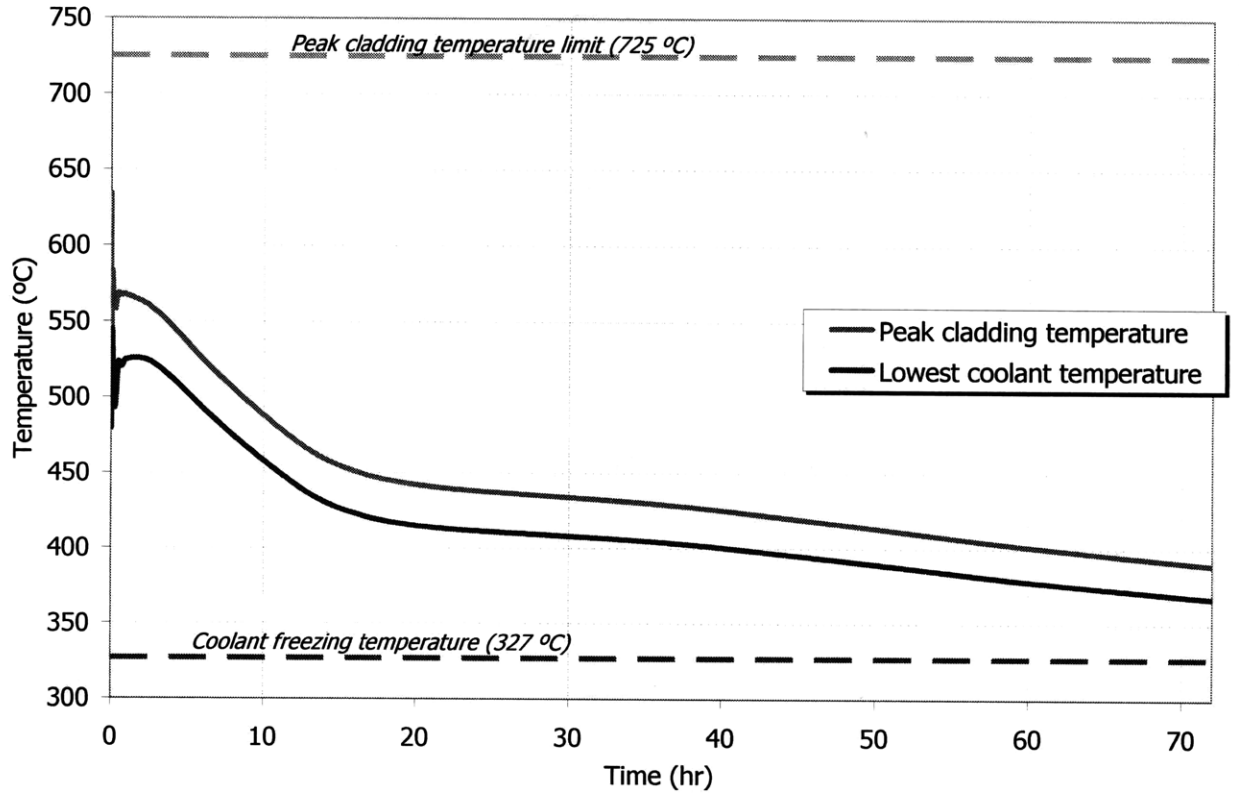

Figure 7-18. Peak cladding temperature and lowest coolant temperature for protected SBO with four operating trains

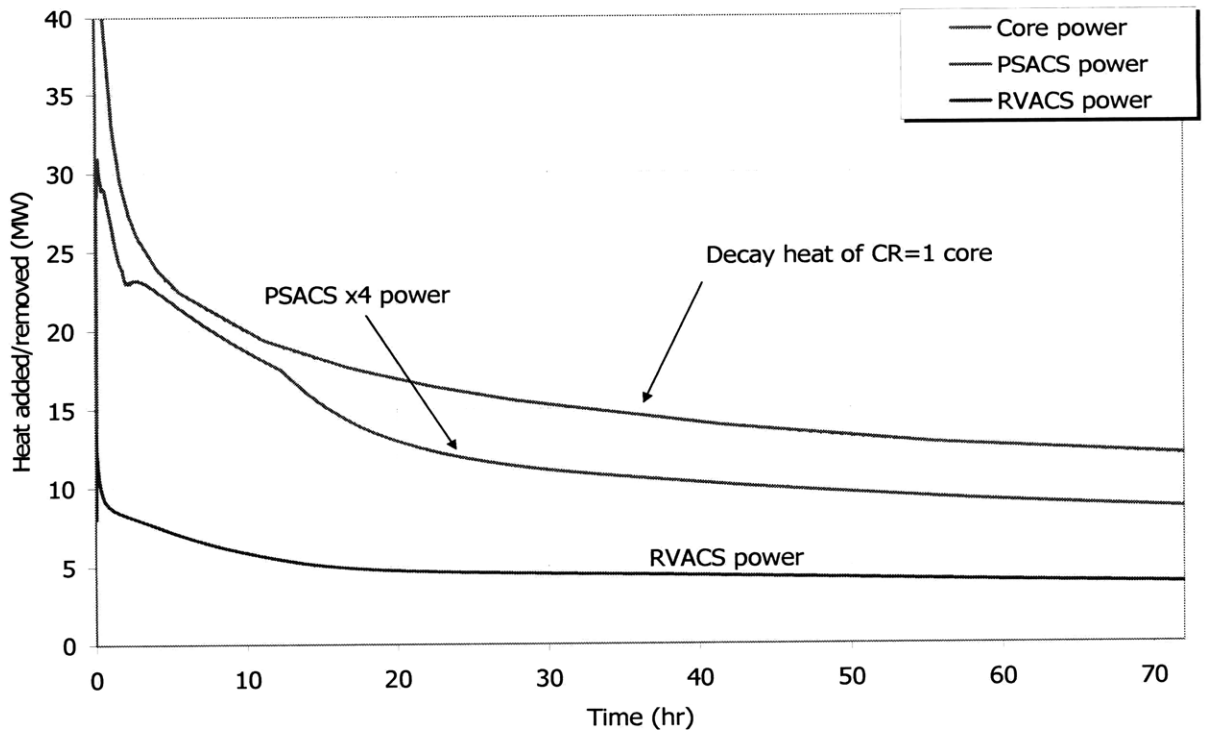

Figure 7-19. Heat added/removed for protected SBO with four operating trains

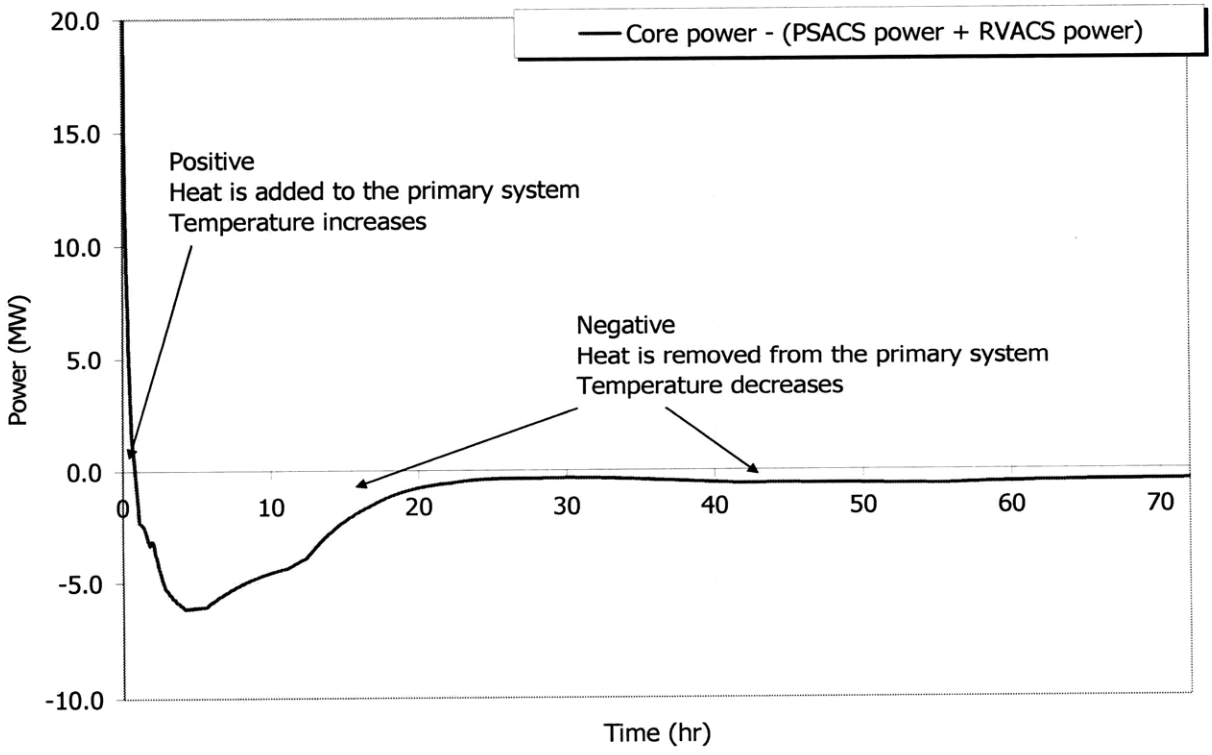

Figure 7-20. Difference between heat produced by the core and heat removed by the safety systems (MW)

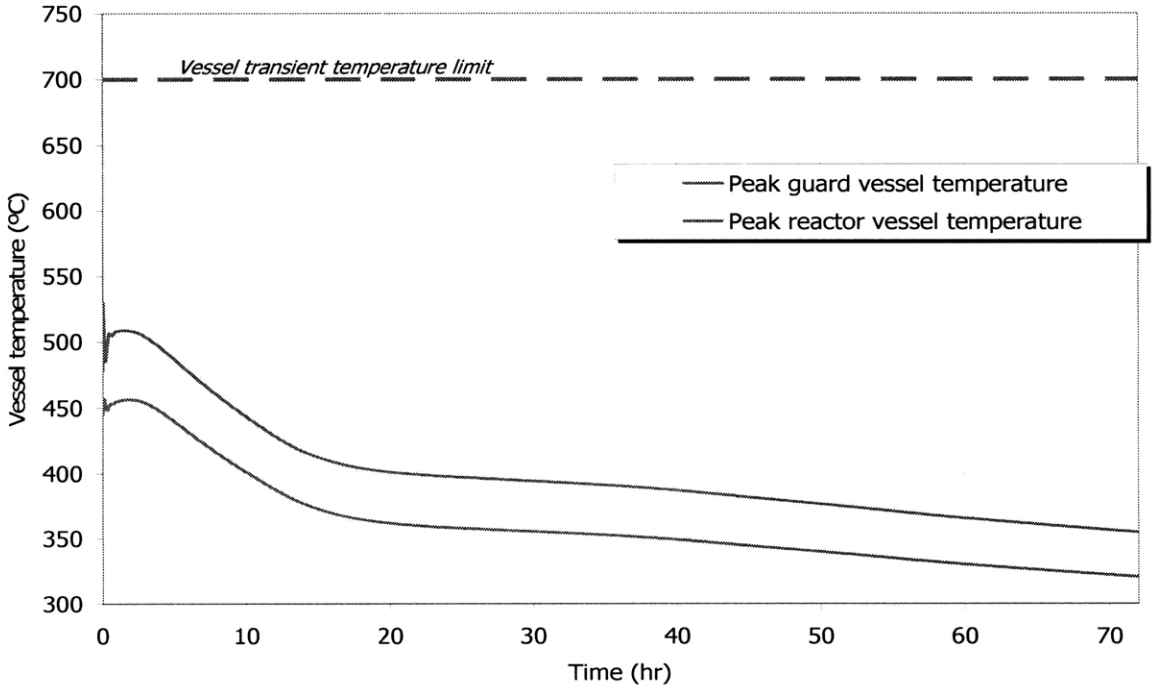

Figure 7-21. Reactor and guard vessel peak membrane temperature during protected SBO with 4 operating loops

7.1.4. Results for Protected Station Blackout for CR=0 core

The protected station blackout with all trains operating for the zero conversion ratio core is more conservative than the CR=1 case. This is because the transient temperatures of the CR=0 are lower than for other core. Thus, the possibility of coolant freezing is higher. Figure 7-22 shows peak cladding temperature and lowest coolant temperature for the CR=0 core. The water in PSACS tanks does not evaporate throughout the 72-hour transient. The lowest coolant temperature is therefore observed at 72 hours and is equal to 356°C (29°C margin to freezing). After 72 hours of transient conditions, it is assumed that the onsite power is restored, and the PSACS can be isolated to avoid later coolant freezing.

Figure 7-23 compares decay power with the heat rate removed through the RVACS and PSACS, and Figure 7-24 plots the net heat rate balance between heat generation and removal. It can be observed that removed heat rate is always larger than the decay heat, confirming the overall decreasing trend of the PCT. Also reactor vessel temperatures remain well below the transient limit, as shown in Figure 7-25.

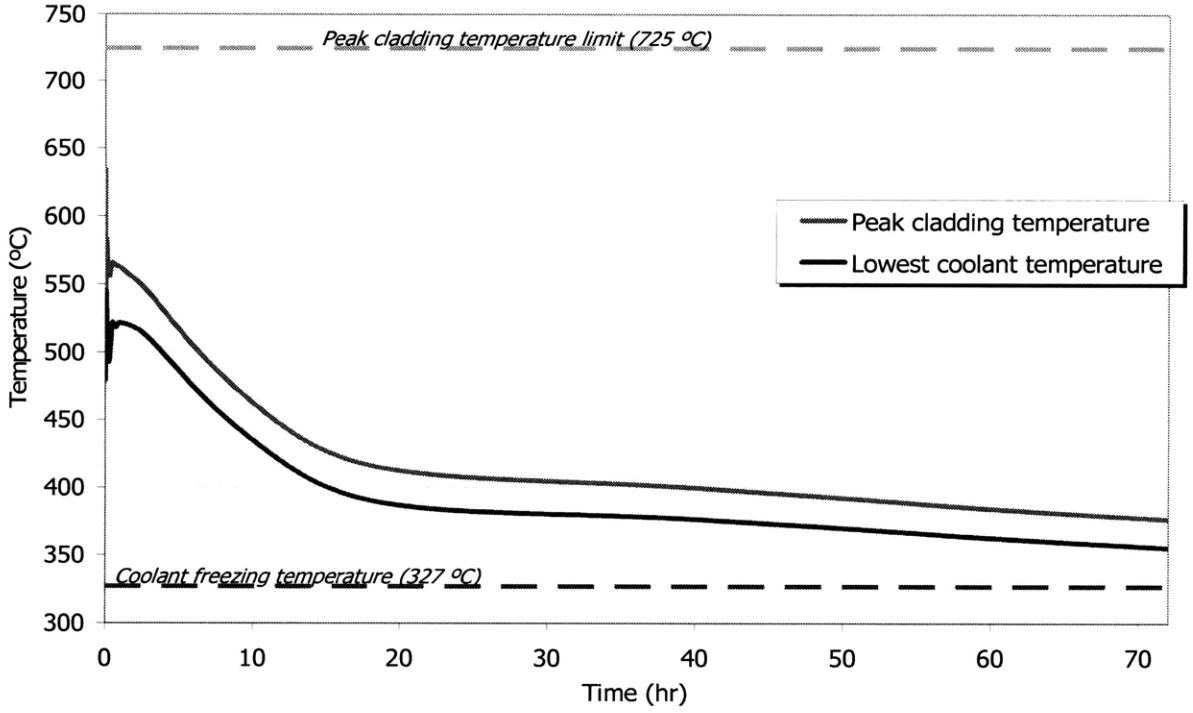

Figure 7-22. Peak cladding temperature and lowest coolant temperature for protected SBO with four operating trains for the CR=0 core

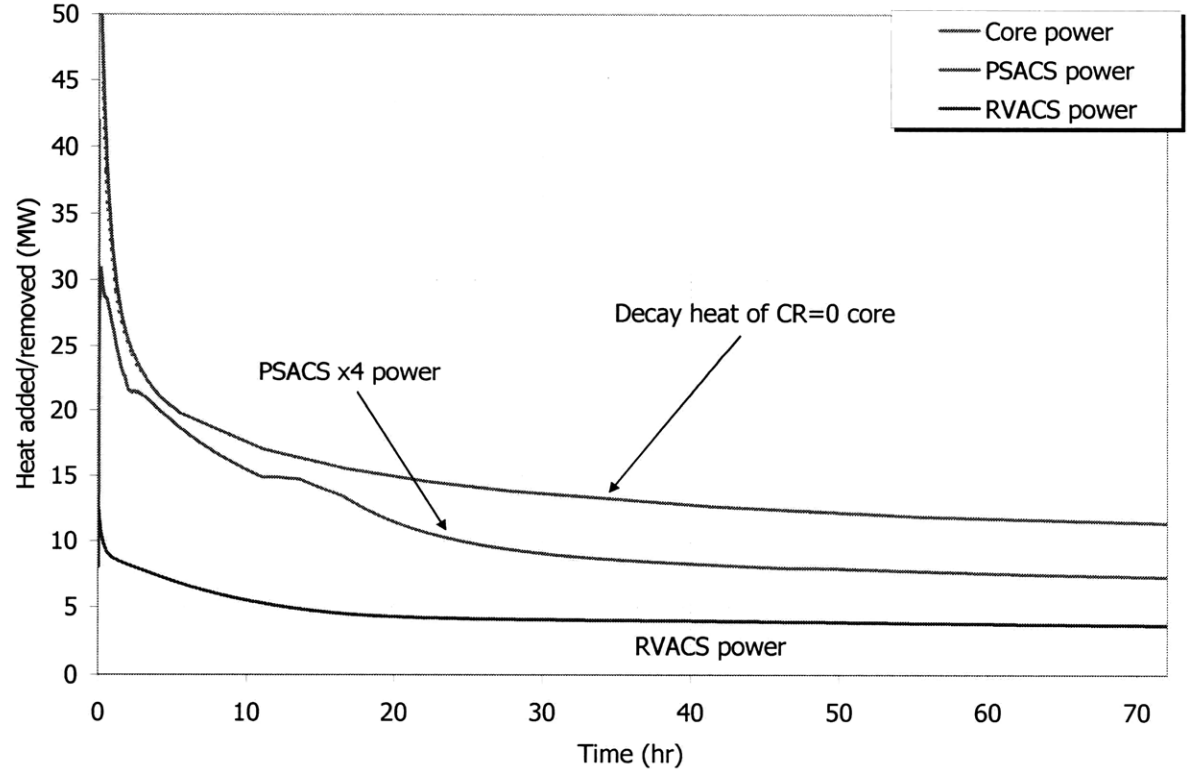

Figure 7-23. Heat added/removed for protected SBO with four operating trains for the CR=0 core

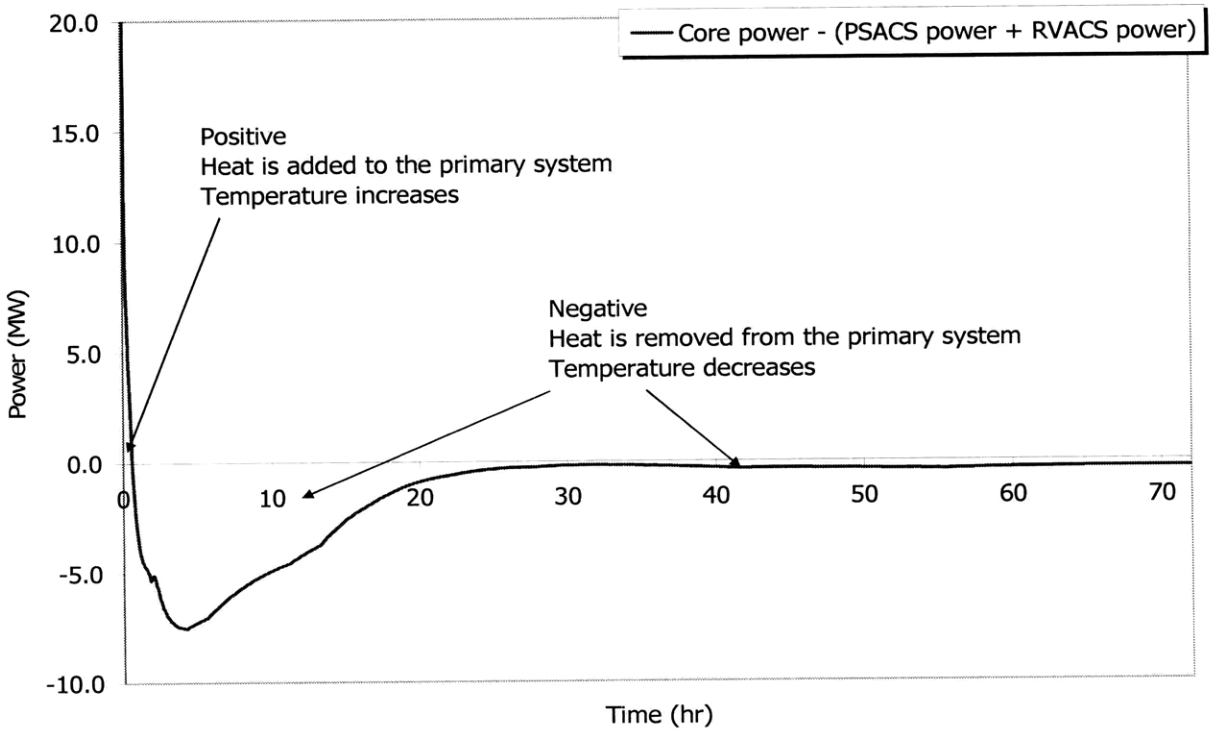

Figure 7-24. Difference between heat produced by the core and heat removed by the safety systems (MW) for the CR=0 core

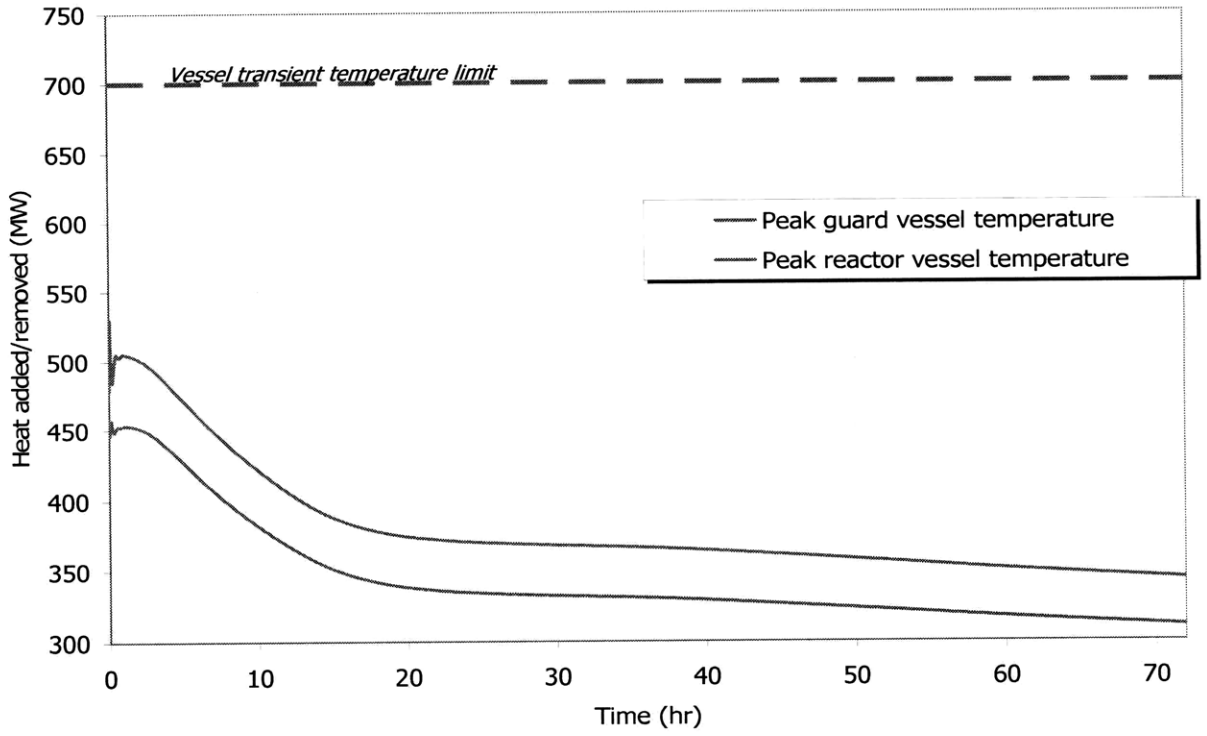

Figure 7-25. Reactor and guard vessel peak membrane temperature during protected SBO with 4 operating loops for the CR=0 core

7.1.5. Conclusions for Station Blackout Accident

The overall conclusion of the station blackout accident simulation is that the safety systems, RVACS and PSACS, are adequate for passive decay heat removal and safe shutdown of both reactors. Regardless of the number of trains operating or core present, the peak cladding temperature and peak membrane vessel temperature remain below the limits during the unprotected transient. In case of protected accident, the coolant is prevented from freezing with a sufficient margin even when all PSACS trains are operated.

Even though the passive safety systems showed acceptable performance during both protected and unprotected SBO accidents, the size of the water tank of PSACS is large and increases cost. Such large tank is needed if completely passive response is required. The system can be redesigned with a smaller size of the water tank provided that some operator action is allowed. Such actions can include manual reactor scram (e.g. within 24 hours) or water tank refill at some point during the unprotected accidents.

7.2. Unprotected Loss of Flow Accident

The unprotected Loss of Flow Accident (LOFA) is caused by the complete loss of the electric power to the primary coolant pumps. This leads to generator trip, lost of heat sink and initiation of PSACS in the same manner as was analyzed in the SBO scenario. Therefore, the SBO results are applicable for unprotected LOFA as well. However, because the Brayton SCO_2 PCS has significant capability for self-sustained operation using heat from the IHX to drive the turbine and compressor and because electricity to precooler pumps is available, it is of high interest to investigate plant response to unprotected LOFA using the PCS. Therefore, the RELAP5-3D model described in the previous section was used to evaluate this scenario using the power conversion system. Thus, the power conversion system is assumed connected to the IHX throughout the entire accident duration, and the precooler pumps are assumed to be active. The water mass flow rate through the precoolers can be controlled. The PSACS trains remain

inoperative during this sequence. The following actions/assumptions were taken during this transient:

- Turbine bypass was used to protect against shaft overspeed after the generator is disconnected from the grid (see Section 5.5.1 for more details on turbine bypass)
- Turbine speed demand for the PID controller that controls turbine bypass valve opening after turbine speed is avoided was set to 50 rad/sec. This speed was selected such to achieve power removed through the PCS to match natural circulation capability of the primary system within desirable core outlet/inlet temperatures.
- Precooler mass flow rate (water) was reduced to 5% of the original flow (460 kg/sec)

The initial conditions are the same as for the SBO and are presented in Table 7-1. In the case of pump trip accident with PCS acting as the main heat removal system, the main concern is to avoid primary system undercooling and consequent reactor restart, since the PCS has a large capacity to remove heat. Therefore, a search had to be performed through preliminary runs and PID controller tune ups to identify the target shaft speed that can circulate a heat rate matching natural circulation –supported reactor power within a desirable temperature range. The temperature range is established such that the core outlet temperature remains sufficiently low to keep peak cladding temperature below the limit of 725°C with margin and the core inlet temperature remains well above the lead freezing point. Moreover, the average core temperature needs to be above the nominal operating temperature to support reactor power reduction through reactivity feedbacks to a value that can be removed by natural circulation of lead. The shaft speed of 50 rad/sec was found to provide this balance.

The results of the unprotected LOFA transient with shaft demand set to 50 rad/s are presented on Figure 7-26 through Figure 7-34. To reduce the length of the report and compare more easily differences between the two conversion ratio designs, both CR=1 and CR=0 are presented on each figure. As shown on Figure 7-26, immediately after the primary coolant pumps trip, primary system temperatures begin to rise. Peak cladding temperature shown on Figure 7-27 follows the trend of the core outlet temperature. The core power starts to decrease due the negative reactivity feedback associated with higher fuel and coolant temperatures. However,

since there is a significant amount of heat removed through the IHXs, the reactor approaches a new steady state with natural circulation and power level of 154 MWt for CR=1 and 148 MWt for CR=0 cores, as depicted on Figure 7-28 (~6.4% of the full power level). Figure 7-29 illustrates the normalized core power and core mass flow rate during the accident. The new steady state conditions are achieved approximately one hour after the start of the accident sequence. The natural circulation core mass flow rate is established at 7.2% of its initial value. Turbine speed and the gas mass flow rate through the turbine are shown on Figure 7-30. Note that the turbine speed converges to the preset value of 50 rad/sec. The rate of convergence is defined by the settings of the P-I controller. More details on PI controller parameters are discussed in Section 5.5.

Figure 7-31 compares the reactivity of both unity and zero conversion ratio cores. It can be seen that CR=0 core exhibits more negative reactivity than the unity conversion ratio core during first 100 seconds into the accident. This is due to the significantly smaller coolant temperature reactivity coefficient of the zero conversion ratio core. Interestingly, the reactivity feedback effect is such that the PCT peak during that time is lower for CR=0 than for CR=1 (recall that the steady state value of PCT for CR=0 is higher by 12°C). This is explained by the lower values of reactivity coefficients.

Figures Figure 7-32 through Figure 7-34 compare the behavior of the zero conversion ratio core as a function of the settings of the P-I controller. Ideally, the turbine speed should be held nearly constant, so the decay heat can be removed for as long as possible through PCS. In this case, the mass flow rate through the turbine must be adjusted in such way that the speed of the shaft remains constant. This can be done through control of the turbine bypass valve open area or can also be extended to other valve configurations. In this example, the turbine bypass was used with the proportional weight held constant and integral weight varied. The integral weight accelerates the conversion of the turbine speed to the setpoint value which was set to 50 rad/sec, to match primary and PCS heat rate, as discussed earlier. It was determined that a relatively small integral weight should be applied to ensure that the turbine velocity has a smoothly decreasing behavior comparable to the decay heat curve. However, if the integral weight is too small, the turbine speed decreases very slowly (integral weight of 0.0025 on Figure 7-32). This

causes higher heat removal rate through the turbine which leads to higher core power (Figure 7-33). Therefore, the integral weight value must be chosen such that the peak cladding temperature is kept below the transient limit of 725°C. Figure 7-34 summarizes the PCT for the three cases discussed. Note from the figure, that the value of integral weight of 0.011 assures that the PCT is below the limit. Thus, the analysis described above used this integral weight.

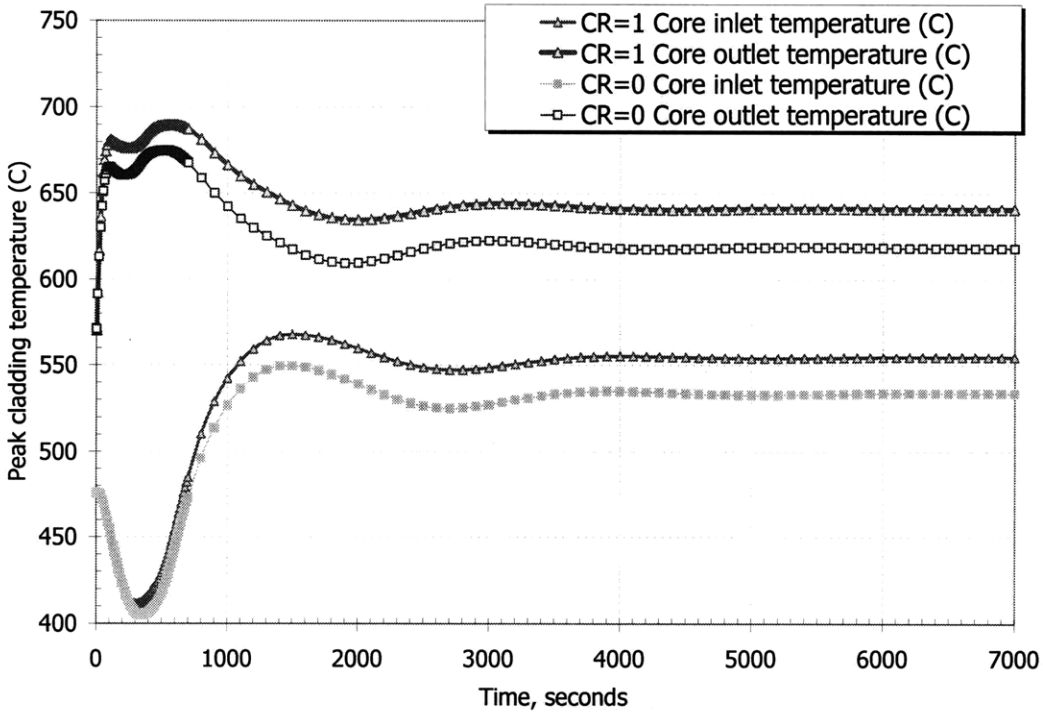

Figure 7-26. Core coolant temperatures during LOFA

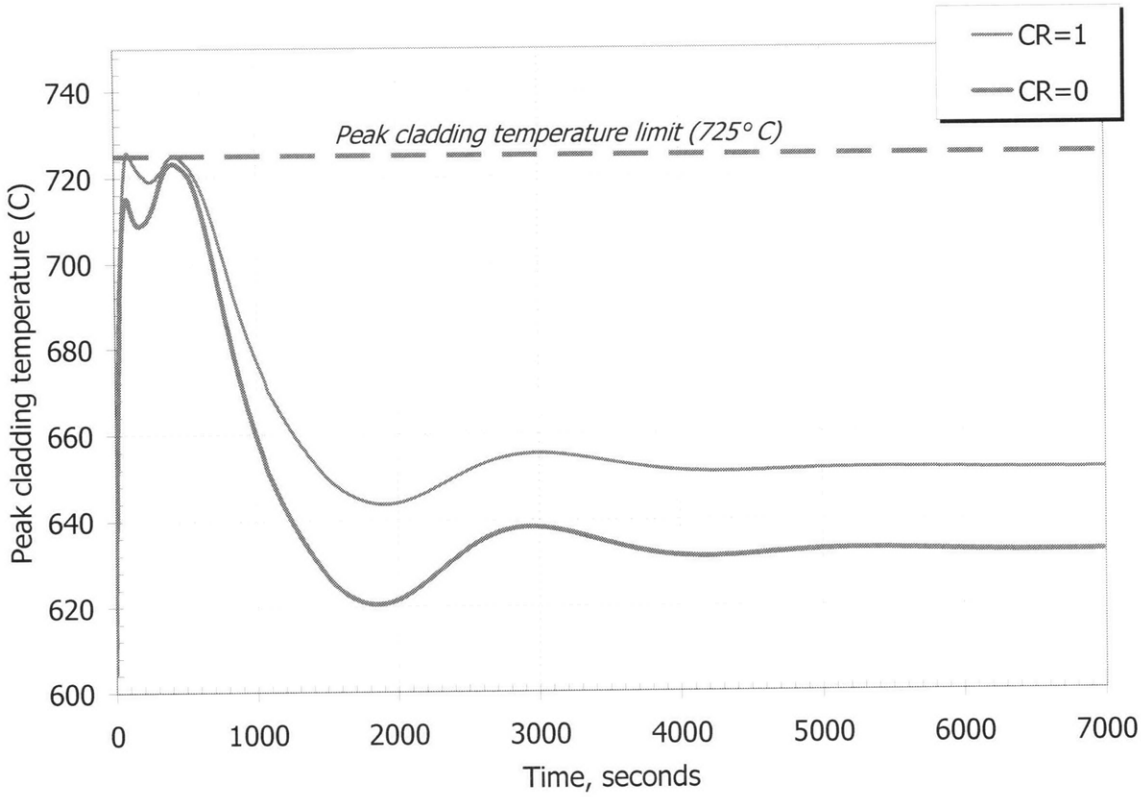

Figure 7-27. Peak cladding temperature during LOFA

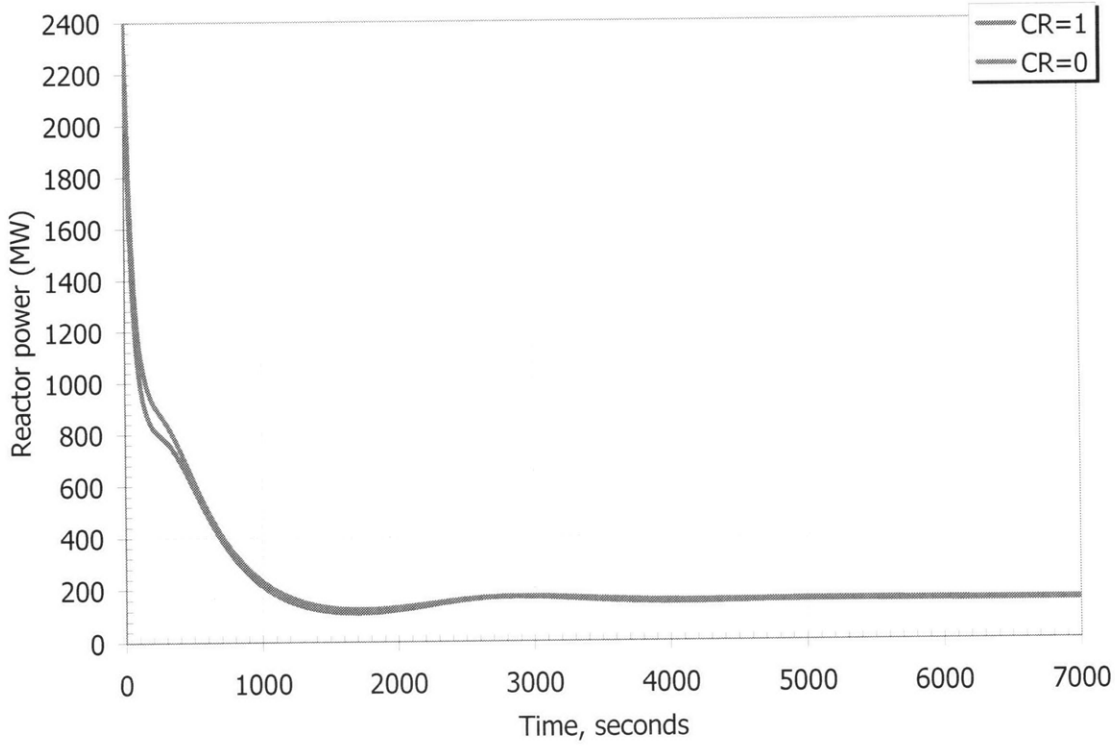

Figure 7-28. Reactor core power during LOFA

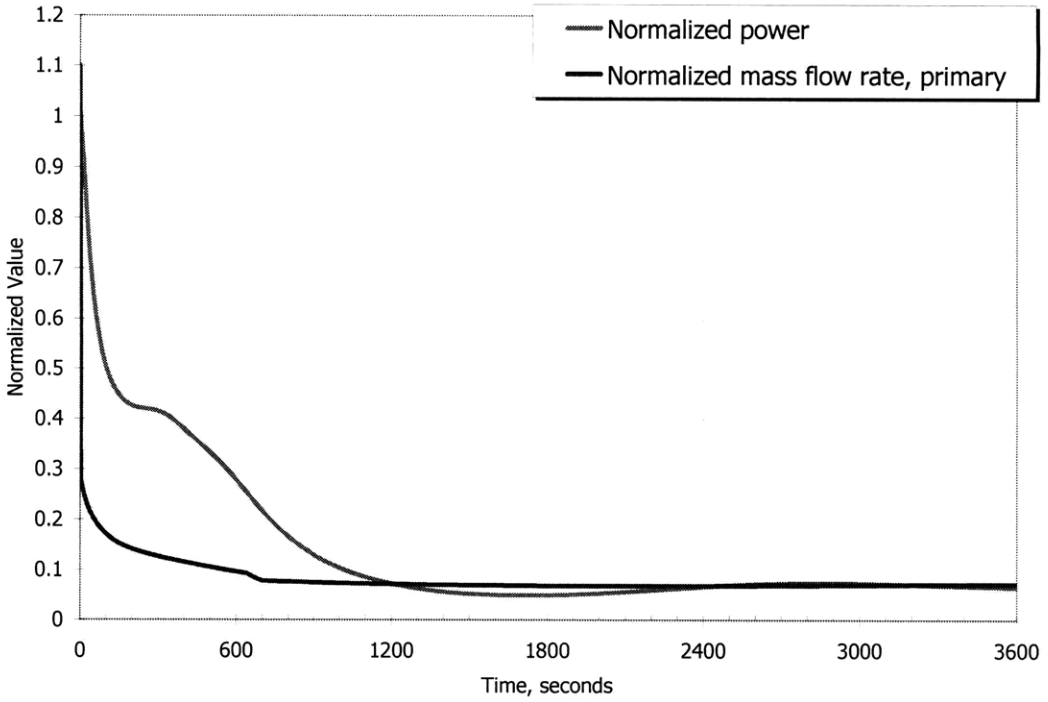

Figure 7-29. Normalized reactor power and primary coolant mass flow rate during LOFA (CR=1 and CR=0 behave very similarly)

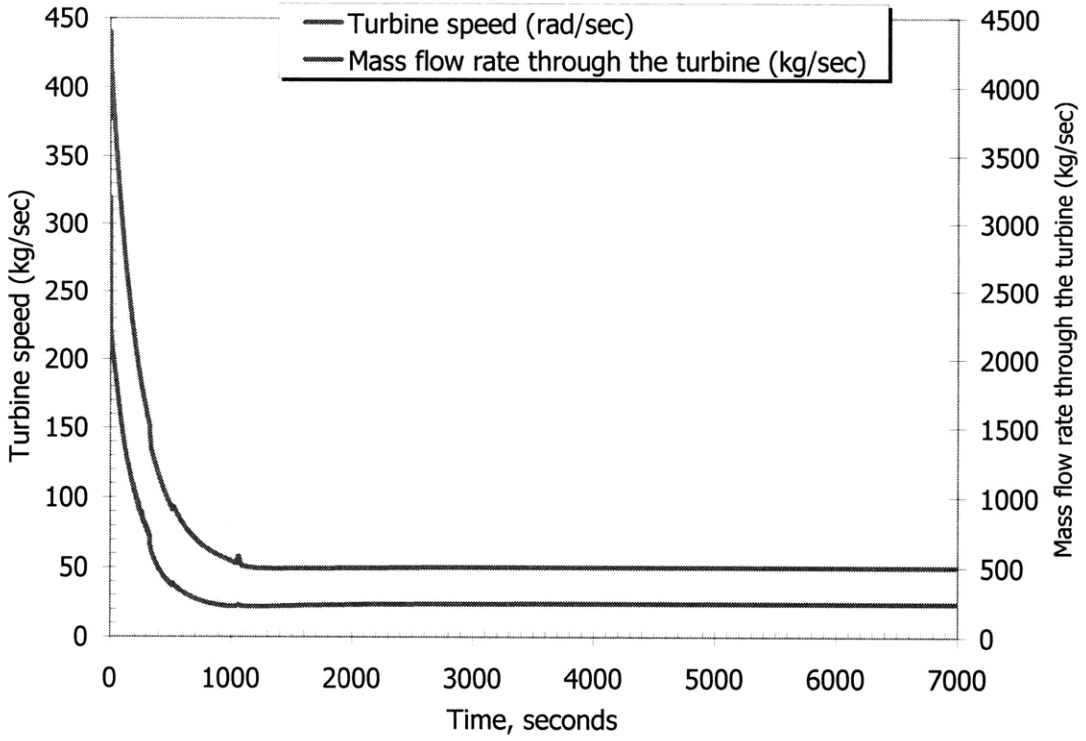

Figure 7-30. Turbine speed and CO_2 mass flow rate during LOFA (CR=1 and CR=0 behave very similarly)

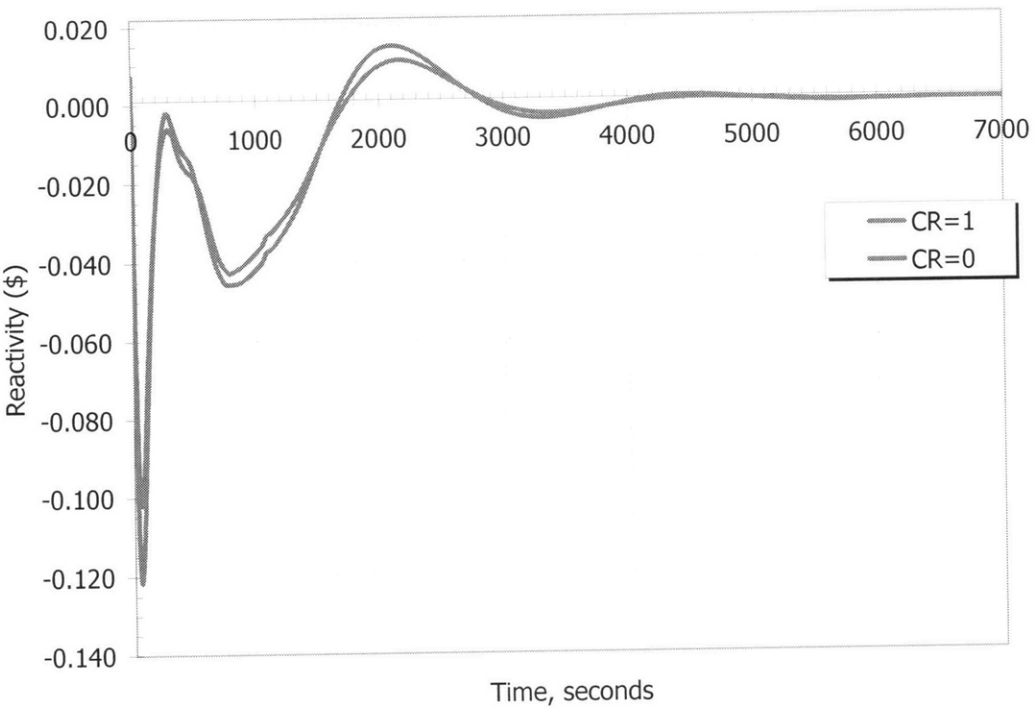

Figure 7-31. Reactivity dynamics during LOFA

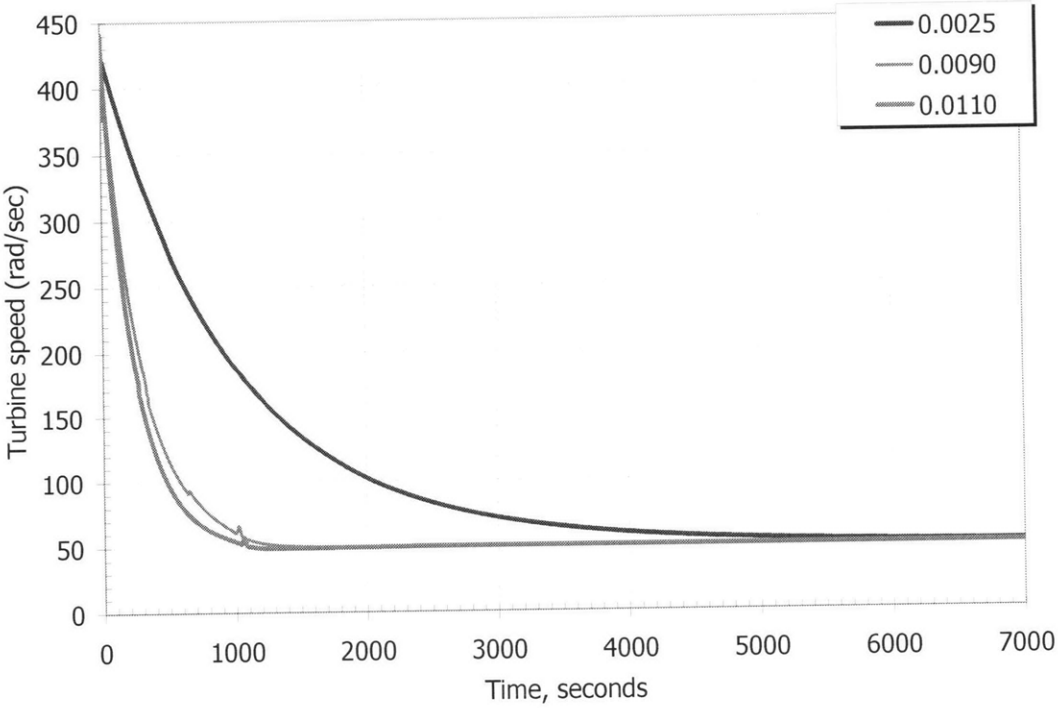

Figure 7-32. Effect of PI controller integral weight on the reactor (CR=0 core)

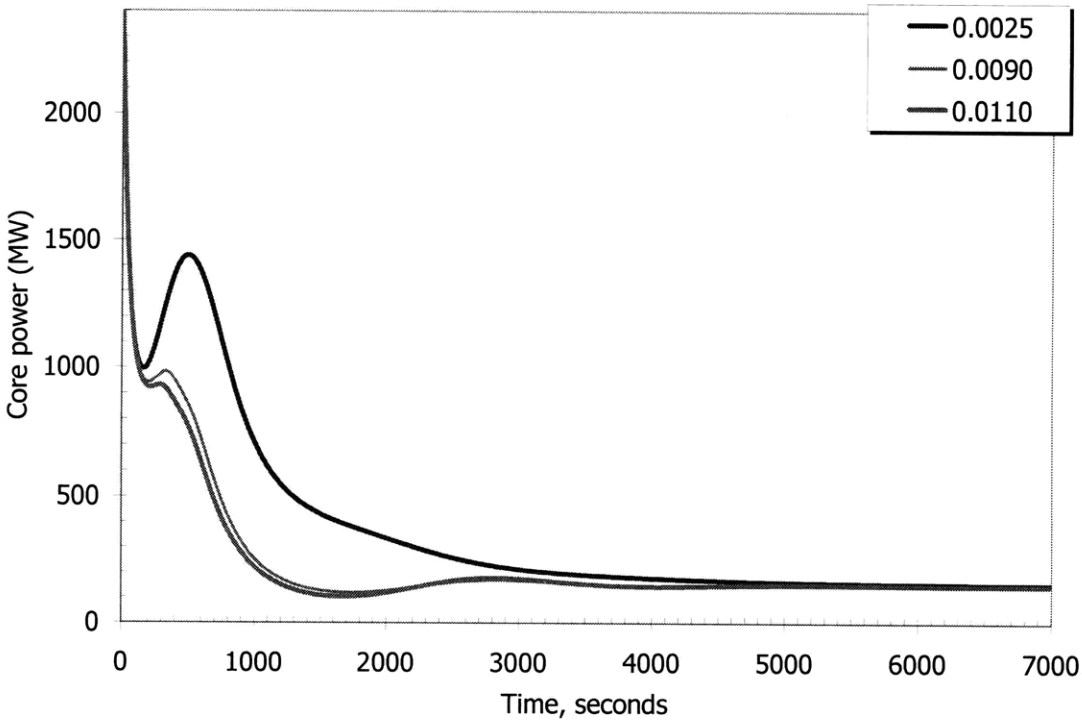

Figure 7-33. Effect of PI controller integral weight on the reactor (CR=0 core)

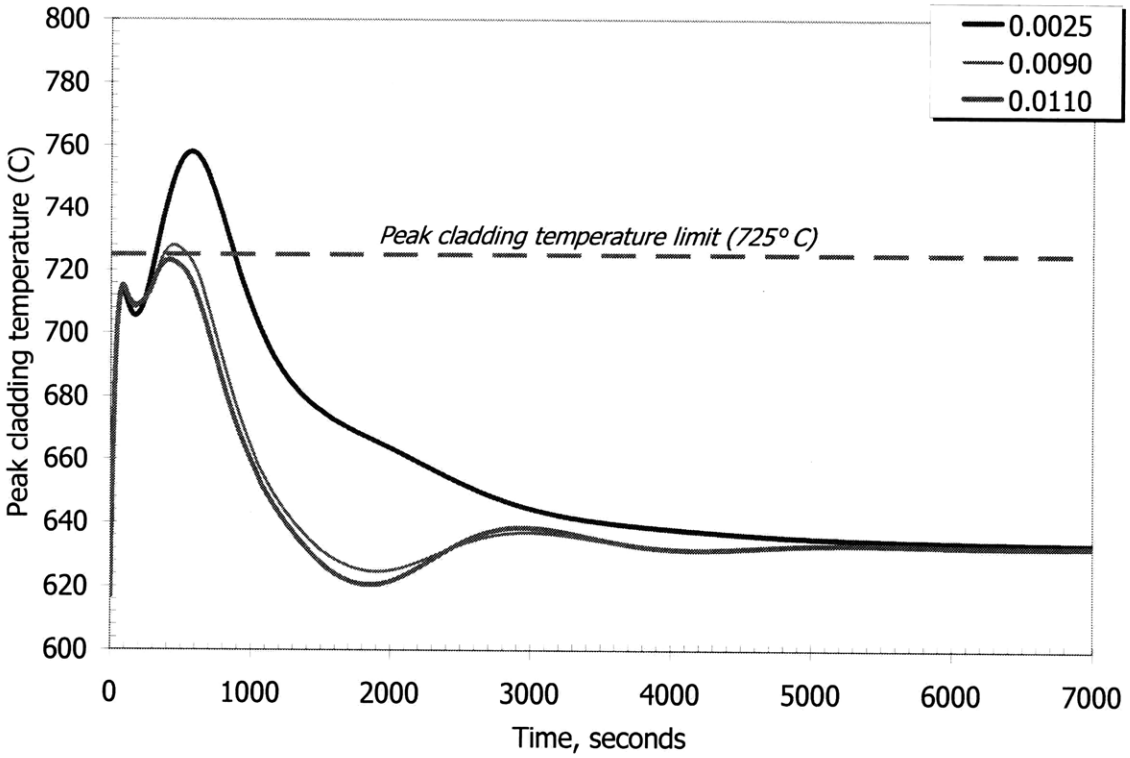

Figure 7-34. Effect of PI controller integral weight on the reactor (CR=0 core)

7.3. Unprotected Overpower Accident

The Unprotected Transient Overpower (UTOP) accident assumes rapid withdrawal of the highest worth control assembly. The control assembly removal speed was assumed to be similar to one used in IFR safety analysis which was limited by the physical drive speed. Failure to scram was assumed in this analysis. However, the primary coolant pumps remained in use, and the PCS was allowed to passively respond to the accident in a load-follow fashion. Thus, the generators were assumed to remain coupled to the grid, and the precooler mass flow rate was kept at the nominal value.

Because it is instructive to compare performance of the CR=1 and CR=0 cores, both cores will be discussed in this section rather than in a separate section on CR=0 core. Table 7-2 summarizes the parameters used to calculate maximum rod worth. In FCR cores, the control rods (CR) are assembled into clusters of 25 rods residing in the middle of an assembly. Thus, in this analysis, the term "assembly" refers to the cluster of 25 rods. The maximum assembly worth is determined by excess reactivity of the core at BOL and the reactivity feedback caused by the Hot Full Power conditions. The value for the assembly withdrawal rate for CR=1 was adopted from IFR safety studies [Wade et al., 1997.] However, two different assumptions can be made for the CR=0 core: the rate of withdrawal equivalent to that of the CR=1 core in terms of withdrawal speed or in terms of $/sec. The former assumption, which means that it would take the same amount of time for both CR=1 and CR=0 control assemblies to be fully withdrawn from the core, was used in the current analysis.

Table 7-3 contains the summary of main results for the UTOP accident. As the control assembly starts the runout, the core power follows the increase in reactivity as shown in Figure 7-35. Immediately, higher core temperatures (PCT is shown on Figure 7-36) trigger negative reactivity feedback. Since the coolant temperature reactivity coefficient of the CR=1 core is more positive than the CR=0 core, the reactivity of the CR=0 core returns back to negative values faster. Also, due to appreciably higher coolant and fuel temperatures of the CR=0 core, the negative feedback of CR=0 core is more noticeable. The reactivity dynamics for both cores are shown on Figure 7-37.

Table 7-2. Maximum rod worth parameters

Parameter	CR=1	CR=0
k-effective (max)	1.020	1.155
Excess reactivity ($)	5.4466	45.9586
CZP to HFP ($)	0.9190	1.14823
total ($)	6.3656	47.1069
# of CR clusters	96	349
$/cluster (x25 rods)	0.0663	0.1350
Maximum peaking factor	1.21	1.34
Maximum assembly worth ($)	0.0971	0.2424
Assembly withdrawal rate ($/sec)	+0.0050*	+0.0125**

* Value used in safety studies of the IFR [Wade et al., 1997]
**Value calculated assuming the same speed of assembly withdrawal as for CR=1 core.

Table 7-3. Main results for UTOP

Parameter	CR=1	CR=0
Peak cladding temperature (°C)	652	705
Peak power, P/P_0*	1.22	1.53
New equilibrium temperature (°C)	650	692
New equilibrium power, P/P_0*	1.06	1.11

*P_0 is the nominal steady state power of 2400 MWth

Since the CR=0 core has much larger maximum rod worth, its PCT during UTOP is higher when compared to the CR=1 core. Consequently, due to the larger reactivity insertion, the CR=0 core relative power increases by ~50% of its original power. Once the control assembly motion ceases, the reactor reaches a new equilibrium at higher power and temperature conditions. A new equilibrium was established at around 500 seconds after the beginning of the accident. Overall, both conversion ratio cores can easily accommodate the unprotected overpower transient. Since the maximum fuel temperature is also required to be within the limits described in Chapter 2, the peak centerline temperature is shown on Figure **7-38**. The fuel temperature remains below the limits during the entire accident with large margin.

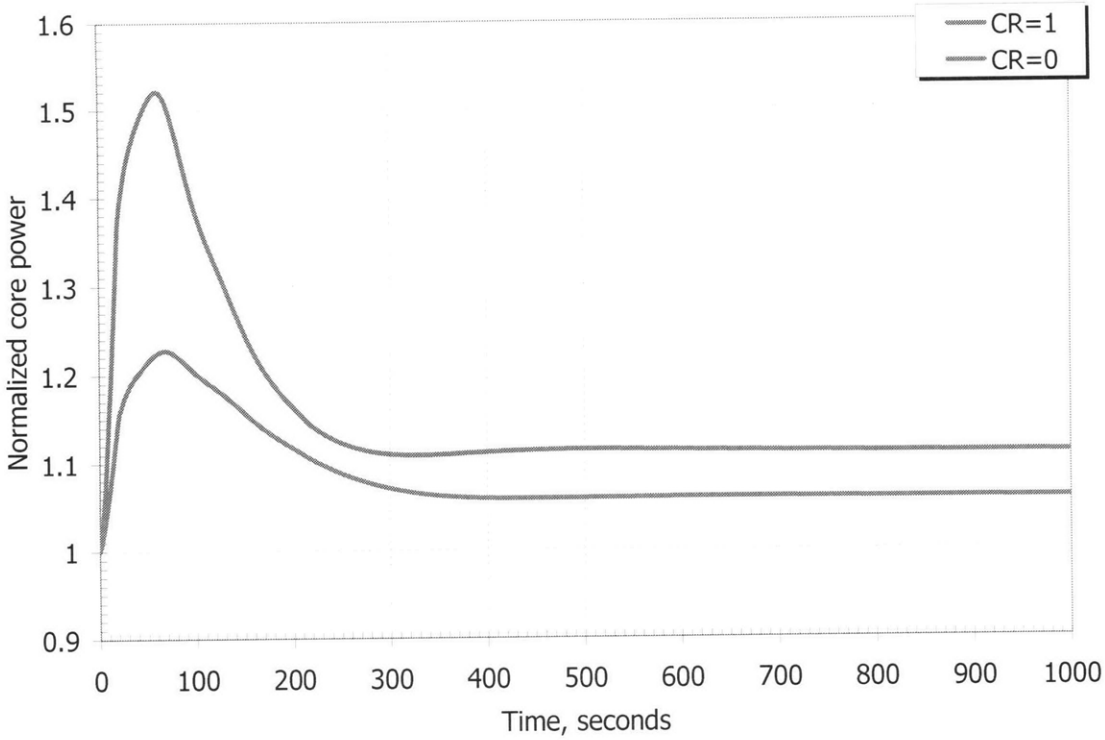

Figure 7-35. Normalized core power during UTOP

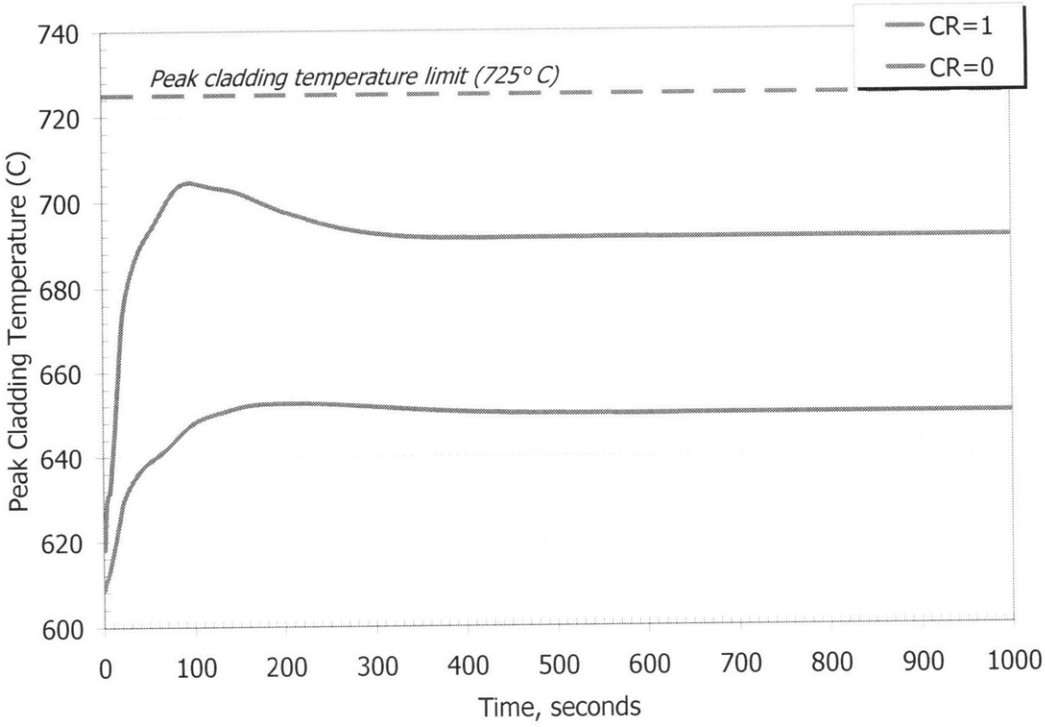

Figure 7-36. Peak cladding temperature (°C) during UTOP

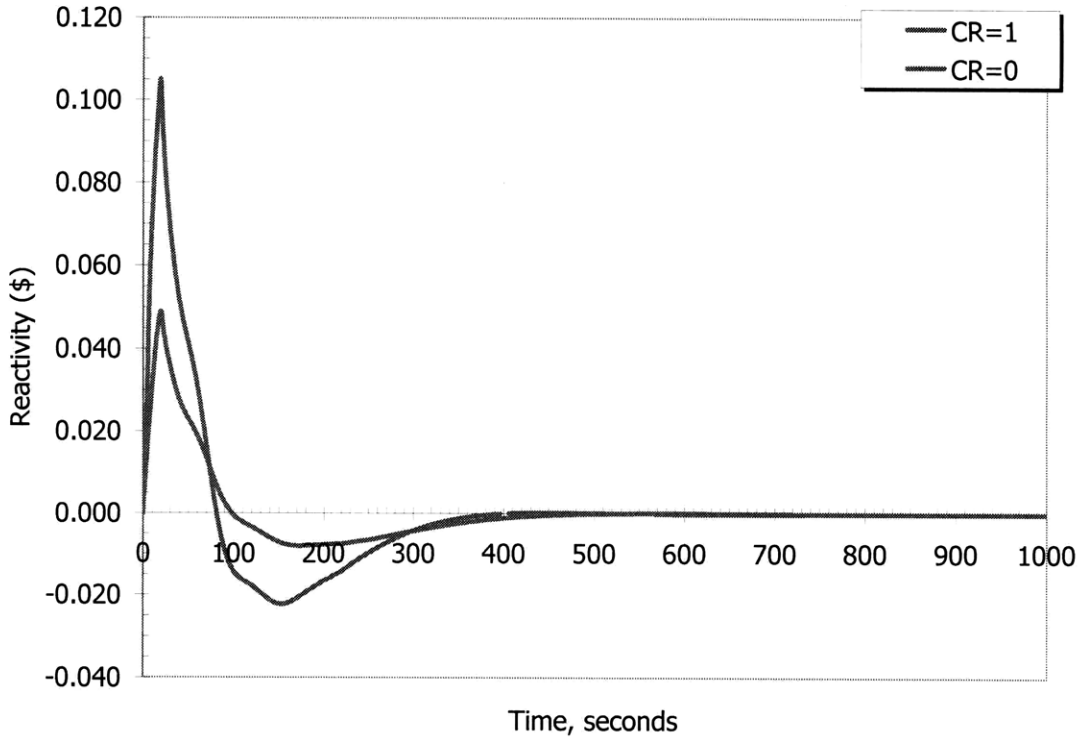

Figure 7-37. Reactivity dynamics during UTOP (note different rates ($/sec) of rod withdrawal)

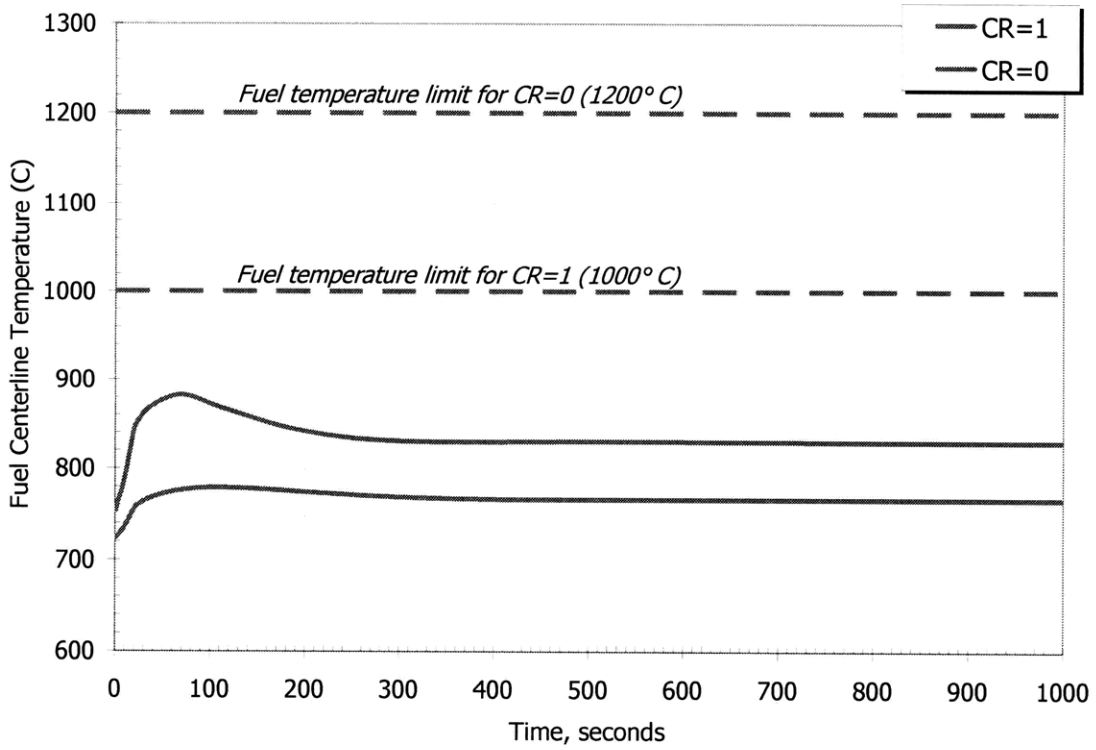

Figure **7-38**. Maximum fuel centerline temperature for both cores during UTOP

7.4. References for Chapter 7

Fridman E., Shwageraus E., Galperin A., "Implementation of multi-group cross-section methodology in BGCore MC-depletion code," Proc. of Physor-2008, Interlaken, Switzerland, September 2008.

Shwageraus E., Fridman E., Abramski E., Galperin A., "BGCore - A Comprehensive Package for Reactor Core and Fuel Storage Analysis", Proc. of 23rd Conference of the Nuclear Societies in Israel, Dead Sea, Israel, February 15-16, 2006.

Todreas N.E., Hejzlar P., Shwageraus E., Petroski R., Nikiforova A., Whitman J., and Fong, C.J., "Flexible Conversion Ratio Fast Reactor Systems Evaluations", Final report, Center for Advanced Nuclear Energy Systems, MIT, MIT-NFC-PR-101, August 2008.

Wade D.C., Wigeland R.A., Hill D.J., "The safety of the IFR", *Progress in Nuclear Energy*, Vol. 31, No. 1/2, pp. 63-82, 1997.

8. CONCLUSIONS AND RECOMMENDATIONS FOR FUTURE WORK

The design of a large lead-cooled 2400 MWth reactor with flexible conversion ratio has been completed, and transient analysis for three unprotected and one protected accidents has been conducted. Further analysis of the reactor systems coupled with the supercritical CO2 Brayton cycle power conversion system showed promise for high efficiency and compactness in design of the plant.

Steady state thermal hydraulic design and analysis of both unity and zero conversion ratio cores confirmed the feasibility of 112 kW/l power density cores to maintain peak cladding temperature within the 650°C limit with appreciable margin. In addition, it was found that it is possible to fit four 600MWt-IHXs in the cavity between the core and the vessel, while keeping acceptably small temperature difference between core outlet and turbine inlet temperatures (23°C) and low CO_2 pressure drop (225 kPa with margin to the target of 500 kPa) to maximize plant efficiency. However, it is noted that although the placement of the 2400MWt core, 4 IHX and 4 pumps within the 10.2 m diameter vessel appears feasible based on thermal hydraulic considerations, further feasibility study such as roof mechanics, in-service inspection, seismic analyses, and refueling system design are necessary to confirm this conclusion.

Transient analysis of both reactor cores was performed for three accidents: Unprotected Station Blackout, Unprotected Loss of Flow, and Unprotected Overpower. The protected SBO was also analyzed to confirm existence of a margin to lead freezing. Both cores showed satisfactory performance during LOFA and UTOP accidents. However, because of the large amount of decay heat generated in the core and reactivity feedback for the shutdown, SBO analysis presented some challenges. An additional safety system for decay heat removal, the Passive Safety Auxiliary Cooling System, was found to be needed. The PSACS design was optimized with a small PSACS heat exchanger and a very large water tank. Such a design prevented the PCT from crossing the transient temperature limit of 725°C while maintaining the coolant temperature above freezing at any combination of accident conditions (protected vs. unprotected) and number of operating trains (two, three, or four). Figure **8-1** summarizes the combinations of

limiting conditions for the SBO accident. The simulation of the accident with different conditions showed that surviving the Station Blackout Accident for both cores for both protected and unprotected conditions for up to 72 hours without exceeding the limits is possible.

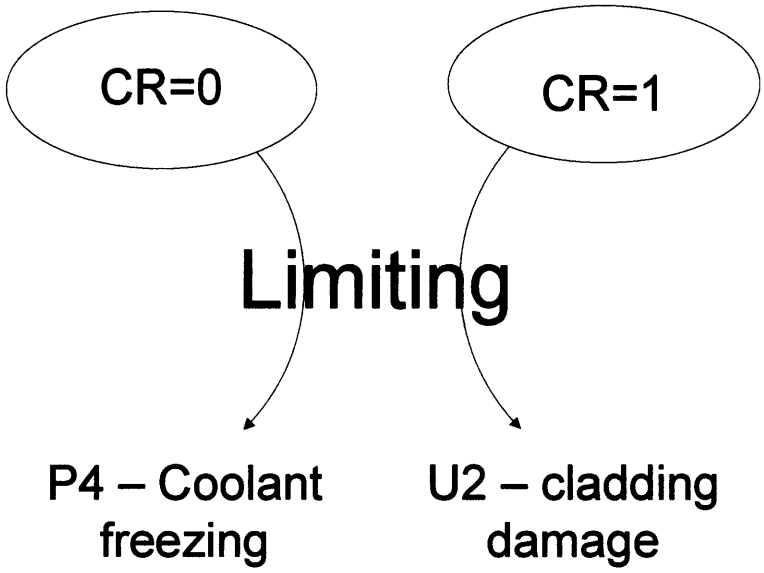

Figure 8-1. Limiting conditions for SBO accident

The design was performed for the "currently" available materials with conservative material limits for coolant velocity, cladding and vessel temperature, and irradiation limits. The design can improve in economic and safety respects if more advanced materials become available.

Therefore, it is recommended that PSACS design be taken further and the air option be implemented as described in details in Todreas et al. [2008]. The advantage of the air coolant PSACS option is larger temperature difference between the heat exchanger and air and thus less susceptibility of the system to coolant freezing during protected accidents.

References for Chapter 8

Todreas N.E., Hejzlar P., Shwageraus E., Petroski R., Nikiforova A., Whitman J., and Fong, C.J., "Flexible Conversion Ratio Fast Reactor Systems Evaluations", Final report, Center for Advanced Nuclear Energy Systems, MIT, MIT-NFC-PR-101, August 2008.

A. APPENDIX A INTERMEDIATE HEAT EXCHANGER MODEL

This appendix describes the analytical model of the intermediate heat exchanger between lead coolant and supercritical CO_2. The design and analysis of the intermediate heat exchangers (IHXs) have been a challenge due to high operating pressures and temperatures. The high pressure (20 MPa) on the CO_2 side required a detailed analysis to determine appropriate tube thickness. Furthermore, the large difference in heat transfer coefficients between the lead coolant and supercritical carbon dioxide stimulated interest in the enhanced heat transfer. Finally, the pressure drop constraint on the S-CO_2 side is directly related to the power conversion system efficiency; thus, the minimum achievable pressure drop was pursued. The above challenges are linked to the material properties.

T-91 alloy (with surface treatment on the CO_2 side) was investigated for the use in heat exchangers since the 316SS alloy is not compatible with lead corrosive environment at temperatures above 550 °C. The 2007 ASME Boiler and Pressure Vessel code included T-91 alloy as an acceptable material for Sec. III, Division 1, Subsection NB/NH for Class 1 components. Note that when the optimization analysis was conducted, the time-dependent properties of T-91 were not available in ASME Boiler and Pressure Vessel code. Thus, the analysis was conducted for very conservative estimated values of the thermal conductivity and design stress intensity. The conclusions obtained in this analysis were later applied to the updated design of the IHX reported in Section 3.3.

The heat exchangers are placed within the annulus between the vessel liner and the core riser; thus, the primary coolant never leaves the vessel. The heat exchanges have a kidney shape to utilize the tight space efficiently. The CO_2 coolant enters the IHX through the large main inlet tube and proceeds to the lower plenum where it is distributed through the smaller tubes. The gas flows upward through the tubes exchanging the heat with lead coolant which is on the shell side. Heated CO_2 then mixes up in the upper plenum and leaves the heat exchanger through two outlet tubes.

A.1. Thermal analysis

The S-CO_2 cycle sets constraints on the secondary fluid temperatures and flow rate. The lead coolant has also predetermined values for the core inlet and outlet temperatures and the mass flow rate. Therefore, the heat exchanger must be designed to satisfy all requirements. The radial size of the heat exchanger is constrained by the vessel and core geometry. The CO_2- and lead-side pressure drops are dependent on the axial length of the IHX tubes. The constraint on the CO_2 pressure drop was set by its effect on Brayton cycle efficiency to 0.7 MPa.

The outlet temperature of the CO_2 can be obtained from the heat transfer balance. The target is around 550°C as optimum temperature for cycle efficiency.

$$\dot{Q} = \bar{k} A \Delta t_{lm} \tag{A.1-1}$$

An important part of the heat exchanger design is the overall heat transfer coefficient. For the tube-and-shell heat exchanger, the following equation is used for the heat transfer:

$$Q = \frac{T_i - T_o}{\frac{1}{h_i A_i} + \frac{R_{fi}}{A_i} + \frac{\ln(r_o / r_i)}{2\pi L k_w} + \frac{R_{fo}}{A_o} + \frac{1}{h_o A_o}} \tag{A.1-2}$$

where R_{fo} and R_{fi} are fouling resistances on the outside and inside of the tubes respectively. In case of the inner side of tubes where CO_2 is present, the fouling layer is generally of negligible size (R_{fi} can be ignored). On the other hand, with lead on the outside of the tubes, the fouling layer plus PbO deposition can reach significant values and must be considered. Such fouling resistance will come mostly from the corrosion of tube materials and can be approximated using oxide layer characteristics. With the oxide layer modeled as a plane, the fouling coefficient of the oxide layer is the ratio of the layer thickness to its thermal conductivity.

$$R_{f,s} = \frac{t_{oxide}}{k_{oxide}} \tag{A.1-3}$$

The average heat transfer coefficient corrected for the oxide layer presence is:

$$\bar{k} = \frac{1}{\frac{1}{h_{CO2}} + \frac{r_i \ln(r_i / r_{IL})}{k_{IL}} + \frac{r_i \ln(r_o / r_i)}{k_w} + \frac{r_i \ln(r_{OL} / r_o)}{k_{OL}} + \frac{r_i}{r_{OL} h_{Pb}}} \tag{A.1-4}$$

where:

$\dot{m}_{Pb}$ = mass flow rate of lead through the IHX

$\dot{m}_{CO2}$ = mass flow rate of CO_2 through the IHX

h_{co2} = CO_2 heat transfer coefficient

h_{Pb} = lead heat transfer coefficient

k_w = wall material thermal conductivity

k_{OL} = oxide layer thermal conductivity

r_i = inner diameter if the IHX tube

r_o = outer diameter if the IHX tube

r_{OL} = outer diameter if the IHX tube with oxide layer on it

Effective heat transfer surface can be calculated as:

$$A = n_{tubes} (AL)_{tube} = n_{tubes} (2\pi r L)_{tube} \tag{A.1-5}$$

Log-mean temperature difference Δt_{lm} is evaluated using equation (A.1-6):

$$\Delta t_{lm} = \frac{(T_{in,Pb} - T_{out,CO_2}) - (T_{out,Pb} - T_{in,CO_2})}{\ln \frac{(T_{in,Pb} - T_{out,CO_2})}{(T_{out,Pb} - T_{in,CO_2})}} \tag{A.1-6}$$

A.2. Pressure Drop on the Tube Side

The pressure drop on the S-CO_2 side is one of the design constraints. Pressure head on the CO_2 side must be limited to 0.7 MPa to ensure cycle efficiency. The total pressure drop is comprised of friction, acceleration, gravity and form losses.

Friction:
$$\Delta P_{fric} = f\left(\frac{L}{D}\right)\frac{\rho V^2}{2} \tag{A.2-1}$$

Acceleration:
$$\Delta P_{acc} = G^2\left(\frac{1}{\rho_{out}} - \frac{1}{\rho_{in}}\right) \tag{A.2-2}$$

Gravity:
$$\Delta P_{grav} = (\rho_{in} - \rho_{out})gL \tag{A.2-3}$$

Form losses:
$$\Delta P_{form} = \left(k\frac{G^2}{2\rho}\right)_{inlet} + \left(k\frac{G^2}{2\rho}\right)_{outlet} \tag{A.2-4}$$

where: f is the friction factor given by McAdams relation

G is the mass flux

k is inlet/outlet form loss coefficient

A.3. Lead heat transfer coefficient and friction factor

The heat transfer coefficient, h, between the heat exchanger tubes and the Pb-Bi coolant were determined from the Lyon-Martinelli correlation [El-Wakil, 1978].

$$Nu_{\infty} = 7.0 + 0.025Pe^{0.8} \tag{A.3-1}$$

$$h_{Pb} = \frac{Nu_{\infty}k_{Pb}}{d} \tag{A.3-2}$$

The pressure drop on the shell side is across a bank of tubes. For lead flow, Rehme's method for solving the turbulent flow case in actual geometry was used. The results of this method were fitted by Cheng and Todreas [1986] with the following polynomial:

$$C_{fit} = a + b_1(P/D-1) + b_2(P/D-1)^2$$

where

$$f_{iT} \equiv \frac{C_{fit}}{(\mathrm{Re}_{iT})^n} \tag{A.3-3}$$

For triangular geometry (assume interior subchannels) with P/D greater 1.1, the following coefficients are applicable:

a = 0.1458

b_1 = 0.03632

b_2 = -0.03333

n = 0.18

A.4. Pressure Drop on the Shell Side

It is important to minimize the shell-side pressure drop in order to reduce size and cost of the primary coolant pumps, maximize natural circulation in LOFA events and minimize free level separation. While calculation of the tube-side pressure drop was rather straightforward, the shell side is more complicated because of the presence of baffles. Also, the effect of different bypass and leakage should be taken into account. For the preliminary heat exchanger design, the effect of spacers on the pressure drop was considered. The pressure drop should further be corrected for different flow streams due to baffle presence. For present analysis, the total pressure drop consists of friction, acceleration and form losses.

Friction:
$$\Delta P_{fric} = f_{iT}\left(\frac{L}{D}\right)\frac{\rho V^2}{2} \tag{A.4-1}$$

Acceleration and form losses:
$$\Delta P_{form} = \left(k\frac{G^2}{2\rho}\right)_{inlet} + \left(k\frac{G^2}{2\rho}\right)_{outlet} + C_v\frac{\rho V_v^2}{2}\left(\frac{A_s}{A_v}\right)^2 \tag{A.4-2}$$

where the last term of form loss was suggested by Rehme to account for the spacer pressure losses [Todreas and Kazimi, 1990].

C_v is modified drag coefficient

$C_v = 6.5 + 3(5 - \log \mathrm{Re})$ for honey-comb type spacer

V_v is average bundle velocity

A_s is projected frontal area of the spacer

A_v is unrestricted flow area away from the spacer

A.5. Tube Thickness

High pressure on the S-CO_2 side requires special attention to the hoop stresses in the tubes. The required tube thickness can be calculated using ASME code requirements for primary membrane intensity in thick cylinders. The tube is considered thick if the following ratio is satisfied:

$$t_{tube} / R_{mean} \geq 0.1. \tag{A.5-1}$$

Primary membrane intensity, S_m, is determined for the straight pipe under internal pressure as defined in ASME Section NB. Thus, the tube thickness is defined as:

$$t_{tube} = \frac{PD_o}{2(S_m + P/2)} = \frac{D_o}{1 + 2\frac{S_m}{P}}. \tag{A.5-2}$$

A.6. CO_2 heat transfer coefficient and friction factor

A.6.1. Smooth tube option

For gases in circular smooth tubes, the simplified correlation for Nusselt number by Gnielinski [1976] is used:

$$Nu = 0.0214(\mathrm{Re}^{0.8} - 100)\mathrm{Pr}^{0.4} \tag{A.6-1}$$

$$h_{CO2} = \frac{Nu_{\infty} k_{CO2}}{d} \qquad \text{(A.6-2)}$$

The friction factor is given by McAdams relation:

$$f = 0.184 \mathrm{Re}^{-0.2} \qquad \text{(A.6-3)}$$

A.6.2. Enhanced Heat Transfer Option

Because the intermediate heat exchanger is constrained by the size, there is a strong interest in enhancement of heat transfer capabilities to reduced IHX dimensions and temperature difference. One of the possible methods to accomplish this goal is improvement of the performance of the heat exchanger through tube roughening on the inside surface. Tube augmentation was considered on the CO_2 side due to its lower heat transfer coefficient when compared to lead (about a factor of 3-5). Surface alternation on the CO_2 side achieved by introducing repeated ribs promotes an increase in heat transfer through disturbance of the surface sublayer [Ravigururajan, 1999].

Thus, tubes with repeated helical ribs on the inner side were used for the IHX. The following requirements and assumptions were followed in the design:

Requirements

- Pressure drop on CO_2 side is around 500 kPa (does not exceed 700kPa)
- Pitch is large enough so that no flow stagnation between the ribs occurs

Assumptions:

- Steady state operation
- Homogeneous material
- No contact resistance between the ribs and the tube (extruded ribs)
- Constant heat transfer coefficient of the rib to the gas flow over the entire rib surface

Literature review and comparison

Due to intensive use of augmented tubes in industry, correlations with different ranges of applicability have been developed and a number of papers on tube augmentation and heat transfer have been published. However, depending on the application of the tubes, a specific type of enhancement must be chosen, i.e. ribs, flutes, wire inserts, or grooves, each in helical configuration. Two approaches for developing correlations are usually employed: the analogy method and a statistical/empirical approach [Ravigururajan, 1999]. Correlations based on a latter approach have certain advantages over the analogy-based ones. They are generally simpler to use, and friction factor and heat transfer coefficient correlations are decoupled.

The following comparison was conducted for the enhanced heat transfer and friction factor correlations for single-phase forced convection flow inside circular ducts. Thus, passive tube augmentation through extended surfaces (i.e. ribbed tubes) is considered in the following evaluation. A common trend in these correlations is improved Nusselt number and an accompanying increase in friction factor.

Analogy Approach

Webb et al. [2000] in his paper provides experimental results as well as correlations developed from experiments for friction and Colburn factors for water in different geometries of augmented tubes. The correlations predict that friction factor and Colburn factor increase with increasing number of starters, rib height to inner diameter ratio, and helical angle, with friction factor being a stronger function of the last two parameters than Colburn [Webb, 2000]. When compared to experimental data, the correlations appear to over-predict the friction factor values by 0-15% while the Colburn j-factor error remains within 10%.

Gee and Webb [1980] performed an experimental investigation of helix angle change impact on single phase flow in circular tubes. The report presented the heat transfer and friction characteristics for air flow with three helix angles (30, 49 and 70°) all having a rib pitch-to-height ratio of 15. The preferred helix angle is approximately 45°. However, Pr number and

pitch variations are not included in the functions. Thus, the applicability range of the correlations is limited.

Statistical Approach

Bergles et al. [1996] attempted to construct a general correlation for friction factor and heat transfer coefficient over a wide range of hydraulic and geometric parameters for internally augmented tubes. Starting with a database previously developed by various authors' experimental and statistical correlations for different fluids and geometries, statistical analysis was applied to put together wide-ranging correlations. Further, different types of commercially available tubes were tested with heated water to validate the obtained correlations. The friction factor and Nu number correlations reduce to smooth-tube correlations as the rib height approaches zero. The friction factor correlation predicts 96% of the database to within + 50% and 77% of the database to within + 20%. Corresponding prediction figures for the heat-transfer correlation are 99% within 50% and 69% within 20% [Bergles at al., 1996].

Selected Correlations

Table **A-1** provides a summary of various heat transfer and friction factor correlations for augmented tubes. The study carried out by Ravigururajan [1999] tested and compared analogy based correlations and correlations developed using the statistical approach. Further, the correlations were evaluated for application to heat exchanger design. His work reveals the limitations of the analogy method. One of the main conclusions drawn from the study is the effectiveness of the statistical empirical methods over the analogy approach in predicting friction factor and Nusselt number [Ravigururajan, 1999]. Due to the generality of the Ravigururajan and Bergles correlations, the former were selected for FCR heat exchanger design.

Heat exchanger with ribbed tubes design

Evaluation of different fin geometries

The thermal design of the modified heat exchanger was unchanged. As in a straight tube IHX, the constant parameters were temperatures, energy balance, and flow rates. However, the CO_2 side correlations were changed to account for enhanced heat transfer.

Correlations suggested by Bergles et al. [1996] were used for the comparison analysis. The friction factor and heat transfer correlations developed by Bergles were intended for a wide range of parameters. Moreover, when applied to smooth tubes (assuming that the rib height approaches zero), such correlations produce results very close to the results obtained from the smooth tube analysis (see Table A-2). Correlations by Bergles et al. were statistically developed for a wide range of experimental data. They are based on correlations by Petukhov and Popov for Nusselt number and Filonenko for friction factor for smooth tubes.

The comparison of friction factor and heat transfer coefficient for a tube of outer diameter of 16 mm and pitch-to-diameter ratio of 1.161 was performed using the smooth tube Gnielinski correlation [1976] and the Bergles et al. correlation with zero rib height. Table A-2 compares these results and shows that the Bergles et al. correlation can closely reproduce smooth correlation results in the limit. Moreover, Bergles et al. provides conservative results for both the heat transfer coefficient and pressure drop.

Table A-1. Summary of different correlations for augmented tubes

Author	Fluid	Range of applicability	Geometry range	Nusselt number (*Nu*) correlation	Friction factor (*f*) correlation	Comments	Nomenclature
Webb, et al. (2000)	Single phase water	Pr: 5.08-6.29 Re: 20,000-80,000	Helically ribbed tube N_s :18-45 α(°) :25-45 e(mm):0.33-0.55	$j = 0.00933\,\mathrm{Re}^{-0.181} N_s^{0.285}\left(\frac{e}{D_i}\right)^{0.323} \times \alpha^{0.505}$ where $j = Colburn\ j\ factor$ $j = St\,\mathrm{Pr}^{2/3}$	$f = 0.108\,\mathrm{Re}^{-0.283} N_s^{0.221}\left(\frac{e}{D_i}\right)^{0.785} \alpha^{0.78}$	Correlations were developed for a specific range of Pr number. While providing good accuracy, they are not applicable for CO_2 heat transfer and friction factor of PR ≈ 0.7.	*f* fanning friction factor *e* rib height, m *d* maximum inside diameter, m α helix angle of rib (deg) *Ns* number of starts
Gee and Webb (1980)	Air	Pr for air Re: 6,000-65,000	Helically ribbed tube	$g = 6.03(e^+)^{0.2}(\alpha/50)^{1}$ $for\ e^+ > 8$ $j = 0.37\ for\ \alpha < 50°$ $j = -0.16\ for\ \alpha > 50°$	$A = 6.83(e^+)^{0.07}(\alpha/50)^{0.16}$ $for\ e^+ > 5$	Re number range is outside of the operating range of FCR IHX	α helix angle of rib (deg) e^+ roughness Re number *g* heat transfer correlator *A* friction correlator
Bergles et al. (1996) with subse-quent correc-tions	Air, water, hydrogen, n-butyl alcohol	Pr : 0.66-37.6 Re : 3,000-500,000	Helical e/d : 0.01-0.2 p/d : 0.1-7.0 α/90: 0.3-1.0	$\frac{Nu_a}{Nu_{sm}} = \left\{1 + \left[2.64\,\mathrm{Re}^{0.036}\left(\frac{e}{d}\right)^{0.212} \times \left(\frac{p}{d}\right)^{-0.21}\left(\frac{\alpha}{90}\right)^{0.29}\mathrm{Pr}^{-0.024}\right]^7\right\}^{1/7}$ Where Nu_{sm} number is given by Petukhov: $Nu_{sm} = \frac{\frac{f}{2}\mathrm{Re}\,\mathrm{Pr}}{1 + 12.7\left(\frac{f}{2}\right)^{0.5}\left(\mathrm{Pr}^{2/3} - 1\right)}$	$\frac{f_a}{f_{sm}} = \left\{1 + \left[29.1\,\mathrm{Re}^{(0.67 - 0.06p/d - 0.49\alpha/90)} \times \left(\frac{e}{d}\right)^{(1.37 - 0.157p/d)}\left(\frac{p}{d}\right)^{(-1.66e/d - 6\mathrm{Re} - 0.33\alpha/90)} \times \left(\frac{\alpha}{90}\right)^{(4.59 + 4.11e/d - 6\mathrm{Re} - 0.15p/d)} \times \left(1 + 2.94/n\sin(\beta)\right)\right]^{15/16}\right\}^{16/15}$ Where f_{sm} is given by Filonenko: $f_{sm} = (1.58\ln\mathrm{Re} - 3.28)^{-2}$	One of the better correlations found. Very wide range of applicability. The friction factor correlation predicts 96% of the database to within + 50% and 77% of the database to within + 20%. Corresponding prediction figures for the heat-transfer correlation are 99% and 69%.	*e* rib height, m *d* maximum inside diameter, m *p* pitch of ribs, m α helix angle of rib (deg) β contact angle of profile (deg) *n* number of sharp corners facing the flow that characterizes the rib profile Subscripts: *a* augmented tube *sm* smooth tube

Table A-2. Comparison of correlations by Bergles, et al. [1996] and correlations used for "smooth" heat exchanger design (same tube geometry)

	SMOOTH	BERGLES (-> SMOOTH)
$h=Nu \cdot k/D$	7360	7290
Nu correlation by	Gnielinski	Petukhov and Popov
Pressure drop	620.96 kPa	643.25 kPa
f correlation by	McAdams	Filonenko
Tube length	7.86 m	8.04 m

The purpose of ribs inside the tubes is twofold: first, they will allow for greater heat transfer area, and second, they will result in a constant turbulent sublayer disturbance enhancing the heat transfer. In the second case, the flow interrupted by the rib will cause the layers close to the wall to separate from the wall and reattach downstream of the rib at a distance of 5 to 8 times the rib height. If the pitch of the ribs is less than the distance required to achieve reattachment, the flow will slide over the ribs causing secondary flow patterns between the ribs [Ravigururajan, 1999]. For highly turbulent flows, the layer height is small; thus small roughness height is required. Helix angle also plays a significant role in the flow patterns.

Before the final heat exchanger design was selected, an evaluation of friction factor and Nusselt number variation with geometry of the internal ribs was conducted. Figure A-1 illustrates fin configuration inside the tube. As can be seen from Figure A-2 and Figure A-3, both quantities increase with a rise in the number of ribs and helix angle.

The effect of the number of ribs on the heat transfer is not as pronounced as the angle of helix. For the comparison, the pitch between the fins was kept less than 5 times the rib height as discussed previously. Thus, the heat transfer enhancement happens mostly due to the turbulent sublayer disturbance, and less due to the increase in area. The friction factor increases exponentially with the rib helix angle while the Nusselt number is linear. Thus, smaller angle values will assure less pressure drop without largely affecting the heat transfer coefficient.

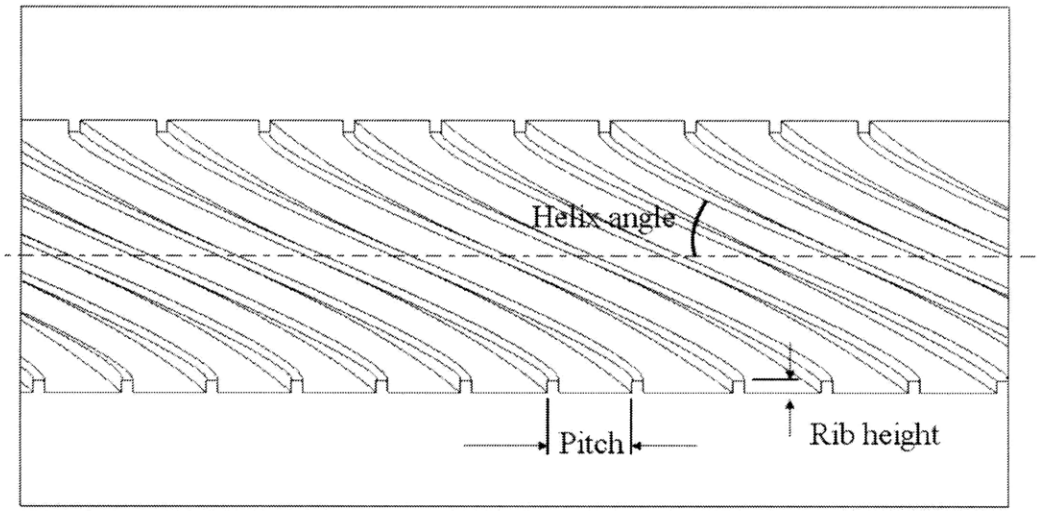

Figure A-1. Schematics of helical ribs inside the tube [Gee and Webb, 1980]

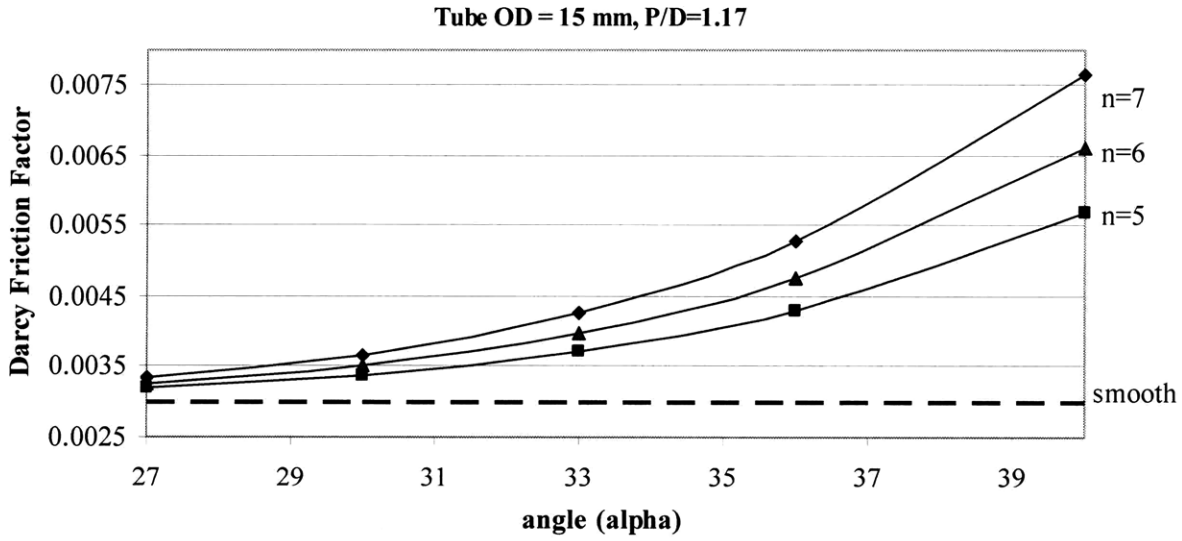

Figure A-2. Friction factor variation with the helix angle and number of fins

Pressure drop and heat transfer of the flow are illustrated in Figure A-4. At first, Nu number shows a strong increase with increasing rib height. However, for a given geometry, it saturates around 1700. On the other hand, the friction factor demonstrates a non-linear increase with increased rib height. Thus, the optimum value for the rib height is around 0.3-0.5 mm.

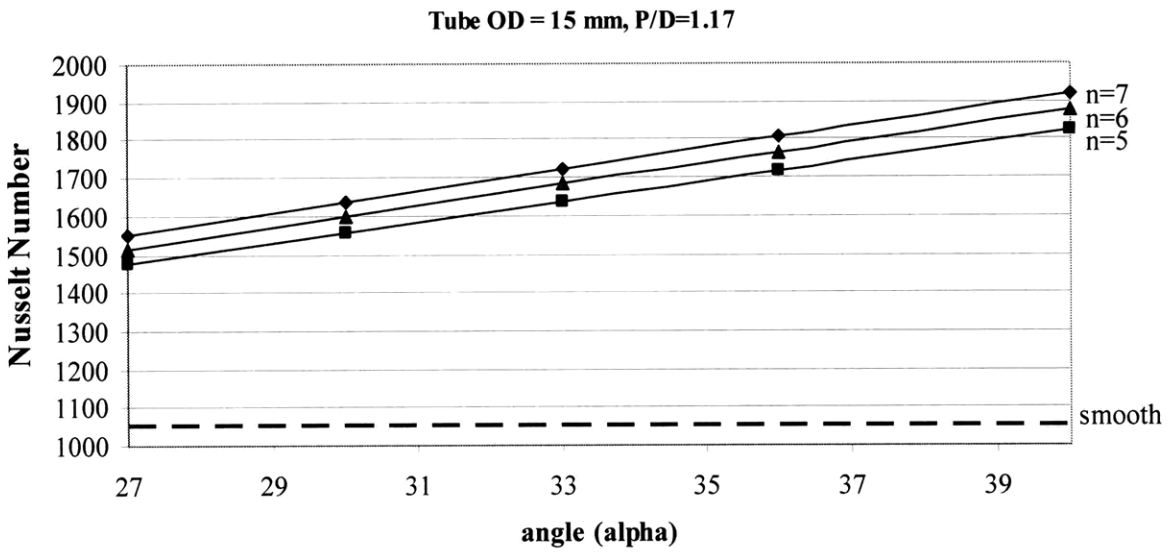

Figure A-3. Nusselt number variation with the helix angle and number of fins

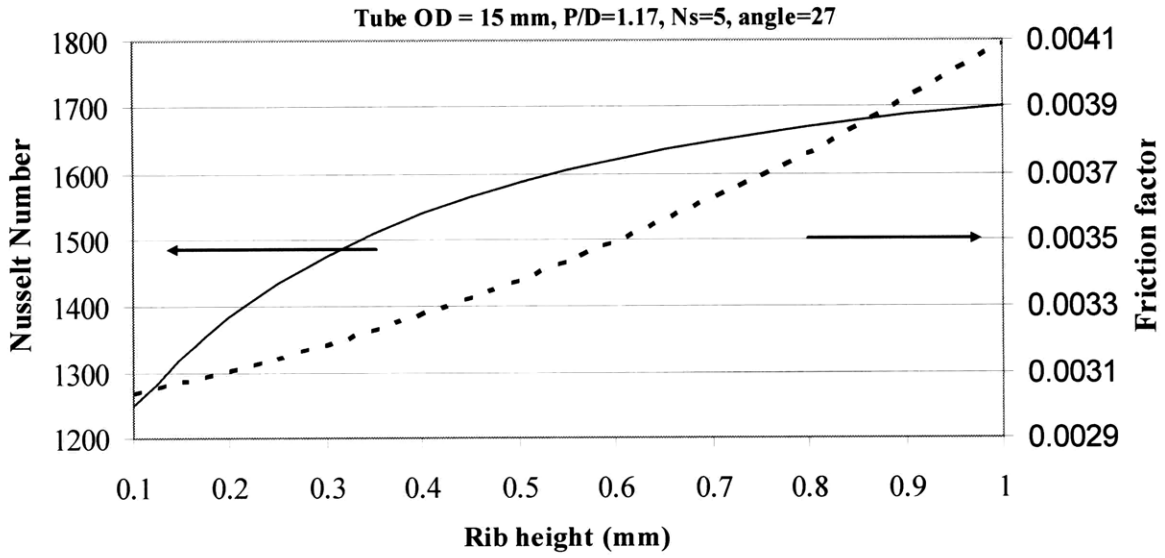

Figure A-4. Nu number and friction factor dependence on the rib height

Evaluation of different IHX tube geometries

Taking all of the above recommendations into consideration, an evaluation of different tube geometries was conducted. The same tube geometry as for smooth tubes was used for the

calculations. Table A-3 summarizes the output values for the IHX with enhanced heat transfer tubes.

Figure A-5 compares the pressure drops for both sides in smooth and augmented tubes. The values are for the tubes with outer diameter of 14 mm. Other geometries exhibit similar behavior. Enhanced heat transfer allowed a reduction in tube length (active heat transfer area) therefore a significant reduction of the pressure drop on the lead side. As a result, the required pumping power values are decreased as well.

In the augmented tubes, the pressure drop of carbon dioxide does not vary significantly with the tube diameter (see Figure A-6). However, it increases rapidly with increasing P/D ratio (smaller number of tubes increases the CO_2 velocity), as can be seen from Figure A-5. The outer diameter of 15 mm yields the smallest pressure drop on the secondary side. Ideally, a pitch-to-diameter ratio of 1.15 or smaller should be used; however, this creates an increase in lead velocity above 3 m/s. Thus, the optimal P/D that also provides a margin to the lead velocity constraint is 1.17.

Heat exchanger tube wall thickness varies with the diameter of the tube. As the outer diameter increases, the wall thickness also increases. As can be seen in Figure A-6, even though the inside diameter of the tube increases, the CO_2 pressure drop continues to increase. This occurs due to the decrease in the overall heat transfer coefficient. The overall heat transfer coefficient strongly depends on the steel wall conduction heat transfer, which becomes dominant heat transfer resistance for thick walls. Thus, longer tubes are needed to accommodate the loss in the overall heat transfer coefficient causing increased pressure drop.

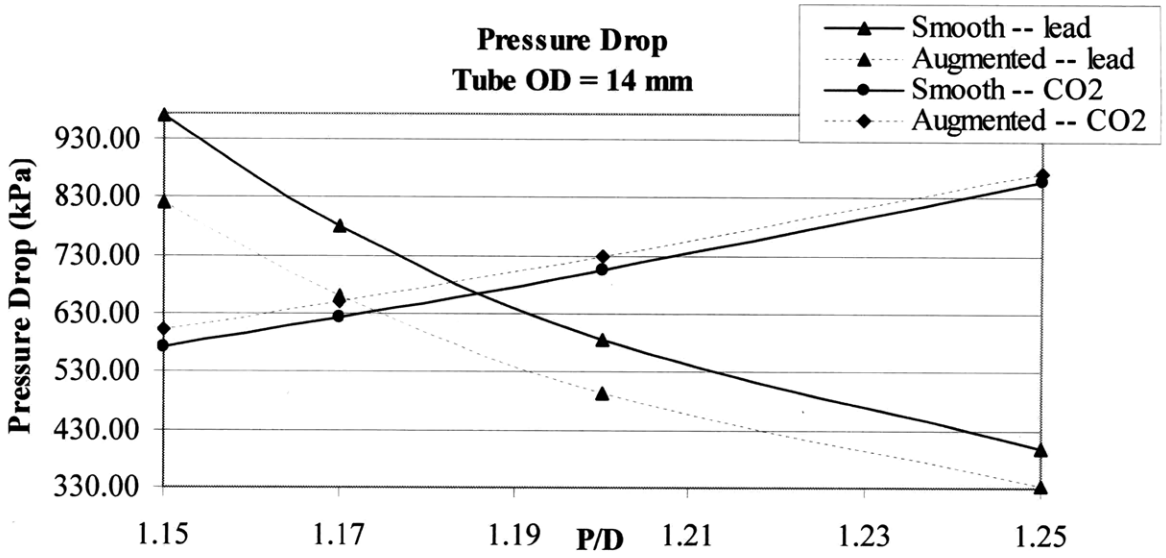

Figure A-5. Pressure drop dependence on the P/D ratio

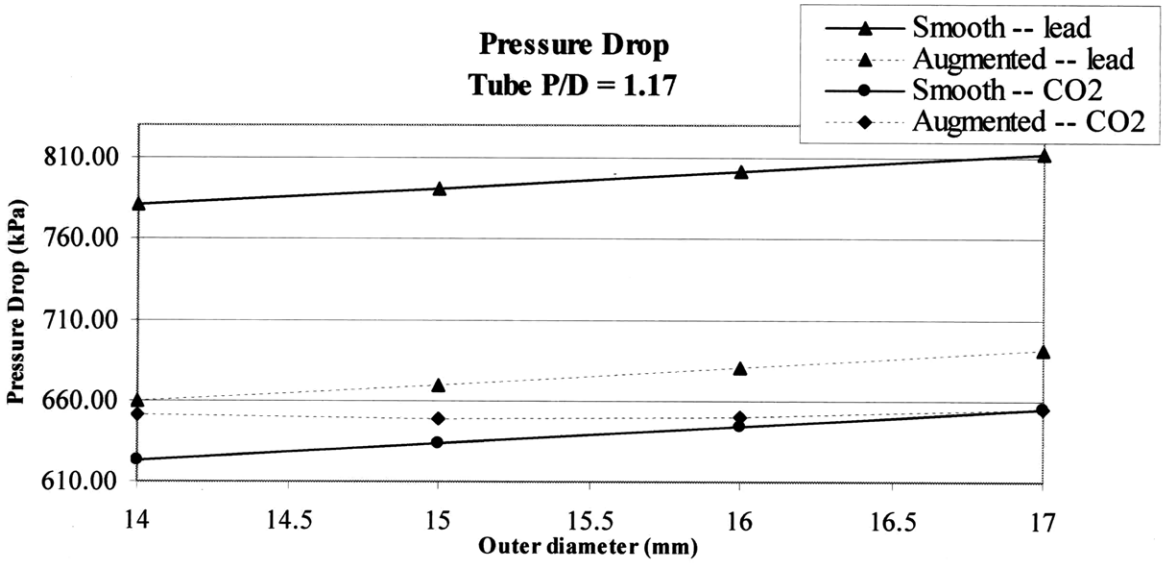

Figure A-6. Pressure drop dependence on the tube outer diameter

Table A-3. Comparison of different tube geometries for IXH with augmented* tubes

P/D	Lead velocity (m/s)	CO_2 velocity (m/s)	Lead pressure drop (kPa)	CO2 pressure drop (kPa)	Tube Length (m)	Lead side pumping power**	HT area (m^2)	Number of tubes
OD=14mm								
1.15	2.99	26.13	823.04	604.72	5.41	1.23	2544.7	19678
1.17	2.79	27.04	660.29	652.10	5.55	1.12	2520.5	19011
1.2	2.54	28.45	494.93	728.59	5.75	1.01	2483.2	18073
1.25	2.24	30.87	333.07	871.98	6.08	0.89	2418.9	16656
OD=15mm								
1.15	2.99	26.11	835.69	601.70	6.04	1.24	2650.4	17142
1.17	2.79	27.02	670.12	649.89	6.20	1.13	2625.5	16561
1.2	2.54	28.43	502.06	727.91	6.42	1.01	2586.9	15743
1.25	2.24	30.84	337.59	874.37	6.79	0.90	2520.6	14509
OD=16mm								
1.15	2.99	26.09	849.20	602.22	6.70	1.25	2754.5	15066
1.17	2.79	27.01	680.72	651.38	6.87	1.14	2728.8	14555
1.2	2.54	28.41	509.67	730.93	7.12	1.02	2689.2	13837
1.25	2.24	30.82	342.52	880.74	7.53	0.90	2620.8	12752
OD=17mm								
1.15	2.99	26.08	863.18	605.25	7.38	1.26	2857.2	13346
1.17	2.79	26.99	691.75	655.46	7.57	1.14	2830.8	12893
1.2	2.54	28.39	517.71	736.72	7.85	1.02	2790.1	12257
1.25	2.24	30.81	347.72	889.92	8.30	0.90	2719.8	11296

* Helical ribs with rib height of 0.35 mm, rib pitch of 1.4 mm and helix angle of 27°.

** Expressed in percent of the total core thermal power. Includes pressure drop through the core and heat exchanger.

A.7. References for Appendix A

Bergles A. E., Ravigururajan T. S., Development and Verification of General Correlations for Pressure Drop and Heat Transfer in Single-Phase Turbulent Flow in Enhanced Tubes, *Experimental Thermal and Fluid Science,* **13**, pp. 55-70, 1996.

Cheng S. K. and Todreas N. E., "Hydrodynamic models and correlations for bare and wire-wrapped hexagonal rod bundles – Bundle friction factors, subchannel friction factors and mixing parameters," *Nuclear Engineering and Design*, **92**, 2, pp. 227-251, April 1986.

El-Wakil M. M., Nuclear Heat Transport, American Nuclear Society, La Grange Park, IL, USA, 1978.

Gee D. L., and Webb R. L., Forced Convection Heat Transfer in Helically Rib-Roughened Tubes, *Int. J. Heat Mass Transfer,* **23**, pp. 1127-1136, 1980.

Gnielinski V., "New Equations for Heat and Mass Transfer in Turbulent Pipe and Channel Flow", *International Chemical Engineering*, **6**, 2, pp. 359-368, April 1976.

Ravigururajan T. S., A Comparative Study of Thermal Design Correlations for Turbulent Flow in Helical-Enhanced Tubes, *Heat Transfer Engineering,* **20**, pp. 54-70, 1999.

Todreas N.E., and Kazimi M.S., Nuclear Systems I: *Thermal Hydraulic Fundamentals*, Taylor and Francis, 1993.

Webb R. L., Narayanamurthy, R., Thors, P., Heat Transfer and Friction Characteristics of Internal Helical-Rib Roughness, *Journal of Heat Transfer,* **122**, pp. 134-142, 2000.

B. APPENDIX B RELAP5/ATHENA INPUT EXAMPLES

This chapter provides input examples for key features of the RELAP5/ATHENA model. All of the examples are given for the unity conversion ratio core, but most are applicable for both cores.

B.1. Core Input

The core is divided into two channels: hot (510) and average (516). The model includes the pressure drop due to the grid spacers and the orificing. The active core is divided into five meshes. With relatively short fuel pins (1.3 m), five meshes is acceptable. However, for larger assemblies, more meshes might be required for accuracy.

```
*------------------------------------------------------------------------------
5100000             avcore           pipe
*------------------------------------------------------------------------------
5100001   8
5100101   7.869982359  8
5100301   1.00         1
5100302   0.30         2
5100303   0.26         7
5100304   1.30         8
5100401   0.0          8
5100601   90.0         8
5100701   1.00         1
5100702   0.30         2
5100703   0.26         7
5100704   1.30         8
**hydro   roughness  hyd diam    vol
5100801   1.524E-6   8.07160E-03 8
5100901   0.0        0.0         2
5100902   0.87       0.87        3
5100903   0.0        0.0         7
5101001   00          8
5101101   001000      7
5101201   0          2004797.    105904.    1082718. 0.       0.    1
5101202   0          1905581.    105905.5   1081939. 0.       0.    2
5101203   0          1862875.    108327.    1081594. 0.       0.    3
5101204   0          1802798.    111483.5   1081099. 0.       0.    4
5101205   0          1763247.    115146.2   1080765. 0.       0.    5
5101206   0          1723775.    117975.5   1080427. 0.       0.    6
5101207   0          1684387.    119718.2   1080084. 0.       0.    7
5101208   0          1566470.    119725.    1079017. 0.       0.    8
5101300    0
5101301   2.1442       2.1442      0.              1 * 171402.
5101302   2.14421      2.14421     0.              2 * 171402.
5101303   2.148173     2.148173    0.              3 * 171402.
5101304   2.153355     2.153355    0.              4 * 171402.
5101305   2.15939      2.15939     0.              5 * 171402.
```

```
5101306   2.164068      2.164068     0.              6 * 171402.
5101307   2.16696       2.16696      0.              7 * 171402.
5101402   8.07160E-03   0.0     1.0      1.0      7
*-------------------------------------------------------------------------
5150000                 avgexit            sngljun
*-------------------------------------------------------------------------
5150101   510010000     520000000      0.0          0.0      0.0     01100
5150201   0             2.16698        2.16698      0. * 171402.
5150110   8.07160E-03   0.0            1.0          1.0
*-------------------------------------------------------------------------
5160000             hotchan            pipe
*-------------------------------------------------------------------------
5160001   8
5160101   0.091246172   8
5160301   1.00          1
5160302   0.30          2
5160303   0.26          7
5160304   1.30          8
5160401   0.0           8
5160601  90.0           8
5160701   1.00          1
5160702   0.30          2
5160703   0.26          7
5160704   1.30          8
**hydro   roughness   hyd diam    vol
5160801   1.524E-6    8.07160E-03 8
5160901   0.0         0.0         2
5160902   0.8708      0.8708      3
5160903   0.0         0.0         7
5161001  00            8
5161101  001000        7
**Corrected pressure drops and temperatures
5161201  0           2043685.    105905.    1082998. 0.       0.    1
5161202  0           1937445.    105906.9   1082193. 0.       0.    2
5161203  0           1891717.    108564.6   1081828. 0.       0.    3
5161204  0           1824243.    112029.4   1081277. 0.       0.    4
5161205  0           1781883.    116049.6   1080923. 0.       0.    5
5161206  0           1739611.    119155.    1080564. 0.       0.    6
5161207  0           1697438.    121068.    1080198. 0.       0.    7
5161208  0           1571234.    121076.    1079061. 0.       0.    8
**Corrected velocities 5161300   0
5161301   2.371556      2.371556     0.              1 * 2197.987
5161302   2.37157       2.37157      0.              2 * 2197.987
5161303   2.37638       2.37638      0.              3 * 2197.987
5161304   2.382674      2.382674     0.              4 * 2197.987
5161305   2.390004      2.390004     0.              5 * 2197.987
5161306   2.39569       2.39569      0.              6 * 2197.987
5161307   2.399205      2.399205     0.              7 * 2197.987
5161402   8.07160E-03   0.0     1.0      1.0      7
*-------------------------------------------------------------------------
5180000                hotexit            sngljun
*-------------------------------------------------------------------------
5180101   516010000     520000000     0.0         0.0     0.0    01100
5180201   0             2.39923       2.39923     0. * 2197.987
5180110   8.07160E-03   0.0           1.0         1.0
*-------------------------------------------------------------------------
```

```
*************************** STRUCTURE 5101 ****************************
* average fuel assembly (1.3 m)
*=====================================================================$
15101000  5    9    2     1      0.0     0
15101100  0         1
15101101  5         0.00271
15101102  1         0.00313
15101103  1         0.00376
15101104  1         0.00377
15101201  1         5
15101202 -2         6
15101203 -13         7
15101204 -4         8
15101301  1.0       5
15101302  0.0       8
15101400  0
15101401  800.0       9
15101501  0         0         0         0         0.0         5
15101601  510030000 10000     110         1      38940.85     5
15101701  10110    0.17286    0.0       0.0       1
15101702  10110    0.22537    0.0       0.0       2
15101703  10110    0.26152    0.0       0.0       3
15101704  10110    0.20199    0.0       0.0       4
15101705  10110    0.12438    0.0       0.0       5
15101900    1
15101901 0.0     10. 10. 10.   10.  0.0   0.0   1.0   1.3  1.3  1.0  5
*************************** STRUCTURE 5161 ****************************
* hot fuel assembly
*=====================================================================$
15161000  5    9    2     1      0.0     0
15161100  0         1
15161101  5         0.00271
15161102  1         0.00313
15161103  1         0.00376
15161104  1         0.00377
15161201  1         5
15161202 -2         6
15161203 -13         7
15161204 -4         8
15161301  1.0       5
15161302  0.0       8
15161400  0
15161401  800.0       9
15161501  0         0         0         0         0.0         5
15161601  516030000 10000     110         1      451.48814    5
15161701  10110    0.0024329  0.0       0.0       1
15161702  10110    0.0031721  0.0       0.0       2
15161703  10110    0.0036808  0.0       0.0       3
15161704  10110    0.0028429  0.0       0.0       4
15161705  10110    0.0017506  0.0       0.0       5
15161900    1
15161901 0.0     10. 10. 10.   10.  0.0   0.0   1.0   1.3  1.3  1.0  5
```

B.2. IHX Input

The lead-side of the IHX (560) is modeled as a bundle of non-communicating parallel channels. Note that this input represents two heat exchangers bundled together. The gas-side of the IHX (399) is similar to the lead. the two fluids exchange heat through the model of the IHX walls (1560). The heat structure includes the tube wall and the oxide layer on the lead-side. The gas-side heat transfer enhancement is modeled as heat transfer multiplier.

```
*==========================================================================
5600000   ihx1-lead      pipe
*--------------------------------------------------------------------------
*         no. vols
5600001   50
*         vol area
5600101   3.937599  50
*         length
5600301   0.114     50
*         volume
5600401   0.0       50
*         azim angle
5600501   0.0       50
*         incl angle
5600601   -90.0     50
5600701   -0.114    50
*         roughness hyd dia
5600801   4.572e-6  9.355E-03 50
*         kf        kr
5600901   0.0       0.0       49
*         pvbfe
5601001   00000     50
*         fvcahs
5601101   001000     49
*         ebt
5601201    0  466918.   119578.6    1063147. 0. 0.    1
5601202    0  472420.   119424.7    1063287. 0. 0.    2
5601203    0  477923.4  119267.2    1063425. 0. 0.    3
5601204    0  483428.   119106.     1063562. 0. 0.    4
5601205    0  488934.   118941.2    1063698. 0. 0.    5
5601206    0  494442.   118772.6    1063833. 0. 0.    6
5601207    0  499951.   118600.     1063967. 0. 0.    7
5601208    0  505461.   118423.5    1064097. 0. 0.    8
5601209    0  510973.   118243.     1064226. 0. 0.    9
5601210    0  516487.   118058.2    1064354. 0. 0.    10
5601211    0  522002.   117869.2    1064480. 0. 0.    11
5601212    0  527519.   117675.9    1064606. 0. 0.    12
5601213    0  533037.   117478.     1064731. 0. 0.    13
5601214    0  538558.   117275.8    1064855. 0. 0.    14
5601215    0  544079.   117068.8    1064978. 0. 0.    15
5601216    0  549603.   116857.1    1065100. 0. 0.    16
5601217    0  555129.   116640.6    1065221. 0. 0.    17
5601218    0  560656.   116419.1    1065341. 0. 0.    18
5601219    0  566185.   116192.5    1065460. 0. 0.    19
5601220    0  571716.   115960.7    1065579. 0. 0.    20
```

```
5601221     0  577250.   115723.6    1065696. 0. 0.    21
5601222     0  582785.   115481.     1065813. 0. 0.    22
5601223     0  588322.   115233.     1065929. 0. 0.    23
5601224     0  593861.   114979.2    1066044. 0. 0.    24
5601225     0  599403.   114719.7    1066158. 0. 0.    25
5601226     0  604946.   114454.3    1066271. 0. 0.    26
5601227     0  610492.   114182.9    1066384. 0. 0.    27
5601228     0  616040.   113905.2    1066496. 0. 0.    28
5601229     0  621591.   113621.3    1066607. 0. 0.    29
5601230     0  627143.   113331.     1066718. 0. 0.    30
5601231     0  632698.   113034.     1066827. 0. 0.    31
5601232     0  638256.   112730.2    1066936. 0. 0.    32
5601233     0  643816.   112419.5    1067044. 0. 0.    33
5601234     0  649379.   112101.8    1067152. 0. 0.    34
5601235     0  654944.   111777.     1067259. 0. 0.    35
5601236     0  660512.   111444.7    1067365. 0. 0.    36
5601237     0  666082.   111105.     1067471. 0. 0.    37
5601238     0  671656.   110757.5    1067576. 0. 0.    38
5601239     0  677232.   110402.3    1067680. 0. 0.    39
5601240     0  682811.   110039.     1067784. 0. 0.    40
5601241     0  688393.   109667.5    1067887. 0. 0.    41
5601242     0  693978.   109287.6    1067989. 0. 0.    42
5601243     0  699565.   108899.2    1068091. 0. 0.    43
5601244     0  705156.   108502.     1068192. 0. 0.    44
5601245     0  710750.   108095.8    1068293. 0. 0.    45
5601246     0  716347.   107680.5    1068393. 0. 0.    46
5601247     0  721948.   107255.8    1068493. 0. 0.    47
5601248     0  727551.   106821.5    1068592. 0. 0.    48
5601249     0  733158.   106377.4    1068690. 0. 0.    49
5601250     0  738769.   105923.5    1068788. 0. 0.    50
*         vel/flow
5601300   0
*         liquid    vapor     int-face
5601301   2.193217  2.233013 0.       1 * 86802.6
5601302   2.19296   2.220006 0.       2 * 86802.6
5601303   2.192693  2.207844 0.       3 * 86802.6
5601304   2.19242   2.19717  0.       4 * 86802.6
5601305   2.192145  2.192145 0.       5 * 86802.6
5601306   2.19186   2.19186  0.       6 * 86802.6
5601307   2.191572  2.191572 0.       7 * 86802.6
5601308   2.191276  2.191276 0.       8 * 86802.6
5601309   2.190973  2.190973 0.       9 * 86802.6
5601310   2.190663  2.190663 0.       10 * 86802.6
5601311   2.190346  2.190346 0.       11 * 86802.6
5601312   2.19002   2.19002  0.       12 * 86802.6
5601313   2.18969   2.18969  0.       13 * 86802.6
5601314   2.18935   2.18935  0.       14 * 86802.6
5601315   2.189003  2.189003 0.       15 * 86802.6
5601316   2.18865   2.18865  0.       16 * 86802.6
5601317   2.188286  2.188286 0.       17 * 86802.6
5601318   2.187915  2.187915 0.       18 * 86802.6
5601319   2.187536  2.187536 0.       19 * 86802.6
5601320   2.187147  2.187147 0.       20 * 86802.6
5601321   2.18675   2.18675  0.       21 * 86802.6
5601322   2.186345  2.186345 0.       22 * 86802.6
5601323   2.18593   2.18593  0.       23 * 86802.6
5601324   2.185506  2.185506 0.       24 * 86802.6
```

```
5601325   2.185072  2.185072 0.       25 * 86802.6
5601326   2.18463   2.18463  0.       26 * 86802.6
5601327   2.184175  2.184175 0.       27 * 86802.6
5601328   2.183712  2.183712 0.       28 * 86802.6
5601329   2.18324   2.18324  0.       29 * 86802.6
5601330   2.182753  2.182753 0.       30 * 86802.6
5601331   2.18226   2.18226  0.       31 * 86802.6
5601332   2.18175   2.18175  0.       32 * 86802.6
5601333   2.181234  2.181234 0.       33 * 86802.6
5601334   2.180705  2.180705 0.       34 * 86802.6
5601335   2.180163  2.180163 0.       35 * 86802.6
5601336   2.17961   2.17961  0.       36 * 86802.6
5601337   2.179045  2.179045 0.       37 * 86802.6
5601338   2.178467  2.178467 0.       38 * 86802.6
5601339   2.177876  2.177876 0.       39 * 86802.6
5601340   2.17727   2.17727  0.       40 * 86802.6
5601341   2.176655  2.176655 0.       41 * 86802.6
5601342   2.176024  2.176024 0.       42 * 86802.6
5601343   2.17538   2.17538  0.       43 * 86802.6
5601344   2.17472   2.17472  0.       44 * 86802.6
5601345   2.174046  2.174046 0.       45 * 86802.6
5601346   2.173357  2.173357 0.       46 * 86802.6
5601347   2.172653  2.172653 0.       47 * 86802.6
5601348   2.171934  2.171934 0.       48 * 86802.6
5601349   2.1712    2.1712   0.       49 * 86802.6
*hydro jun diam      beta  intercept slope    jun
5601401   9.355E-03  0.0     1.0     1.0      49



*=============================================================================
3990000   IHX-CO2      pipe
*-----------------------------------------------------------------------------
*         no. vols
3990001   50
*         vol area
3990101   2.737    50
*         length
3990301   0.114    50
*         volume
3990401   0.0      50
*         azim angle
3990501   0.0      50
*         incl angle
3990601   90.0     50
*         roughness hyd dia
3990801   1.0e-6    8.990E-03 50
*         kf         kr
3990901   0.0        0.0       49
*         pvbfe
3991001   00000     50
*         fvcahs
3991101   001000     49
*         ebt
3991201    0  19776750. 722620.     722620.  1. 0.    1
3991202    0  19773172. 727594.     727594.  1. 0.    2
```

```
3991203    0  19769584. 732456.     732456.  1. 0.    3
3991204    0  19765974. 737209.     737209.  1. 0.    4
3991205    0  19762346. 741856.     741856.  1. 0.    5
3991206    0  19758696. 746399.     746399.  1. 0.    6
3991207    0  19755030. 750857.     750857.  1. 0.    7
3991208    0  19751346. 755217.     755217.  1. 0.    8
3991209    0  19747644. 759479.     759479.  1. 0.    9
3991210    0  19743924. 763646.     763646.  1. 0.    10
3991211    0  19740186. 767720.     767720.  1. 0.    11
3991212    0  19736430. 771703.     771703.  1. 0.    12
3991213    0  19732658. 775596.     775596.  1. 0.    13
3991214    0  19728870. 779411.     779411.  1. 0.    14
3991215    0  19725066. 783146.     783146.  1. 0.    15
3991216    0  19721248. 786797.     786797.  1. 0.    16
3991217    0  19717414. 790366.     790366.  1. 0.    17
3991218    0  19713566. 793855.     793855.  1. 0.    18
3991219    0  19709702. 797265.     797265.  1. 0.    19
3991220    0  19705824. 800598.     800598.  1. 0.    20
3991221    0  19701930. 803856.     803856.  1. 0.    21
3991222    0  19698024. 807040.     807040.  1. 0.    22
3991223    0  19694104. 810163.     810163.  1. 0.    23
3991224    0  19690172. 813216.     813216.  1. 0.    24
3991225    0  19686228. 816200.     816200.  1. 0.    25
3991226    0  19682272. 819116.     819116.  1. 0.    26
3991227    0  19678302. 821967.     821967.  1. 0.    27
3991228    0  19674320. 824754.     824754.  1. 0.    28
3991229    0  19670326. 827477.     827477.  1. 0.    29
3991230    0  19666320. 830138.     830138.  1. 0.    30
3991231    0  19662302. 832739.     832739.  1. 0.    31
3991232    0  19658274. 835280.     835280.  1. 0.    32
3991233    0  19654234. 837763.     837763.  1. 0.    33
3991234    0  19650184. 840198.     840198.  1. 0.    34
3991235    0  19646124. 842578.     842578.  1. 0.    35
3991236    0  19642054. 844903.     844903.  1. 0.    36
3991237    0  19637976. 847176.     847176.  1. 0.    37
3991238    0  19633886. 849397.     849397.  1. 0.    38
3991239    0  19629786. 851567.     851567.  1. 0.    39
3991240    0  19625678. 853688.     853688.  1. 0.    40
3991241    0  19621560. 855761.     855761.  1. 0.    41
3991242    0  19617432. 857786.     857786.  1. 0.    42
3991243    0  19613296. 859766.     859766.  1. 0.    43
3991244    0  19609152. 861700.     861700.  1. 0.    44
3991245    0  1.9605+7  863590.     863590.  1. 0.    45
3991246    0  19600836. 865438.     865438.  1. 0.    46
3991247    0  19596666. 867243.     867243.  1. 0.    47
3991248    0  19592488. 869010.     869010.  1. 0.    48
3991249    0  19588302. 870739.     870739.  1. 0.    49
3991250    0  19584110. 872430.     872430.  1. 0.    50
*        vel/flow
3991300  0
*        liquid    vapor     int-face
3991301  15.0442    15.0442   0.     1 * 6372.
3991302  15.1794    15.1794   0.     2 * 6372.
3991303  15.31168   15.31168  0.     3 * 6372.
3991304  15.44113   15.44113  0.     4 * 6372.
3991305  15.5678    15.5678   0.     5 * 6372.
3991306  15.69174   15.69174  0.     6 * 6372.
```

```
3991307   15.81104   15.81104  0.      7 * 6372.
3991308   15.92762   15.92762  0.      8 * 6372.
3991309   16.0417    16.0417   0.      9 * 6372.
3991310   16.15336   16.15336  0.      10 * 6372.
3991311   16.26263   16.26263  0.      11 * 6372.
3991312   16.36956   16.36956  0.      12 * 6372.
3991313   16.4742    16.4742   0.      13 * 6372.
3991314   16.5755    16.5755   0.      14 * 6372.
3991315   16.6741    16.6741   0.      15 * 6372.
3991316   16.77058   16.77058  0.      16 * 6372.
3991317   16.86502   16.86502  0.      17 * 6372.
3991318   16.95745   16.95745  0.      18 * 6372.
3991319   17.0479    17.0479   0.      19 * 6372.
3991320   17.13643   17.13643  0.      20 * 6372.
3991321   17.22308   17.22308  0.      21 * 6372.
3991322   17.30787   17.30787  0.      22 * 6372.
3991323   17.38967   17.38967  0.      23 * 6372.
3991324   17.46968   17.46968  0.      24 * 6372.
3991325   17.548     17.548    0.      25 * 6372.
3991326   17.62466   17.62466  0.      26 * 6372.
3991327   17.6997    17.6997   0.      27 * 6372.
3991328   17.77317   17.77317  0.      28 * 6372.
3991329   17.84508   17.84508  0.      29 * 6372.
3991330   17.91546   17.91546  0.      30 * 6372.
3991331   17.98436   17.98436  0.      31 * 6372.
3991332   18.0518    18.0518   0.      32 * 6372.
3991333   18.1178    18.1178   0.      33 * 6372.
3991334   18.18154   18.18154  0.      34 * 6372.
3991335   18.24393   18.24393  0.      35 * 6372.
3991336   18.30502   18.30502  0.      36 * 6372.
3991337   18.36483   18.36483  0.      37 * 6372.
3991338   18.4234    18.4234   0.      38 * 6372.
3991339   18.48075   18.48075  0.      39 * 6372.
3991340   18.5369    18.5369   0.      40 * 6372.
3991341   18.59188   18.59188  0.      41 * 6372.
3991342   18.64573   18.64573  0.      42 * 6372.
3991343   18.69846   18.69846  0.      43 * 6372.
3991344   18.7501    18.7501   0.      44 * 6372.
3991345   18.8007    18.8007   0.      45 * 6372.
3991346   18.85024   18.85024  0.      46 * 6372.
3991347   18.89878   18.89878  0.      47 * 6372.
3991348   18.94613   18.94613  0.      48 * 6372.
3991349   18.99212   18.99212  0.      49 * 6372.
*hydro jun diam      beta  intercept slope    jun
3991401   8.990E-03  0.0     1.0     1.0     49

*************************** STRUCTURE 5601 ***************************
* 1 IHX heat structure
*=====================================================================$
*ht str ht.strs  m.pts  geom  init  l.coord  refl  b.vol
15601000   50      6    2     1    0.004780844  0
*
*        loc      flag
15601100  0         1
*
*         #         r
15601101  4         0.00700
```

```
15601102  1          0.00701
*
*         compos.    #
15601201    13        4
15601202    4         5
*
*          source    #
15601301  0.0        5
*
*         temperature flag
15601400  0
*
*          temperature #
15601401  750.00       6
*
*          vol        inc        type       code       factor
15601501  399010000   10000     160          1         4371.44    50
*          vol        inc        type       code       factor
15601601  560500000  -10000     110          1         4371.44    50
*
*
*          type       mult       D-lt       D-rt       #    *sour
15601701   0          0.0        0.0        0.0        50
*
15601800    1
*          Dhe    LHEf      LHEr      LGSf LGSr Kfwd Krev  Fboi   nclf povd  ff
#
15601801  0.0  10.0     10.0    10.0 10.0 0.0   0.0   1.0  5.7  1.23  1.36   1
15601802  0.0  10.0     10.0    10.0 10.0 0.0   0.0   1.0  5.7  1.23  1.36  25
15601803  0.0  10.0     10.0    10.0 10.0 0.0   0.0   1.0  5.7  1.23  1.36  50
*
15601900    1
*          Dhe    LHEf      LHEr     LGSf  LGSr Kfwd  Krev  Fbo
15601901  0.0  10.0     10.0    10.0 10.0 0.0   0.0   1.0  5.7  1.23  1.0    50
*=================================================================$
*
```

B.3. Primary Coolant Pump Input

```
*-------------------------------------------------------------------------
5950000   rcp1       pump
*-------------------------------------------------------------------------
*
5950101   1.332                2.05             0.0
*
5950102   0.00           -90.0             -2.05        00000
*
5950108   590000000  0.0       0.02       0.02    001000
*
5950109   500010004  0.0       0.02       0.02    001000
*
5950110   0.65       0.00      1.00       1.00
5950111   0.65       0.00      1.00       1.00
*
```

```
5950200   0          932207.       106282.7     1071856.      0.
*
5950201   0          12.83528  13.83774 0. * 173600.
*
5950202   0          12.8354   12.8354  0. * 173600.
5950301    -2     -1    -3    -1    0    595    0
*      Pump description
*           Rated pump velocity (rads/sec)
*           |           Ratio of initial pump velocity to rated pump velocity
*           |           |     Rated flow (m3/s)
*           |           |     |     rated head (m)
*           |           |     |     |
5950302    102.77    .99124   17.087 8.76143
*           Rated torque (N*m)
*           |           Moment of inertia (kg*m2)
*           |           |     Rated density (kg/m3)
*           |           |     |           Rated pump motor torque (N*m)
*           |           |     |           |
5950303  1.45187E+05  2819.6 10160.      0.00
*           Second frictional torque coefficient (N*m)
*           |     Constant frictional torque coefficient (N*m)
*           |     |           First frictional torque coefficient (N*m)
*           |     |           |     Third frictional torque coefficient (N*m)
*           |     |           |     |
5950304  1451.87  1451.87     0.00  0.00
5956100  594     cntrlvar    570
5956101    0.0     0.0
5956102  200.0     200.0
*-------------------------------------------------------------------------------
```

B.4. RVACS Input

The RVACS model consists of hydrodynamic volumes, heat structures and radiation model.

```
*===============================================================================
8000000   supply    tmdpvol
*-------------------------------------------------------------------------------
*         area                 length          volume
8000101   1.e5                  1.0              0.0
*         azim angle           incl angle       delta z
8000102   0.00                -90.0              -1.0
*         roughness            hyd dia          pvbfe
8000103   0.00000              0.0000           00010
*         ebt       trip           search var
8000200   004       0
*         indep var
8000201   0.00      1.e5     310.93  0.0
*===============================================================================
*8000000   supply    tmdpvol
*-------------------------------------------------------------------------------
*         area                 length          volume
*8000101   13.823               20.0              0.0
*         azim angle           incl angle       delta z
```

```
*8000102   0.00                -90.0              -20.0
*          roughness           hyd dia          pvbfe
*8000103   4.572e-5             0.8              00010
*          ebt       trip          search var
*8000200   004       0
*          indep var
*8000201   0.00      1.e5     310.93  0.0
*=============================================================================
*hydro             component name      component type
8050000               inlet               sngljun
*-----------------------------------------------------------------------------
*hydro    from          to           area      f loss    r loss  vcahs
8050101   800010000     810000000    29.6566   0.5       1.0     01000
*
*hydro    vel/flw       f flowrate     g flowrate     j flowrate
8050201   0             2.370757       2.370757       0. * 78.7705
*hydro    dhjun         beta           c            m
8050110   1.6           0.0            1.0          1.0
*
*=============================================================================
8100000   dwncmr    pipe
*-----------------------------------------------------------------------------
*         no. vols
8100001   15
*         vol area
8100101   29.6566  15  *~AN
*         length
8100301   1.0       1
8100302   1.0      11
8100303   1.3      13  *~AN
8100304   1.30     14
8100305   1.50     15
*         volume
8100401   0.0      15
*         azim angle
8100501   0.00     15
*         incl angle
8100601  -90.0     15
*         delta z
8100701  -1.0       1
8100702  -1.0      11
8100703  -1.3      13
8100704  -1.30     14
8100705  -1.50     15
*         roughness hyd dia
8100801   4.572e-5  1.6   15
*         pvbfe
8101001   00000      15
*         fvcahs
8101101   001000     14
*         ebt
8101201    6    100000.8   381656.    381656.     1.  1.  1
8101202    6    100011.7   381852.    381852.     1.  1.  2
8101203    6    100022.6   382097.    382097.     1.  1.  3
8101204    6    100033.5   382332.    382332.     1.  1.  4
8101205    6    100044.4   382557.5   382557.5    1.  1.  5
8101206    6    100055.3   382773.    382773.     1.  1.  6
```

```
8101207    6    100066.2   382979.    382979.     1.  1.  7
8101208    6    100077.1   383174.    383174.     1.  1.  8
8101209    6    100088.    383359.5   383359.5    1.  1.  9
8101210    6    100098.9   383534.4   383534.4    1.  1.  10
8101211    6    100109.7   383699.    383699.     1.  1.  11
8101212    6    100122.2   383898.    383898.     1.  1.  12
8101213    6    100136.3   384080.    384080.     1.  1.  13
8101214    6    100150.4   384244.    384244.     1.  1.  14
8101215    6    100165.6   384409.    384409.     1.  1.  15
*         vel/flow
8101300   0
*         liquid    vapor     int-face
8101301    2.372416  2.372416 0.  1   * 78.7705
8101302    2.374226  2.374226 0.  2   * 78.7705
8101303    2.376557  2.376557 0.  3   * 78.7705
8101304    2.378784  2.378784 0.  4   * 78.7705
8101305    2.380907  2.380907 0.  5   * 78.7705
8101306    2.382925  2.382925 0.  6   * 78.7705
8101307    2.384836  2.384836 0.  7   * 78.7705
8101308    2.38664   2.38664  0.  8   * 78.7705
8101309    2.38834   2.38834  0.  9   * 78.7705
8101310    2.389926  2.389926 0.  10   * 78.7705
8101311    2.391402  2.391402 0.  11   * 78.7705
8101312    2.393204  2.393204 0.  12   * 78.7705
8101313    2.394787  2.394787 0.  13   * 78.7705
8101314    2.39618   2.39618  0.  14   * 78.7705
*                                          jun
8101402   1.6       0.0      1.0      1.0      14
*
*=============================================================================
*hydro              component name       component type
8150000               turn                 sngljun
*-----------------------------------------------------------------------------
*hydro     from          to           area       f loss     r loss   vcahs
8150101   810010000     820000000    0.0         0.327      0.327   01000
*
*hydro     vel/flw       f flowrate     g flowrate      j flowrate
8150201   0             5.6242         5.6242          0. * 78.7705
*hydro     dhjun         beta             c              m
8150110   0.5         0.0              1.0           1.0
*
*=============================================================================
8200000   riser     pipe
*-----------------------------------------------------------------------------
*         no. vols
8200001   15
*         vol area
8200101   12.6424  15
*         length
8200301   1.50      1
8200302   1.30      2
8200303   1.3       4
8200304   1.00      14
8200305   1.00      15
*         volume
8200401   0.0       15
*         azim angle
```

```
8200501   0.00     15
*         incl angle
8200601   90.0     15
*         delta z
8200701   1.50     1
8200702   1.30     2
8200703   1.3      4
8200704   1.00     14
8200705   1.00     15
*         roughness hyd dia
8200801   4.572e-5  0.475  15
*         pvbfe
8201001   00000      15
*         fvcahs
8201101   001000     14
*         ebt
8201201    6    100145.4   391277.    391277.     1.  1.  1
8201202    6    100129.    397190.    397190.     1.  1.  2
8201203    6    100114.    403011.4   403011.4    1.  1.  3
8201204    6    100099.3   408741.    408741.     1.  1.  4
8201205    6    100086.4   413093.    413093.     1.  1.  5
8201206    6    100075.5   417391.    417391.     1.  1.  6
8201207    6    100064.7   421635.    421635.     1.  1.  7
8201208    6    100054.    425825.    425825.     1.  1.  8
8201209    6    100043.6   429961.    429961.     1.  1.  9
8201210    6    100033.2   434043.    434043.     1.  1.  10
8201211    6    100023.    438070.    438070.     1.  1.  11
8201212    6    100012.8   442045.    442045.     1.  1.  12
8201213    6    100002.8  445971.    445971.     1.  1.  13
8201214    6    99993.    447776.    447776.     1.  1.  14
8201215    6    99983.4   447650.    447650.     1.  1.  15
*         vel/flow
8201300   0
*         liquid    vapor     int-face
8201301    5.79518    5.79518  0.  1   * 78.7705
8201302    5.9422     5.9422   0.  2   * 78.7705
8201303    6.08676    6.08676  0.  3   * 78.7705
8201304    6.2289     6.2289   0.  4   * 78.7705
8201305    6.3369     6.3369   0.  5   * 78.7705
8201306    6.44339    6.44339  0.  6   * 78.7705
8201307    6.54848    6.54848  0.  7   * 78.7705
8201308    6.65215    6.65215  0.  8   * 78.7705
8201309    6.75443    6.75443  0.  9   * 78.7705
8201310    6.85531    6.85531  0.  10   * 78.7705
8201311    6.9548     6.9548   0.  11   * 78.7705
8201312    7.05292    7.05292  0.  12   * 78.7705
8201313    7.14981    7.14981  0.  13   * 78.7705
8201314    7.1947     7.1947   0.  14   * 78.7705
*                                          jun
8201402   0.475       0.0      1.0     1.0     14
*
*=======================================================================
*hydro              component name      component type
8250000                outlet             sngljun
*-----------------------------------------------------------------------
*hydro    from          to            area      f loss     r loss  vcahs
8250101   820010000     830000000     12.6424    0.0        0.0     01000
```

```
*
*hydro    vel/flw       f flowrate     g flowrate     j flowrate
8250201   0             7.19229      7.19229      0. * 78.7705
*hydro    dhjun         beta           c            m
8250110   0.475         0.0            1.0          1.0
*
*=============================================================================
8300000   sink      tmdpvol
*-----------------------------------------------------------------------------
*         area                  length          volume
8300101   56.                   20.0              0.0
*         azim angle            incl angle      delta z
8300102   0.00                  90.0              20.0
*         roughness             hyd dia         pvbfe
8300103   0.00000               4.2000          00010
*         ebt       trip            search var
8300200   004       0
*         indep var
8300201   0.00      1.e5     310.93  0.0

*************************** STRUCTURE 8201 ***************************
* reactor and containment vessel walls; gap filled with lead bismuth
*=====================================================================$
*ht str ht.strs  m.pts  geom  init  l.coord  refl  b.vol   ax.incr.
18201000   16      13    2     1    4.920E+00 0
*
*        loc      flag
18201100  0         1
*
*         #         r
18201101  4         4.970E+00
18201102  2         5.000
18201103  6         5.100
*
*        compos.    #
18201201    3       4
18201202    6       6
18201203    3      12
*
*         source    #
18201301  0.0      12
*
*        temperature flag
18201400  0
*
*         temperature #
18201401  600.00     13
*
*         vol       inc       type      code      factor      #
18201501 500010000    0        1         1         1.500       1
18201502 580010000    0        1         1         1.300       2
18201503 580020000    10000    1         1         1.300       4
18201504 580040000    10000    1         1         1.000      14
18201505 580140000    10000    1         1         0.500      16
*
*         vol       inc       type      code      factor      #
18201601 820010000    0        1         1         1.500       1
```

```
18201602 820020000    0        1          1        1.300      2
18201603 820030000    10000    1          1        1.300      4
18201604 820050000    10000    1          1        1.000      14
18201605 820150000    0        1          1        0.500      16
*
*         type      mult      D-lt      D-rt      #   *source
18201701   0        0.0       0.0       0.0       16
*
18201800    1
*        Dhe  LHEf  LHEr LGSf  LGSr Kfwd  Krev  Fboil nclf povd ff   #
18201801 0.0  10.   10.  10.   10.  0.0   0.0   1.0   1.50 1.0  1.0  1
18201802 0.0  10.   10.  10.   10.  0.0   0.0   1.0  14.90 1.0  1.0  16
*
18201900    1
*        Dhe  LHEf  LHEr LGSf  LGSr Kfwd  Krev  Fboil nclf povd ff   #
18201901 0.0  10.   10.  10.   10.  0.0   0.0   1.0  16.4  1.0  2.5  16
*
**************************** STRUCTURE 8202 ****************************
* collector cylinder wall
*=========================================================================$
*ht str ht.strs  m.pts  geom  init  l.coord  refl  b.vol   ax.incr.
18202000   16       5    2     1    5.490    0
*
*        loc      flag
18202100  0         1
*
*         #         r
18202101  4         5.500
*18202102  1         3.604325
*
*        compos.    #
18202201    3       4
*18202202    5       5             *asbestos
*
*         source    #
18202301  0.0       4
*
*        temperature flag
18202400  0
*
*         temperature #
18202401  600.00      5
*
*         vol       inc       type      code      factor      #
18202501  820010000   0         1         1         1.50        1
18202502  820020000   0         1         1         1.30        2
18202503  820030000   10000     1         1         1.300       4
18202504  820050000   10000     1         1         1.00       14
18202505  820150000   0         1         1         0.50       16
*
*         vol       inc       type      code      factor      #
18202601  810150000   0         1         1         1.50        1
18202602  810140000   0         1         1         1.30        2
18202603  810130000  -10000     1         1         1.300       4
18202604  810110000  -10000     1         1         1.00       14
18202605  810010000   0         1         1         0.50       16
*
```

```
*         type      mult      D-lt      D-rt      #   *source
18202701   0        0.0       0.0       0.0       16
*
18202800    1
*        Dhe  LHEf  LHEr LGSf  LGSr Kfwd  Krev  Fboil nclf povd ff   #
18202801 0.0  10.   10.  10.   10.  0.0   0.0   1.0  16.4 1.0  2.0  16
*
18202900    1
*        Dhe  LHEf  LHEr LGSf  LGSr Kfwd  Krev  Fboil nclf povd ff   #
18202901 0.0  10.   10.  10.   10.  0.0   0.0   1.0  16.4 1.0  1.0  16
*
*************************** STRUCTURE 8203 ****************************
* perforated plate
*=====================================================================$
*ht str ht.strs  m.pts  geom  init  l.coord  refl  b.vol   ax.incr.
18203000   16       3    2     1    5.290    0
*
*        loc      flag
18203100  0         1
*
*         #         r
18203101  2         5.300
*
*        compos.    #
18203201    3       2
*
*         source    #
18203301  0.0       2
*
*        temperature flag
18203400  0
*
*         temperature #
18203401  600.00      3
*
*         vol       inc       type      code      factor      #
18203501  820010000   0         1         1         0.90        1
18203502  820020000   0         1         1         0.78        2
18203503  820030000   10000     1         1         0.78        4
18203504  820050000   10000     1         1         0.60       14
18203505  820150000   0         1         1         0.30       16
*
*         vol       inc       type      code      factor      #
18203601  820010000   0         1         1         0.90        1
18203602  820020000   0         1         1         0.78        2
18203603  820030000   10000     1         1         0.78        4
18203604  820050000   10000     1         1         0.60       14
18203605  820150000   0         1         1         0.30       16
*
*         type      mult      D-lt      D-rt      #   *source
18203701   0        0.0       0.0       0.0       16
*
18203800    1
*        Dhe  LHEf  LHEr LGSf  LGSr Kfwd  Krev  Fboil nclf povd ff   #
18203801 0.0  10.   10.  10.   10.  0.0   0.0   1.0  16.4 1.0  2.0  16
*
18203900    1
```

```
*        Dhe   LHEf   LHEr LGSf   LGSr Kfwd   Krev   Fboil nclf povd ff    #
18203901 0.0   10.    10.  10.    10.  0.0    0.0    1.0   16.4 1.0  2.0   16
*
*************************** radiation ********************************
*                  nset
60000000           16
***********************************************************************
*  from outer wall of containment vessel to inner wall of collector
***********************************************************************
*         nrh    trmin  alpha  set
60100000   4      273.  0.0
*         htnum     jlr emis
60101001 8201001   1   0.75
60102001 8203001   0   0.75
60103001 8203001   1   0.75
60104001 8202001   0   0.75
*
* 1       view factor  surface
60101101    0.0           1    * F1-1
60101102    0.60          2    * F1-2
60101103    0.0           3    * F1-3
60101104    0.40          4    * F1-4
* 2
60102101    0.964083      1    * F2-1
60102102    0.035917      2    * F2-2
60102103    0.0           3    * F2-3
60102104    0.0           4    * F2-4
* 3
60103101    0.0           1    * F3-1
60103102    0.0           2    * F3-2
60103103    0.0           3    * F3-3
60103104    1.0           4    * F3-4
* 4
60104101    0.371585      1    * F4-1
60104102    0.0           2    * F4-2
60104103    0.579235      3    * F4-3
60104104    0.049180      4    * F4-4
*
*         nrh    trmin  alpha  set
60200000   4      273.  0.0    01
*         htnum     jlr emis
60201001 8201002   1   0.75
60202001 8203002   0   0.75
60203001 8203002   1   0.75
60204001 8202002   0   0.75
*
*         nrh    trmin  alpha  set
60300000   4      273.  0.0    01
*         htnum     jlr emis
60301001 8201003   1   0.75
60302001 8203003   0   0.75
60303001 8203003   1   0.75
60304001 8202003   0   0.75
*
*         nrh    trmin  alpha  set
60400000   4      273.  0.0    01
*         htnum     jlr emis
```

```
60401001 8201004   1   0.75
60402001 8203004   0   0.75
60403001 8203004   1   0.75
60404001 8202004   0   0.75
*
*         nrh   trmin  alpha  set
60500000   4     273.  0.0    01
*         htnum    jlr emis
60501001 8201005   1   0.75
60502001 8203005   0   0.75
60503001 8203005   1   0.75
60504001 8202005   0   0.75
*
*         nrh   trmin  alpha  set
60600000   4     273.  0.0    01
*         htnum    jlr emis
60601001 8201006   1   0.75
60602001 8203006   0   0.75
60603001 8203006   1   0.75
60604001 8202006   0   0.75
*
*         nrh   trmin  alpha  set
60700000   4     273.  0.0    01
*         htnum    jlr emis
60701001 8201007   1   0.75
60702001 8203007   0   0.75
60703001 8203007   1   0.75
60704001 8202007   0   0.75
*
*         nrh   trmin  alpha  set
60800000   4     273.  0.0    01
*         htnum    jlr emis
60801001 8201008   1   0.75
60802001 8203008   0   0.75
60803001 8203008   1   0.75
60804001 8202008   0   0.75
*
*         nrh   trmin  alpha  set
60900000   4     273.  0.0    01
*         htnum    jlr emis
60901001 8201009   1   0.75
60902001 8203009   0   0.75
60903001 8203009   1   0.75
60904001 8202009   0   0.75
*
*         nrh   trmin  alpha  set
61000000   4     273.  0.0    01
*         htnum    jlr emis
61001001 8201010   1   0.75
61002001 8203010   0   0.75
61003001 8203010   1   0.75
61004001 8202010   0   0.75
*
*         nrh   trmin  alpha  set
61100000   4     273.  0.0    01
*         htnum    jlr emis
61101001 8201011   1   0.75
```

```
61102001 8203011   0   0.75
61103001 8203011   1   0.75
61104001 8202011   0   0.75
*
*         nrh    trmin  alpha  set
61200000   4      273.  0.0    01
*         htnum     jlr emis
61201001 8201012   1   0.75
61202001 8203012   0   0.75
61203001 8203012   1   0.75
61204001 8202012   0   0.75
*
*         nrh    trmin  alpha  set
61300000   4      273.  0.0    01
*         htnum     jlr emis
61301001 8201013   1   0.75
61302001 8203013   0   0.75
61303001 8203013   1   0.75
61304001 8202013   0   0.75
*
*         nrh    trmin  alpha  set
61400000   4      273.  0.0    01
*         htnum     jlr emis
61401001 8201014   1   0.75
61402001 8203014   0   0.75
61403001 8203014   1   0.75
61404001 8202014   0   0.75
*
*         nrh    trmin  alpha  set
61500000   4      273.  0.0    01
*         htnum     jlr emis
61501001 8201015   1   0.75
61502001 8203015   0   0.75
61503001 8203015   1   0.75
61504001 8202015   0   0.75
*
*         nrh    trmin  alpha  set
61600000   4      273.  0.0    01
*         htnum     jlr emis
61601001 8201016   1   0.75
61602001 8203016   0   0.75
61603001 8203016   1   0.75
61604001 8202016   0   0.75
*
```

B.5. Decay Heat Curve Model

```
*-------------------------------------------------------------------------
20270600    power      510    1.0   1.0
*           time           p/po
20270601   -1.0            0.0
20270602    0.1            0.0589144
20270603    1.0            0.0551549
20270604    1.5            0.0536907
```

```
20270605    2.0             0.0524328
20270606    4.0             0.0487971
20270607    6.0             0.0464603
20270608    8.0             0.0447893
20270609    10.0            0.0435018
20270610    15.0            0.0411928
20270611    20.0            0.0395791
20270612    40.0            0.0357397
20270613    60.0            0.0334909
20270614    80.0            0.0319063
20270615    100.0           0.0307046
20270616    150.0           0.0286318
20270617    200.0           0.0272649
20270618    400.0           0.0242200
20270619    600.0           0.0224554
20270620    800.0           0.0211546
20270621    1000.0          0.0201120
20270622    1500.0          0.0181624
20270623    2000.0          0.0167732
20270624    4000.0          0.0137039
20270625    6000.0          0.0122575
20270626    8000.0          0.0114053
20270627    10000.0         0.0108279
20270628    15000.0         0.0099174
20270629    20000.0         0.0093461
20270630    40000.0         0.0080769
20270631    60000.0         0.0073531
20270632    80000.0         0.0068500
20270633    100000.0        0.0064680
20270634    150000.0        0.0057910
20270635    200000.0        0.0053224
20270636    400000.0        0.0042407
20270637    600000.0        0.0036697
20270638    800000.0        0.0033155
20270639    1000000.0       0.0030754
*=========================================================================
```